INFORMATION TO USERS

This manuscript has been reproduced from the microfilm master. UMI films the text directly from the original or copy submitted. Thus, some thesis and dissertation copies are in typewriter face, while others may be from any type of computer printer.

The quality of this reproduction is dependent upon the quality of the copy submitted. Broken or indistinct print, colored or poor quality illustrations and photographs, print bleedthrough, substandard margins, and improper alignment can adversely affect reproduction.

In the unlikely event that the author did not send UMI a complete manuscript and there are missing pages, these will be noted. Also, if unauthorized copyright material had to be removed, a note will indicate the deletion.

Oversize materials (e.g., maps, drawings, charts) are reproduced by sectioning the original, beginning at the upper left-hand corner and continuing from left to right in equal sections with small overlaps.

ProQuest Information and Learning
300 North Zeeb Road, Ann Arbor, MI 48106-1346 USA
800-521-0600

Calcium phosphate compatible bone cement: characterization, bonding properties and tissue response

by

Maria Lynn Roemhildt

A dissertation submitted to the graduate faculty

in partial fulfillment of the requirements for the degree of

DOCTOR OF PHILOSOPHY

Major: Biomedical Engineering

Program of Study Committee:
Thomas McGee, Major Professor
David Cann
Mary Helen Greer
Dennis Johnson
Surya Mallapragada
Stanley Wagner

Iowa State University

Ames, Iowa

2002

Graduate College
Iowa State University

This is to certify that the dissertation of

Maria Lynn Roemhildt

has met the dissertation requirements of Iowa State University

Signature was redacted for privacy.

Committee Member

Signature was redacted for privacy.

Committee Member

Signature was redacted for privacy.

Committee Member

Signature was redacted for privacy.

Committee Member

Signature was redacted for privacy.

Committee Member

Signature was redacted for privacy.

Major Professor

Signature was redacted for privacy.

For the Major Program

TABLE OF CONTENTS

LIST OF FIGURES

LIST OF TABLES

I. INTRODUCTION

Bone cement is used in orthopaedic surgery to replace or bind bone fragments resulting from trauma, to fill cavities, or to secure an implanted prosthesis. Any enduring bone cement must be biocompatible, be stable in the physiological environment, and have adequate mechanical properties for stresses applied during daily activity.

Joint replacement is a common procedure to replace diseased joints. 139,000 total hip replacement surgeries and 247,000 total knee replacement surgeries were performed in the United States in 1996 (NCHS, 1999). In joint replacement, the cement serves to anchor the prostheses as well as transfer the applied load from the stiff prosthesis to the relatively less rigid bone. In addition to biocompatibility and adequate mechanical properties, a bone cement should have flow properties to allow proper placement and an appropriate setting time so that joint articulation can be verified before closure of the wound.

Common bone cements are based on polymerizing methacrylate or reactions with salts of calcium phosphates. Poly(methyl-methacrylate), PMMA, is currently widely used for prosthesis fixation and cavity filling applications. However, PMMA has many shortcomings including: tissue necrosis resulting from the exothermic setting reaction, lack of bonding (except for mechanical interlocking), degradation fragments which cause irritation and inflammation, and suspected toxicity of the monomer (Planell, 1995). To date, calcium phosphates cements have shown excellent tissue compatibility, but mechanical properties have been poor and inadequate for load bearing application.

In previous research, cement made from a combination of calcium aluminate and calcium phosphate was studied *in vitro* and was found to have mechanical and setting properties that would be suitable for use as a bone cement (Roemhildt, 1998). This cement is referred to as OC-cement in this paper. It is postulated that the hydrated calcium aluminate binder would provide adequate strength and be stable in the physiological environment, while the calcium phosphate aggregate would enhance the biocompatibility of the material and lead to bioactivity.

The objective of the present study was to investigate the following characteristics of OC-cement:

- flow and setting properties,
- compressive strength and phase composition of OC-cement with aging,
- bonding strength between the OC-cement and a metal prosthesis,
- bonding strength between the OC-cement and natural bone,
- and tissue response to the OC-cement *in vivo*.

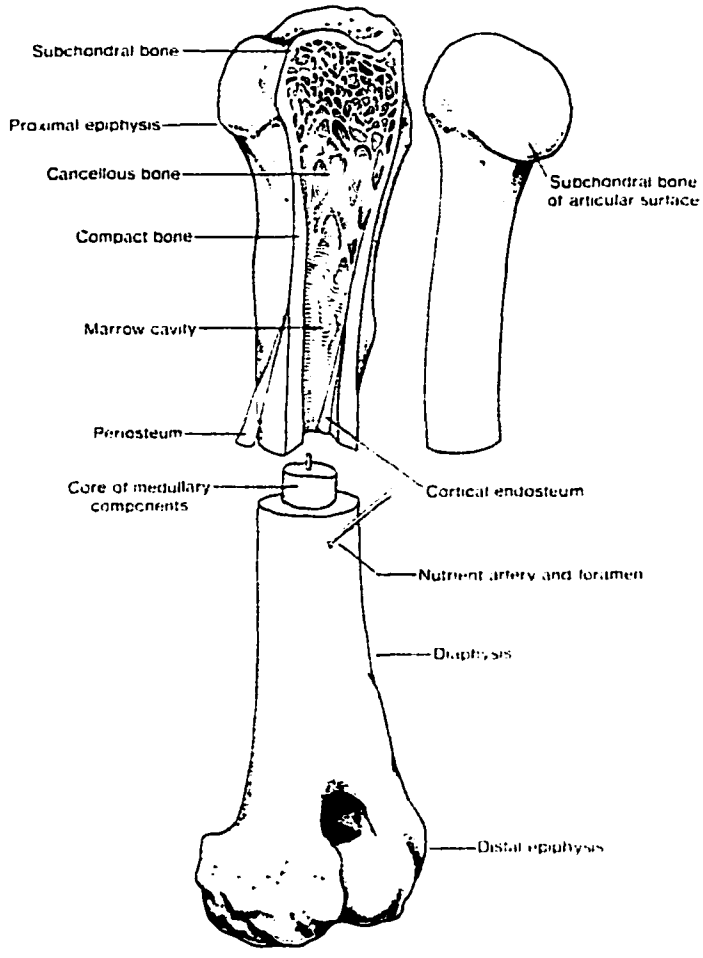

Figure 1. Longitudinal section through a growing long bone (Banks, 1986)

Table 1. Composition of adult mammalian bone

Component	*Amount (wt%)*	*Approximate distribution (wt%)*
mineral matrix	50-70%	calcium 39%, phosphate 17%, sodium 0.7%, magnesium 0.5%, carbonate 0.5%, potassium 0.2%
organic matrix	20-40%	collagen 96%, noncollagenous protein, proteoglycan, hyaluronan, and gylcoprotein
water	5-10%	
lipids	< 3%	

From Lian et al., 2000 and Martini, 1995.

The organic matrix mostly contains type I collagen fibers that are oriented in a preferential direction. The preferential orientation of the collagen fibers alternates from layer to layer in adult bone to give bone its typical lamellar structure (Baron, 1999). The mineral phase forms spindle- or plate-shaped crystals (~30-70 x 200Å) of a poorly crystalline, carbonated apatite similar to hydroxyapatite [$Ca_{10}(PO_4)_6(OH_2)$]. These mineral crystals are found on and within the collagen fibers and in the ground substance. The crystals are typically oriented in the same direction as the collagen fibers (Baron, 1999). Substitutions of carbonate, magnesium, acid phosphate and OH^- vacancies create small, imperfect crystals that are somewhat soluble, allowing bone to act as a reserve for calcium, phosphate, and magnesium ions (Lian et al., 1999).

4. Types of bone

According to structure and function, there are two main types of bone: dense cortical (compact) and cancellous (trabecular). They are constituted of the same matrix elements and the same cells, but are different in structure and function. The main structural difference is that 80-90% of the volume of cortical bone is mineralized, while only 15-25% is mineralized in cancellous bone. The remaining volume is occupied by bone marrow, blood vessels, and connective tissue (Baron, 1999).

In cortical bone, the main structural unit is the osteon that is composed of approximately 20-30 concentric lamellae (Figure 2). A typical osteon is cylindrically shaped and approximately 200-250 μm in diameter. At the center of each osteon is the Haversian canal providing a pathway for blood vessels. Perforating (Volkmann's) canals provide a transverse, interconnected network through the lamellae for blood vessels to supply nutrients to osteons deeper in the bone and to the marrow cavity (Martini, 1995). Inside the concentric lamellae are small cavities called lacunae where osteocytes are found. Canaliculi provide a narrow passageway for diffusion of nutrients between lacunae. Surrounding each osteon is a cement line, a 1-2 μm thick layer of mineralized tissue that lacks collagen fibers.

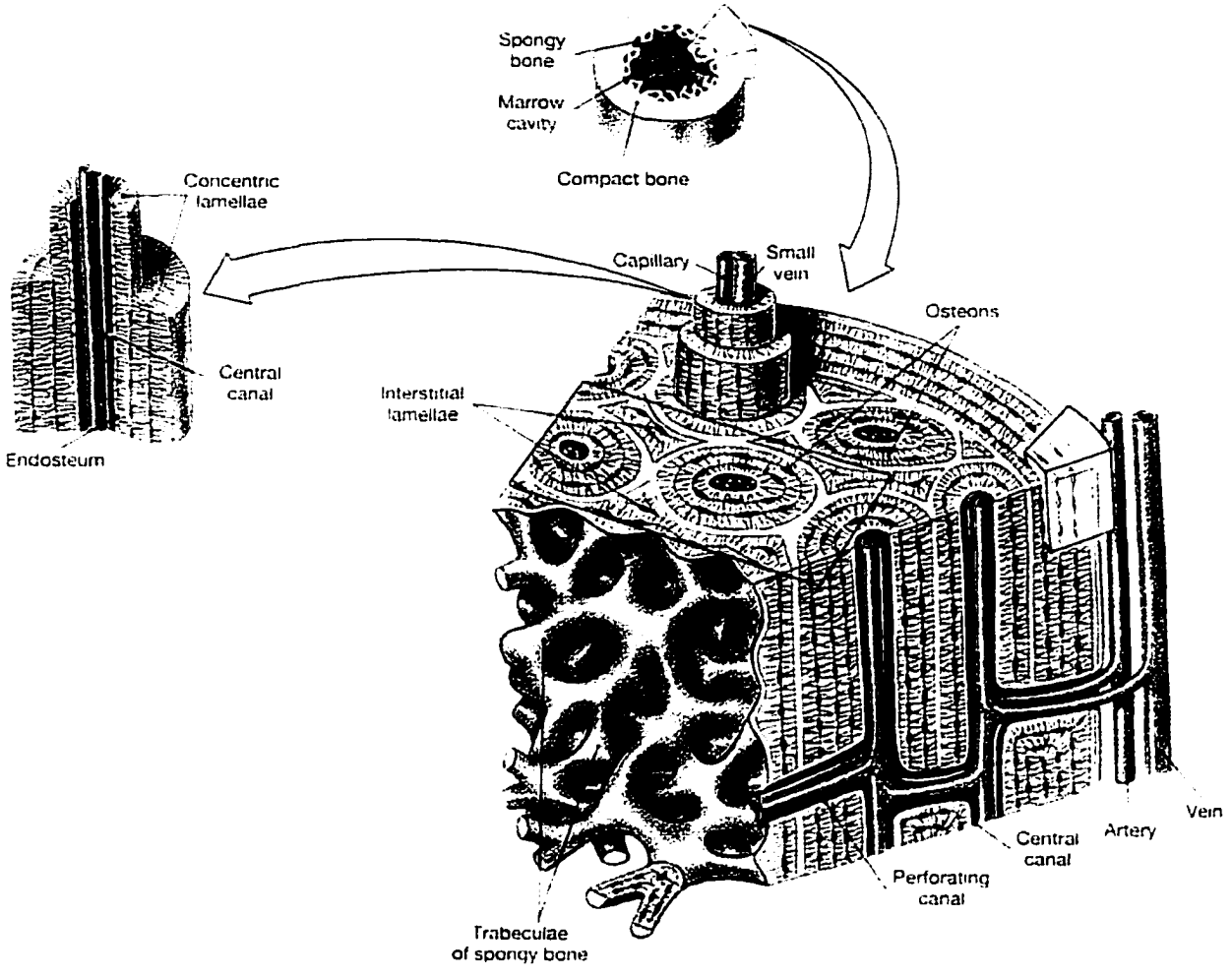

Figure 2. Structure of osteon system (Martini, 1995)

In cancellous bone the structural unit is shallow, crescent hemiosteon, or trabecular packet, approximately 600 μm radius, 50 μm thick, and 1 mm in length (Jee, 1999). The architecture of the trabeculae serves to distribute a load over a larger area. With a surface to volume ratio eight times greater than cortical bone, cancellous bone surface provides more than 66% of the total bone surface (Jee, 1999). Table 2 shows a comparison of the basic structural units in cortical versus cancellous bone.

Table 2. Comparison of adult cortical and cancellous bone structural units

Parameter	*Cortical (Osteonal)*	*Cancellous (Trabecular packet)*
Circumference (mm)	0.6	0.6
Length (mm)	2.5	1.0
Wall thickness (mm)	0.075	0.040
Number / mm^3 bone volume	15	40
Total # in skeleton	$21 * 10^6$	$14 * 10^6$
Resorption time (days)	24	21
Formation time (days)	124	91
Bone turnover rate (% / yr)	3	26
Shape	cylindrical	crescent

Modified from Recker, 1983.

5. Types of bone cells

The main cellular elements of bone are osteoblasts, osteocytes, osteoclasts, and bone lining cells (Figure 3, Table 3). Osteoblasts, osteocytes, and bone lining cells emanate from local progenitor cells whereas osteoclasts arise from precursors originating in various hemapoietic tissues.

Osteoblasts are bone-forming cells that synthesize and secrete unmineralized bone matrix, participate in calcification and resorption, as well as help to regulate the ion flux in and out of bone. In their active state, they are found in clusters of cuboidal cells along a bone surface. Osteoblasts contain an abundance of alkaline phosphatase and osteo-inductive cell markers (Jee, 1999). At the end of its secreting period, an osteoblast becomes a bone lining cell or an osteocyte (Baron, 1999). Osteocytes are mature osteoblasts that ceased producing matrix and have become embedded with bone. They are found in lacunae and are incapable of dividing. Slender processes extend from the osteocyte through the canaliculi to communicate with other osteocytes or bone lining cells. The role of osteocytes is to stabilize bone mineral, detect microfractures, and respond to the amount and distribution of strain within bone (Jee, 1999).

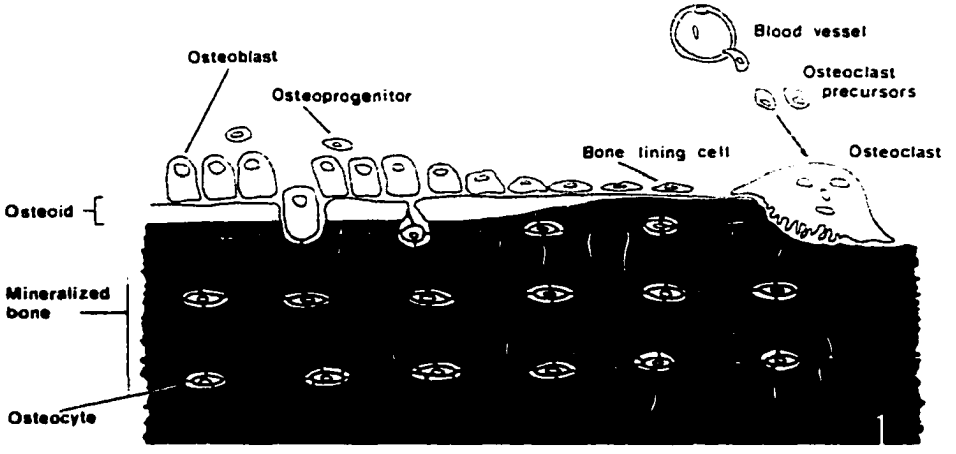

Figure 3. Types of bone cells (Marks and Popoff, 1988)

Table 3. Comparison of types of bone cells

	Osteoblast	*Osteocyte*	*Bone lining cells*	*Osteoclast*
Size	15-30 μm length	~20 μm long	1 μm thick 12 μm long	20-100 μm diameter
Shape	cuboidal	elliptical with processes	flattened ellipsoidal	multinucleated
Function	synthesize and secrete bone matrix	regulation of mineral content and architecture of bone mass	cover inactive bone surfaces	erode bone
Location	mineralization front	lacunae	inactive bone surface	cavities on bone surface
Precursor	mesenchymal progenitors	osteoblast	inactive osteoblasts	macrophage
Life-span	n/a	n/a	n/a	7 wks

From Jee, 1999 and Puzas and Lewis, 1999.

Osteoclasts are multinucleated, giant cells that are found on bone surfaces; eroding and resorbing bone matrix. A ruffled border that is sealed on each side characterizes their zone of contact with bone. The osteoclast lowers the pH of the extracellular compartment to approximately 5 and dissolves the crystals of calcium phosphate (Puzas and Lewis, 1999). Next, lysosomes and enzymes degrade and digest the exposed matrix and collagen fibers. It is thought that the osteoclast undergoes apoptosis after a cycle of resorption (Baron, 1999).

Bone lining cells are flat, elongated, inactive cells that cover bone surfaces that are not undergoing resorption or formation (Marks and Hermey, 1996).

6. Bone growth, repair, and remodeling

Specialized receptors in bone cells respond to hormonal, mechanical, and other signals to control bone growth, repair, and remodeling (Lian et al., 1999).

Bone growth occurs through intramembrous or endochondral ossification. Most growth of long bones occurs through endochondral ossification, in which growth of bone proceeds from cartilage. Mesenchymal cells proliferate and differentiate into prechondroblasts and chondroblasts. A chondroblast secretes cartilaginous matrix in which it can become embedded and differentiate into a chondrocyte (Baron, 1999). The cartilage enlarges, a series of struts calcify, followed by the death of the chondrocytes.

In contrast, growth of flat bone and some bone repair proceeds through intramembrous ossification. Mesenchymal cells proliferate and differentiate into preosteoblasts and then to osteoblasts. In intramembrous ossification, osteoblasts synthesize bone matrix without a preferential orientation, osteocytes are large and numerous, and calcification is delayed and irregular. This results in what is called woven bone, which is later remodeled into compact bone (Baron, 1999).

The body's normal response to bone fracture involves three stages: inflammation, reparation, and remodeling. Immediately after the injury, hemorrhage and cell death elicit an inflammatory response that works to phagocytize necrotic tissue and produce rudimentary scar tissue. Clinically, this phase of healing is associated with swelling, pain, and warmth lasting 3-4 days. In the reparation phase, necrotic debris is removed and replaced with new cell matrix and an external callus is formed to provide stability. The last phase, remodeling, can begin after 4 to 6 weeks and last up to 12 months. During this time, the periosteal bony callus is gradually resorbed, maturate bone is formed, and the bone structure is restored (An et al., 1999, Caputo, 1999). The rate at which the repair proceeds is species dependent as shown in Table 4.

Table 4. Timetable of interface formation for an endosseous implant in cortical bone

Stage of repair	*Time in weeks*		
	Rabbit	Canine	Human
Woven callus formation	2	4	6
Lamellar compaction	6	12	18
Interface remodeling	6	12	18
Maturation	18	36	54

From Roberts et al., 1987.

Bone remodeling is a coordinated mechanism of bone resorption and bone formation, through which old bone is removed and replaced by new bone. Though cortical and cancellous bone vary in structure, the remodeling of each follows the same principles. Remodeling can be divided into five phases: resorption, reversal, initial mineralization, formation, and mineralization (Figure 4). Figure 5 depicts bone-remodeling activity along a longitudinal sequence. First, a "cutting cone" tunnels out bone matrix followed by a "closing cone" that leads to the formation of a new haversian system.

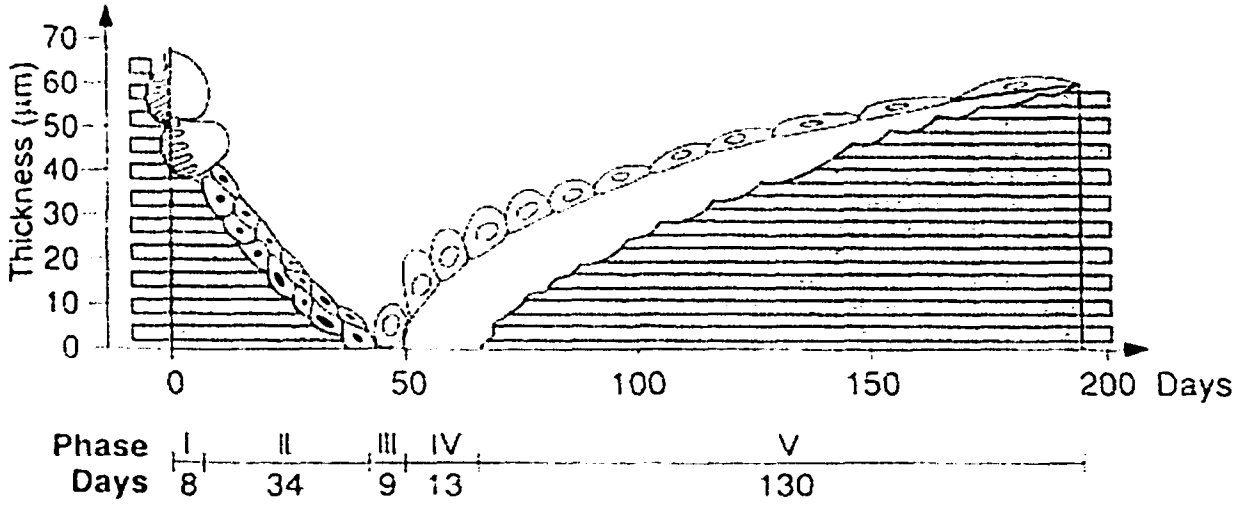

Figure 4. Bone remodeling in cancellous bone (Baron, 1999)

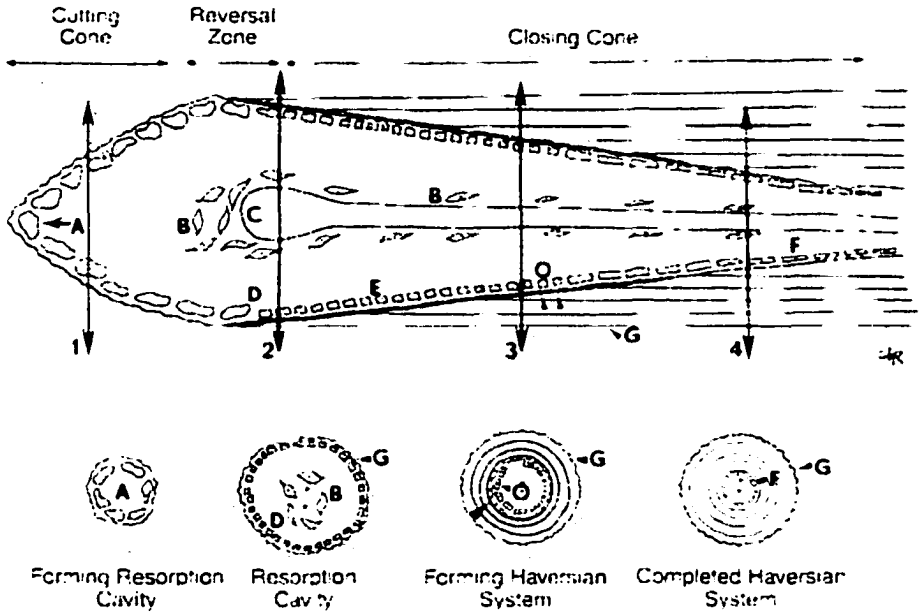

Figure 5. Bone resorption cone (from Baron, 1999)

On average, 18% of the total bone mass is remodeled each year in an adult human (Ganong, 1995). Remodeling serves to help maintain the overall skeletal mass, reform fracture callus to new bone, adapt bone to applied stresses, and aid in the control of mineral homeostasis (Puzas and Lewis, 1999). Bones that are heavily stressed become thicker and stronger, whereas bones not subjected to ordinary stresses will become thin and brittle (Ganong, 1995). The relationship between the forces acting on bone and remodeling were studied by Wolff who found that bone is reshaped in response to the forces acting on it (1892). Others have suggested these additional principles:

- Remodeling is triggered not by principal stress but by "flexure."
- Repetitive dynamic loads on bone trigger remodeling. Static loads do not.
- Dynamic flexure causes all affected bone surfaces to drift toward concavity that arises during the act of dynamic flexure (Park and Lakes, 1992).

Also of interest is the phenomenon of stress shielding. This occurs where a load-bearing implant reduces the local stress at a previously load-bearing site resulting in atrophy or tissue loss in adjacent tissue (Black, 1999). In total hip replacement (THR) cement serves not only to anchor the

prosthesis but to transfer the load from the relatively stiff prosthesis to the surrounding tissue (Park and Lakes, 1992).

7. Hormonal regulation of bone

Although there are many hormones that may have an effect on bone, there are three main regulating hormones for the control of calcium metabolism and bone physiology: 1,25-dihydroxycholecalciferol, parathyroid hormone (PTH), and calcitonin. 1,25-dihydroxycholecalciferol is a steroid formed from vitamin D that functions to increase the calcium absorption in the intestine. PTH acts directly on bone to mobilize calcium from bone. It also indirectly decreases calcium excretion. Calcitonin acts to decrease the calcium concentration in the extracellular fluid by inhibiting bone resorption (Ganong, 1995).

8. Factors affecting bone loss

When bone loss is accelerated or exaggerated, it contributes to a decrease in bone mass and strength and increases the possibility of fracture. As adults age, they begin to lose bone mass in their later decades. This is due in part to the low calcium intake in the elderly population as well as decreased vitamin D consumption (Rosen et al., 1999). Estrogen deficiency has also been recognized as a major cause of bone loss in women after menopause. In addition to nutritional and hormonal factors, level of exercise, alcohol consumption, smoking, heredity, and environmental factors contribute to overall bone loss (Rosen et al., 1999).

B. Mechanical Properties of Bone

Bone is a complex composite of materials that contribute to its overall mechanical properties. The structure of bone is anisotropic, leading to the anisotropy of its properties. It has been difficult for researchers to determine accurate values for the mechanical properties of bone and a broad range of values has been reported in the literature, as shown in Table 5. The intrinsic strength of bone is dependent upon the type of bone, bone architecture, species, age, and composition in terms of porosity, density, and mineralization.

Table 5. General mechanical properties of bone

Bone property	*Range*	*Average*
Cortical bone		
Comp. strength (MPa)	133-295	200±36
Comp. elastic modulus (GPa)	14.7-34.3	23±4.8
Tensile strength (MPa)	92-188	141±28
Tensile elastic modulus (GPa)	7.1-28.2	19.6±6.2
Cancellous bone (average)		
Strength (MPa)	1.5-38	
Elastic modulus (GPa)	.01-1.57	

From An, 2000.

In vitro factors also influence the values obtained when testing the mechanical properties of bone. Factors of influence include storage history of the bone sample, dryness, rate of mechanical loading, and direction and distribution of the applied load. It has been recommended that bone samples be kept moist with saline at all times and that samples be frozen to minimize degradation if storage is necessary. Freezing of bone specimens to -20°C for up to eight months was not found to significantly affect the mechanical properties of bone (Zioupos et al., 2000).

C. Orthopaedic Biomaterials

1. Bone repair and replacement materials

In addition to autografts, allografts, and xenographs, various metals, ceramics, and polymers have been used in orthopaedic surgery to repair and/or replace bones and joints. Any material that is implanted must be biocompatible. Williams defines biocompatibility as the ability of a material to perform with an appropriate host response in a specific application (1999). An orthopaedic biomaterial must be appropriate in terms of its mechanical and biological properties. Materials are described as toxic, bioinert, bioactive, or bioresorbable based upon the host's response to the biomaterial. These terms are described in Table 6. Also of concern in the use of orthopaedic biomaterials are the possibilities and effects of wear debris, corrosion, and infection on the biomaterial as well as on the tissue (Tanner, 1998).

Table 6. Types of biomaterial based on host response

Type of material	*Tissue response to the material*	*Examples*
Toxic	provoke inflammatory or disadvantageous response, body tries to reject or remove the material, necrosis of surrounding tissue	particulate debris
Biotolerant	foreign body response forms a fibrous capsule that surrounds and isolates the material	PMMA, 316L stainless steel
Bioinert	limited response with the formation of a thin fibrous capsule	alumina, zirconia
Bioactive	body's response is advantageous, formation of biomaterial-tissue interface results	glass-ceramics, hydroxyapatite
Bioresorbable	material is nontoxic, dissolves, and is replaced by surrounding tissue	tricalcium phosphate, some polymers

From Hench, 1996 and Park and Lakes, 1992.

In general, metals have a high strength and elastic modulus, are tough and ductile, and usually have good fatigue resistance and stress-corrosion resistance. Commonly used metals include low carbon stainless steel and alloys of Ti-Al-V or Co-Cr-Mo. Metals are frequently used for load bearing applications such as prostheses, nails, pins, rods, and plates. Polymers, long chain, high molecular weight molecules, generally have substantially lower strength, lower elastic moduli, and deform at lower stresses than metals. Poly(ethylene) is often used to form the artificial acetabular cup and poly(methyl-methacrylate) is commonly used in bone cement. Ceramic materials such as calcium phosphates, zirconia, and alumina have been found to have good tissue response and are typically strong, but brittle in nature. For this reason they are generally used as coatings or for non-load bearing applications; however, in Europe the use of alumina for the ball and socket of the total hip replacement is popular due to its superior wear resistance compared to presently used materials. The mechanical properties of selected biomaterials are compiled in Table 7.

Table 7. Properties of common biomaterials

Material	*Compressive strength (MPa)*	*Tensile strength (MPa)*	*Elastic modulus (GPa)*	*Density[b] (g/cm^3)*
316L Steel	---	505-860	190	7.9
Ti-6Al-4V	---	860	116	4.5
Co-Cr-Mo	---	430-1038	210	9.2
PMMA bone cement	92	30	3	1.1
Alumina (100% dense)	4,000-5,000	260-350	365 -400	3.9
Alumina (25% porosity)	500	---	150	2.9
Glass-ceramic	300	200	30-35	2.5
Hydroxyapatite[c]	917	40-200	40-120	3.2
ß-TCP[c]	10-28	40-120	90-120	3.14
Calcium aluminate[d]	118-186	---	124-141	2.8-3.0

From Ratner et al., 1996 and [b] Park and Lakes, 1992. [c]Jarcho, 1981. [d] Mendoza et al., 1989.

2. Ceramic biomaterials

As mentioned above, ceramics are strong but brittle, non-ductile materials. The mechanical properties of ceramic materials are generally much higher in compression than in tension. Failure often generates at cracks or sites of imperfections and results in catastrophic failure. The strength of ceramic materials often decreases exponentially as porosity increases. When a ceramic biomaterial is implanted, the chemical nature of the material and its structure influence the response. Ceramics having interconnecting pores with a minimum size of 75-100 μm have been found to allow the ingrowth of bone into porous structures (Hulbert et al., 1970).

A disadvantage of ceramic biomaterials is that they are generally only available in preshaped forms and sizes. Powders or beads of ceramic have been used to provide flexible sizes and shapes, but were found to migrate from the original site after implantation (Driessens, 1995).

a). Calcium phosphate

Calcium phosphates are the most widely used ceramics for orthopaedic applications. The $CaO \cdot P_2O_5$ phase diagram in Figure 6 displays the various phases of anhydrous calcium phosphate that form depending upon the molar ratio of reactants and the firing temperature for the ceramic. The calcium phosphates common for biological applications are listed in Table 8 along with their common abbreviation, calcium to phosphate ratio, and solubility product. Hydroxyapatite, HA, and β-tricalcium phosphate, β-TCP, can also be precipitated from aqueous solutions, although this involves

a complex series of events that can be affected by subtle changes in the reaction conditions as well as the presence of trace elements (Jarcho, 1981).

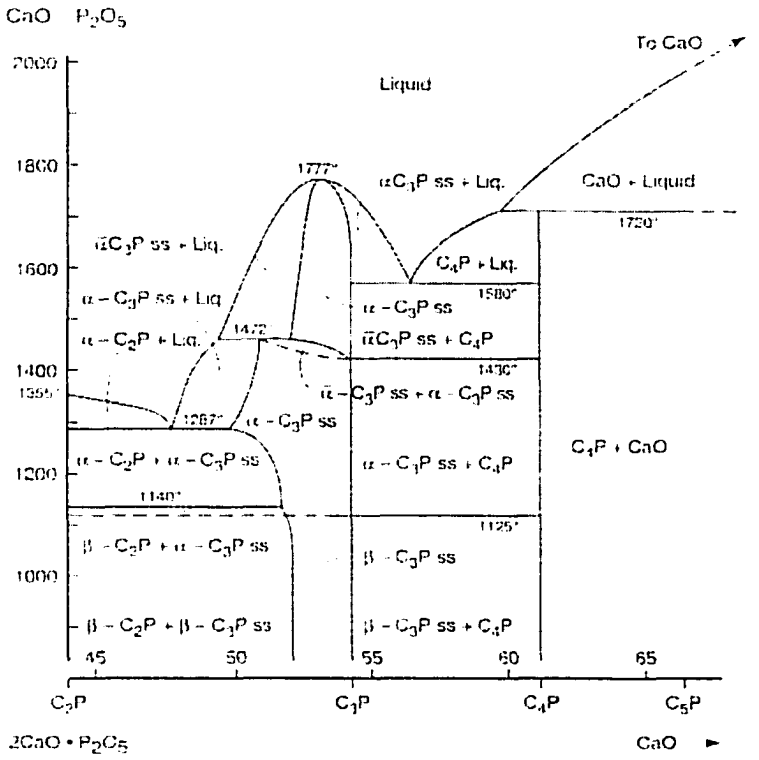

Figure 6. Calcium phosphate phase diagram (Welch and Gut, 1961)

Table 8. Common calcium phosphates and selected properties

Calcium phosphate	*Symbol*	*Formula*	*Ca:P ratio*	*Solubility product (calc.)*[b]
Hydroxyapatite	HA	$Ca_{10}(PO_4)_6(OH)_2$	1.67	6.62×10^{-126}
β-tricalcium phosphate	β-TCP	$Ca_3(PO_4)_2$	1.50	2.07×10^{-33}
α-tricalcium phosphate	α-TCP	$Ca_3(PO_4)_2$	1.50	8.46×10^{-32}
Dicalcium phosphate	DCP	$CaHPO_4$	1.00	2.59×10^{-7}
Octacalcium phosphate	OCP	$Ca_4H(PO_4)_3 2.5\ H_2O$	1.33	5.01×10^{-25}
Biological apatite	--	---	1.61	---

From Lacout, 1992 and [b]Elliot, 1994. (Mejdoubi, 1994 for Lacout)

The use of calcium phosphates in orthopaedic applications has been of great interest due to its favorable tissue response. Calcium phosphates with a calcium to phosphate ratio between 1 to 2 have good *in vivo* response, while compounds with ratios in the range of 1.50 to 1.67 Ca:P have been found to have excellent bioactivity (Bhaskar, 1971, Driessens, 1995, Donath, 1990). After implantation of calcium phosphates there is a lack of local or systemic toxicity, lack of inflammatory or foreign body response, absence of fibrous tissue at the implant-tissue interface, and the apparent ability to become directly bonded to bone tissue (Jarcho, 1981). HA has a limited solubility and normally appears integrated, but not resorbed when implanted, whereas β-tricalcium phosphate is biodegradable and is replaced with bone over time, due to its higher solubility (Driessens, 1995, Figure 7).

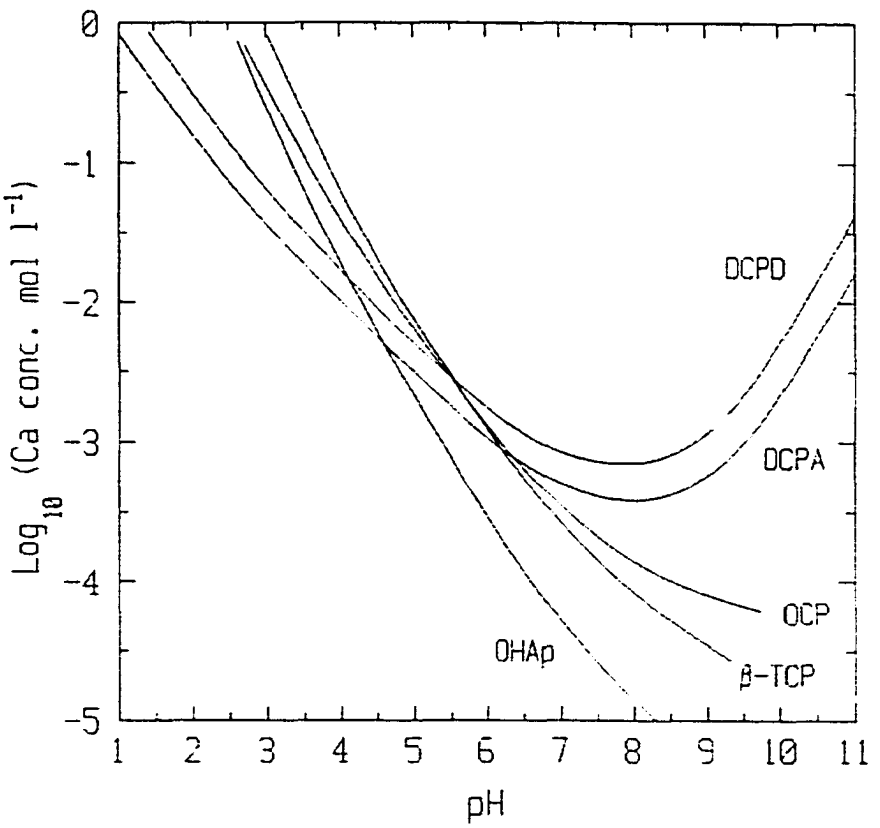

Figure 7. Calculated solubility isotherms for common calcium phosphates (Elliot, 1994)

b). Calcium aluminate

Calcium aluminate ceramic is prepared by combining calcium oxide with aluminum oxide and sintering to the given temperature, as displayed in the phase diagram (Figure 8). When referring to calcium aluminates, C = CaO, A = Al_2O_3, and H = H_2O. Research has been conducted since the 1970's on calcium aluminate ceramics for use as a biomaterial. *In vitro* culture testing as well as *in vivo* studies in rats, rabbits, canines, rhesus monkeys and humans have been performed without serious, adverse response to the material (Autian, et al., 1972, Hentrich et al., 1971, Carvalho et al., 1975, Hulbert et al., 1970, Hulbert et al., 1981). Despite the large amount of research regarding calcium aluminate ceramics that has been done from 1970 through the 1980's, direct comparisons of the results are difficult due to variations in composition, processing, and porosity of the calcium aluminate ceramics that were used.

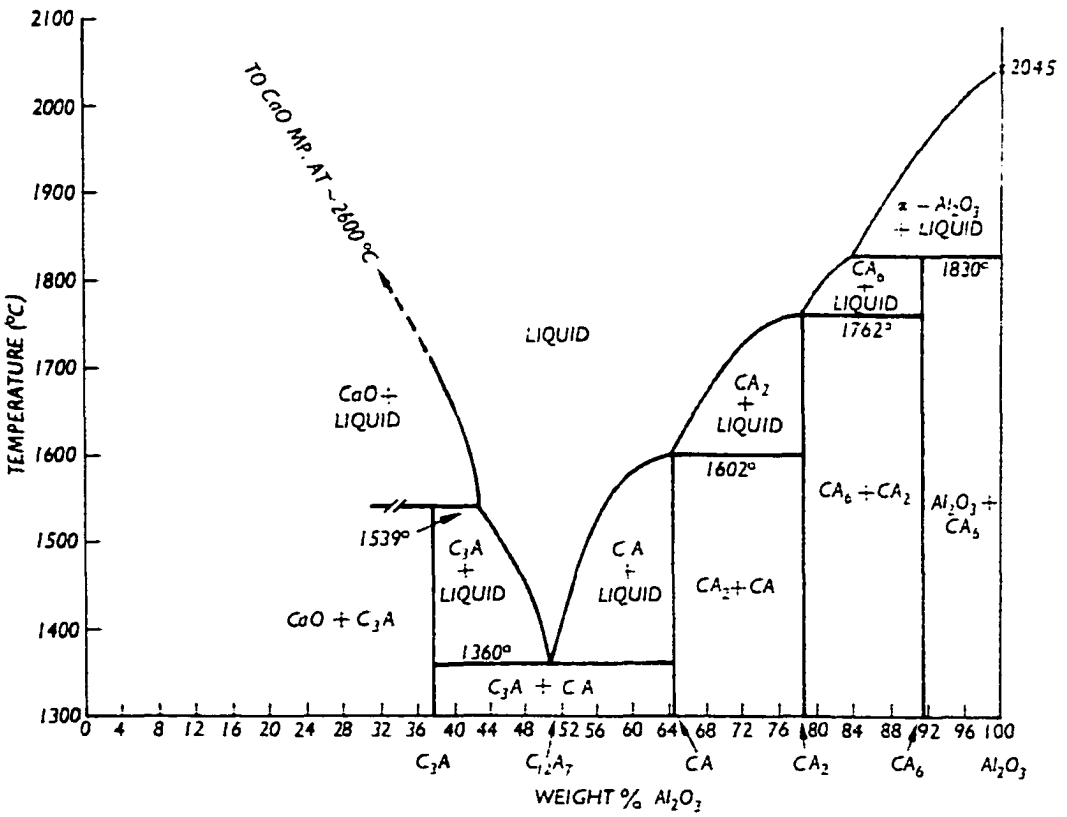

Figure 8. Phase diagram of calcium aluminate (Nurse et al., 1965)

to achieve a high strength within 24 hrs, durability in saline environments and proposed biocompatibility has led to its evaluation for use in bone cement.

The main phases of calcium aluminate cement are CA, CA_2, C_3A, and $C_{12}A_7$. The hydration products: hexagonal, low density CAH_{10}; C_2AH_8; high density, cubic C_3AH_6; and AH_3 are the same for all calcium aluminate cements, only the relative concentrations differ (Lea et al. 1973). CAH_{10} is a metastable hydrate that can convert to C_2AH_8 and later C_3AH_6 depending on the environmental conditions. Conversion from the low density CAH_{10} to C_3AH_6 involves a 53% decrease in volume (Taylor, 1997). The strength of the calcium aluminate cement is primarily determined by the concentration of CA (Lea, 1971).

Factors influencing the properties of the resulting hydrated cement include water to cement (w/c) ratio, temperature during setting, pH, presence of additives, and the storage environment (Sersale, 1957). The setting reactions for calcium aluminate cements are exothermic. Gitzen et al. (1957) reported a temperature rise between 10 and 28°C for 2.5 inch cubes of neat cements cured nonadiabatically at 32°C.

i) Effect of water to cement ratio

Additional water contributes to porosity in the cement, thus decreasing the strength. According to Midgley (1990) the water to cement (w/c) ratio for high aluminate cement must be less than 0.4 for enduring strength. The theoretical w/c ratios for complete hydration are as follows:

Reaction	w/c	volume	ρ of hydrate (g/cm^3)
$CA + 10H_2O \rightarrow CAH_{10}$	1.14	3.64x	1.7
$2\,CA + {}^{11}/_{2}H_2O \rightarrow C_2AH_8 + AH_3$	0.63	2.31x	1.9
$CA + 4H_2O \rightarrow {}^{1}/_{3}\,C_3AH_6 + {}^{2}/_{3}AH_3$	0.46	1.7b	2.45-2.54

In a cement prepared with a high w/c ratio, all of the calcium aluminate hydrates. If a low w/c ratio is used, only a portion of the calcium aluminate hydrates. A subsequent conversion of calcium aluminate hydrates releases water that can be used for further hydration, usually resulting in strong cement with low porosity (Taylor, 1997, Figure 9).

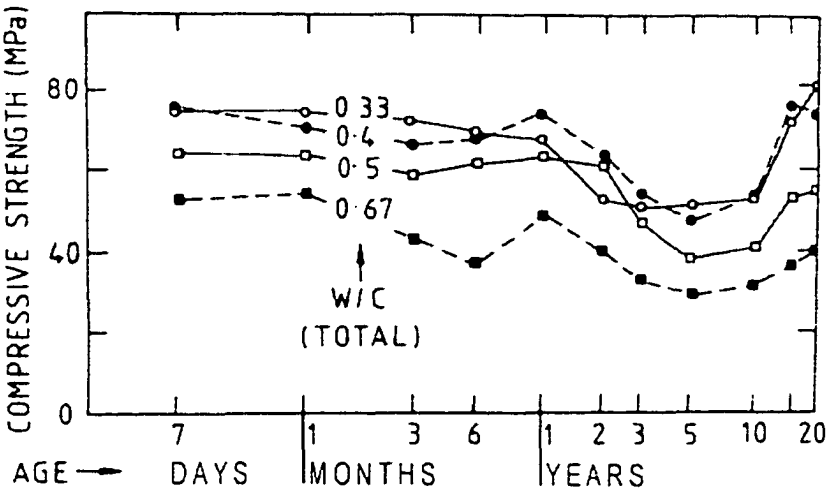

Figure 9. Strength of cements with varying water to cement ratios (Taylor, 1997)

ii) *Effect of temperature during setting and storage*

According to Capmas et al. (1990), as the temperature is increased from 18°C to 30°C, the setting is retarded due to the difficult nucleation of CAH_{10}. As temperatures increase above 30°C, the setting rate accelerates. Lea (1971) reports that temperatures greater than 56°C during setting and hardening over the first 24 hrs cause a considerable loss in strength and a regression at later ages. The strength after conversion is affected by the rate at which it occurs, the crystallization of AH_3, and the initial w/c ratio (Taylor, 1997, Midgley, 1967).

Figure 10 shows the hydration products after hydration at various temperatures. Depending upon temperature, conversion and further hydration can proceed from the initial hydration as follows:

at T< 21°C

$CA + 10H \rightarrow CAH_{10}$

$3CAH_{10} \rightarrow {}^{3}/_{2}\, C_2AH_8 + {}^{3}/_{2}\, AH_3 + {}^{27}/_{2}\, H$

at 27°C < T < 54°C

$2CA + 11H \rightarrow C_2AH_8 + AH_3$

$^{3}/_{2}\, C_2AH_8 \rightarrow C_3AH_6 + \frac{1}{2}\, AH_3 + {}^{9}/_{2}\, H$

at T > 50°C

$3\, CAH_{10} \rightarrow C_3AH_6 + 2AH_3 + 18H$

$3CA + 12H \rightarrow C_3AH_6 + 2AH_3$ (Kosmac et al., 1993).

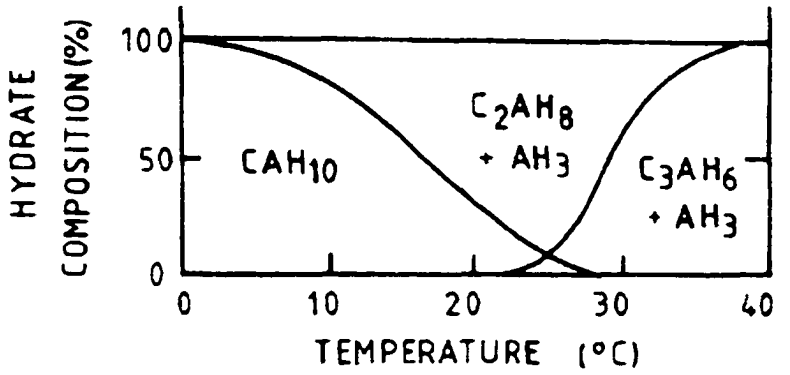

Figure 10. Calcium aluminate hydration products at various temperatures (Taylor, 1997)

CAH_{10} is the hydrate formed at temperatures below 20°C, while C_3AH_6 is formed at temperatures greater than 50°C (George, 1990). In cement that is hydrated at low temperatures and later exposed to higher temperature, the low-density hydrate converts to the high-density form. The higher the temperature, the faster the conversion takes place (George, 1990).

iii) Effect of additives and aggregates

The use of admixtures is common to alter the properties of cement. Of most interest in the present study is the use of accelerators to reduce the working and setting time of the cement. The effect an additive has on a cement is often complicated and can depend on concentration, ambient temperature, and the use of other additives.

Parker (1952) and Robson (1967) found that a decrease in setting time is observed with the addition of basic additives that increase the pH. Conversely, acids were found to promote a delay in the hydration process in high alumina cement (Lea, 1971). Curell et al. (1987) state that the setting times of calcium aluminate cement with additives follow:

$Li^+ < Na^+ <$ pure water $< K^+$, $Ca^{2+} < Mg^{2+}$, $Sr^{2+} < NH^{+4}$ and

$OH^- <$ pure water $< Cl^-$, $NO_3^- < Br^- <$ Acetate.

Nilfoushan and Sharp (1995) studied the effect of alkaline-earth metal chlorides ($MgCl_2$, $CaCl_2$, $SrCl_2$, and $BaCl_2$) from 0.025-0.5M on the setting behavior of calcium aluminate cements. At 12°C, all chlorides retarded set time and increased their effect with increasing concentration. At 20°C, low concentrations brought about acceleration, while high concentrations retarded setting. At

28°C and 36°C, retardation of setting was observed and increased in effect with increasing concentration of the additive.

$CaCl_2$ has long been used as an accelerator and allows near normal strength without significantly influencing the workability, air content, or water to cement ratio of the cement into which it is incorporated (Rixom and Mailvaganam, 1986). The addition of 2% $CaCl_2$ cement was not found to adversely affect the long-term strength of concrete (Glenkinsop, 1963). Addition of finely ground calcite to cement was found to prevent loss of strength through the formation of the hydrate $C_4ACO_2H_{11}$, which limited or prevented conversion (Cussino and Negro, 1980). Also, concrete made with equal parts cement and blast furnace slag were found to increase in compressive strength over one year, while neat cement samples showed the normal decrease in compressive strength typically associated with conversion (Majumdar et al., 1990).

iv) Other factors

Concretes made with calcium aluminate cement are highly resistant to sulfate solutions, seawater, and dilute acids with pH greater than 4. The resistance increases with decreasing w/c ratios and increasing cement concentration (Crammond, 1990).

Kurdowski et al. (1990) studied the behavior of high alumina cement in chloride solutions. Shrinkage of 11mm/m was observed in one month, after which the cement was stable. The formation of a thin, dense layer of AH_3 and CAH_{10} was observed on the external layer of the cement sample while the internal region had cubic C_3AH_6 and high strength.

d). Calcium aluminate chloride hydrates

Previous work in the field of calcium aluminate chloride hydrates has focused on concretes and mortars of various compositions, often containing SiO_2 or FeO_2 and C_3A as the calcium aluminate phase. It is not known if results from these studies correlate with the calcium aluminate based cement used in the present study. They are the only such compounds found in available literature. The findings are presented here in hopes of better understanding the current system under investigation.

When $CaCl_2$ is added to calcium aluminate cement, it reacts with the calcium aluminate phases to form chloroaluminates that generally conform to the formula: $C_3A{\cdot}CaX_2{\cdot}nH_2O$ or $C_3A{\cdot}CaCl_2{\cdot}nH_2O$ (Poellman, 1986). $C_3A{\cdot}CaCl_2{\cdot}H_{10}$ has been found to crystallize in thin hexagonal plates. This monoclinic α-$C_3A{\cdot}CaCl_2{\cdot}H_{10}$ is stable at 25°C, but transforms to rhombohedral β-$C_3A{\cdot}CaCl_2{\cdot}H_{10}$ at 35°C through a reversible reaction (Kuzel, 1968). In practice, a solid solution of these two phases is often found (Poellman and Kuzel, 1988).

The addition of $CaCl_2$ to calcium aluminate cements retards or prevents the formation of the cubic C_3AH_6 phase (Traetteberg and Bellow, 1975). Darr and Ludwig studied the incorporation of chloride into calcium aluminum hydrates (1974). Additions of 0.33 or 0.66 mole $CaCl_2$ per mole of hydrate (C_4AH_{13}) were incorporated within four and seven days, respectively. The maximum amount of chloride incorporation was 0.92 mole $CaCl_2$ at 5°C and 0.82 mole at reaction temperatures between 20° and 40°C with a considerably longer time required to reach equilibrium.

Hannawayya reported that the addition of $CaCl_2$ to cement reduced the alkalinity of the aqueous phase in the hydrating cement (1990). The system compensates for the lower pH, by liberating more lime through an increased rate of hydrolysis of the cement. Hannawayya also found that reinforced concrete with $CaCl_2$ added did not suffer any serious or rapid damage from steel corrosion (1990).

3. Bone cements

Bone cement is used for cavity filling, bone replacement, fixation of prostheses, and transfer of the load from the stiff prosthesis to the relatively less rigid bone. Cements discussed in this section include PMMA, calcium phosphate cements, and OC-cement. The only ASTM standard for bone cement is that for acrylic cement. This specifies a maximum working time of 5.0 minutes, a setting time of 5-15 minutes, a maximum temperature less than 90°C during setting, and a minimum compressive strength after 7 days of 70 MPa while not losing more than 10% of the initial compressive strength as measured after 24 hrs (ASTM 451, 1986).

a). Poly(methyl-methacrylate)

PMMA is currently the most commonly used cement for orthopedic applications. This cement is primarily composed of PMMA powder and methyl methacrylate monomer liquid, with additions of hydroquinone to prevent premature polymerization, *N*, *N*-dimethyl-*p*-toluidine to accelerate the curing, barium sulphate or zirconium dioxide to add radiopacity, and dibenzoyl peroxide as an initiator. The use of PMMA led to the widespread practice of the total hip replacement (Charnley, 1972) and after three decades of use, it remains the gold standard in joint replacement surgery.

The main advantage of PMMA is its rapid strength development that allows for fast recovery following joint replacement. Although the mechanical properties of PMMA may vary with temperature, environment, mixing procedure, porosity, strain rate, and the brand of cement, a typical range of values is as follows: elastic modulus 2.2-3.7 GPa, compressive strength 78-120 MPa, and tensile strength 13.2- 48.2 MPa (Planell, 1995). *In vivo* experiments have found that the mechanical properties increase during an initial time period, generally days to months, followed by a slow decrease over the succeeding years. The fatigue behavior of PMMA bone cement *in vivo* depends mostly on the behavior of crack propagation (Planell, 1995).

The bonding at the cement-prosthesis interface depends on the surface roughness of the prosthesis; mechanical interlocking predominates for rough surfaces while atomic interactions predominate for smooth surfaces. The strength of the interfacial bonding also depends on the type of metal used to form the prosthesis. It has been found that 316L stainless steel has the highest interfacial strength, followed by Co-Cr-Mo, and lastly Ti-6Al-4V (Planell, 1995). The bonding at the cement-bone interface relies upon mechanical interlocking from the protrusion of the cement into the trabeculae of the bone.

The biological response to PMMA is generally the formation of fibrous membrane between the cement and bone. In animal models, this membrane has been found to contain macrophages, giant cells, and granuloma formation (Planell, 1995).

The main disadvantage of PMMA bone cement for use in joint replacement surgery is that approximately 10% of the patients may require a revision within 10 years (Planell, 1995). Aseptic loosening often occurs which has been attributed to: lack of chemical bonding, mechanical failure of the cement, fibrous tissue formation resulting from heat induced necrosis, and osteolysis induced by wear debris particles (Planell, 1995). Another concern in the use of PMMA is the suspected toxicity of the monomer.

b). Calcium phosphate cements

As mentioned previously, calcium phosphate ceramics have been found to have good tissue response and no mutagenic effects (Driessens, 1995). In addition, tissue may attach directly to the implant without the formation of a fibrous capsule. A calcium phosphate cement would allow the benefits of the ceramic material, but could also be shaped to the desired form at the time of implantation or *in vivo*. Current research efforts to develop calcium phosphate cements (CP-cements) are based on an aqueous reaction of calcium and phosphate containing compounds resulting in the precipitation of hydroxyapatite, dicalcium phosphate, dihydrate, or octacalcium phosphate. The temperature rise during setting is generally negligible; less than 1°C. The pH during setting ranges from 6.5 to 10 depending on the specific formulation (Driessens et al., 1995). The handling of CP-cements does not appear to cause allergy for either patient or the practitioner.

The properties of the CP-cements depend upon formulation, mixing environment, particle size, porosity, and additives, among other factors. The working time of these cements has ranged from 4-25 minutes and the setting time from 10-100 minutes, with full strength generally achieved within 1 to 14 hrs. Driessens et al. (1995), report that for CP-cements compressive strength can vary from approximated 4-120 MPa, with typical values between 20-40 MPa. Tensile strength ranged from 0.5 to 8 MPa. It should be noted that the storage conditions and length of aging time before testing often were not indicated.

Disadvantages of calcium phosphate cements include the brittleness of the resulting porous cement, difficulties of setting *in vivo*, wash out of implanted cement paste, and the relatively low

strength. Much research is currently underway to study these issues and to improve the mechanical characteristics of CP-cements.

c). OC-cement

An OC-cement has been developed at ISU in response to the need for an improved cement for prosthesis fixation and other orthopedic applications. This cement is a combination of a calcium aluminate binder and calcium phosphate that sets when mixed with water. The setting properties of the cement can be controlled with additives. Additives and other methods are also being investigated to optimize the flow characteristics of this cement. The OC-cement is expected to have sufficient mechanical properties for load bearing applications as well as a friendly tissue response.

Initial study of the mechanical properties of OC-cement showed that compressive strength after aging 1 wk under simulated physiological conditions ranged from 91-138 MPa (Roemhildt, 1998). The study of the mechanical properties of OC-cement and the effects of aging continue with ongoing efforts to improve the overall properties of OC-cement. A major difference between OC-cement compared to traditional PMMA cement is that OC-cement is a dilatent mixture in that the shear is dependent upon the rate of strain. This cement flows best when vibration is applied as opposed to solely pressure.

D. Assessment of Compatibility of Biomaterial Implants

1. Tissue reaction to biomaterials and evaluation

The body's response to the implantation of a biomaterial involves a complex series of events. A local response occurs due to damage of surrounding tissue from the implantation procedure and the presence of the biomaterial in the tissue. The sequence of the local responses to the implantation of a biomaterial is injury, acute inflammation, chronic inflammation, formation of granulation tissue, foreign body response, and fibrosis (Figure 11). The tissue reaction varies in response to the physical and chemical nature of the biomaterial, including the size, shape, angularity, surface roughness, and porosity of the material (Anderson, 1996). In addition to any tissue response to the

biomaterial, micromotion, loosening, degradation products, and wear debris also affect the overall tissue reaction (Ratner, 1996).

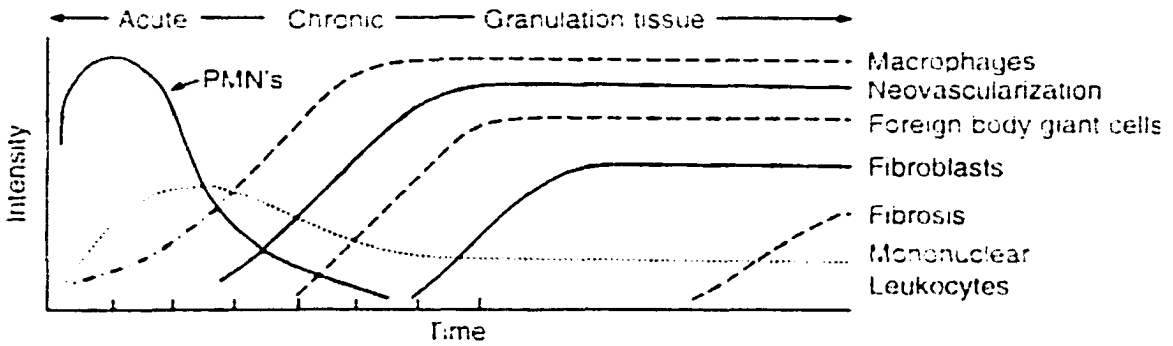

Figure 11. Timetable of body's response to biomaterial (Anderson, 1996)

Inflammation is a nonspecific response to tissue damage that is characterized by redness, swelling, pain, and heat (Black, 1999). Acute inflammation generally lasts a matter of minutes to days, during which time monocytes and neutrophils try to phagocytize the foreign material. In cells, lysosomes are present to digest dead or foreign material (Anderson, 1996). However, if the implant is large, it will not be possible to engulf the foreign matter, which leads to chronic inflammation. Monocytes, macrophages, lymphocytes, blood vessels and connective tissue are prevalent during chronic inflammation. The formation of granulation tissue is a normal part of the healing process that occurs 3-5 days after tissue damage. During this stage monocytes differentiate into macrophages, fibroblasts and vascular endothelial cells proliferate at the implant site, and granulation tissue begins to form (Black, 1999). Foreign body reaction occurs as monocytes and macrophages fuse together to form foreign body giant cells (FBGC) and a continuation of granulation tissue formation. The end-stage in the healing process is often fibrosis or fibrous tissue encapsulation to isolate the implant from the local environment. Cells surrounding the implant regenerate, fibroblasts form, and scar tissue results (Anderson, 1996).

Deep infection is a serious complication that can result from implantation of a biomaterial. Infections occur in approximately 1% of joint replacement surgeries and often require a subsequent surgery and/or implant removal for effective treatment (Black 1999). Due to the difficulty of treating

deep infections, efforts have been made to decrease the incidence of infection by incorporating antibiotic into PMMA bone cement.

The biocompatibility of a biomaterial may be tested using a variety of *in vitro* and *in vivo* techniques. In the field of orthopaedic biomaterials, microradiography, light microscopy, fluorescent microscopy, and/or scanning electron microscopy (SEM) are often utilized to analyze local tissue response of the explanted tissue in contact with a biomaterial. Radiography is used to show the gross structure of the bone and the biomaterial. This technique is often useful to confirm proper placement of the implant. Light microscopy in conjunction with thinly sliced, stained sections can be used to identify the types of cells present. Fluorescence microscopy can be used to analyze specimens from test subjects that have received bone-labeling agents to observe regions and time frame of bone mineralization. Tetracycline antibiotics form stable tetracycline-calcium chelates that fluoresce at specific wavelengths. *In vivo*, tetracyclines bind to Ca^{2+} and can be used as bone labels. Chelates form only at sites of new bone deposition where bone contains 20% or less of the maximum mineral content (Gruber and Stasky, 1999). These chelates remain immobile until resorption occurs. Lastly, scanning electron microscopy, SEM, can be used analyze the 3-d surfaces of specimens at a much higher magnification than the other techniques mentioned here.

2. Mechanical testing of bone-biomaterial interface

Push-out and pull-out tests are commonly used to measure the shear strength of the *ex vivo* bone-implant interface of orthopaedic and dental implants (Berzins and Sumner, 2000). A load is applied to the implant via a fixture connected to the crosshead of a materials testing machine. The test is run until the interface fails, which is represented on a force versus displacement curve as a sudden displacement of the implant. The ultimate shear strength is calculated by dividing the maximum force by the interfacial area. A combination of factors such as friction, mechanical interlock, and chemical bonding determine this shear strength. For smooth materials the shear strength is mainly due to chemical bonding, while the shear strength for rougher materials is primarily due to mechanical interlocking between the implant and bone (McKoy et al., 2000). A number of

aspects have been found to affect the strength at the bone-biomaterial interface including implant characteristics, local factors, medications, surgical factors, and patient factors as detailed in Table 9.

Table 9. Factors affecting the strength at bone-biomaterial interfaces

Implant and local factors	surface configurations, surface coatings, implant geometry, material properties, quality of cementing procedure, particle debris, design and stress shielding
Medications	affect bone growth and resorption
In vitro factors	storage before testing, specimen preparation
Surgical and hospital factors	skill of surgeon, post operative care
Patient factors	age, lifestyle, inflammation, infection

From McKoy et al, 2000.

a). Pull-out test

Pull-out tests are frequently used to evaluate the stability of orthopaedic implants such as posts, screws, or nails. These can be placed directly in bone to compare implant materials or surface treatments, or cemented in place to study the stability of the cement and implant. There is a wide variety of test conditions for pull-out test protocols, which could bias the test results. As with push-out tests, care must be taken to avoid comparing results of pull-out tests with differences in boundary conditions or material or design arrangements (Berzins and Sumner, 2000). For intramedullary pull-out tests it is recommended that the post occupy at least 80% of the cross-sectional area of the medullary canal (Canale, 1998).

Mueller and Schurmann found the shear strength of the PMMA–metal interface *in vitro* varies greatly with the metal surface texture as well as the storage condition during aging. Smooth and rough specimens aged 60 days under physiological conditions failed at the cement-metal interface with a shear strength of 0 MPa (1999).

b). Push-out test

Push-out specimens are typically implanted transcortically in a long bone such as the femur or longitudinally in the medullary canal. After the allotted time the specimen is retrieved and prepared for testing. Interfacial shear strength can be determined from: $S = F / (\pi * d * t)$; where S is the interface shear strength (MPa), F is the push-out force (N), d is the plug diameter (mm), and t is the average bone thickness in contact with the implant (Dhert et al., 1992).

Critical aspects of push-out tests include precise alignment of the implant and the testing fixture and clearance between the specimen support and the implant to be displaced. Dhert et al. found that a clearance no less than 0.7 mm is required to minimize non-uniform stress distribution (1992). Because the strength calculation assumes uniform stress distribution at the interface, one must avoid comparisons between implants with different interfacial stress distributions (Berzins and Sumner, 2000).

III. MATERIALS AND METHODS

A. Materials

Characterization of the calcium aluminate cement, β-tricalcium phosphate, hydration solution, and stainless steel posts is given below.

1. Calcium aluminate cement

Commercial calcium aluminate (La Farge Calcium Aluminates, Inc., Chesapeake, VA) was used. The molar ratio of calcium to alumina was approximately 0.82 to 1.00. This cement contained only calcium aluminate phases CA, CA_2, and $C_{12}A_7$ and alumina without any detectable additives (Table 10, Figure 12).

Table 10. Manufacturer's specification for the chemical composition of CA

Al_2O_3	≥ 68.5	bulk density: 1.04-1.23 g/cm^3
CaO	≤ 31.0	specific density 3.0 g/cm^3
SiO_2	< 0.8	fineness: 3600-4100 cm^2/g
Fe_2O_3	< 0.3	residue at 90 microns < 5%
MgO	< 0.5	
TiO_2	<0.25	
SO_3	< 0.3	
$K_2O + Na_2O$ soluble	< 0.5	

From La Farge product data

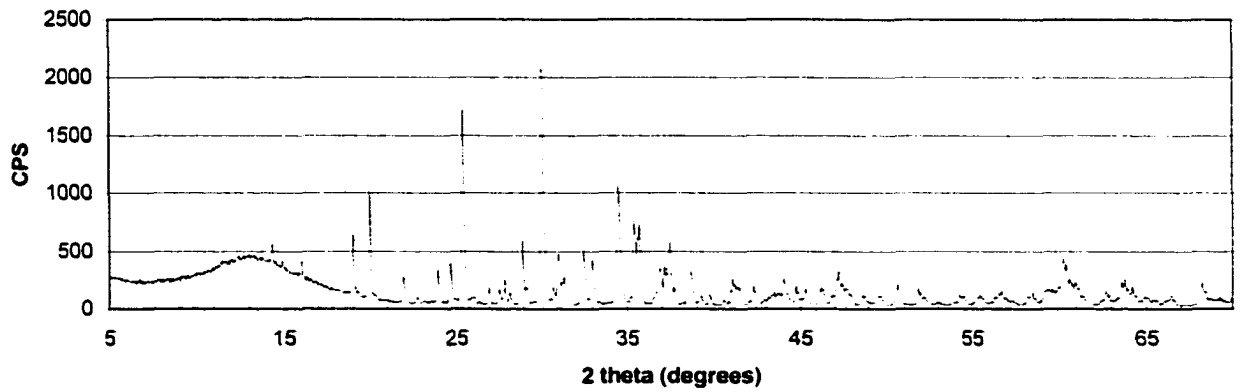

Figure 12. XRD of calcium aluminate cement

The median particle size was 5.91 μm, standard deviation of 7.16 μm and the particle size distribution shown in Figure 13, as determined with a Horiba CAPA-700 Particle Size Distribution Analyzer (Horiba Ltd., Kyoto, Japan) based on liquid-phase sedimentation.

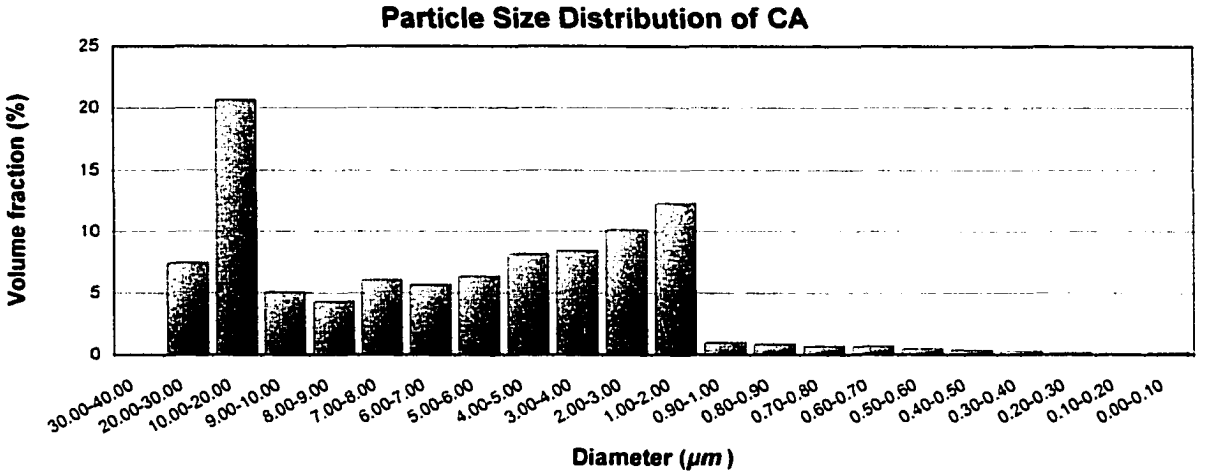

Figure 13. Particle size distribution of calcium aluminate cement

2. ß-tricalcium phosphate

β-tricalcium phosphate (Fluka Chemicals, Neu-Ulm, Switzerland) was used. The chemical composition is shown in Table 11 and x-ray diffraction in Figure 14. The median particle size of the β-tricalcium phosphate was found to be 3.62 μm with a standard deviation of 2.10 μm and the particle size distribution is shown in Figure 15. Particle size measurements were conducted using a Horiba Particle Size Analyzer as above.

Table 11. Manufacturer's specification for the chemical composition of β-TCP

Cu ≤0.005%	K ≤ 0.01%
Cl ≤ 0.05%	Na ≤ 0.01%
SO4 ≤ 0.1%	Ni ≤ 0.005%
Cd ≤ 0.005%	Pb ≤ 0.005%
Co ≤ 0.005%	Zn ≤ 0.005%
Fe ≤ 0.02%	

From Fluka product data

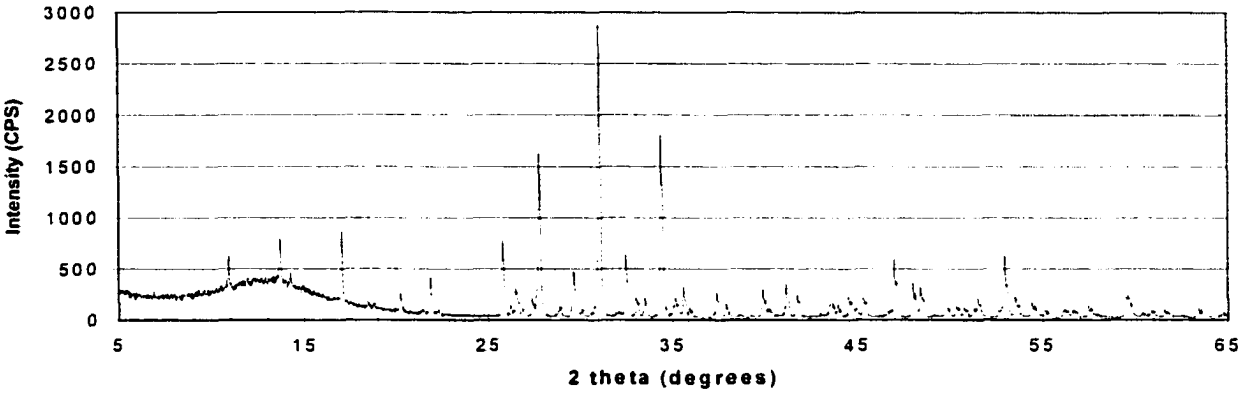

Figure 14. XRD of β-tricalcium phosphate

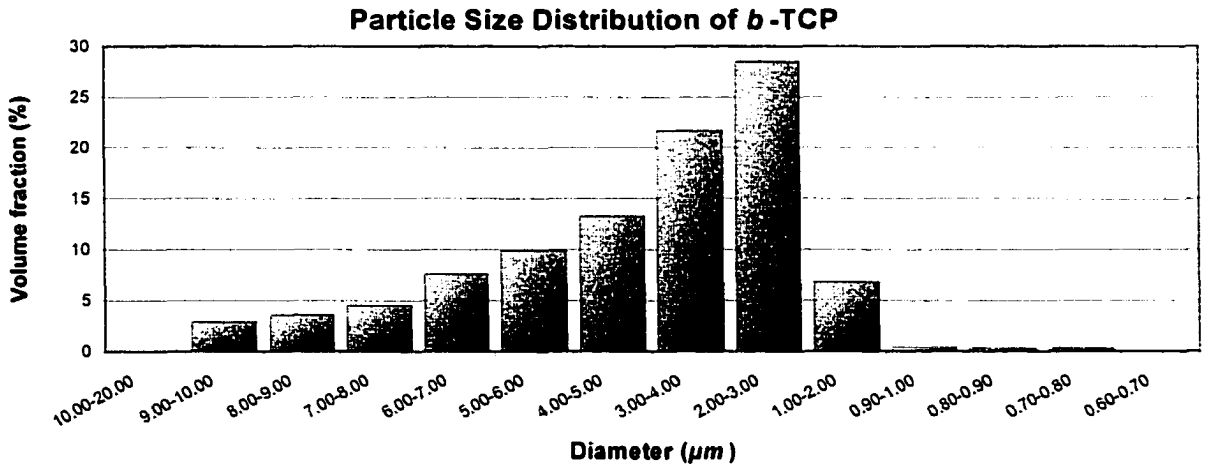

Figure 15. β-Tricalcium phosphate particle size distribution

3. Hydration solution

The hydration solution for the cement was 2.00 M calcium chloride prepared from calcium chloride (Fisher Scientific, Fairlawn, NJ) and de-ionized water that had been boiled for at least 10 minutes to remove carbon dioxide. The solution was acidic with a pH of 4.1 ± 0.5 and had a density of 1.2 g/cm^3.

4. Stainless steel posts

Metal posts, 6 mm diameter x 100 mm length, were machined from medical grade 316L stainless steel for use in the pull-out experiment. Care was taken not to scratch or mar the surface. Prior to testing, posts were washed in a mixture of mild detergent and water, placed in an ultrasonic cleaner for 5 minutes, rinsed with de-ionized water and dried. The surface roughness of the posts was measured using a Dektak IIA profilometer (Veeco, S. A., Plainview, NY). A typical scan is displayed in Figure 16. The average surface roughness was determined by a sample of 15 posts with three measurements collected per post. The mean surface roughness was found to be 2322 ± 388 Å. Before using the posts for pull-out testing, the bottom tip was coated in paraffin wax to act as a release agent. The second shipment of 316 L stainless steel that was received had a rougher surface finish. These posts were polished with 0.3 μm alumina to obtain a surface roughness comparable to the initial 316L stainless steel posts.

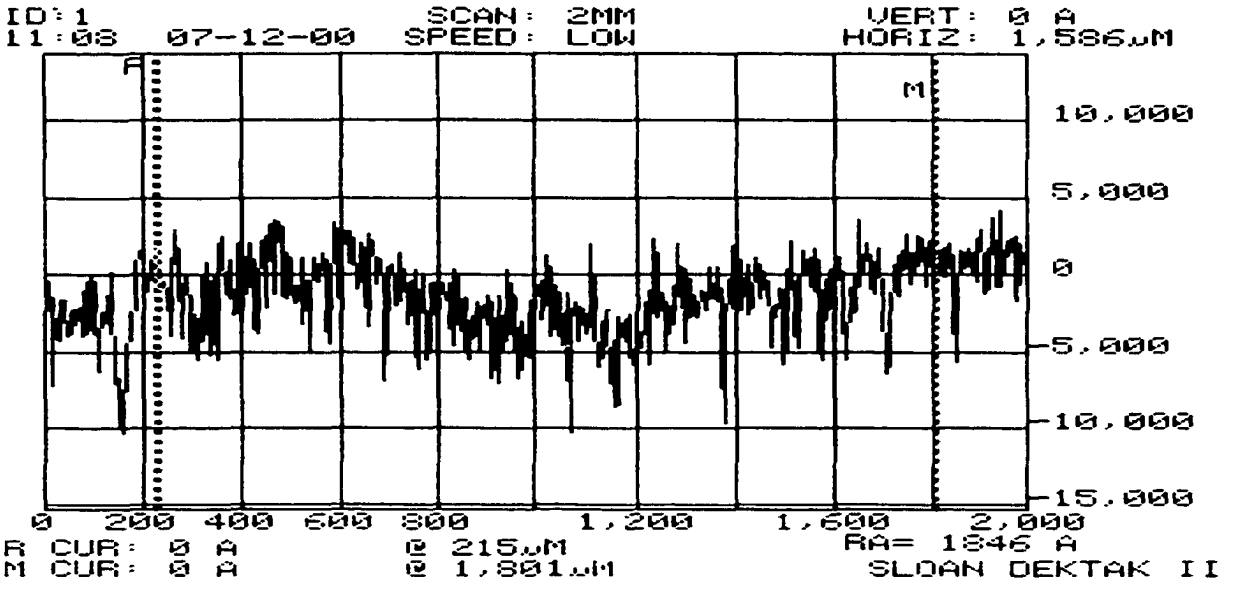

Figure 16. Typical surface roughness graph

B. Methods

1. Preparation and characterization of OC-cement

OC-cement was prepared according to the formula: 10.00 g calcium aluminate cement, 5.00 g β-tricalcium phosphate and 4.70 g of 2.00 M $CaCl_2$ solution. The dry powders were mixed together with in a mortar and pestle until uniform. The dry components were then added to the pre-measured amount of hydration solution, the components were mixed for 1 minute, and vibration was applied with a hand massager for 45 seconds at high speed to aid in mixing and removal of entrapped air.

2. Measurement of flow

The consistency of the cement was that of a thick paste. To measure the flow of the OC-cement, procedures by Katsumura et al. (1998) and the American Dental Association Specification No. 8 for zinc dental cement (1977) were followed with appropriate modifications. The cement was placed in a syringe with an inner diameter of 0.8 cm and a disc was prepared using 0.5 ml of cement. The cement disc was placed on a smooth glass plate. An additional glass plate and weight (120 g total) were placed on top of the cement disc for 20 minutes. For the vibrated condition, immediately after disc formation, vibration with a hand massager was applied to the lower glass plate for the designated time. In general, the cement flowed outward between the plates in a radial manner. The diameter of the cement disc was measured initially, immediately after vibration, and subsequently at five-minute increments. The average disc diameter for each trial was calculated from three measurements taken at 60° increments. The mean diameter for each condition was determined from 10 trials.

3. Measurement of working and setting time

Working and setting times were estimated by a procedure similar to that used for calcium phosphate cements and dental cements (Mirtichi et al., 1990, Driessens et al., 1995). Working time was determined to be the point of zero flow, which indicates the end of moldability without damage to the developing cement structure. The working time was considered to have ended when a small, stainless steel spatula inserted into the paste could be withdrawn without pulling out any cement.

The setting time was defined as the point beyond which it is possible to handle the cement without causing damage to the cement (Driessens et al., 1995). It was determined as the time at which a small, stainless steel spatula pressed against the surface of the cement with moderate force did not damage the cement nor leave a noticeable mark on the surface.

4. Strength testing

Specimens, 12 mm diameter x 16 mm height, were prepared for compressive strength testing. Following preparation the cement paste was next placed in a Plexiglas mold and allowed to set in a water bath maintained at 37°C. 20 minutes after setting, the specimens were removed from the molds and placed in small containers containing lactated Ringer's solution (Abbott Laboratories, North Chicago, IL). Samples were stored at 37°C until tested. The force required for failure was measured using an Instron 4202 universal testing machine (Instron Corp., Canton, MA), equipped with a 50 kN load cell and the cross-head speed was set at 1 mm/min. The compressive strength (CS) was calculated as follows: $CS = Force_{max} / Area$. The mean compressive strength from at least 6 specimens is reported for each condition.

The tensile strength of the cement was measured using a diametral tensile test with the same Instron settings as used for compressive strength testing. Specimens approximately 12 mm diameter x 4.8 mm in height were prepared and stored as described above for compressive testing. The mean diametral strength determined from at least 10 specimens is reported for each condition. Diametral tensile strength (DTS) was calculated as: $DTS = Force_{max} / (\pi * t * {}^{d}/_{2})$, where t is the thickness and d is the diameter of the cement disc.

5. Physical changes

Changes in the mass and diameter of OC-cement specimens prepared and stored in the same manner as for compressive strength testing were recorded from 1 hour after setting up to 14 months. Each specimen was labeled and the diameter was measured with calipers using care to take readings from the same location on the specimen each time. Specimens were blotted dry with paper towels before measuring the mass.

applied to the post to facilitate its placement. Following the setting of the cement, test specimens were stored at 37°C for the desired time period. The cement was kept moist by irrigation with lactated Ringer's solution after setting until testing.

Pull-out tests were conducted at 4 hrs, 24 hrs, and 60 days after preparation. At least 7 specimens were tested for each cement type at each of the three time periods. Specimens were randomly assigned a testing period of 4 or 24 hrs. Due to complications in aging femurs under test conditions longer than 24 hrs, rigid, textured, plastic tubing was used to simulate femurs for the specimens tested at 60 days.

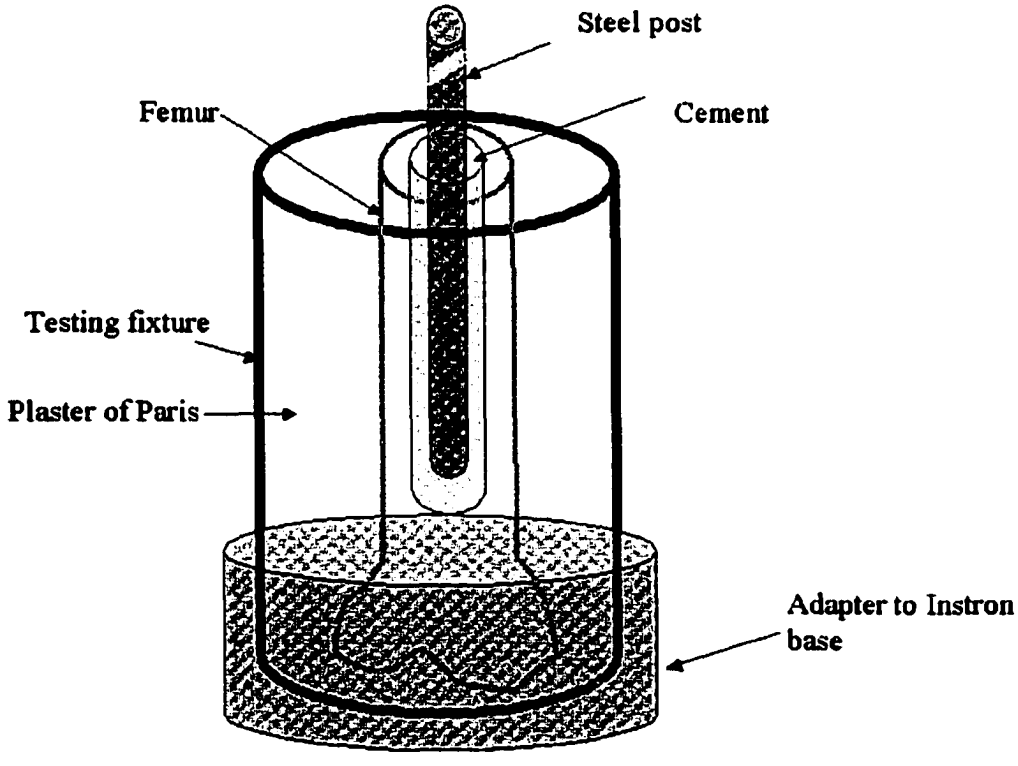

Figure 17. Drawing of pull-out test fixture and specimen

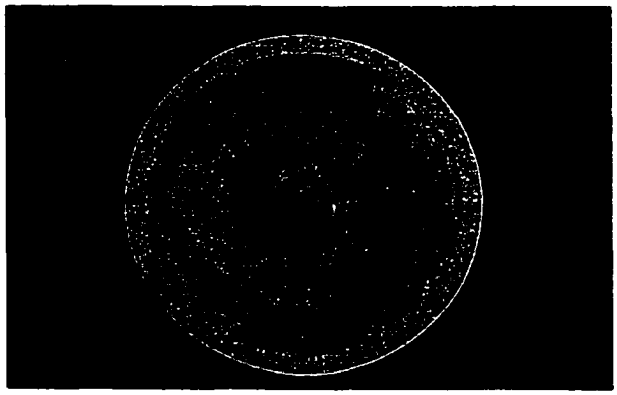

Figure 18. Centered, cemented post for pull-out testing

After the designated time, the potted specimens were fixed to the testing jig and attached to the Instron machine (Figure 19). The rate of displacement for the crosshead was 1 mm/minute. The maximum tensile force to displace the prosthesis and method of failure were recorded for each specimen. Interfacial shear strength was determined by calculating the force/area for failure.

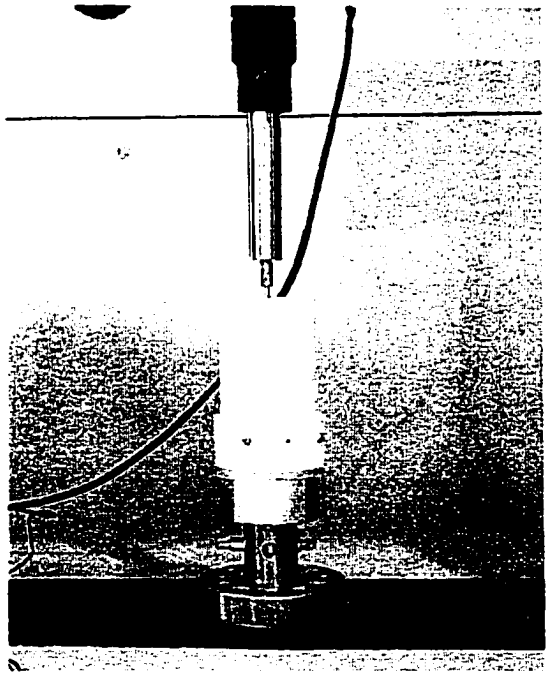

Figure 19. Instron set-up for pull-out testing

9. *In vivo* testing

In vivo testing was used to assess the tissue response to the experimental cement and to measure the shear strength between the implanted cement and cortical bone. *In vivo* testing was performed following guidelines from ASTM procedures F 763-87, *Standard practice for short-term screening of implant materials*, and F 981-93, *Assessment of compatibility of biomaterials for surgical implants with respect to effect of materials on muscle and bone* as applicable to this experimental material and projected applications. ASTM 763-87 provides a procedure for evaluating the short-term tissue response to biomaterials that have been implanted into muscle tissue (1987), whereas ASTM 981-93 assesses the long-term response to biomaterials in bone or muscle. Both procedures assume a solid biomaterial that is formed to desired shape before surgical implantation. Next, these small specimens are implanted into muscle or transcortically into a long bone. However, to best evaluate the OC-cement under conditions similar to its proposed use, tissue response was evaluated after the cement paste was placed in the medullary canal of the femur.

Adult, mixed breed canines were used for *in vivo* testing. Historically, canines have had a dominant role in orthopaedic research and are thought to be the closest *in vivo* condition to human, aside from primates (An and Friedman, 1999). Also influencing the selection of canines, as the animal model in this study was their availability and the relative ease of the surgical procedure in dogs as compared to smaller, commonly used experimental animals.

The experimental design is given in Table 12. Twelve animals were used for the experimental conditions and 9 for control. The implant and surrounding tissue were evaluated 2, 6, and 12 wks following implantation. Seven animals were sacrificed at each time period: 4 experimental and 3 control. Femurs that had been implanted with cement were retrieved and radiographed. From each femur, at least 4 specimens for tissue analysis and 5 specimens for push-out testing were prepared.

Table 12. Experimental design for *in vivo* tests

n	*Implantation time (wks)*	*Cement type*	*PSR*	*Time of FI label (wks)*			*Histology specimens*	*Push-out test specimens*
1	2	OC	✓	-	-	-	✓	✓
2	2	OC	✓	-	-	-	✓	✓
3	2	OC	✓	-	-	-	✓	✓
4	2	OC	✓	-	-	-	✓	✓
5	2	PMMA	✓	-	-	-	✓	✓
6	2	PMMA	✓	-	-	-	✓	✓
7	2	PMMA	✓	-	-	-	✓	✓
8	6	OC	✓	2	5	-	✓	✓
9	6	OC	✓	2	5	-	✓	✓
10	6	OC	✓	2	5	-	✓	✓
11	6	OC	✓	2	5	-	✓	✓
12	6	PMMA	✓	2	5	-	✓	✓
13	6	PMMA	✓	2	5	-	✓	✓
14	6	PMMA	✓	2	5	-	✓	✓
15	12	OC	✓	2	7	11	✓	✓
16	12	OC	✓	2	7	11	✓	✓
17	12	OC	✓	2	7	11	✓	✓
18	12	OC	✓	2	7	11	✓	✓
19	12	PMMA	✓	2	7	11	✓	✓
20	12	PMMA	✓	2	7	11	✓	✓
21	12	PMMA	✓	2	7	11	✓	✓

PSR: post surgery radiograph, FI = fluorescent labeling

Prior to surgery, the dry, OC-cement powder was gas sterilized with ethylene oxide. Calcium chloride powder was autoclaved, then diluted with sterile, de-ionized water to the proper concentration. OC-cement prepared under aseptic conditions was cultured and no aerobic or anaerobic growth was found after 48 hrs or 4 days incubation, confirming that the sterilization procedures used were sufficient.

a). Pre-surgery Conditioning

Approval was obtained for the experimental protocol by the Animal Care and Use Committee at Iowa State University. Upon procurement of the dogs used in this study, their health was evaluated by Laboratory Animal Resource Veterinary Faculty. Following vaccination (Vanguard®, Pfizer Animal Health, Exton, PA), animals were quarantined for two weeks before beginning experimental procedures. Throughout the test period animals were cared for according to Laboratory Animal Resources protocol. Animals were free to roam about the caged area and given food and water ad libetum.

b). Premedication and anesthesia

Animals were pretreated with Acepropzine (0.04 mg/kg) and Butorphanol (0.4 mg/kg). Thiopental (10 mg/kg) was given before intubation. Once intubated, animals were placed on Isoflourane (1.5-2.0%) in oxygen until completion of the surgical procedure. Heart rate and respiratory rate were monitored throughout the procedure.

Implant surgeries were performed by a skilled, veterinary orthopedic surgeon. The implantation procedure was similar to that by Takahasi and Koshino (1995). The right, rear leg was clipped from the hock to the midline of the animal's back. Following a 5 minute sterile surgical preparation, an approach was made to the greater trochanter. The medullary canal of the femur was entered with an intramedullary pin. Intramedullary pins of increasing size and a bone file were used to increase the size of the opening. A 6.0-8.0 mm opening was created in the greater trochanter to the marrow cavity of the diaphysis. Suction was used to clean the medullary canal.

The selected cement was prepared as described previously and the medullary canal was filled. PMMA cement was placed in a 20 ml disposable syringe and inserted under pressure. OC-cement was placed inside a Teflon tube, pressure was applied to the top end of the tube, and the OC-cement was pushed out and slid into place in the intramedullary canal. Fluoroscopy was used throughout the procedure to guide location of the opening and proper placement of the cement. Once the cement had set, the fascia was closed with 3-0 polydioxanone sutures in a simple interrupted pattern and the skin closed using 2-0 nylon sutures.

c). Postoperative care

Postoperative analgesic (Morphine, Elkins-Sinn, Inc., Cherry Hill, NJ, 08003) was given, once immediately after coming out of anesthesia and a second dose four hours later. The animals and their surgical incisions were monitored daily throughout the study. Animals were given recommended laboratory care and feeding. Fluorescent bone labeling agents were administered approximately 3, 6, and 11 wks post surgery as shown in Table 13. Tetracycline hydrochloride and oxytetracycline (Sigma Chemical Co., St. Louis, MO) were used. Depending on weight, animals were given 200 or 250 mg orally, approximately every eight hours, for a three-day period.

Table 13. Schedule of fluorochrome administration

Animal ID #	*Implant time (wks)*	*Cement type*	*Days F1*	*Total dose (mg)*	*Days F2*	*Total dose (mg)*	*Days F3*	*Total dose (mg)*
6629	2	PMMA	---	---	---	---	---	---
6668	2	PMMA	---	---	---	---	---	---
6672	2	PMMA	---	---	---	---	---	---
6657	6	PMMA	24, 25, 26	2000	34, 35, 36	1800	---	---
6596	6	PMMA	25, 26, 27	2000	36, 37, 38	1800	---	---
6649	6	PMMA	24, 25, 26	2000	34, 35, 36	1800	---	---
6615	12	PMMA	24, 25, 26	2000	49, 50, 51	1800	78, 79, 80	2000
6587	12	PMMA	24, 25, 26	2000	49, 50, 51	1800	78, 79, 80	1750
6640	12	PMMA	22, 23, 24	2000	47, 48, 49	1800	76, 77, 78	2000
6673	2	OC	---	---	---	---	---	---
6669	2	OC	---	---	---	---	---	---
6746	2	OC	---	---	---	---	---	---
6740	2	OC	---	---	---	---	---	---
6569	6	OC	23, 24, 25	2250	34, 35, 36	2250	---	---
6698	6	OC	21, 22, 23	2250	34, 35, 36	2250		
6656	6	OC	22, 23, 24	2250	36, 37, 38	2250	---	---
6661	6	OC	22, 23, 24	2250	36, 37, 38	2250	---	---
6662	12	OC	21, 22, 23	2200	47, 48, 49	2250	74, 75, 76	2250
6663	12	OC	21, 22, 23	2200	47, 48, 49	2250	74, 75, 76	2250
6652	12	OC	21, 22, 23	2250	53, 54, 55	2250	75, 76, 77	2250
6681	12	OC	21, 22, 23	2250	53, 54, 55	2250	75, 76, 77	2250

F1 = tetracycline hydrochloride, F2 = oxytetracycline, F3 = tetracycline hydrochloride

d). Sacrifice and implant retrieval

After the given time interval, animals were euthanized using Beuthanasia™ (Schering-Plough Animal Health, Union, NJ) given intravenously at 2 ml/10 kg body weight. Operated femurs were harvested, taking care to note physical observations such as color and any abnormalities of surrounding tissue. Femurs were wrapped in towels saturated with lactated Ringer's solution. Medial-lateral and cranial caudal macroradiographs were taken of each femur immediately after it was retrieved. Next, femurs were transversely sectioned using an Isomet low-speed saw (Buehler Ltd., Evanston, IL) and lactated Ringer's solution as a cutting fluid. At least 5 slices, approximately 3-4 mm thick, were prepared for push-out testing while four additional sections were collected for tissue analysis (Figure 20). Immediately after sectioning, specimens for tissue analysis were placed in the appropriate fixative and push-out specimens were kept moist using lactated Ringer's solution.

testing. Push-out testing was performed as soon as possible after sectioning, typically within four hours of harvesting.

The push-out force was measured using an Instron universal testing machine, a 1 kN load cell, and a crosshead speed of 0.5 mm/min. The maximum force for interface failure was determined as a sudden drop in force on a force vs. displacement chart. The maximum shear force and mode of failure were recorded for each specimen. Initially the maximum diameter at the cement-bone interface was measured, the specimen was rotated 90 degrees and a secondary diameter was measured. Measurements were taken on the top and bottom surfaces. The area of the cement-bone interface was approximated by assuming an elliptical shape for the bone-cement interface and averaging the circumference of the top and bottom surfaces. Since some specimens did not have complete contact between the bone and cement, the above calculation of interfacial surface area was not always accurate. Therefore, a digital image was collected of each specimen at the Iowa State University Image Analysis Facility using a Zeiss Image analysis system (Zeiss-Kontron; BAS version 2.00). Images were captured using a Sony 3CCD color video camera. The area of direct contact between the cement and bone was calculated for each specimen. Using these area measurements, the shear strength was calculated as the force divided by area. The mean interfacial shear strength was determined for each experimental condition.

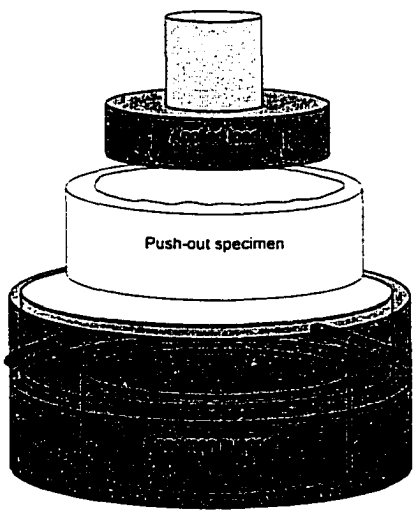

Figure 21. Push-out testing fixture

11. Evaluation of tissue response

Evaluation of tissue response included gross observation, light microscopy, fluorescent microscopy and microradiography.

a). Light microscopy

Specimens for light microscopy work were fixed with 10% neutral buffered formalin for at least 24 hr before processing by Iowa State University Veterinary Histology Services. Specimens were demineralized using 25% formic acid. Ammonium oxalate solution was used to determine the endpoint of decalcification. Following demineralization, specimens were dehydrated in a series of graded alcohol solutions and xylene, and embedded in paraffin. Thin sections, 5 μm thick, were cut from the paraffin blocks using a microtome. These thin sections were mounted on glass slides. Slides were stained with hematoxylin and eosin or Gomori's trichrome to facilitate the observation of cellular elements, fibrous tissue, and new bone. Slides from at least one cortical bone section and one cancellous bone section were prepared from each experimental femur.

The cellular response to implanted cement was evaluated by a veterinary pathologist from the Iowa State University Veterinary Pathology department. A general, qualitative assessment was made for each slide based on the cellular elements present, the degree of necrosis, and the presence of any fibrous capsule. Slides were examined using a Zeiss Axioplan 2 microscope equipped with an Axioplan HRc camera to acquire digital photos. A stage micrometer was used to calibrate the internal scaling feature of the software.

b). Fluorescence microscopy

Specimens for analysis using fluorescence microscopy were fixed in 70% ethanol for at least 24 hr. Non-decalcified sections were dehydrated using a graded series of ethanol solutions and acetone. The specimens remained in for each of the following solutions for at least 24 hr: 70% ethanol, 90% ethanol, 95% ethanol, 100% ethanol, 100% ethanol, acetone, acetone. Control specimens containing PMMA cement were dried for 24 hr under vacuum after being removed from 100% ethanol, then embedded in Spurr's resin because acetone would have dissolved the PMMA cement. After dehydration, specimens were placed in Spurr's media: 10.0 g 4-vinylcyclohexene

dioxide, 6.0 g diglycidyl ether of polypropylene glycol, 26.0 g nonenylsuccinic anhydride, and 0.40 g of dimethylamino ethanol. The specimens in unpolymerized Spurr's resin were placed under vacuum and shaken for 2-3 days to remove residual acetone and to promote complete infiltration of the resin into the bone specimen. After the resin had begun to thicken, generally around day 5, the specimens were placed in an oven at 70° for at least 24 hr to complete polymerization.

The hardened blocks containing embedded bone specimens were cut into sections approximately 500 μm thick using an Isomet, low-speed saw and water as a lubricant. After being cut, the sections were rinsed thoroughly, dried on paper towels, and stored in the dark. The sectioned wafers were next mounted on Lexan® slides using Duro® superglue and pressed for 24 hr. The mounted sections were polished to 300 ± 50 μm using a series of 400, 600, 1200 grit paper, and 0.3 μm alumina on a lapping wheel.

These sections were examined on an Olympus AH-2 microscope (Olympus Corp., Lake Success, NY) or Zeiss D-7082 Photomicroscope (Carl Zeiss Microimaging, Inc., Thornwood, NY) with reflected light using blue or violet filters.

c). Microradiography

After fluorescence microscopy, microradiographs of the thick sections were collected to study mineralization around the implanted cement. Digital microradiographs were obtained using specialized, high-resolution, x-ray equipment at the Center for Nondestructive Evaluation, an IPRT Center at Iowa State University. Equipment included a Kevek microfocus x-ray tube at 30-35 kV with a 5 μm spot size, Varian amorphous silicon detector with a gadolium sulfyotide screen, x-ray detector, with a Daedel 4 axis micro stepper positioner.

d). Scanning electron microscopy

The resin embedded cement-bone sections used for fluorescence analysis were analyzed without coating with a Hitachi 2460N Scanning electron microscope, SEM, (Hitachi Scientific Instruments, Pleasanton, CA), using secondary electrons (SE) or backscattered electrons (BSE) operating between 5-30 kV.

12. Statistical analysis

Means and standard deviation are presented for the experimental data. The Student's t-test was used to assess whether the observed differences between the means of different groups were statistically significant.

IV. RESULTS AND DISCUSSION

A. Cement Characterization

1. Characterization of OC-cement

The setting, flow properties, strength over time in a simulated body environment, change in mass and size over time, and phases present during hydration were studied to further understand the composition and characteristics of OC-cement.

a). Setting

The working and setting times of OC-cement are dependent on cement composition, the presence of additives, and the mixing environment. Setting properties have been evaluated from 10-40°C and are displayed in Table 14 and Figure 22. Both working and setting times were highly influenced by temperature. The working time decreased progressively: 28.2, 14.2, 8.6, 6.3, 4.4 minutes, with increasing temperature. Similarly, the setting times decreased: 64.4, 27.5, 17.92, 12.8, 10.2 minutes, as the temperature increased. The setting time of OC-cement at 37°C was found to range from 12.5 to 13.5 minutes. This is similar to that of commercial PMMA cements such as Palacos R®, Simplex P®, and Zimmer D® (Kindt-Larsen et al., 1995).

The graph of ln time vs. absolute temperature^{-1} in Figure 23 shows high correlation and approximately the same slope for both the working and setting times. With the slopes from the regression line, the ΔH was estimated to be -42 kJ/mole.

Table 14. Setting properties of OC-cement

Working and setting times of OC-cement (minutes)										
	10 °C		20 °C		30 °C		37 °C		40 °C	
n	*WT*	*ST*	*WT*	*ST*	*WT*	*ST*	*WT*	*ST*	*WT*	*ST*
1	27.0	61.0	15.0	27.0	9.0	19.0	6.5	12.5	4.0	10.5
2	37.0	68.0	15.0	28.0	9.0	18.5	6.0	13.0	4.5	10.5
3	27.0	63.0	14.0	27.0	8.5	16.0	6.5	12.5	4.5	10.5
4	27.0	64.5	14.0	29.0	9.0	20.0	6.0	12.5	3.5	10.0
5	26.0	64.0	13.5	28.0	8.0	17.5	6.5	13.5	4.8	10.3
6	24.5	66.0	13.5	26.0	8.0	16.5	6.5	13.0	5.0	9.5
AVG	*28.1*	*64.4*	*14.2*	*27.5*	*8.6*	*17.9*	*6.3*	*12.8*	*4.4*	*10.2*
SD	*4.5*	*2.4*	*0.7*	*1.1*	*0.5*	*1.5*	*0.3*	*0.4*	*0.5*	*0.4*

WT = Working time, ST = Setting time

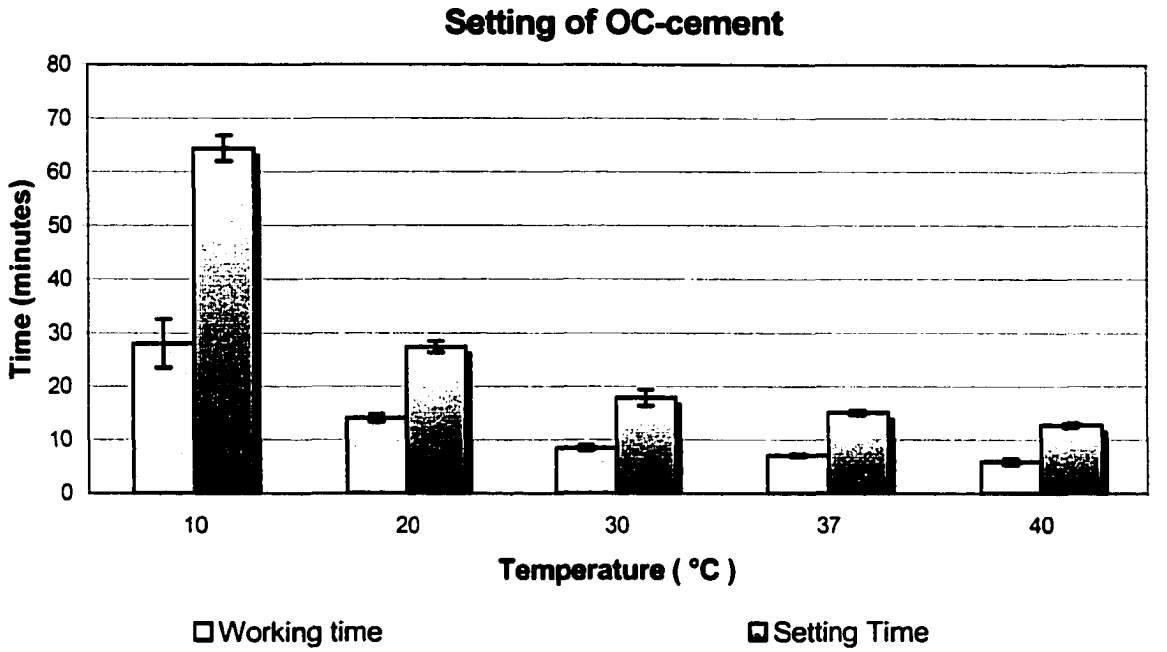

Figure 22. Working and setting times of OC-cement vs. temperature (mean ± standard deviation)

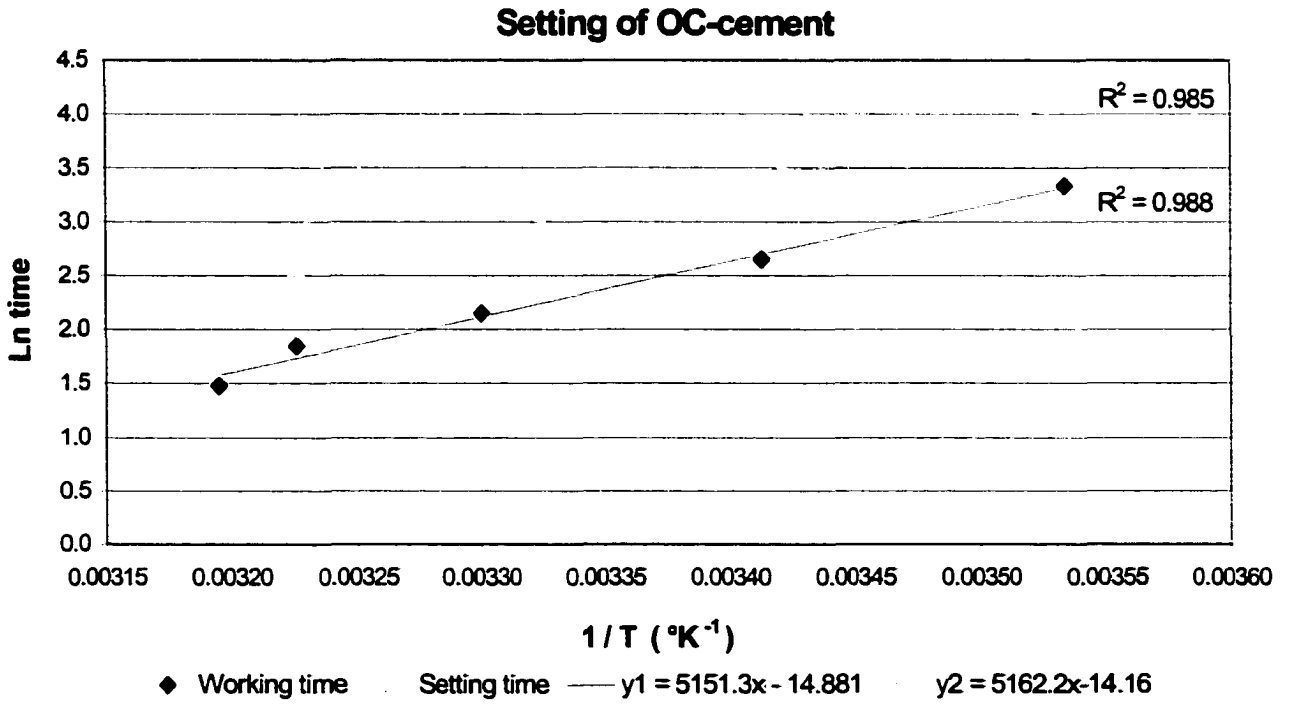

Figure 23. Working and setting times of OC-cement vs. 1 / temperature ($^{\circ}K^{-1}$)

b). OC-cement flow

The experimental cement mixture exhibits dilatent flow, the resistance to flow is increased as the rate of shear increases. The cement is similar to Portland cements in that it flows better under light vibration. The effect of vibration on the flow of the cement was studied to aid in effectively placing the cement. For OC-cement, the average diameter of a standard cylinder, under a standard load, without vibration increased from 0.938±0.72 to 1.395±0.218 cm, 49%, over the 20 minute period. The greatest change took place during the initial 5 minute period (Table 15, Figure 24). OC-cement that had been vibrated showed an immense increase in mean diameter following vibration. Total increases in diameter over the 20 minute test period of 438%, 442% and 629% were found for OC-cement vibrated 15, 30, and 45 seconds, respectively (Tables 16, 17,18). Following vibration up to 20 minutes, the mean diameters increased 3.2%, 1.8%, and 0.9%, respectively, for the 15, 30, and 45 second vibration durations. These small changes were not statistically different.

These results show that under specific conditions, OC-cement flows readily and its unique flow properties could be advantageous for some applications. The dilatent nature of the cement could prevent cement from being forced into the cavities of trabecular bone, as frequently occurs with PMMA cement implanted with applied pressure. However, adapting to the differences in flow may require modifications to the typical PMMA cement placement procedure.

Table 15. Flow of OC-cement – no vibration

	Diameter of OC-cement disc (cm)				
N	*0 min*	*5 min*	*10 min*	*15 min*	*20 min*
1	0.970	1.217	1.300	1.363	1.333
2	0.873	1.180	1.180	1.170	1.200
3	0.873	1.040	1.280	1.290	1.300
4	0.857	1.183	1.293	1.317	1.327
5	0.860	1.083	1.430	1.430	1.447
6	1.033	1.597	1.877	1.883	1.883
7	0.993	1.833	1.467	1.490	1.490
8	0.920	1.240	1.373	1.353	1.353
9	1.050	1.020	1.030	1.080	1.080
10	0.950	1.350	1.480	1.520	1.540
Total AVG	*0.938*	*1.274*	*1.371*	*1.390*	*1.395*
SD	*0.072*	*0.258*	*0.224*	*0.220*	*0.218*

Table 16. Flow of OC-cement – vibrated 15 seconds

	Diameter of OC-cement disc (cm)					
N	*0 min*	*After Vib.*	*5 min*	*10 min*	*15 min*	*20 min*
1	0.922	4.977	5.167	5.180	5.183	5.183
2	0.906	5.387	5.417	5.417	5.417	5.610
3	0.868	4.763	5.097	5.103	5.103	5.103
4	0.863	5.467	5.573	5.607	5.610	5.723
5	0.917	4.660	4.687	4.690	4.693	4.695
6	0.962	5.553	5.723	5.723	5.723	5.723
7	0.982	5.540	5.633	5.643	5.643	5.643
8	0.988	2.003	2.003	2.033	2.037	2.037
9	0.973	4.867	4.967	4.967	4.967	4.967
10	0.995	5.617	5.683	5.700	5.700	5.700
Total AVG	*0.936*	*4.883*	*4.995*	*5.006*	*5.008*	*5.038*
SD	*0.047*	*1.074*	*1.106*	*1.101*	*1.100*	*1.117*

Table 17. Flow of OC-cement – vibrated 30 seconds

	Diameter of OC-cement disc (cm)					
n	*0 min*	*After Vib.*	*5 min*	*10 min*	*15 min*	*20 min*
1	1.067	5.200	5.230	5.320	5.320	5.320
2	1.140	4.610	4.613	4.627	4.627	4.627
3	1.146	6.683	6.850	6.863	6.863	6.863
4	1.347	6.620	6.650	6.680	6.680	6.680
5	1.133	6.767	6.800	6.803	6.837	6.837
6	1.157	5.313	5.370	5.380	5.383	5.383
7	1.050	5.997	6.080	6.130	6.130	6.130
8	0.983	6.337	6.503	6.553	6.560	6.560
9	1.017	6.417	6.523	6.570	6.587	6.587
10	1.290	6.463	6.493	6.503	6.517	6.517
Total AVG	*1.133*	*6.041*	*6.111*	*6.143*	*6.150*	*6.150*
SD	*0.115*	*0.743*	*0.771*	*0.766*	*0.771*	*0.771*

Table 18. Flow of OC-cement – vibrated 45 seconds

	Diameter of OC-cement disc (cm)					
N	*0*	*After Vib.*	*5 min*	*10 min*	*15 min*	*20 min*
1	0.977	5.490	5.523	5.537	5.537	5.537
2	1.017	7.387	7.570	7.583	7.583	7.583
3	0.923	6.647	6.667	6.667	6.667	6.667
4	0.920	7.330	7.658	7.658	7.658	7.658
5	0.930	6.490	6.983	7.097	7.097	7.097
6	0.933	6.087	6.870	6.887	6.887	6.887
7	0.937	6.750	6.513	6.513	6.513	6.513
8	0.903	7.573	6.127	6.127	6.127	6.127
9	0.903	6.983	6.803	6.803	6.803	6.803
10	0.907	6.860	7.347	7.347	7.347	7.347
Total AVG	*0.935*	*6.760*	*6.806*	*6.822*	*6.822*	*6.822*
SD	*0.036*	*0.632*	*0.654*	*0.657*	*0.657*	*0.657*

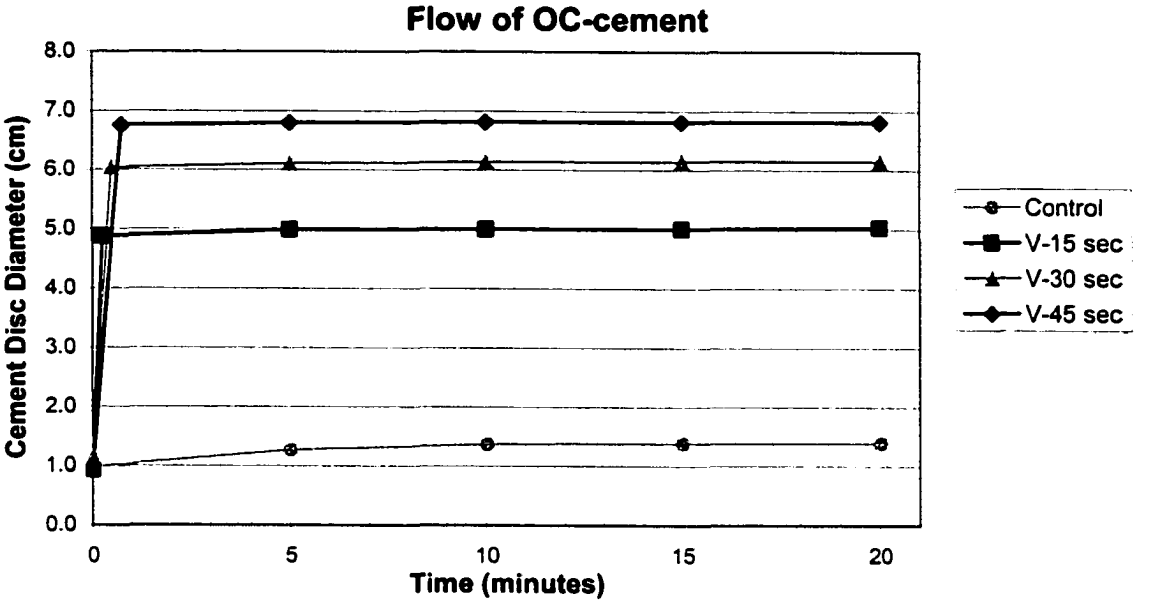

Figure 24. OC-cement flow: standard and vibrated conditions

c). Strength

The compressive strength (CS) was used to evaluate the mechanical properties of OC-cement. The compressive strength of the cement was measured for OC-cement aged 1 day up to 2 years. These results are displayed in Table 19 and Figure 25. Initially, OC-cement was prepared using either 20 or 33wt% β-tricalcium phosphate. Compressive strength results for the cement made with 33wt% β-TCP were significantly higher when measured at 1 month and 6 months; therefore, 33wt% β-TCP was used in subsequent experiments. For OC-cement (33wt% β-TCP), the mean compressive strength progressively increased from 61.70±14.89, 108.93±22.41, 139.93±19.74 MPa at 1 day, 1 week, to 1 month. The compressive strength at 6 months showed a reduction in compressive strength, approximately 30%, as compared to 1 month values. Mean strength values for OC-cement (33wt β-TCP) at 6 months and 1 year were not found to be significantly different, but a decrease was noted from 1 to 2 years.

Table 19. Compressive strength of OC-cement over time (MPa)

	Cement A: 20wt% β-TCP				*Cement B: 33wt% β-TCP*					
n	*1 d*	*1 wk*	*1 m*	*6 m*	*1 d*	*1 wk*	*1 m*	*6 m*	*1 yr*	*2 yr*
1	79.45	134.03	78.91	54.10	79.89	95.16	108.55	98.34	99.03	67.68
2	90.03	108.81	78.24	62.61	46.38	125.35	163.44	81.43	74.24	80.03
3	63.95	83.15	86.25	33.70	78.70	139.16	151.69	134.19	109.80	78.27
4	61.59	91.28	110.09	87.44	72.55	97.16	143.73	88.17	68.85	65.03
5	75.23	102.78	109.51	80.25	50.87	95.41	152.50	82.76	87.82	73.90
6	82.78	101.17	43.60	64.67	70.01	126.59	146.34	112.33	86.71	87.44
7	62.12	68.43	53.89	43.66	40.85	122.07	168.66	87.83	85.43	68.88
8	78.91	83.16	51.38	43.28	70.53	84.99	149.45	88.17	99.43	49.92
9	76.10	97.26	103.70	94.42	42.97	142.13	129.13	50.67	78.43	109.42
10	68.16	114.67	93.59	56.67	72.75	89.39	111.65	124.87	89.77	61.85
11	63.21	118.98	91.99	35.15	53.25	80.85	116.28	87.18	---	63.04
12	---	94.75	---	59.12	---	---	137.74	108.11	---	65.72
AVG	*72.87*	*99.87*	*81.92*	*59.59*	*61.70*	*108.93*	*139.93*	*95.34*	*87.95*	*72.60*
SD	*9.63*	*17.83*	*23.44*	*19.72*	*14.89*	*22.41*	*19.74*	*22.19*	*12.41*	*15.16*

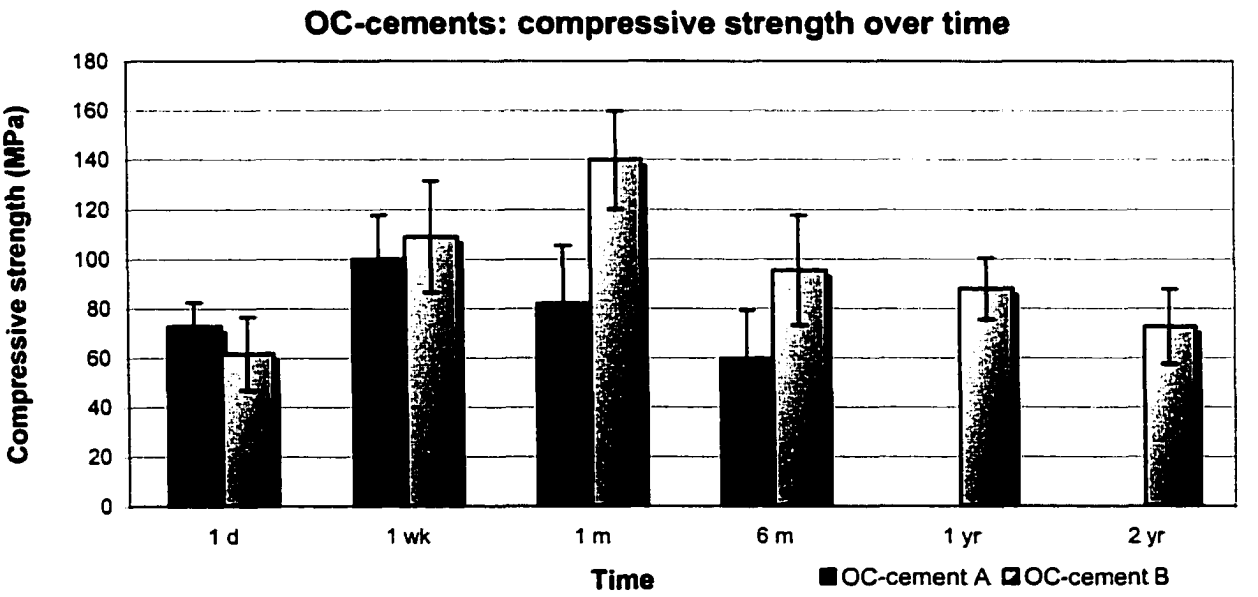

Figure 25. Compressive strength of OC-cement over time (mean ± standard deviation)

Throughout the above segment of testing, improvements were made in the mixing, forming, and testing techniques. The compressive strength experiment was repeated with the addition of several time periods. Testing was performed at 1 hr, 4 hr, 12 hr, 24 hr, 48 hr, 5 d, 1 wk, 4 wk, 8 wk,

16 wk, 32 wk and 52 wk. Mean compressive strengths were 30.34, 71.26, 77.94, 74.73, 66.16, 92.27, 105.91, 111.56, 101.20,111.75, 99.71, and 92.00 MPa, respectively. The same trend of compressive strength over time that was observed in the first experiment was confirmed with similar values for compressive strength (Table 20, Figure 26). Although a small, temporary decease in strength was observed at 48 hours, the general trend in strength increased up to 1 month. The mean strength after 52 wk was 82% of the maximum strength that was measured at 1 month.

Table 20. Compressive strength of OC-cement over time (MPa)

n	*1 hr*	*4 hr*	*12 hr*	*24 hr*	*48 hr*	*5 d*	*1 wk*	*4 wk*	*8 wk*	*16 wk*	*32 wk*	*52 wk*
1	31.58	69.56	92.72	77.88	68.54	82.70	95.44	95.87	78.27	123.89	82.23	128.01
2	26.71	66.05	69.11	75.08	64.43	96.04	122.08	111.86	120.96	81.23	78.29	75.59
3	34.33	70.54	70.04	74.95	63.70	97.48	94.26	97.25	75.64	105.99	117.09	93.37
4	32.29	76.15	63.62	78.08	60.97	73.28	106.59	94.88	111.09	120.14	116.76	109.01
5	33.13	68.64	64.47	67.26	73.42	76.92	122.21	112.48	112.78	97.71	96.85	87.07
6	32.12	75.40	78.94	67.04	69.50	109.86	109.13	102.83	87.72	125.73	114.32	71.39
7	27.54	75.20	89.44	67.15	83.59	73.29	116.95	116.67	113.29	102.74	94.09	99.87
8	30.07	79.59	95.56	72.72	60.62	85.16	86.97	120.49	111.20	136.60	114.98	87.21
9	28.97	60.19	70.81	77.40	66.75	114.51	99.59	134.15	99.81	98.01	80.26	79.62
10	28.52	74.13	85.78	80.94	60.34	113.48	---	113.38	---	125.47	102.32	88.81
11	28.52	82.30	81.66	82.08	55.92	---	---	127.35	---	---	99.57	---
12	---	75.06	73.10	76.18	---	---	---	---	---	---	---	---
AVG	*30.34*	*71.26*	*77.94*	*74.73*	*66.16*	*92.27*	*105.91*	*111.56*	*101.20*	*111.75*	*99.71*	*92.00*
SD	*2.49*	*5.98*	*12.02*	*5.22*	*7.61*	*16.31*	*12.77*	*12.94*	*16.70*	*17.16*	*14.93*	*16.85*

The diametral tensile strength of OC-cement was measured at 1 day and 1 week. Values for mean diametral tensile strength were 7.02±0.79 and 11.34±1.3 MPa, respectively (Table 21). This is approximately $^1/_{10}$ of the compressive strength for the same time periods which is typical for ceramic materials.

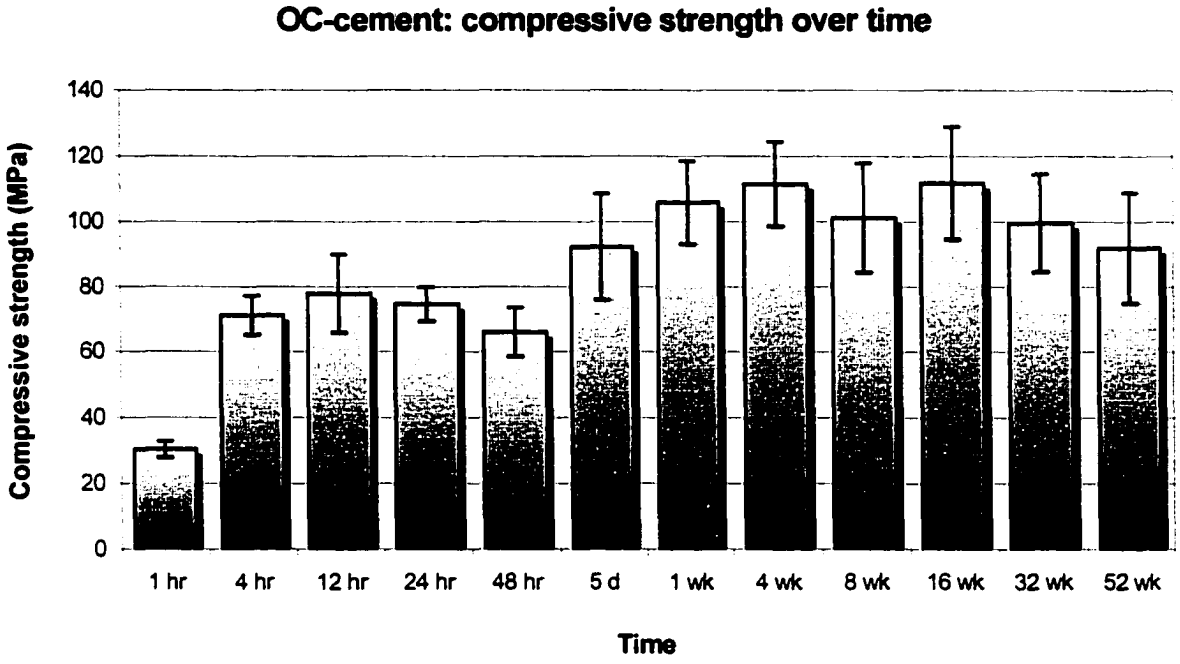

Figure 26. Compressive strength of OC-cement over time (mean ± standard deviation)

Table 21. Diametral tensile strength of OC-cement

	24 hr				*1 wk*			
n	*Diameter (cm)*	*Thickness (cm)*	*Load (N)*	*DTS (MPa)*	*Diameter (cm)*	*Thickness (cm)*	*Load (N)*	*DTS (MPa)*
1	1.271	0.420	562	6.71	1.278	0.546	1129	10.30
2	1.270	0.415	592	7.15	1.270	0.533	1059	9.95
3	1.270	0.486	775	7.99	1.280	0.538	1468	13.56
4	1.265	0.384	452	5.93	1.275	0.538	1346	12.48
5	1.275	0.411	509	6.18	1.273	0.521	1225	11.77
6	1.277	0.462	777	8.39	1.270	0.523	1281	12.27
7	1.276	0.495	729	7.35	1.270	0.536	1454	13.60
8	1.271	0.496	652	6.59	1.278	0.513	1111	10.79
9	1.278	0.549	742	6.74	1.278	0.538	1210	11.20
10	1.291	0.468	717	7.55	1.285	0.533	1236	11.48
11	1.272	0.462	616	6.67	1.288	0.538	1258	11.55
12	1.271	0.461	725	7.88	1.283	0.516	1093	10.52
13	1.286	0.345	505	7.24	1.280	0.533	952	8.87
14	1.275	0.456	501	5.48	1.280	0.541	1254	11.53
15	1.266	0.907	1313	7.28	1.283	0.538	1106	10.19
AVG				*7.02*				*11.34*
SD				*0.79*				*1.30*

OC-cement achieves high strengths within 4 hours of preparation. The mixing technique and experience of the processor are thought to affect the resulting strength. Although the values for compressive strength of OC-cement are comparable with values for commercial PMMA bone cement, the tensile strength is approximately $^1/_3$ to ½ values reported for PMMA (Haas et al., 1975). In the future, it may be possible to further improve the strength properties of OC-cement by decreasing porosity through techniques such as vacuum mixing.

2. Hydration of OC-cement

a). Physical changes during hydration

OC-cement pellets were immersed in lactated Ringer's solution and stored at 37°C. Mass and diameter were measured from 1 hour after setting up to 14 months. Over a one-month period, the mass of the pellets was found to increase 5.95±0.51% (Table 22 and Figure 27). During the remainder of the experimental period, the mass of cement pellets continued to increase, but at a slower rate. A total increase in mass of 8.23±0.65% was observed after 14 months. This increase in mass is thought to be a result of absorption of water from the Ringer's solution that allows for continued hydration of calcium aluminate in the cement. The diameter of the same pellets increased 0.71±0.39% over the 14 month test period. (Table 23 and Figure 29).

These effects may be diffusion controlled, as the correlation of percentage change versus time$^{1/2}$ is highly correlated and typical of diffusion-controlled reactions (Figures 28 and 29). The continued uptake of water may lead to the continued hydration of calcium aluminate phases present. With time, conversions in calcium aluminate phases occur. The variation in densities of these hydrated phases in the cement is also believed to play a role in the physical changes observed.

Table 22. Percentage change in mass of OC-cement pellets over time

n	*1 hr*	*2 hr*	*4 hr*	*18 hr*	*24 hr*	*48 hr*	*5 d*	*7 d*	*1 m*	*4 m*	*6 m*	*9 m*	*14 m*
1	0.23	0.91	1.33	2.27	2.50	3.62	4.20	4.41	5.40	6.12	6.12	6.38	7.31
2	0.32	0.82	1.34	2.21	2.53	3.72	4.74	5.13	6.06	6.93	6.95	7.41	8.46
3	0.23	0.68	1.27	2.19	2.44	3.21	4.91	5.54	6.86	7.71	7.74	8.17	8.71
4	0.41	0.82	1.18	1.93	2.18	3.04	5.08	5.64	6.59	7.48	7.61	8.18	8.91
5	0.56	1.08	1.52	2.45	2.64	3.25	4.96	5.38	6.45	7.18	7.32	7.81	8.32
6	0.49	0.90	1.28	2.09	2.29	3.44	5.05	5.37	6.18	6.96	7.17	7.59	8.58
7	-0.64	0.41	0.75	1.68	1.84	2.75	4.25	4.75	5.84	6.81	6.84	7.04	7.47
8	-0.84	0.21	0.64	1.53	1.60	2.48	3.87	4.26	5.24	6.13	6.04	6.36	7.13
9	-0.70	0.68	1.20	2.12	2.17	3.32	5.03	5.42	6.39	7.54	7.68	7.93	8.29
10	0.61	0.68	0.92	1.58	1.73	2.41	3.94	4.21	5.33	6.10	6.19	6.46	7.67
11	0.63	0.72	0.93	1.54	1.67	2.53	4.34	4.72	5.83	6.84	7.03	7.21	8.54
12	0.68	0.74	1.04	1.71	1.96	2.75	4.41	4.80	5.90	6.98	7.20	7.27	8.33
13	0.74	0.90	1.13	1.78	2.07	2.79	3.87	4.12	5.18	5.85	6.08	6.05	7.56
14	1.07	1.14	1.39	1.99	2.29	3.50	4.78	5.10	6.27	7.36	7.64	7.94	9.31
15	1.02	1.12	1.32	1.89	2.23	3.41	4.42	6.08	5.78	6.94	7.15	7.46	8.81
AVG	*0.32*	*0.79*	*1.15*	*1.93*	*2.14*	*3.08*	*4.52*	*4.99*	*5.95*	*6.86*	*6.98*	*7.28*	*8.23*
SD	*0.60*	*0.25*	*0.25*	*0.29*	*0.33*	*0.43*	*0.44*	*0.59*	*0.51*	*0.58*	*0.61*	*0.70*	*0.65*

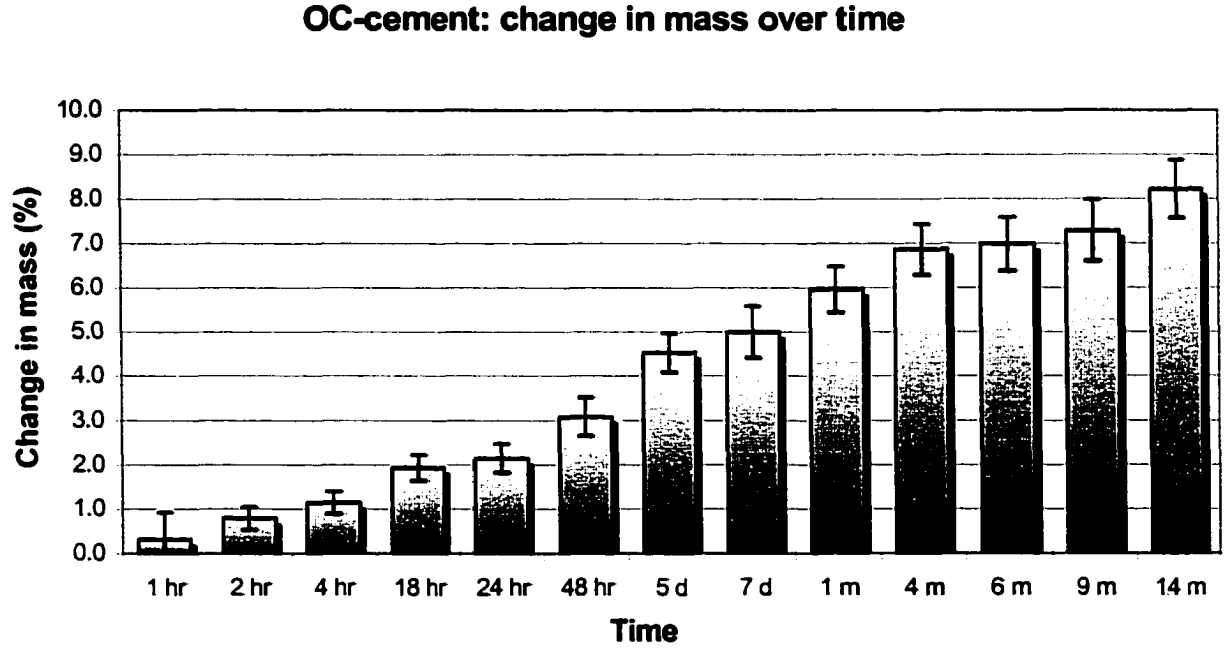

Figure 27. Change in mass over time (mean ± standard deviation)

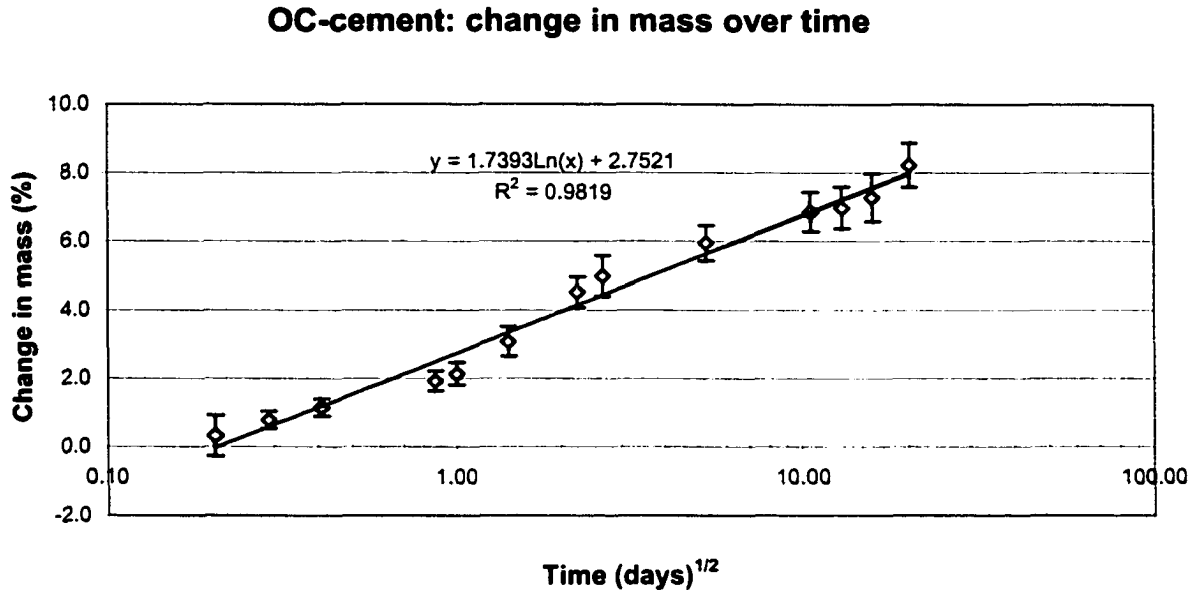

Figure 28. OC-cement change in mass versus square root of time (mean ± standard deviation)

Table 23. Percent change in OC-cement pellet diameter over time

n	*1 hr*	*2 hr*	*4 hr*	*18 hr*	*24 hr*	*48 hr*	*5 d*	*7 d*	*1 m*	*4 m*	*6 m*	*9 m*	*14 m*
1	0.000	0.000	-0.211	0.000	0.000	0.000	0.000	0.000	0.211	0.000	0.211	-0.211	1.01
2	-0.210	0.000	0.000	0.000	0.210	0.210	0.420	0.630	0.630	0.420	0.420	0.420	0.67
3	0.000	0.214	0.214	0.000	0.000	0.214	0.642	0.214	0.642	0.642	0.642	0.642	0.84
4	0.427	0.427	0.427	0.427	0.427	0.427	0.855	0.641	0.855	1.068	0.855	0.855	0.96
5	0.000	0.000	0.000	0.216	0.216	0.216	0.431	0.431	0.431	0.647	0.647	0.431	0.88
6	0.211	0.211	0.211	0.211	0.211	0.632	0.842	0.632	0.842	0.842	0.842	0.842	0.84
7	-0.215	-0.215	-0.215	-0.215	-0.215	0.000	0.215	0.000	0.215	0.215	0.429	0.429	0.39
8	0.210	-0.210	0.000	0.000	0.000	0.210	0.630	0.420	0.420	0.630	0.630	0.630	0.53
9	0.000	0.000	0.213	0.213	0.000	0.213	0.426	0.426	0.640	0.853	0.853	0.640	1.07
10	-0.421	-1.053	-1.053	-1.053	-0.842	-0.842	-0.842	-0.842	-0.632	-0.421	-0.421	-0.632	-0.53
11	0.210	0.000	0.210	0.210	0.419	0.419	0.419	0.629	0.629	0.629	0.629	0.629	1.01
12	0.419	0.000	0.210	0.210	0.210	0.210	0.629	0.629	0.419	0.629	0.629	0.419	0.73
13	0.210	0.210	0.210	0.210	0.210	0.210	0.420	0.420	0.630	0.840	0.840	0.630	0.84
14	0.210	0.000	0.210	0.210	0.000	0.000	0.210	0.419	0.419	0.629	0.419	0.419	0.63
15	0.630	0.420	0.420	0.420	0.420	0.630	0.840	0.840	0.630	0.840	0.840	0.630	0.80
AVG	*0.112*	*0.000*	*0.056*	*0.071*	*0.084*	*0.183*	*0.409*	*0.366*	*0.466*	*0.564*	*0.564*	*0.452*	0.71
SD	*0.275*	*0.348*	*0.361*	*0.354*	*0.317*	*0.346*	*0.426*	*0.409*	*0.359*	*0.381*	*0.336*	*0.390*	0.39

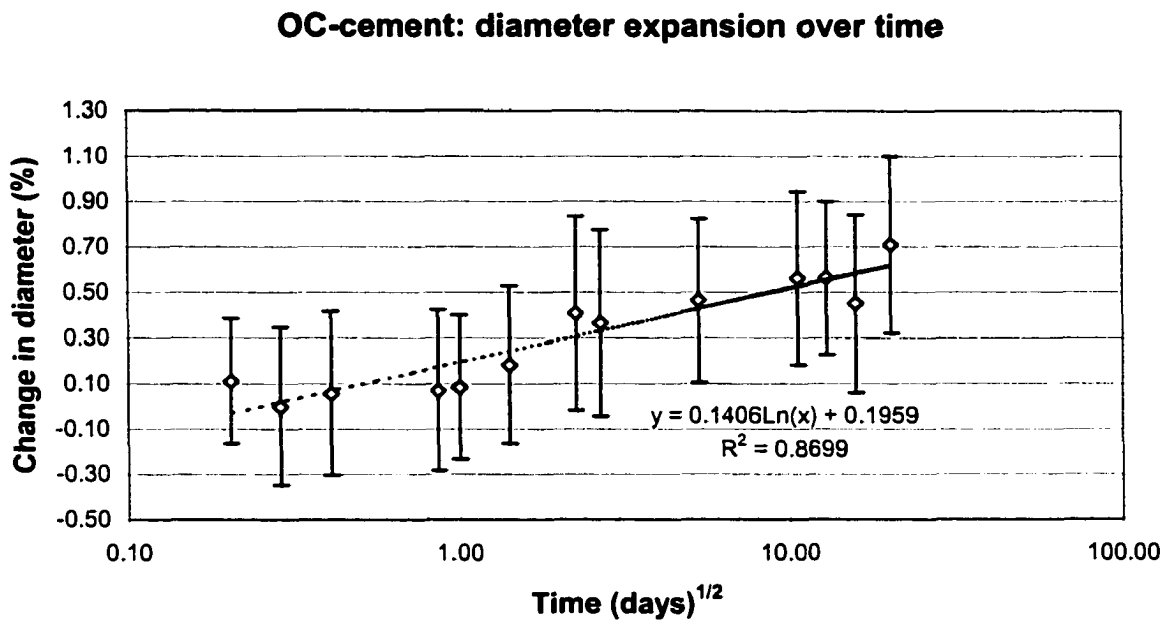

Figure 29. OC-cement diameter expansion over time (mean ± standard deviation)

b). X-ray diffraction analysis

X-ray diffraction (XRD) was used to study the phases present in the hydrated OC-cement over time. XRD scans were collected at 1, 5, 7, 14, 28 days, 6, 14 months and 2 years. Graphs of XRD scans from each time, a table showing changes in peaks over time, and an XRD scan of OC-cement with peak matching are compiled in Appendix A. Figure 30 shows a compilation of XRD scans for all times, while characteristic XRD peaks of key components are shown in Figures 31 and 32.

The CA peak decreased significantly within the first 7 days. It continued to decrease and was hardly discernible at 14 months. The CA_2 peak showed little change up to 28 days. A decrease was noted at 6 and 14 months while some CA_2 remained present up to 2 years. The β-TCP peak was not observed to change during the testing period. Of particular interest was the initial absence of the typical calcium aluminate hydration peaks: CAH_{10}, C_2AH_8, and C_3AH_6. Instead, the $CaCl_2$ in the hydration solution led to the formation of calcium aluminate chloride hydrates. There are multiple

types and phases of calcium aluminate chloride hydrates and given that hydrate peaks often appear broad; at times up to 6 months it was not possible to resolve the peaks to determine which ones were present. Additional slower rate scans collected at 11-12 degrees and 21.5-23.0 degrees 2 theta on the 14 months and 2 year samples found hydrate peaks consistent with α-$Ca_4Al_2H_{0.34}O_{6.34}Cl_{1.67}$ and $Ca_2Al(OH)_6Cl \cdot 2H_2O$. Most likely, a solid solution exists as was reported for the hydrated calcium chloride aluminate studied by Poellman and Kuzel (1988). At seven days, the presence of AH_3 was observed. After 2 years, the AH_3 peaks had become more prominent and sharpened. Small peaks corresponding to C_3AH_6 began to emerge after 28 days; over time, they became slightly larger and more defined.

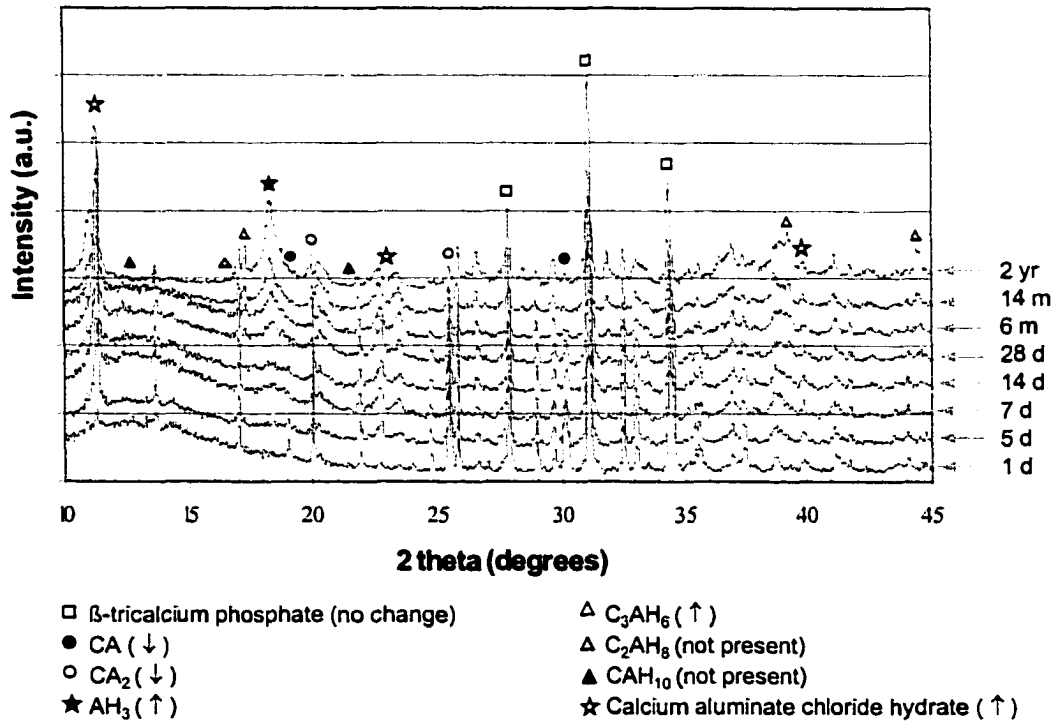

Figure 30. Compilation of XRD scans of OC-cement: 1 day to 2 years

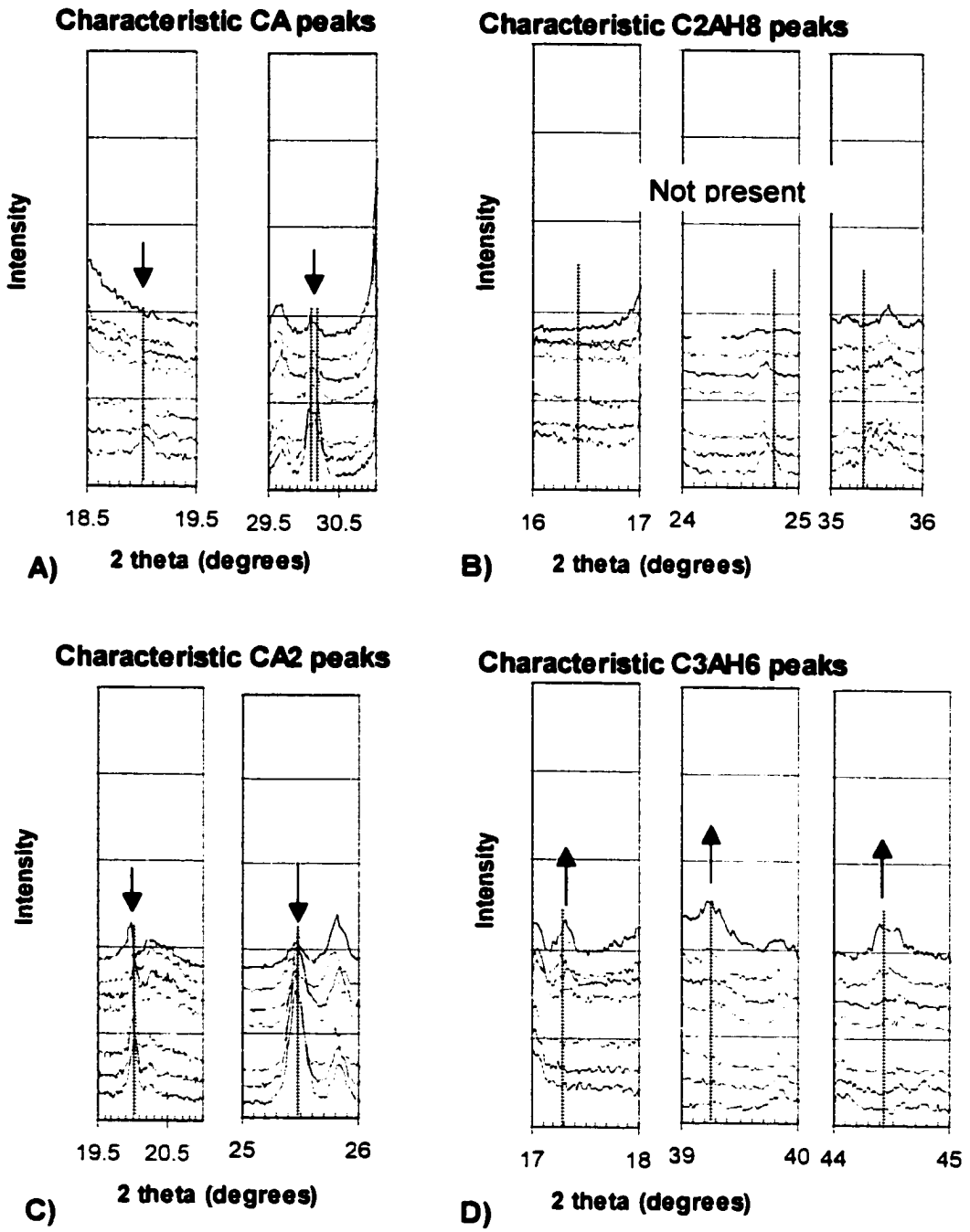

Figure 31. Characteristic XRD peaks: A) calcium aluminate, CA, peaks decreased with time B) calcium aluminate hydrate, C_2AH_8, peaks were not present C) calcium aluminate, CA_2, decreased over time D) Calcium aluminate hydrate, C_3AH_6, peaks became more prominent at later time periods

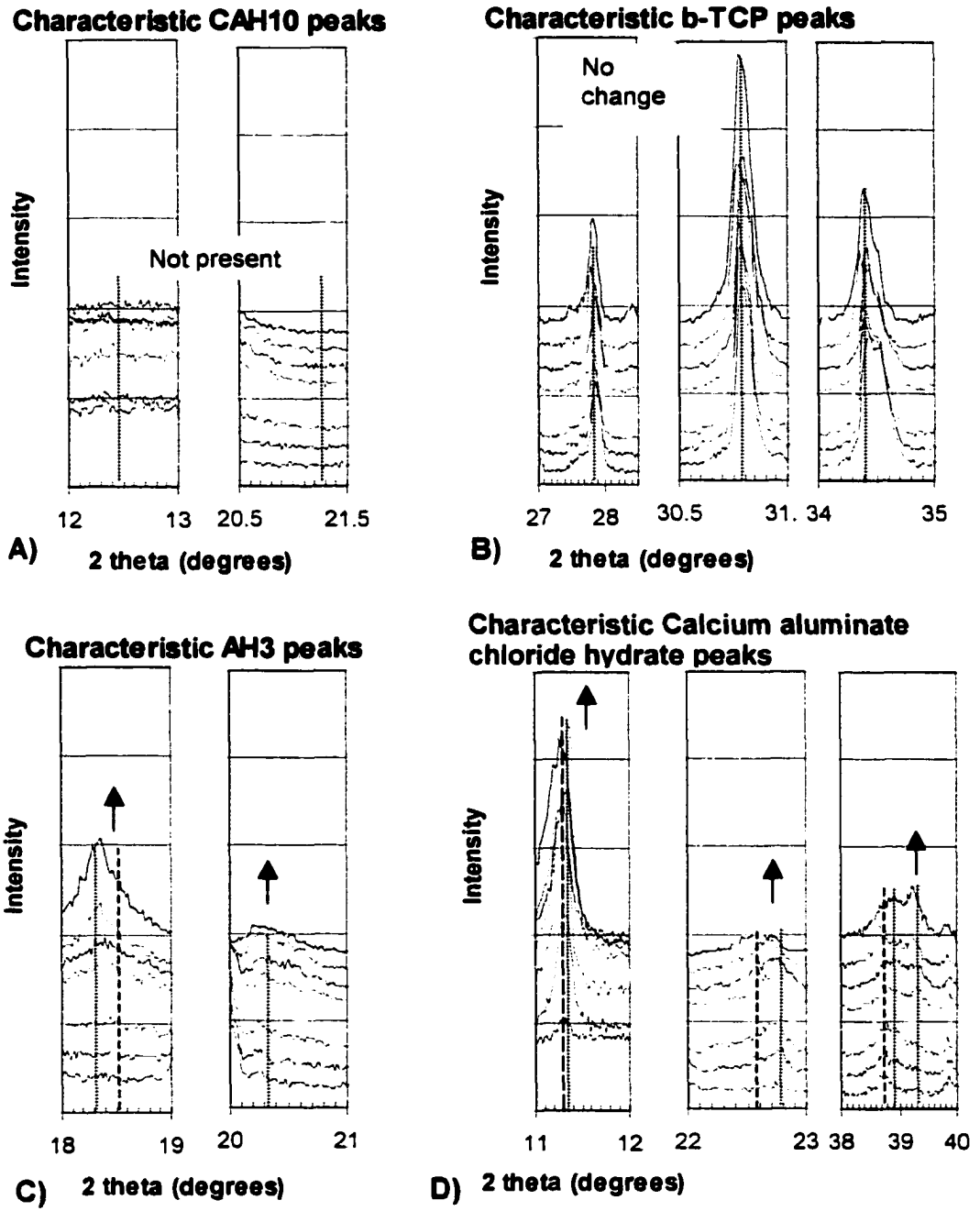

Figure 32. Characteristic XRD peaks: A) calcium aluminate hydrate, CAH_{10}, peaks were not observed B) β-tricalcium phosphate peaks were prominent and remained unaltered throughout the test period C) aluminum oxide hydrate, AH_3, peaks emerged and sharpened with time D) Calcium aluminate chloride hydrate, $CA_2Al(OH)_6Cl{\cdot}2H_20$ and α-$Ca_4Al_2H_{0.34}O_{6.34}$ $I_{1.67}$, peaks were initially observed and increased in intensity during the next few time periods.

3. Cement-prosthesis bonding strength

The cement-prosthesis bond strength was measured using canine cadaver femurs. During pull-out testing, failure occurred at the cement-prosthesis interface for all specimens. Macroscopic evaluation of specimens that had been cut longitudinally showed good filling and close contact of the cement with the post. A summary of the data is shown in Table 24 and Figure 33. Mean interfacial shear strengths (ISS) for OC-cement were 1.18±0.27, 1.11±0.21 and 1.18±0.34 MPa at 4 hr, 24 hr, and 60 days, respectively; PMMA results for corresponding time periods were 1.45±0.70, 1.18±0.66 and 1.48±0.92 MPa. The differences in means for OC-cement and PMMA at each time were not found to be statistically significant ($p < 0.05$).

The values obtained for the PMMA-prosthesis ISS at 60 days were greater than anticipated. Other researchers have reported high initial shear strength for PMMA-prosthesis interface when stored under dry conditions (Beaumont et al., 1977), but a decrease was found after 18 hours submersion in saline, (Davies et al., 1994) and values decreased to 0 MPa when test specimens were aged for 60 days in saline at 37°C (Müller et al., 1999). Even for the dry interface, a range of values has been given in the literature. Some authors have tried to explain these variations based on shrinkage of the PMMA cement that results from polymerization (Müller et al., 1999, Ahmed et al., 1984, Kühn, 2000). The temperature gradient between the inner and outer surface of the PMMA cement can influence whether polymerization begins at the inner surface leading to shrinkage onto the prosthesis or at the outer surface inducing shrinkage of the cement away from the prosthesis.

Table 24. Summary of interfacial shear strengths (MPa)

	OC-cement			PMMA		
n	*4 hr*	*24 hr*	*60 d*	*4 hr*	*24 hr*	*60 d*
1	1.21	1.39	0.85	1.11	2.45	2.63
2	0.91	1.17	1.17	1.09	1.01	2.69
3	1.14	0.92	1.03	1.05	1.51	1.50
4	1.13	1.11	1.04	2.58	0.36	2.06
5	0.90	0.85	0.87	1.07	1.16	1.11
6	1.70	0.98	1.71	2.35	0.84	0.28
7	1.26	1.37	1.61	0.88	0.91	1.12
8						0.43
AVG	*1.18*	*1.11*	*1.18*	*1.45*	*1.18*	*1.48*
ST DEV	*0.27*	*0.21*	*0.34*	*0.70*	*0.66*	*0.92*

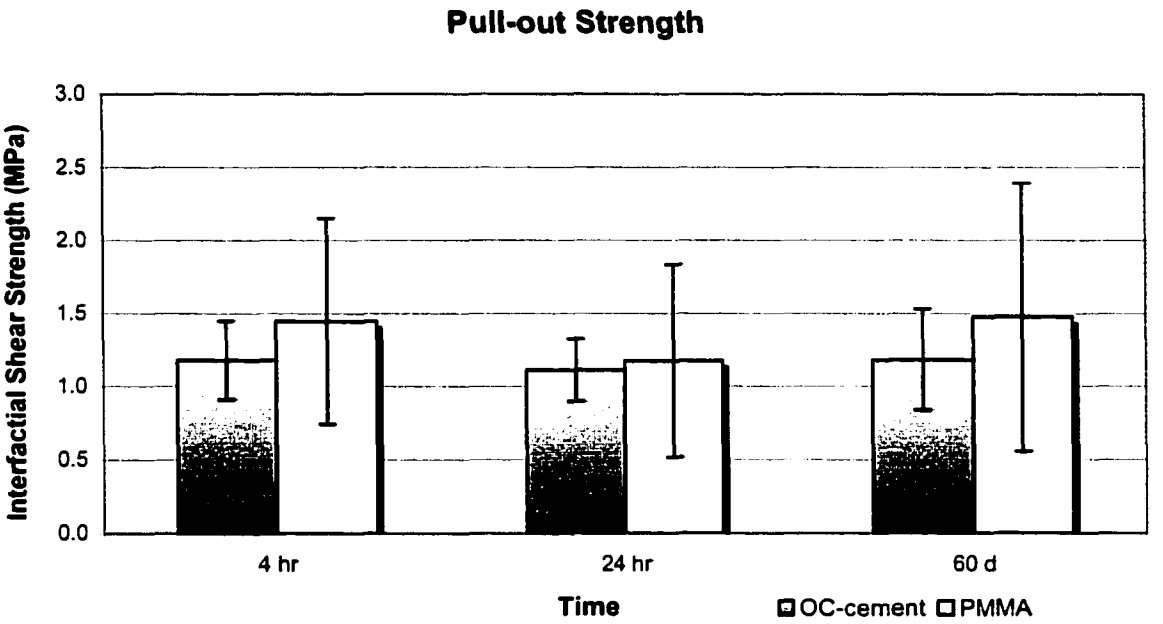

Figure 33. Interfacial shear strength of OC-cement and PMMA (mean ± standard deviation)

Force versus displacement was recorded during testing. Typical plots are shown in Figures 34 and 35. The initial portion of the graphs typically indicated a gradual increase in load as the fixture and specimen became firmly seated. This was followed by a linear segment that rapidly increased in load until failure. Failure was sometimes accompanied by an audible "pop". Following failure there was a dramatic reduction in load to a new level referred to as the residual load. This residual load continued to decline until the post was completely withdrawn. These were the general features of most plots. Differences where found in the shape of the graph following failure that appear related to cement type and aging time. For nearly all specimens the shape of the plot following failure was smooth as in Figure 34 or saw-toothed as in Figure 35 indicating "slip-stick" failure mechanism. Differences observed in the residual strength, width and height of saw-teeth are summarized in Table 25.

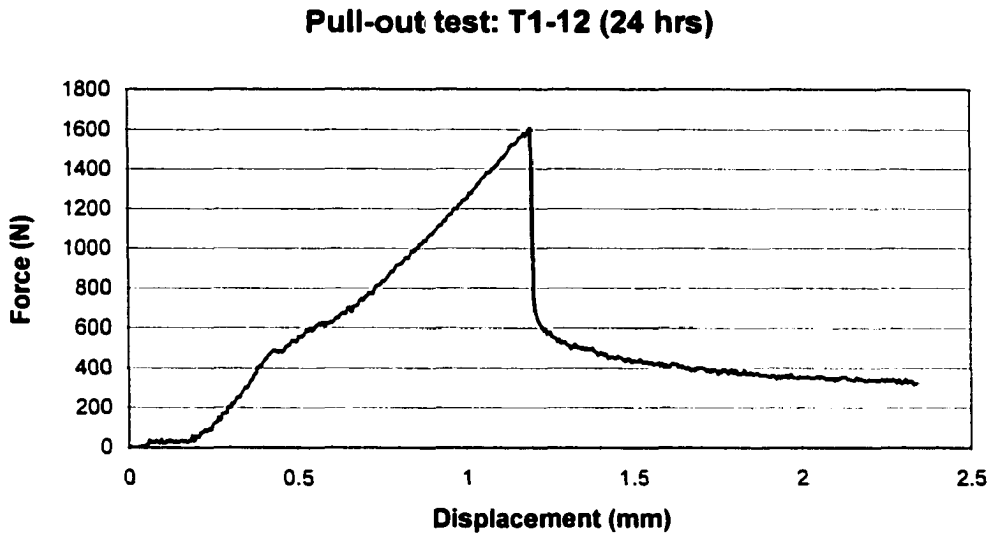

Figure 34. Typical force displacement graph with "normal" behavior following failure

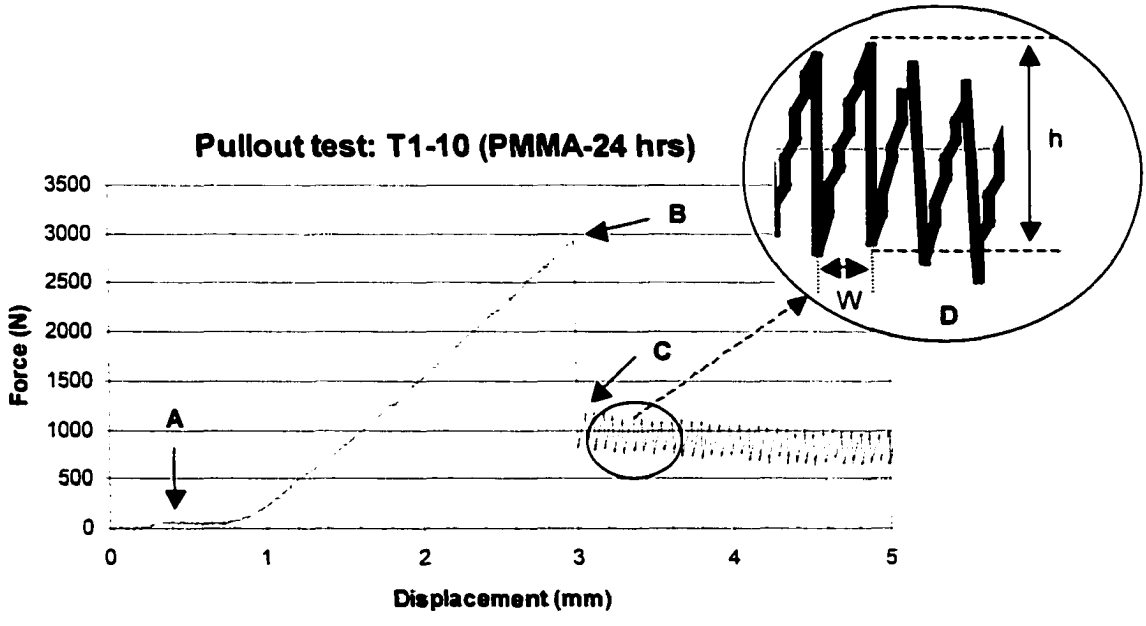

Figure 35. Typical force vs. displacement graph showing "slip-stick' behavior A) tightening of testing fixture and specimen B) maximum load at failure C) residual load after failure D) magnification of saw-tooth region: W - width of saw-tooth slip, h – height of saw-tooth slip

Overall, the residual loads for OC-cement at 4 and 24 hr were higher than for PMMA at 4 and 24 hr; 74 and 59% compared to 38 and 36%, respectively. "Slip-stick" failure occurred in all the OC-cement: 4 hr graphs, most PMMA: 4 hr and 24 hr graphs, and some OC-cement: 24 hr graphs. The average length moved during each slip was approximately 0.01 mm for OC-cement at 4 and 24 hr. Others have correlated the width of the saw-tooth to the distance between valleys of roughness on the metal posts (Beaumont et al., 1977). In the present research the width of the teeth appear of the same magnitude of the surface irregularities of the steel posts, but are more regular than the distance between the surface irregularities of the stainless steel posts. Furthermore, the variation of this distance between test groups indicates that factors beyond post surface features influence the distance moved per slip.

Table 25. Approximate values for residual load, h, and W

		OC-cement	*PMMA*
Avg. residual load (Percent of original load)	4 hr	74 %	38 %
	24 hr	59 %	36 %
	60 days	>95 %	15 %
H	4 hr	568 N	390 N
	24 hr	500 N	533 N
	60 days	<50 N	< 50 N
W	4 hr	.01 mm	.05
	24 hr	.01 mm	.075
	60 days	---	---

The shape of typical OC-cement: 60 days graphs displayed unique behavior following failure. The graphs were mountain-shaped and retained most of their interfacial shear strength after failure (Figure 36). The residual load gradually decreased from the maximum value as the post was pulled out. The mean values for ISS of OC-cement did not change over the 60 day test period. The initial ISS value is thought to be due to bonding and the residual load attributable to friction. The slight expansion that occurs in the OC-cement over time likely explains the increase observed in residual load in the 60 days specimens.

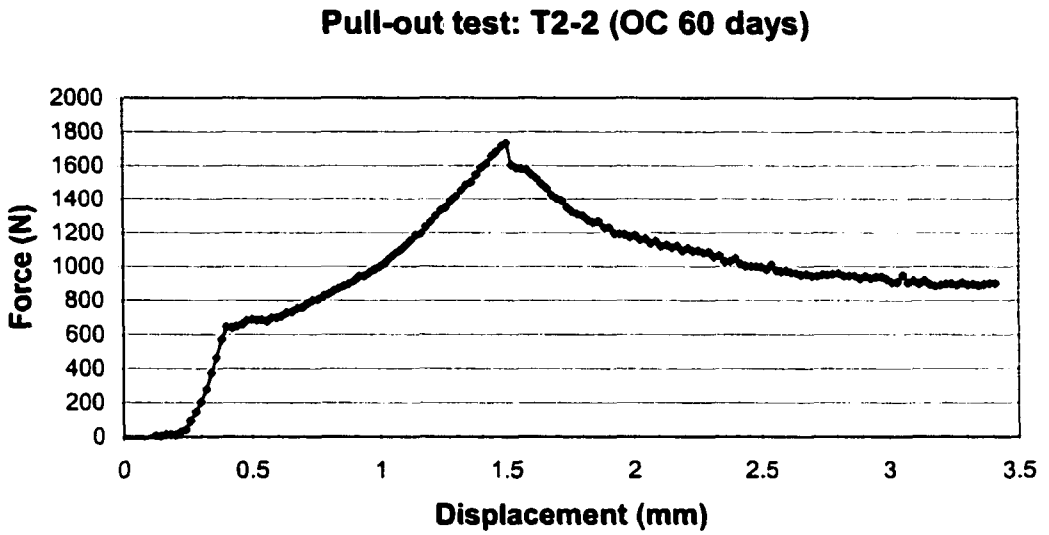

Figure 36. Force vs. displacement graph for OC-cement at 60 days

B. *In vivo* Testing

1. Implantation observations

The surgical procedure to implant the cement was demanding; skill in the formation of the defect and proper alignment of the reaming device were critical. If the reaming device was not in proper alignment, a hole could be created in the wall of the diaphysis of the femur through which cement was able to leave the femur and enter the soft tissue. Since PMMA was inserted under pressure any hole in the diaphysis resulted in a significant amount of PMMA outside of the femur. If possible, this cement was removed prior to closing the incision.

Initially the OC-cement was placed under vibration so that it could flow into the medullary canal. This approach proved problematic and resulted in the OC-cement mixing with blood or being inadvertently spread on the surrounding soft tissue, as in animal #6569. To avoid these complications, plugs of OC-cement paste were formed that were next slid into position. This technique was preferred and used throughout the remaining surgeries. Implantation using the "plug" technique was most successful when the size of the defect created closely matched the size of the

medullary canal. This allowed insertion of the largest possible size of cement plug and resulted in a better fill of the medullary canal.

Comments regarding the surgical procedure and observations regarding the animal after surgery are compiled in Appendix C. Fluoroscope images taken after implantation to confirm cement placement are compiled in Appendix D. OC-cement was innately radiopaque and easily visible on the images collected.

2. Post-surgery and recovery observations

All dogs recovered from surgery without complications. Animals typically began using their surgical leg immediately after surgery or within days. Full-weight bearing and normal use generally occurred within one week. Sutures were removed within two weeks of surgery. Blood was collected from select animals at various times post surgery. The bloodwork results presented in Appendix C did not indicate any abnormalities. All animals were taken outdoors for walks daily while housed at Iowa State University Laboratory Animal Resources. Observations regarding animal activity at the end of the experimental period are also given in Appendix C. Animals were healthy and active, aside from dog #6569. The incision on this animal started to drain after approximately 2 weeks and a drain was placed. This animal was lethargic during periods when its incision was draining and lost weight over the course of the study. It should be noted that during surgery on this animal, OC-cement mixed with blood and covered much of the soft tissue surrounding the incision site.

3. Post retrieval radiographs

Radiographs were collected on the femurs with implanted cement immediately after removal. Observations from the radiographs are compiled in Appendix E. From the radiographs the success of filling the intramedullary canal could be evaluated, as well as, any new bone formation.

With optimal conditions, it was possible to fill the intramedullary canal with OC-cement as shown in Figure 37. The cement was observed to remain in place and intact throughout the testing period. The cement implanted into animals #6652 and #6681 was fragmented in some locations. In animal #6652, the fragmented segment was outside of the bone. In both occurrences it is believed that the fragmentation occurred at the time of implantation and was a result of applying force to the

cement after the working time, but before the cement was completely set. Porosity was readily apparent in many PMMA cement specimens. Some porosity existed in OC-cement as well as a few defects created by the plunger used to slide the cement into the medullary canal. Also apparent in the radiographs were a fracture of the cement and diaphysis in #6587 and a defect in a section of cortical bone in #6640. Both conditions were held to be iatrogenic.

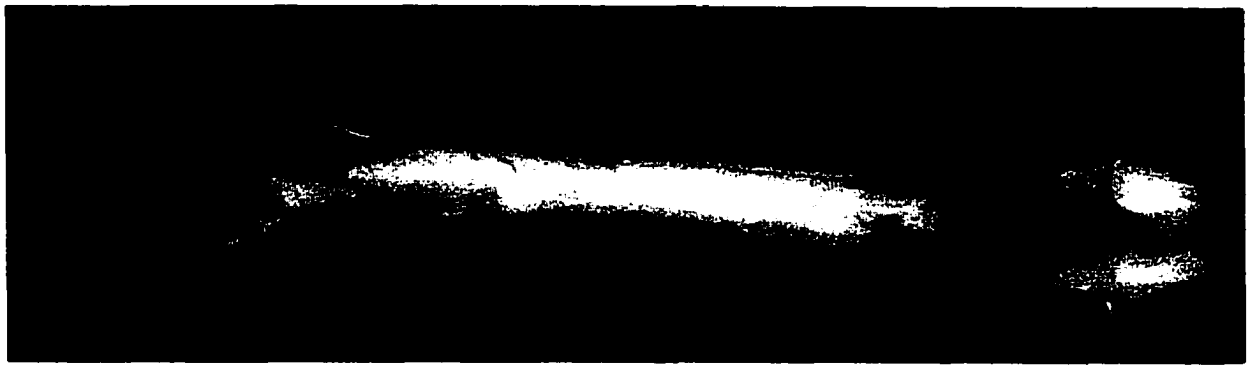

Figure 37. Radiograph of retrieved femur from # 6663, 12 wk after implantation

In the proposed application of using OC-cement for prosthesis anchoring in total joint replacement, it is common procedure to remove the head of the femur. If this procedure were used, access to the intramedullary canal, alignment and placement of the cement would be facilitated due to an improved physical approach and ease of creating a large entry to the medullary canal. Furthermore, insertion of a prosthesis into the cement would shift the cement outward and promote good contact between the bone and OC-cement.

4. Light microscopy

Tissue specimens from each experimental animal were qualitatively examined using light microscopy to evaluate the tissue that surrounded the implanted cement. In order to create paraffin embedded blocks that could be cut with a microtome, the specimens were decalcified after fixation. An extended decalcification period was necessary to soften or remove the OC-cement, while PMMA specimens were placed in acetone following the dehydration series to remove the poly(methyl-methacrylate) cement. It was possible to produce sections suitable for analysis using these

procedures; however, some sections, shattered when cut with the microtome and suitable sections could not be obtained. It is thought that the procedures for decalcification and cement removal led to these difficulties. Extreme attention must be exercised not to leave specimens in the decalcification or cement removing solutions past the end-point for these procedures.

Sections from cortical bone specimens proved more consistent than sections from cancellous bone specimens in regard to the defect created and contact between the bone and implanted cement. In light of this, the present analysis focuses primarily on sections prepared from cortical bone specimens. Since the cement had been removed, the implant-bone interface was no longer intact. Fibrous tissue growth between the cement and bone remained in the specimens, although sometimes it had pulled away slightly from the bone. Similarly, cement or cellular debris particles in the specimens remained intact adjacent to the lumen of the bone.

a). Cement-cortical bone sections

OC-cement 2 wk: No reaction was observed in the bone surrounding the implanted cement 2 weeks following implantation of OC-cement. Some cellular and cement debris was observed adjacent to the inner circumferential bone, but fibrous tissue was not observed (Figure 38-A).

OC-cement 6 wk: In specimens 6 weeks following implantation, some sections contained particulates from OC-cement, which were being walled off in #6656. Other sections were clean with no particles or fibrous tissue observed (#6661, Figure 38-B). Some lacunae appeared empty adjacent to the lumen and more osteocytes were observed as distance from the lumen increased. The bone was considered healthy and the scattered empty lacunae were thought to result from the trauma of the surgical procedure. Newly formed bone was found in the medullary canal several inches below the implanted cement in animal #6656 (Figure 38-A). The marrow cavities in this area appeared normal apart from some isolated areas where fibrous tissue and macrophages were present. The reason for this bone growth in the medullary canal is not understood.

OC-cement 12 wk: Cortical bone sections from 12 weeks (#6663) showed a similar reaction as at 6 weeks (Figure 38-C). Apart from some cement and cellular debris, the sections were clean and showed no fibrous tissue formation. Similarly, the number of osteocytes in the inner

circumferential bone may have been fewer than in outer regions of the bone, still the bone was considered healthy (Figure 40-A).

PMMA 2 wk: Osteoclasts and the beginning of fibrous tissue formation were observed between the bone and implanted cement 2 weeks after implantation (Figure 39-A). Osteocytes were present throughout the cortical bone. Along the exterior edge of the cortical bone, periosteal remodeling and growth were observed as well as fibrosis.

PMMA 6 wk: A thin band of fibrous tissue, usually continuous, was observed around the lumen of the cortical bone (Figure 39-B). Some granulation tissue was also observed, but the bone under the fibrous tissue was normal. As in PMMA 2 wk specimens, remodeling and growth were observed along the outer edge of the cortical bone.

PMMA 12 wk: A thicker, irregular band of fibrous tissue was observed with mature connective tissue at 12 weeks (Figure 39-C). A thin area of necrosis of bone was observed in bone in contact with fibrous tissue in #6615. The underlying bone was mature and healthy. Sections from #6640 showed osteomylitis extending into the marrow cavity. The defect in the cortical bone was filled in by connective tissue. Neutrophil reaction, macrophages, plasma cells, and blood vessels were observed as well as acute/chronic inflammatory cells and fibrous tissue formation between the cement and bone.

b). Cement-cancellous bone sections

Evaluation of cancellous bone sections was more complicated due to variations in bone structure and cement filling. Bone fragments resulting from the formation of the surgical defect were found in the cancellous bone around the defect site. PMMA cement frequently penetrated deeply into the cavities of the cancellous bone structure while OC-cement may or may not completely fill the defect that was created. The outer band of OC-cement in this area had generally mixed with some blood and particles of cement at times had washed out and were observed in adjacent marrow cavities of the cancellous bone.

PMMA: The response to PMMA cement in cancellous bone was consistent with results in cortical bone. A fibrous tissue was typically observed between the PMMA cement and cancellous bone (Figure 40-B). Heat-induced necrosis was less prominent in the cancellous bone sections.

OC-cement: In cancellous bone, no response was observed in the 2 wk specimens (#6740) while in section (#6673) inflammation, necrosis, and minimal fibrous tissue formation were noted (Figure 41-B, C). Sections at 6 weeks showed normal bone. Bony spicule fragments had not yet been removed and appeared there to stay. Marrow appeared normal and occasional giant cells were observed. At 12 weeks the inflammation was generally minimal, osteoid was being laid down adjacent to the cement in places, but had not yet calcified. A band of fibrous connective tissue formed in some locations, but was not complete. Figure 40-C shows an adjacent cancellous cell filling with collagen and fibroblasts (#6656). In #6681, cement particles had spread through many cancellous cells and bone fragments had not yet been removed. Macrophages were observed surrounding cement particles, while no reaction was noted in other areas. In summary, the reaction of OC-cement in cancellous bone depends greatly on how successfully the cement was implanted. The presence of OC-cement particles in cancellous bone tended to initiate fibrous tissue formation, as would be expected for most known biomaterials in particle form. Fibrous tissue formation would also be anticipated around any implant that was not securely placed and allowed movement. Reaction of cancellous bone to OC-cement appeared delayed at times as cellular and cement debris as well as dead bone fragments had not yet been removed. Additional analysis is recommended to better understand the tissue response to OC-cement in cancellous bone.

c). Lymph tissue

Popliteal lymph nodes were retrieved from animals #6669, 6740, 6746, 6596, 6569, and 6681. Analysis of the lymph nodes revealed reactive lymph nodes with prominent follicles and active germinal centers. The paracortical and medullary zones contained increased numbers of plasma cells. The sinusoids were infiltrated by plasma cells and hemosiderin-laden macrophages. No particulate materials or bacteria were observed in the lymph node sections. This response is considered a normal reaction to hemorrhage induced by the surgical procedure.

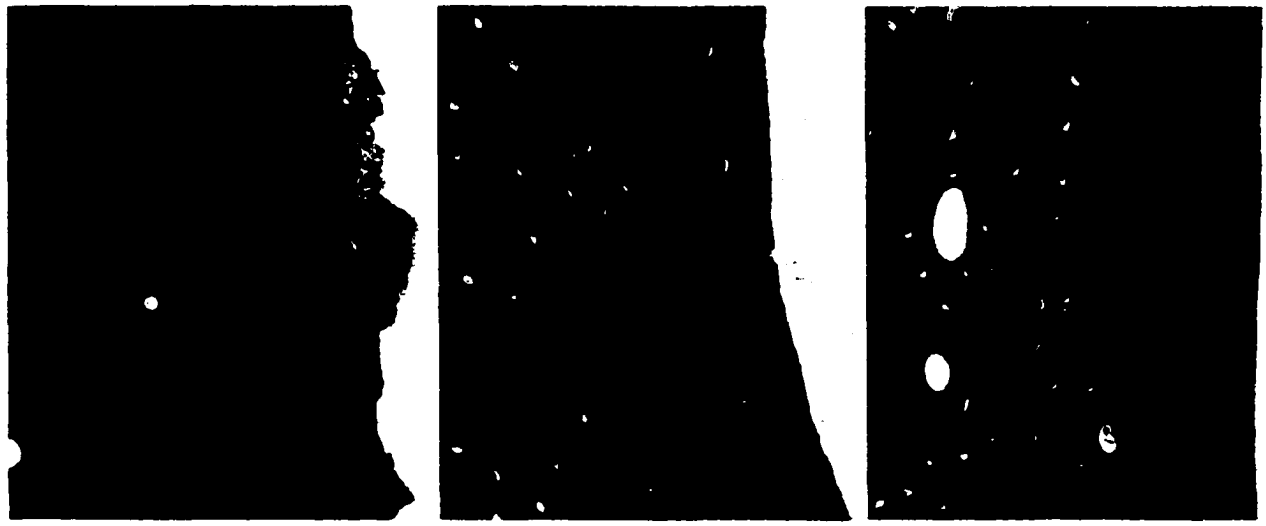

Figure 38. Light micrographs of decalcified cortical bone sections from OC-cement groups, H&E stain, x 40: A) 2 wk (#6673) B) 6 wk (#6661) C) 12 wk (#6663) * indicates cellular and cement debris. Sections were typically free of fibrous tissue and clean as shown in B and C or contained a layer of cement and cellular debris as in A.

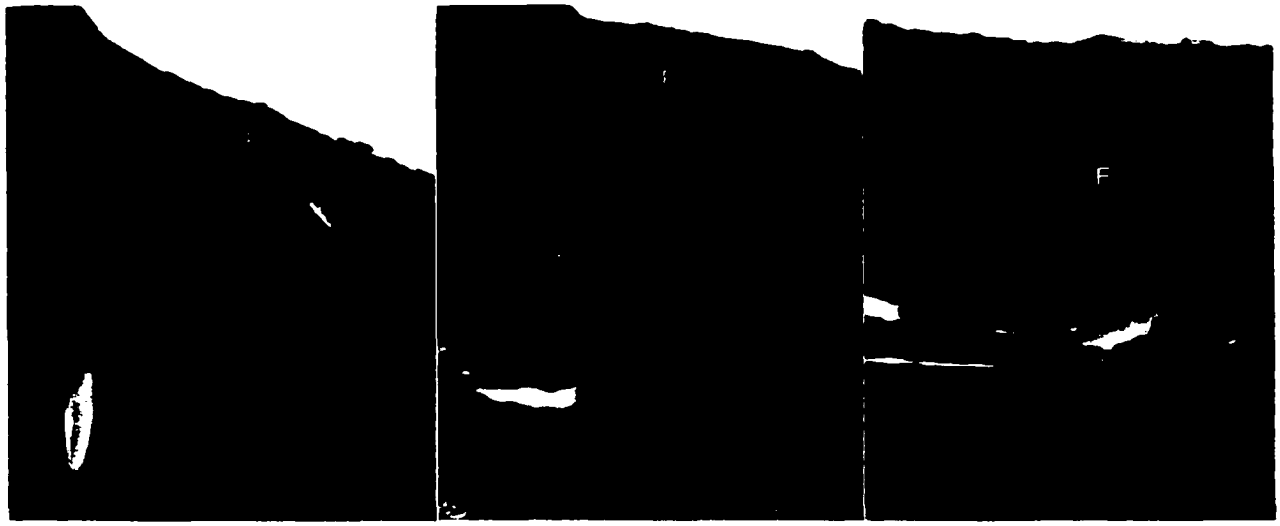

Figure 39. Light micrographs of decalcified cortical bone sections from PMMA cement groups, H&E stain, x 40: A) 2 wk (#6629) B) 6 wk (#6657) C) 12 wk (#6615), F indicates fibrous tissue formation. A layer of fibrous tissue was typically observed around the lumen of the cortical bone sections. In general, the thickness of the fibrous tissue increased over the testing period.

Figure 40. Light micrographs of decalcified bone sections, H&E stain: A) cortical bone-OC-cement section (#6663), x 40, showing osteocytes (O) in lacunae adjacent to the cement at 12 wk B) cancellous bone-PMMA cement section at 12 wk (#6587), x 40, showing trabeculae (T) with scalloped edges on the left, indicative of bone resorption, and a band of fibrous tissue separating the bone from implanted cement. Normal marrow cavity (MC) is present on the right side of the trabeculae C) cancellous bone-OC-cement section (6656) 6 wk, x 40, trabeculae in contact with cement cavity on the upper edge showing no reaction in contact with OC-cement. The nearby marrow cavity filled with collagenous soft tissue (ST) and fibroblasts

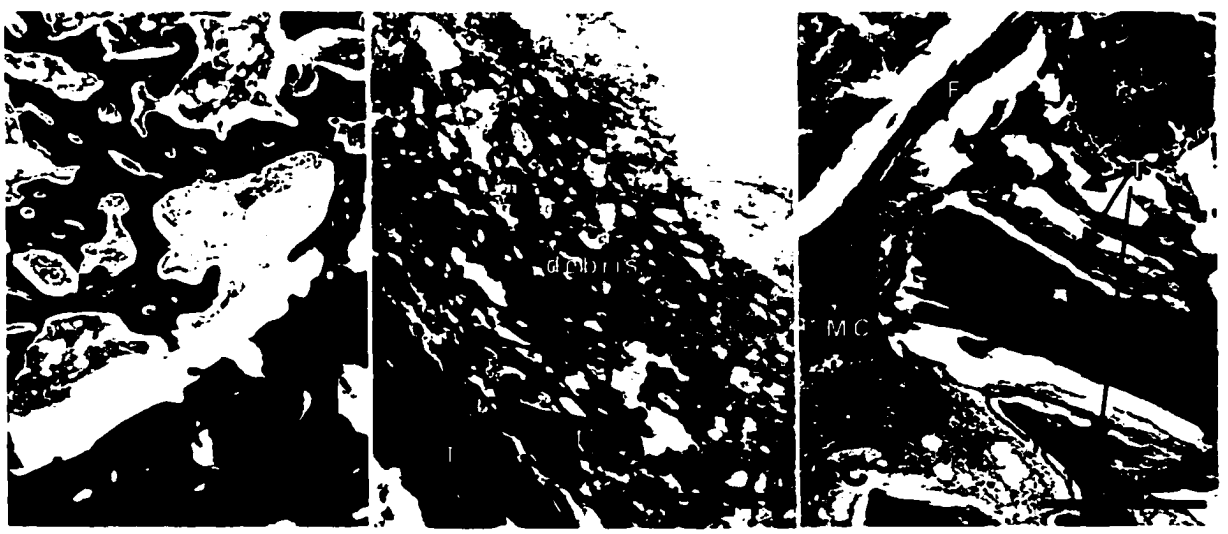

Figure 41. Light micrographs of decalcified bone sections: A) cortical bone-OC-cement section (#6569), Gomori's stain, x 5, showing new bone growth in the medullary canal at 6 wk B) cancellous bone-OC-cement section (#6740) 2 wk, Gomori's stain, x 40, cement and cellular debris adjacent to a trabeculae, but no reaction C) cancellous bone-OC-cement section (#6673) 2 wk, H & E stain, x 10, cement and cellular debris (*), thin band of fibrous tissue (F), and osteoclasts eroding bony spicules, (T) indicates trabeculae, and (MC) identifies the marrow cavity

5. Fluorescence microscopy

Fluorescence microscopy was used to qualitatively assess the amount and location of fluorescent bone labels around the implant and throughout the cement-bone specimen. All animals in the 6 and 12 wk groups received bone labels. Typically, at least one specimen from cortical bone and one specimen from cancellous bone were evaluated from each animal. A table summarizing the observations for each specimen is given in Appendix G.

OC-cement 6 wk: Specimens containing OC-cement characteristically showed a very, thin incomplete or thin continuous band of growth at the periosteum at 6 weeks (Figure 42-A, B, C). Growth and remodeling of haversian systems were prevalent throughout the cortical bone. However, very little growth was observed in direct contact with the cement at the cement-bone interface (Figure 42-D, E). In specimens from cancellous bone, growth and remodeling were active throughout the bone and occasionally in direct contact to the cement. There was often a band of cellular and cement debris separating the cement and bone. In these instances, bone activity was observed at the bone-debris interface. A soft tissue layer between the implanted cement plug and surrounding bone was observed in #6698-3b. In animal #6569, growth of new bone was observed in the medullary canal below the area where the cement had been implanted (Figure 42-F). A portion of the cement was placed outside the bone in animal #6698; no bone growth was observed surrounding this portion of the cement.

PMMA 6 wk: In PMMA specimens at 6 weeks, a thicker, irregular, complete band of growth occurred at the periosteum (Figure 43-A, B, C). Throughout the whole of the cortical bone, less mineralization was observed compared to the OC-cement specimens. Short, thin lines of growth were observed near the cement-bone on #6649-5b and 6657-6a (Figure 43-D). In cancellous bone specimens, an irregular band of growth was generally observed at the periosteum, as in the cortical specimens. Where cement had infiltrated deeply into the marrow cavities of the cancellous bone, mineralization activity was sometimes observed in direct contact with the bone. Bone mineralization activity decreased with increased proximity to the central plug of cement (Figure 43-E). Although there was some activity at the cement-bone interface, it was usually separated by soft tissue.

OC-cement 12 wk: Thin rings of growth were observed at the periosteum of cortical bone in #6652 and 6663-5a, while specimens #6662 and 6681 displayed very little periosteal bone growth (Figure 44-B, C). Mineralization activity was observed throughout the cortical bone for all specimens. Generally, no activity was observed in direct contact with the cement, however, #6652 and 6662 did show small areas with mineralization activity adjacent to cement (Figure 44-D, E, F). In cancellous bone, a thin band of growth around the periosteal bone was found in specimens #6662-4c and 6663-4. Growth and remodeling was observed throughout cancellous bone (Figure 44-A). In #6681-4b and 6663-4 small areas were observed with bone growth in direct contact to cement. In specimens where there was no direct contact between bone and implanted cement (#6652 and 6662-4), soft tissue formed in the gap and bone mineralization activity was observed adjacent to the soft tissue. As in the 6 wk specimens, when the cement was placed outside the bone in soft tissue, no bone mineralization was observed.

PMMA 12 wk: The right femur and implanted cement fractured in animal #6587. Before this occurred, a ring of growth near the original periosteum was observed. Following the fracture, a massive, mineralized callus around the exterior of the bone was formed for stabilization. Little growth was observed throughout the original cortical bone, but active mineralization was observed throughout cancellous bone. Soft tissue separated the bone and cement in cancellous and cortical bone. A portion of the cortical bone was missing from the femur in animal #6640; this defect is thought to have occurred during surgery. The gap created was filled in with soft tissue. The remaining cortical bone showed a large amount mineralization and the cortical wall had thickened significantly. Specimens from the final animal in this group displayed a band of bone growth of medium thickness emanating from the periosteum in the cortical bone specimen and a thin, irregular band of growth at the periosteum in the cancellous bone specimen. Bone mineralization was observed throughout the cortical and cancellous bone. A very thin line of growth was observed around 80-90% of bone surrounding implanted cement. Soft tissue was present between the cement and bone in all specimens in this group.

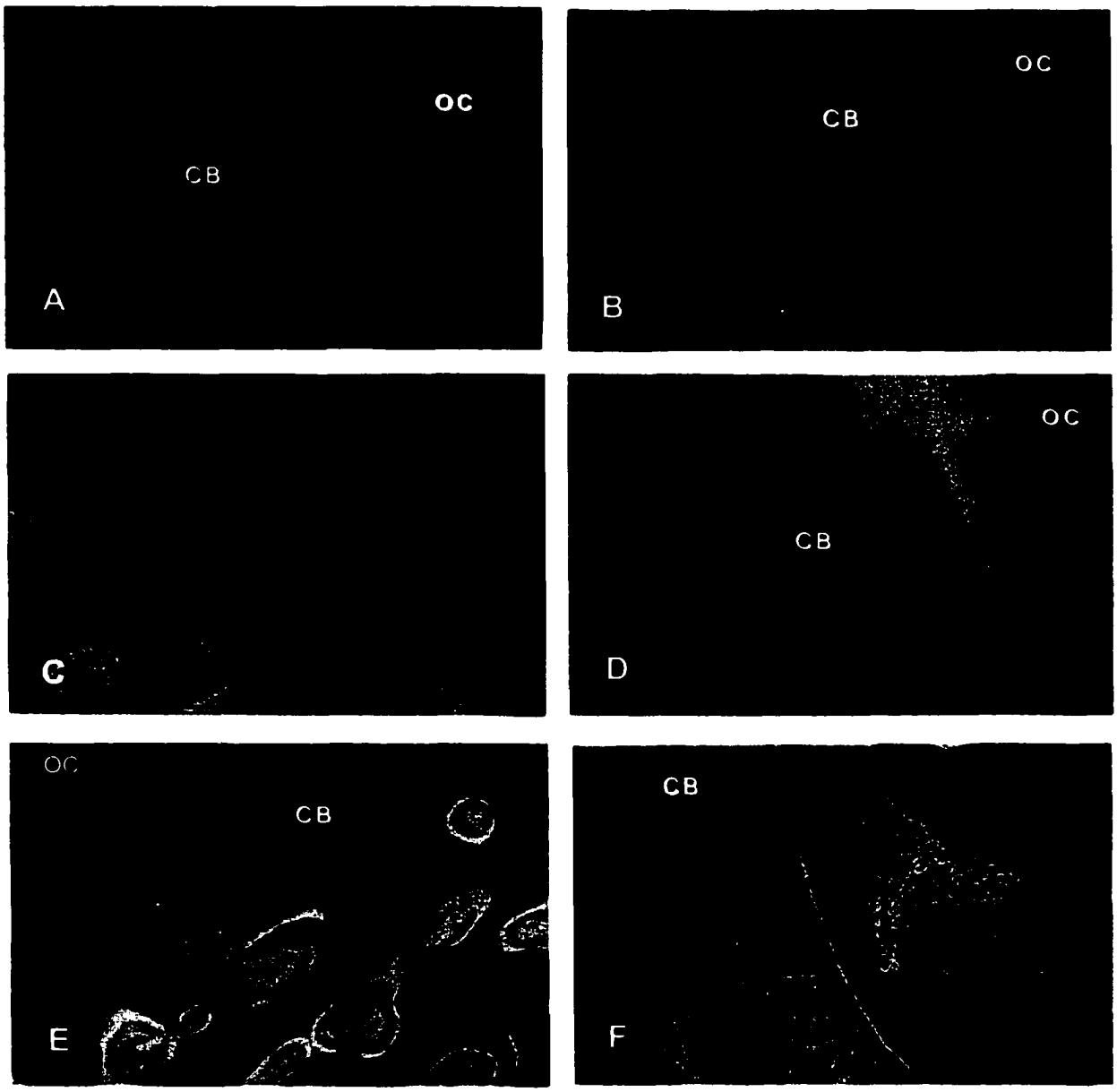

Figure 42. Fluorescence photomicrographs of OC-cement- bone specimens at 6 wk, cortical bone is labeled CB and the implanted cement labeled OC: A) #6661-5c, x 3.125, mineralization throughout cortical bone B) #6656-6b, x 3.125 C) #6661-4, x 25, mineralization of small band at the periosteum and in the remodeling of haversian systems in cortical bone D) #6661-5, x 25, thin line of fluorescence adjacent to cement E) #6661-5, x 25, remodeling of haversian systems close to implanted cement F) #6569-5a, x 1.6, growth of bone in the intramedullary canal below area with implanted cement

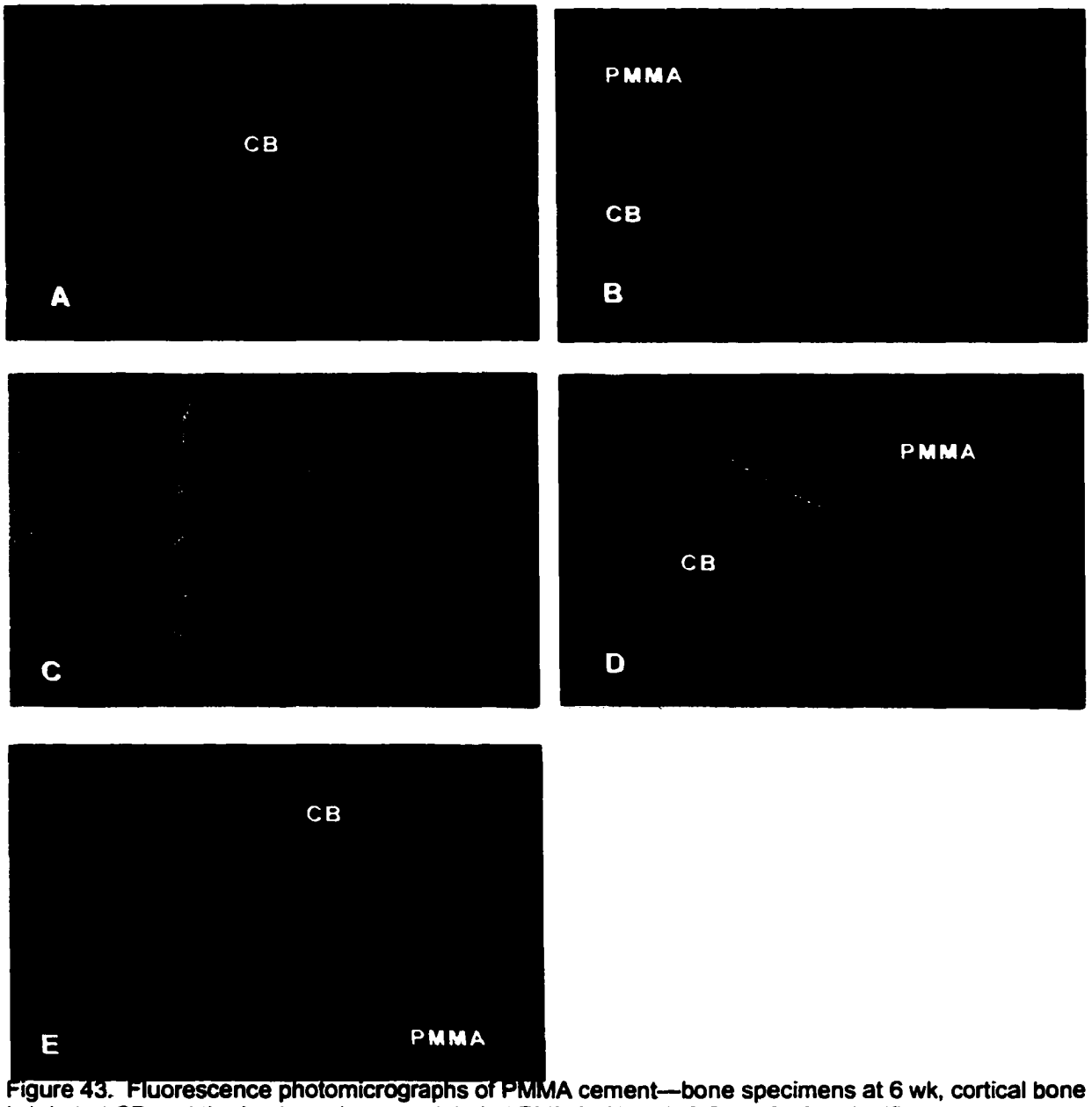

Figure 43. Fluorescence photomicrographs of PMMA cement—bone specimens at 6 wk, cortical bone is labeled CB and the implanted cement labeled PMMA: A) #6649-5b, x 3.125, significant growth at the periosteum. Little growth through-out original cortical bone B) #6657-6c, x 1.6 C) #6657-6b, x 25, close-up of bone at outer edge D) #6649-5b, x 25, thin line of mineralization adjacent to PMMA cement E) #6596-4c, x 3.125, mineralization in outer regions of cortical bone

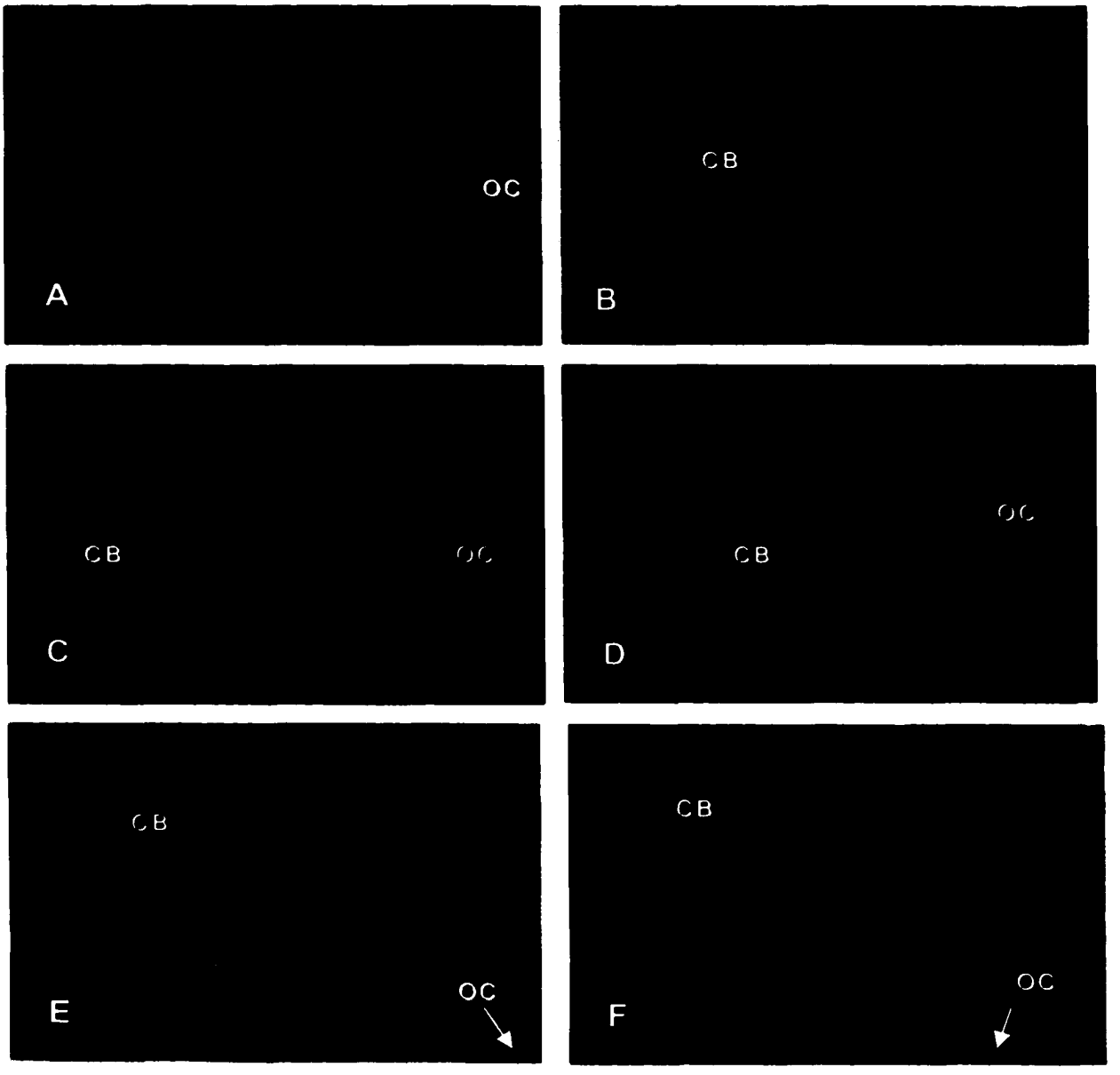

Figure 44. Fluorescence photomicrographs of OC-cement-bone specimens at 12 wk, cortical bone is labeled CB and the implanted cement OC: A) #6663-4a, x 1.6, mineralization throughout cancellous bone B) #6681-6b, x 25, mineralization near periosteum C) #6681-7c, x 3.125, mineralization throughout cortical bone D) #6663-5a, x 3.125, mineralization throughout cortical bone E) #6663-5n, x 25, close-up of osteonal systems near cement F) #6663-5a, x 12.5, osteonal systems near medullary canal

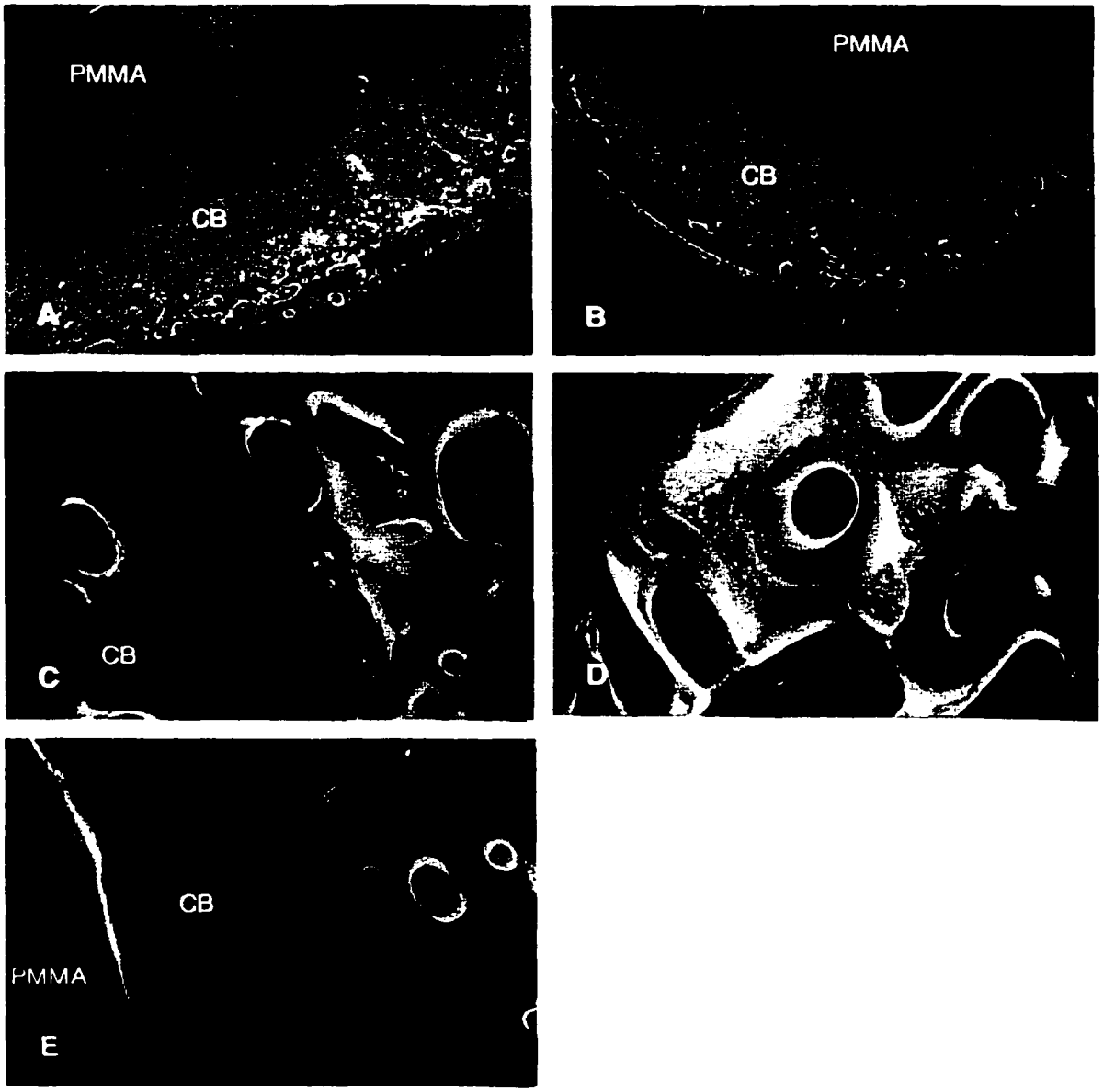

Figure 45. Fluorescence photomicrographs of PMMA cement-bone specimens at 12 wk, cortical bone is labeled CF and the implanted cement labeled PMMA: A) #6615-4b, x 1.6, mineralization around outer edge of bone B) #6615-5nc, x 1.6 C) #6587-5b,x 25, close up of region showing cortical bone-ring of outer growth interface D) #6615-5nc, x 25, close-up of new bone along the outer edge of the cortical bone E) #6615-5nc, x 25, cortical bone showing a thin line of mineralization along the endosteum

6. Microradiography

Microradiographs of polished, thick sections of specimens from cancellous and cortical bone and a summary of observations are compiled in Appendix F. Qualitative evaluation assessed bone structure, mineral density, and if applicable, the thickness of the gap between the bone and cement.

Contingent on successful placement of OC-cement, the microradiographs showed good contact between OC-cement and cortical bone with no gap detected as illustrated in Figure 46. Bone surrounding the implanted cement appeared normal and a thin band of periosteal bone growth was typically observed. In cancellous bone, OC-cement penetrated very little if at all into the surrounding marrow cavities as shown in Figure 47. The trabeculae surrounding the implant appeared normal and remained in direct contact with the cement. Very little periosteal bone growth was observed in cancellous bone implanted with OC-cement. No differences based on implantation time were observed for these specimens.

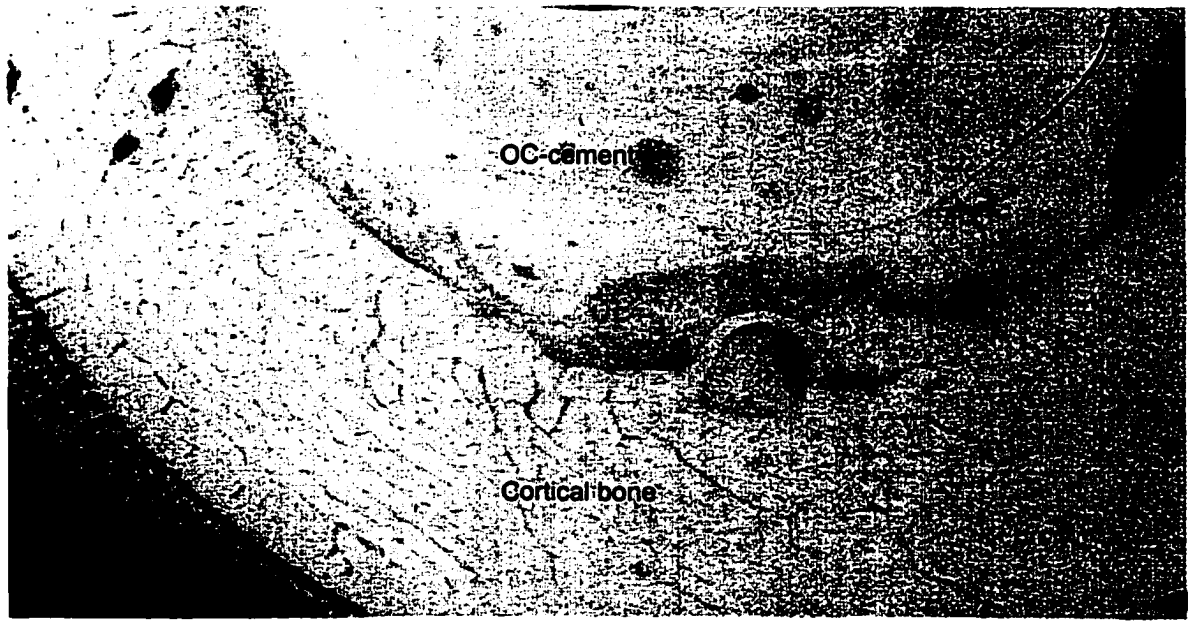

Figure 46. Close-up microradiograph of OC-cement (#6746-2 wk)

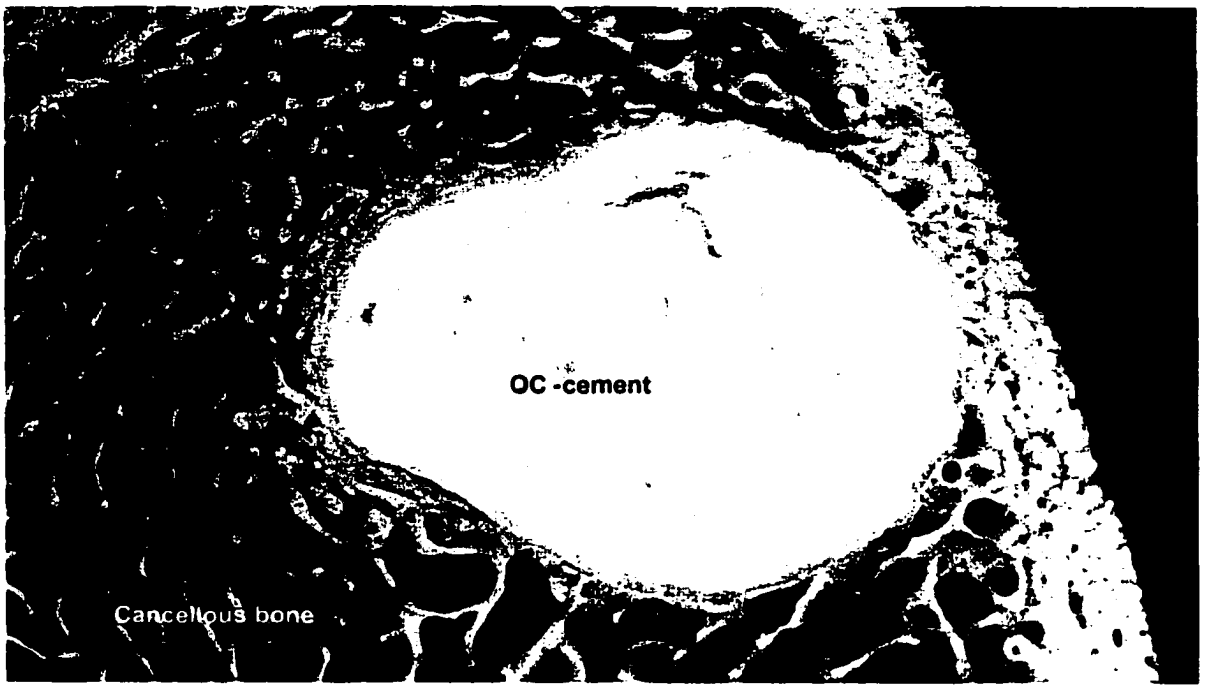

Figure 47. Microradiograph of OC-cement in cancellous bone (#6656-6 wk)

Representative microradiographs for PMMA cement in cancellous and cortical bone are displayed in Figure 48. Analysis of control specimens found that the PMMA cement frequently penetrated deeply into the marrow cavities of cancellous bone during placement (Figure 48-A). A gap between the bone and cement was present in all samples, and was not found to change in thickness over the time-period studied. Periosteal bone growth was observed in both cancellous and cortical specimens at 2 weeks. Mineralization of the periosteal bone continued in the 6 and 12 wk specimens. The periosteal growth was much more prevalent in PMMA specimens as compared to OC-cement specimens. This growth is believed to be induced by tissue necrosis caused by the exothermic setting reaction of the PMMA cement.

Anomalous microradiographs from PMMA sections occurred in animals #6587 and #6640, both euthanized at 12 weeks. Animal #6587 had fractured the right femur and implanted cement. Although the exact time of the fracture is not known, a band of initial periosteal bone growth is observed that was later surrounded by an immense callus formation. Animal #6640 was missing a

section of cortical bone. From intraoperative fluoroscope images, it is evident that a defect was created in the diaphysis through which a large amount of PMMA cement was unintentionally placed outside of the femur. After the cement had hardened, the exterior portion was removed. It is unclear whether the bone defect evident in the microradiograph was due solely to the surgical defect created or if bone resorption occurred in response to heat necrosis from the polymerization of the cement. An extensive callus has formed around the remaining $^{2}/_{3}$ to ¾ of the cortical bone.

Also of interest is the intramedullary surface of the cortical bone sections. As the microradiographs demonstrate, the medullary canal is not perfectly elliptical in shape and the bone surface can contain small irregularities in shape. The effect of these small protrusions of bone and conversely the intrusions of cement into the bone on the strength of the bone-cement interface will be discussed in more detail in the later cement-bone interfacial strength section.

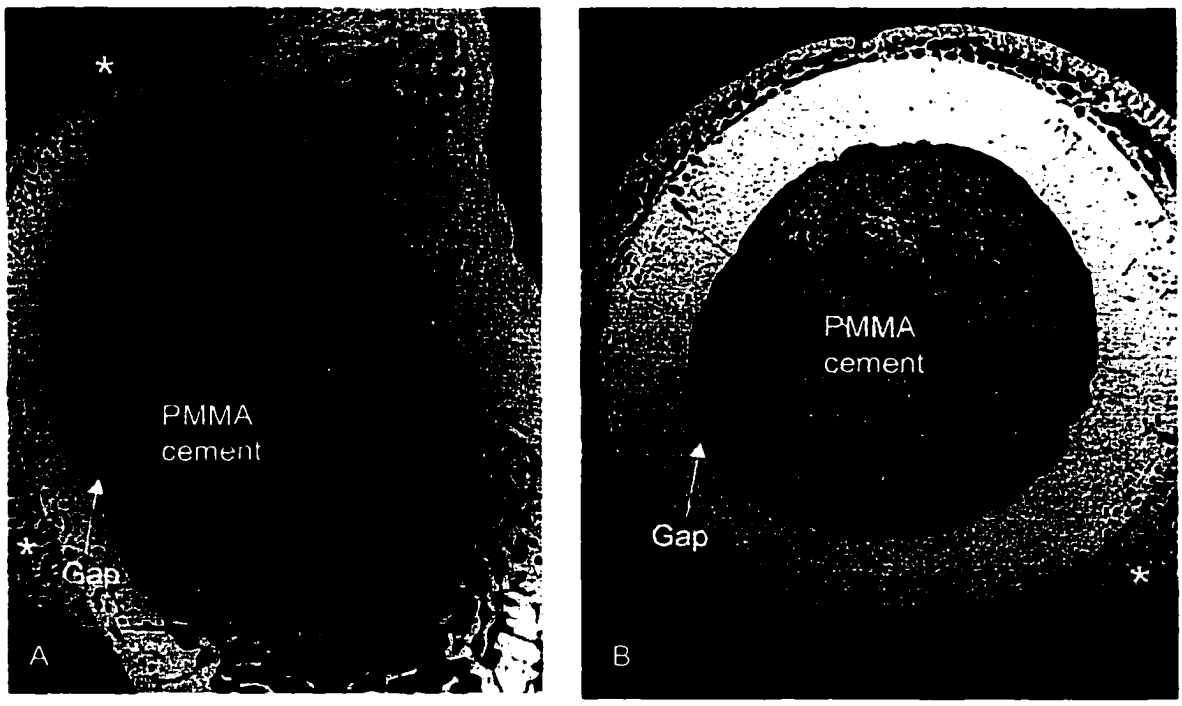

Figure 48. Microradiographs of PMMA specimens: A) Cancellous bone (#6649- 6 wk), B) Cortical bone (#6657- 6 wk), * Indicate areas of periosteal bone growth.

7. Scanning electron microscopy analysis

Polished bone-cement specimens previously used for fluorescent microscopy and microradiography were analyzed using scanning electron microscopy (SEM) with x-ray analysis and elemental mapping. The implanted OC-cement was found to contain a calcium aluminate chloride phase as well as discreet particles of calcium phosphate and calcium aluminate (Figures 49, 50 and 51). The energy dispersive spectrum confirmed the presence of calcium, phosphate, aluminum, chlorine and oxygen. Additionally, carbon was identified in the OC-cement indicating that the Spurr's resin had infiltrated some pores of the cement, confirming a porous pathway whereby calcium phosphate could be leached from the cement to promote bone growth. Figure 49 demonstrates direct contact between OC-cement and bone 2 weeks after implantation. The line scans shown in Figures 50 and 51 illustrate the differences in elemental composition in bone, hydrated cement, calcium phosphate, and unhydrated calcium aluminate. Compositional mapping of the area displayed in Figure 49 did not reveal any variation in the composition of phases at the interface surfaces of the OC-cement or bone (Figure 52).

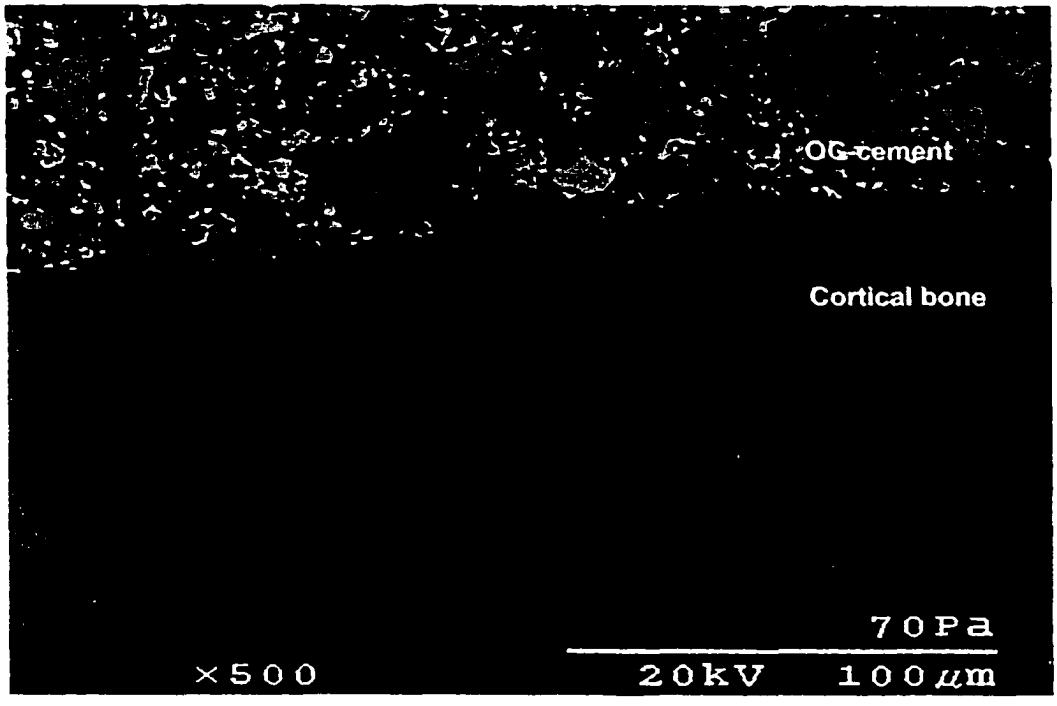

Figure 49. Scanning electron micrograph of OC-cement 2 wk (#6673)

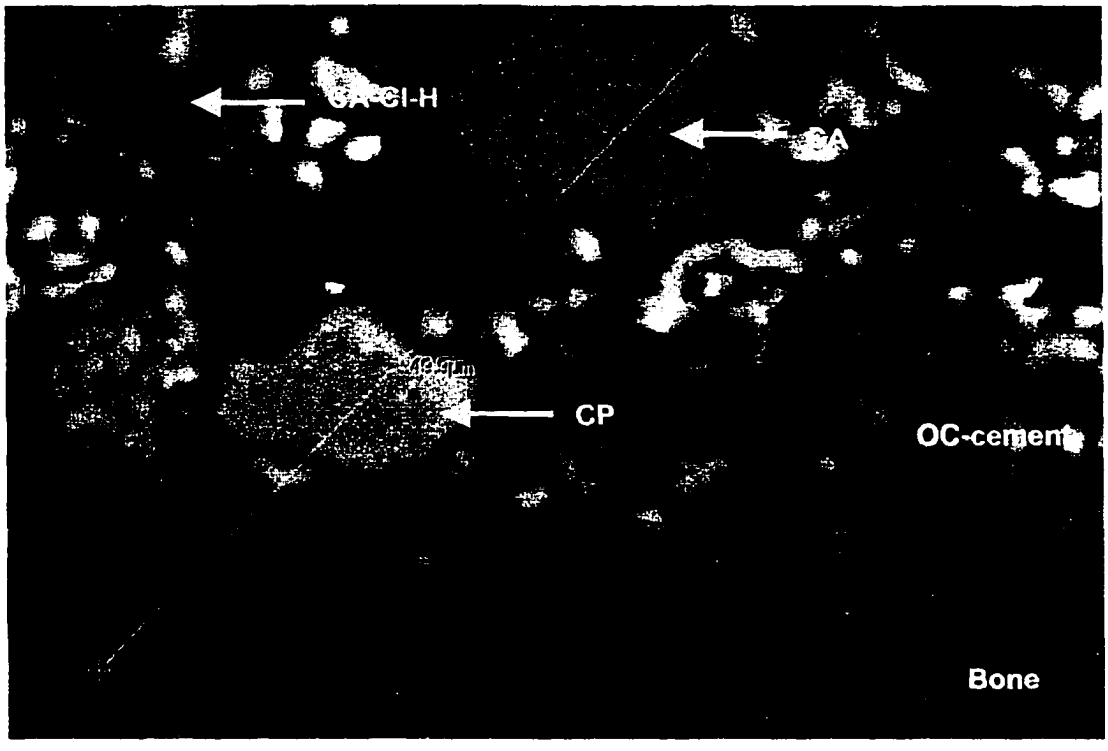

Figure 50. Scanning electron micrograph of OC-cement 2 wk (#6673) showing line scan
CA = calcium aluminate, CP = calcium phosphate, CA-Cl-H = calcium aluminate chloride hydrate

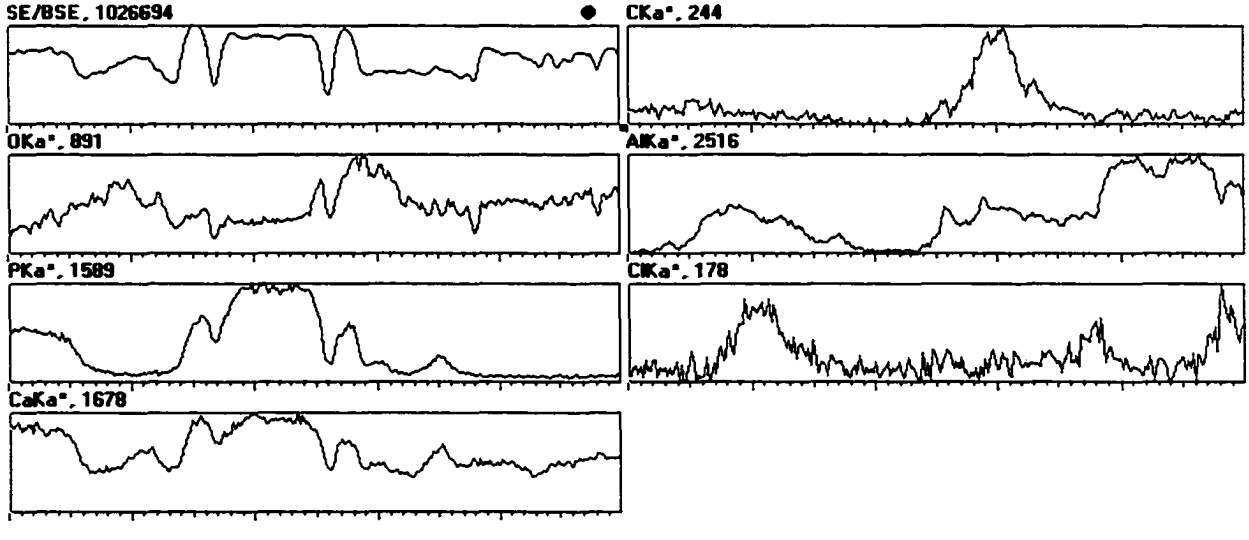

Figure 51. Line scans of C, O, P, Al, Cl, and Ca corresponding to the line indicated on Figure 25 (OC-cement 2 wk #6673)

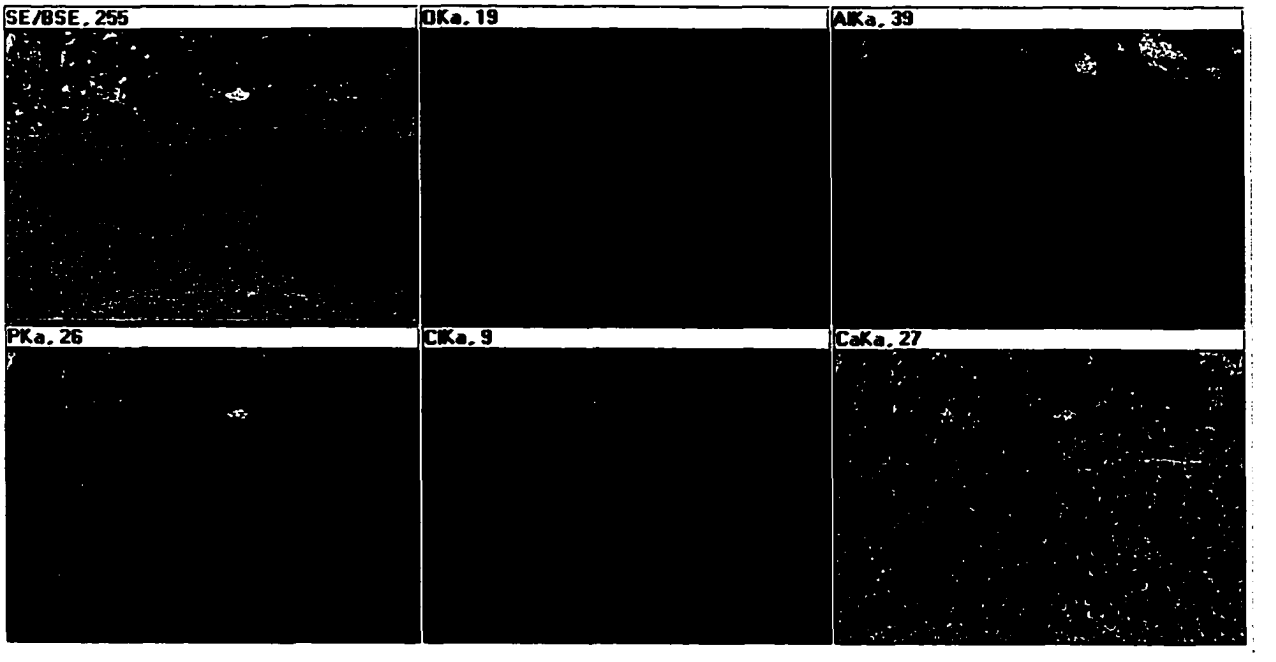

Figure 52. Scanning electron micrograph and compositional mapping of OC-cement 2 wk (#6673)

Similarly, a scanning electron micrograph of an OC-cement specimen that had been implanted for 12 weeks is shown Figure 53. In this specimen, the cracking was an artifact that occurred in processing. Compositional maps in Figures 54 and 55 show the distribution of calcium, phosphorus, chlorine, oxygen, and aluminum in the sample. Variations in composition naturally exist throughout a sample of OC-cement. Analysis did not find evidence of leaching of any elements from the cement surface at 12 weeks.

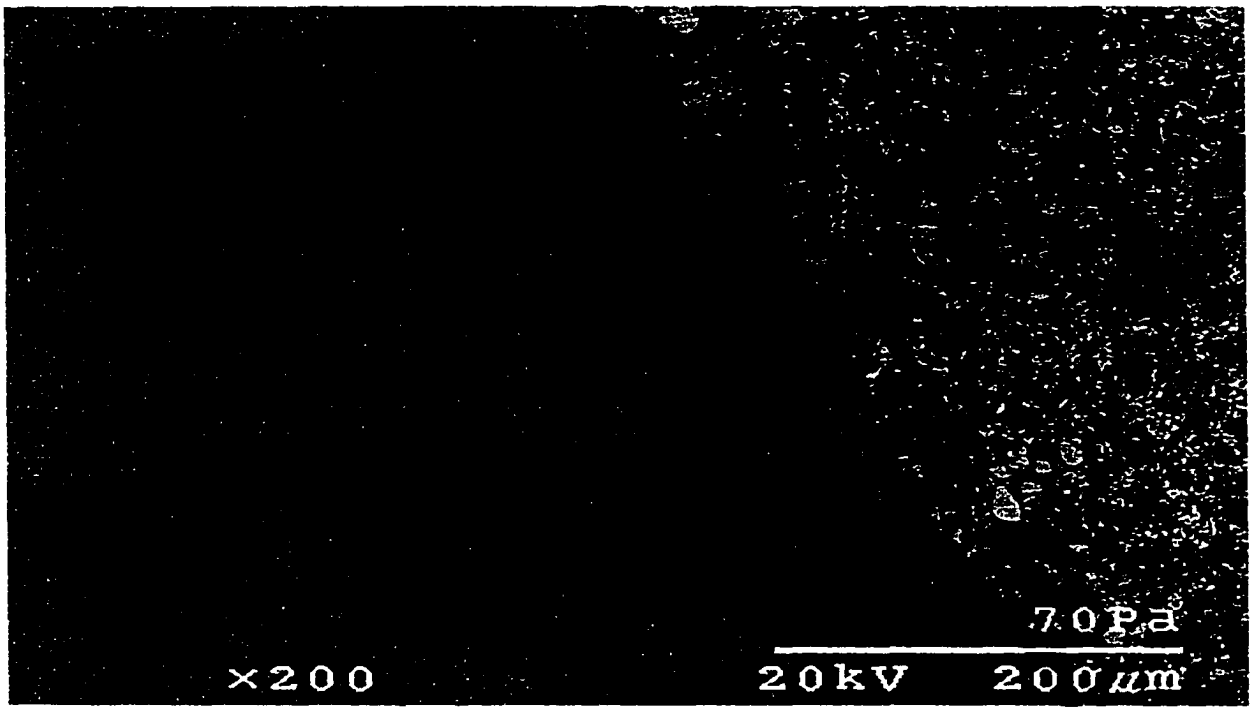

Figure 53. Scanning electron micrograph OC-cement 12 wk (#6663)

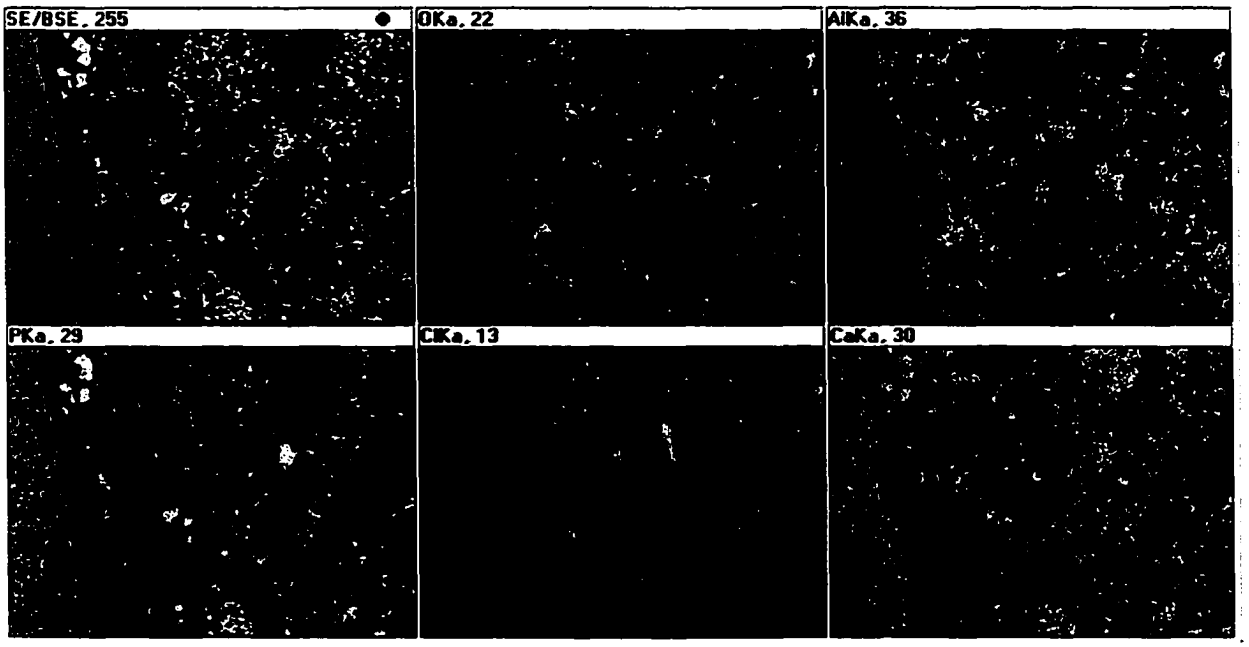

Figure 54. Scanning electron micrograph and compositional map of OC-cement 12 wk at 500x (#6663)

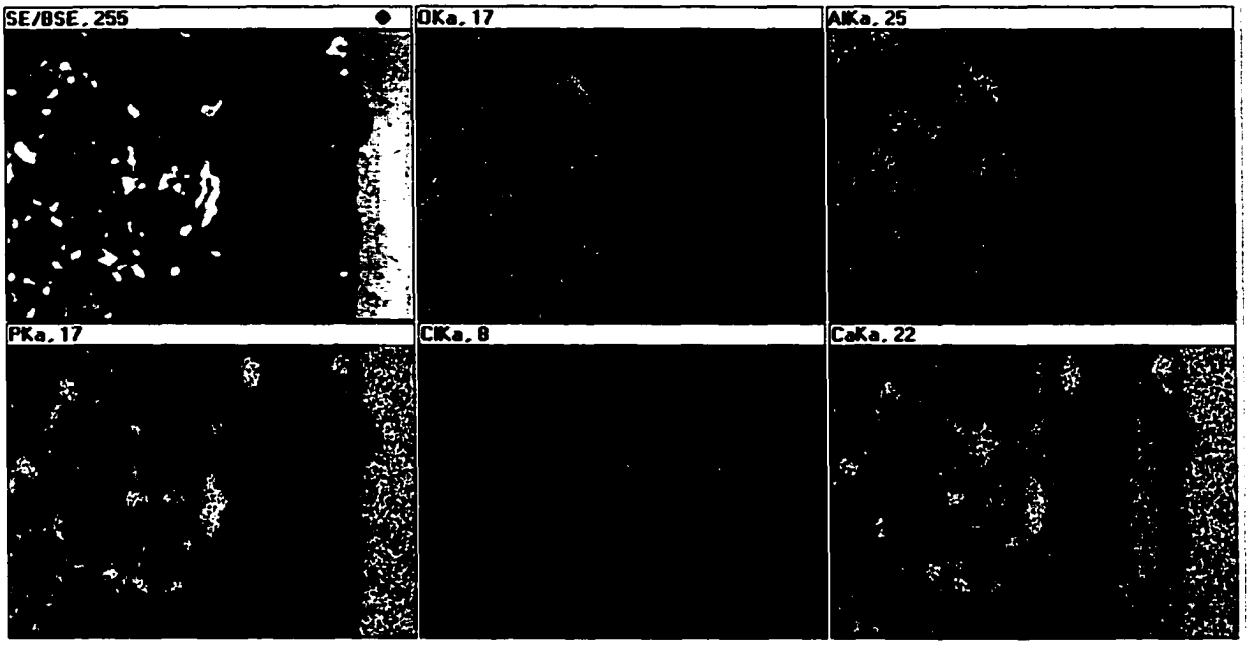

Figure 55. Scanning electron micrograph and compositional mapping of OC-cement 12 wk, 2000x (#6663)

8. Mechanical testing of cement-bone interface

Results from push-out tests of cement from cortical bone after 2, 6, and 12 weeks of implantation in the canine femur are presented in Tables 26 and 27 for OC-cement and PMMA cement, respectively. Full data is given in Appendix I and a summary is presented in Figure 56. The average push-out strength that was calculated for each experimental femur as well as the overall average for all specimens in the given cement type-time group are given. The overall mean push-out strengths for OC-cement were 3.93±2.39, 3.30±1.34, and 2.70±1.28 MPa at 2, 6, and 12 weeks. For PMMA cement, the overall mean push-out strengths were 0.46±1.27, 0.52±0.42, and 0.54±0.65 MPa at 2, 6, and 12 weeks. The experiment was designed to have each femur filled with cement provide at least 6 push-out test specimens. For some animals, it was not possible to prepare six suitable specimens due to incomplete filling of the medullary canal, less than optimal cement-bone contact, or unexpected defects in the femur. Therefore, specimens from each cement-time group are grouped together, and the overall mean and variance are used for statistical comparisons.

Table 26. Mean push-out strengths for OC-cement specimens

	AVG Push-out Strength (MPa)	*Standard Deviation*	*(n)*
OC-2 wk	4.34	3.00	8
	2.21	0.50	8
	1.68	0.58	4
	5.54	1.79	12
Total	*3.93*	*2.39*	*32*
OC-6 wk	2.71	1.68	6
	2.84	0.82	8
	4.19	1.13	8
Total	*3.30*	*1.34*	*22*
OC-12 wk	2.20	1.35	5
	3.31	0.82	11
	2.17	1.51	8
Total	*2.70*	*1.28*	*24*

Table 27. Mean push-out strengths for PMMA cement specimens

	AVG Push-out Strength (MPa)	*Standard Deviation*	*(n)*
PMMA-2 wk	0.07	0.08	6
	0.03	0.04	8
	1.42	2.14	6
Total	*0.46*	*1.27*	*20*
PMMA-6 wk	0.12	0.09	8
	0.83	0.40	11
	0.49	0.27	6
Total	*0.52*	*0.42*	*25*
PMMA-12 wk	0.27	0.32	13
	0.42	0.36	3
	1.25	0.90	5
Total	*0.54*	*0.65*	*21*

The mean push-out strengths of OC-cement from cortical bone decreased over the test period, but means were not found to be statistically different for 2 wk vs. 6 wk and 6 wk vs. 12 wk. However, the difference between the 2 and 12 wk means was statistically significant ($p < 0.05$). It is evident from radiographs that the filling of the femur was not as complete for many of the OC-cement

12 wk specimens as for the 2 wk specimens. Many of the animals in the 12 wk group underwent the implantation surgery earlier than the animals in the 2 wk group. The downward trend in the data may not represent a degradation of the cement–bone interface, but rather a sign of improved placement of the OC-cement with increased surgical experience. The means for the PMMA push-out strengths at 2, 6, and 12 weeks were not statistically different. The means for OC-cement were significantly higher compared to PMMA means for the corresponding time periods; $p < 0.001$ for each.

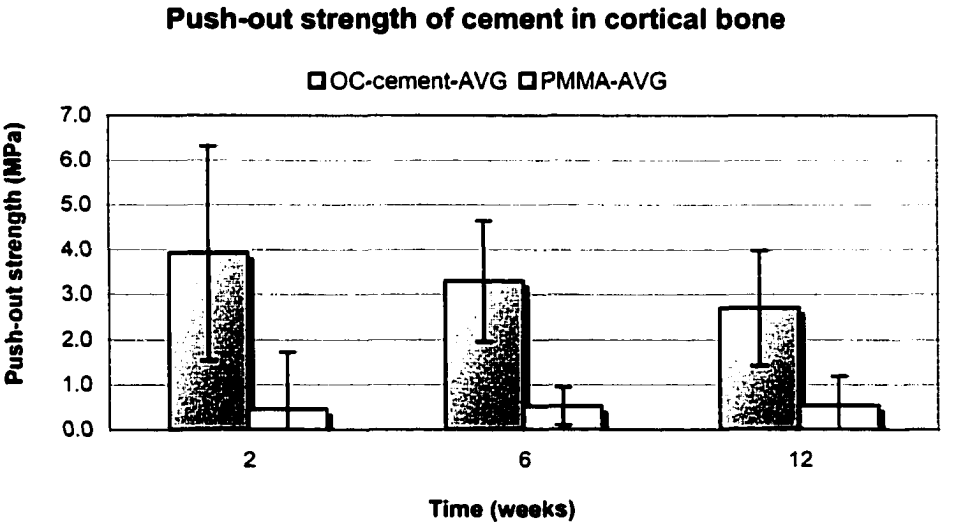

Figure 56. Push-out strengths for cement in cortical bone (mean ± standard deviation)

Typical forces versus displacement charts collected with the Instron test machine are presented in Figures 57 and 58 for OC-cement and PMMA cement, respectively. As testing was performed, a flat segment was observed on the chart as the specimen and testing fixture became firmly seated, after which there was a linear segment where the load quickly increased, followed by interface failure and a dramatic decrease in load.

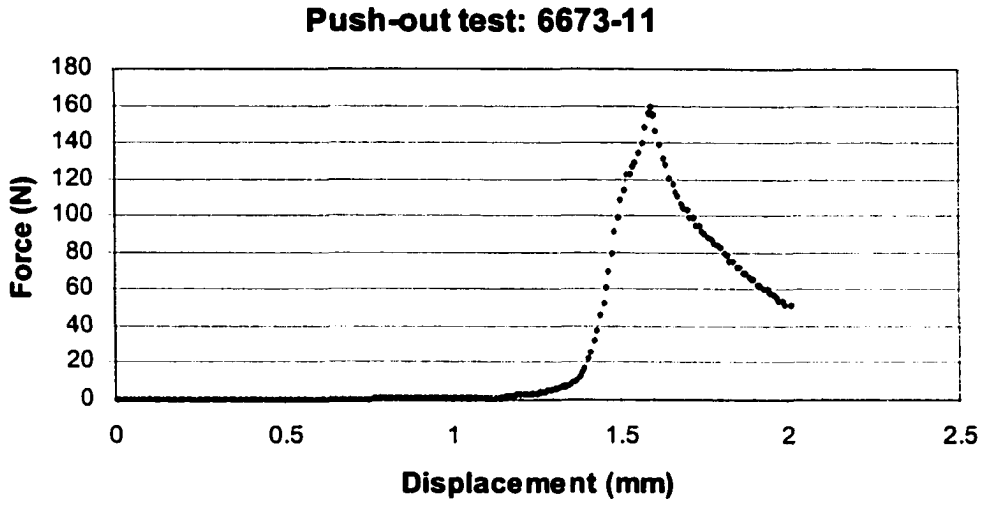

Figure 57. Typical push-out graph of OC-cement in cortical bone

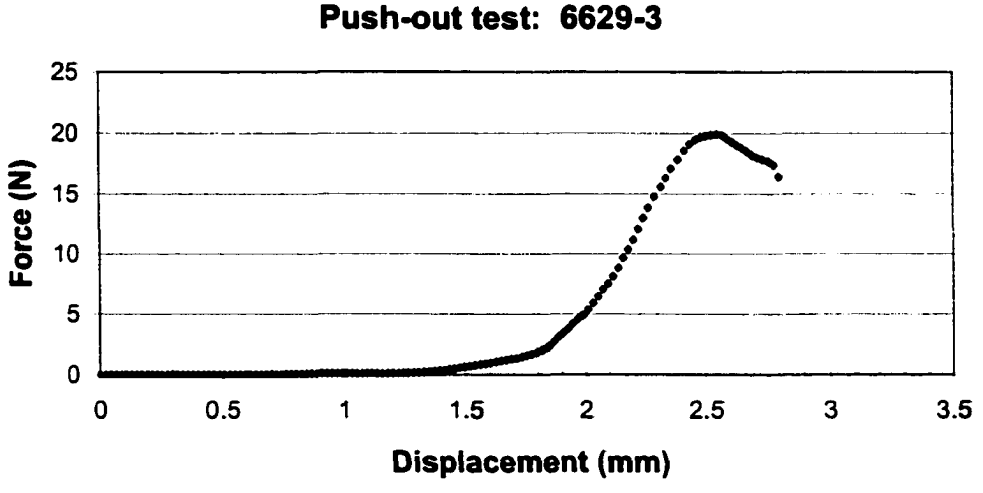

Figure 58. Typical push-out graph for PMMA cement in cortical bone

Using the described testing procedure, failure of the cement-bone interface and displacement was observed on some PMMA-bone specimens while the load continued to increase. This

phenomenon was observed only for PMMA specimens. It was previously shown from histological work and microradiographs, that a layer of fibrous tissue generally separated the PMMA cement from the surrounding cortical bone. It was also noted that the inner surface of the medullary canal is not completely smooth or free from surface artifacts. It is believed that if fibrous tissue exists between the cement and bone, the actual interfacial shear strength would be low as noted by previous researchers (Matsuda, et al., 1997). If, however, cement protruded into pores in the bone or vice versa, the force observed at failure would indicate the force required to shear these PMMA cement or bone spicules; therefore, a much higher shear force would be observed, as found by Stone et al. (1996) and MacDonald et al. (1993). Previous researchers also found that the shear strength of the cement-bone interface was dependent on location, cement penetration, and the gap interface (Stone et al., 1996). Dai et al. (1991) observed a decrease in interfacial shear strength of serially cut PMMA-bone specimens as the anatomic location of the specimens became more distal. In the diaphysis of canine femurs, mean interfacial shear strengths of 0.41, 0.23 and 0.32 MPa were reported which are supported by the present data.

It is observed from the force vs. displacement charts that the distance traveled from onset of load until failure was approximately 3 times greater for PMMA as compared to OC-cement specimen, 0.6 mm versus 0.2 mm. Although OC-cement is a stiffer material than PMMA cement, PMMA would require less force to deform. The force required to create this amount deformation in the PMMA cement would be more than a 100 times greater than the forces observed during push-out testing. Presumably, shrinkage of the PMMA cement during polymerization creates a small gap between the cement and bone allowing for movement at the interface before failure is detected on a force vs. displacement chart. The PMMA cement was inserted under pressure and cement was often forced into any openings in the bone, while much less pressure was applied to place the OC-cement. This difference in applied pressure during insertion may explain why displacement before load failure was observed only in PMMA specimens.

V. CONCLUSIONS

A novel cement consisting of calcium aluminate and β-tricalcium phosphate was evaluated for use as a bone cement. Hydration with a calcium chloride solution achieved working and setting times appropriate for orthopaedic applications. Calcium aluminate chloride hydrate phases were formed during hydration and aging while the β-tricalcium phosphate remained stable. The compressive strength of this cement was 70 MPa four hours following hydration. The strength continued to increase up to 1 month and a high strength was maintained when tested up to 2 years. These values for setting times and compressive strength are comparable to values reported for commercially used PMMA bone cement.

Shrinkage of PMMA bone cement resulting from polymerization is well documented and is thought to give rise to low interfacial strengths, micromotion of the implant, and aseptic loosening. The experimental OC-cement was found to expand slightly, 0.11% within 1 hour of hydration up to 0.71% after 14 months. This slight expansion of the OC-cement over time may be beneficial and help promote implant stability. The mean interfacial shear strengths of the OC-cement-prosthesis bond did not change significantly over the test period and ranged from 1.11-1.18 MPa. Mean values for the PMMA-prosthesis interfacial strength were slightly higher ranging from 1.18-1.48 MPa.

The OC-cement was successfully implanted into the femoral, medullary canal in canines. Care was necessary to avoid washout of the cement and dispersing particles of cement in surrounding tissue. The OC-cement set *in situ*. Intact OC-cement was not found to produce any adverse response in cortical bone for implantation times up to 12 weeks. The patterns of mineralization and remodeling, as observed using fluorescence microscopy, were distinct for PMMA and OC-cement sections. A heavy band of growth emanating from the periosteum was observed for PMMA sections with little activity occurring in the original cortical bone, while bone from OC-cement sections displayed less growth around the outer edge of the cortical bone, but more remodeling throughout the existing cortical bone.

In PMMA sections, a gap was observed between the cement and bone that generally filled in with fibrous tissue. In well-filled OC-cement specimens, direct contact between the cement and bone

was found with no intermediary fibrous tissue. In scattered locations, osteocytes were absent from lacunae adjacent to the implanted OC-cement; however, this response was not atypical given the trauma of the surgical procedure. Furthermore, the filling of the intramedullary canal with cement would presumably disrupt the blood supply to the bone in the inner circumferential system. Histological evaluation found the bone healthy for both PMMA and OC-cement sections from cortical bone.

SEM analysis found no evidence of OC-cement materials leaching into surrounding bone or variation in the composition of bone surrounding the implanted cement after 2 to 12 weeks implantation. At times up to 12 weeks, no bone growth into the OC-cement was observed. Push-out tests used to measure the cement-bone interfacial shear strength found the mean interfacial shear strengths of the OC-cement-bone interface generally 5-8 times greater than the values obtained for PMMA-bone interface at corresponding time periods.

Results of these tests indicate that OC-cement has appropriate and sufficient physical and mechanical properties for orthopaedic applications. Initial evaluations of the short-term tissue response indicate that this experimental OC-cement is biocompatible when implanted into the femoral medullary canal in canines. Although particles of cement in soft tissue induced fibrous tissue formation, when OC-cement was implanted into cortical bone no adverse response was observed and the surrounding cortical bone was healthy.

Future recommendations in the development of OC-cement include increasing the volume of β-tricalcium phosphate in the composition through additional powder or the addition of larger aggregates. If the cement is to be placed in an area in direct contact with blood, the investigation of additives to decrease the effects of wash out is recommended. The present *in vivo* research assessed the relatively short-term response to implanted cement. A long-term study is recommended to evaluate the performance of the OC-cement *in vivo* and tissue response over a number of years as well as performance while bearing a load, as would be the case if this cement were used for prosthesis fixation.

REFERENCES

Ahmed, A. M., S. Raab, and J. E. Miller. 1984. Metal/cement interface strength in cemented stem fixation. Journal of Orthopedic Research, 2: 105-118.

American National Standards Institute/American Dental Association. 1977. Specification No. 8 for dental zinc phosphate cement. Journal of the American Dental Association, 96:121-123.

An, Y. H. and R. J. Friedman. 1999. Animal selections in orthopaedic research. Pages 39 - 57 **in** Y. H. An and R. J. Friedman, ed. Animal Models in Orthopaedic Research. CRC Press, Boca Raton, Florida.

Anderegg, F. O. and D. S. Hubbell. 1995. **in** H. W. Taylor, ed. Cement Chemistry, 2nd ed. Thomas Telford, New York, New York.

Anderson, J. 1996. Pages 165-173 **in** Ratner, B., A. Hoffman, F. Schoen and J. Lemons. Biomaterials Science – An Introduction of Materials in Medicine. Academic Press, San Diego, California.

Annual Book of ASTM Standards. 1993. F981-93: Standard practice for assessment of compatibility of biomaterials for surgical implants with respect to effect of materials on muscle and bone. American Society for Testing and Materials, Conshohocken, Pennsylvania.

Annual Book of ASTM Standards. 1995. F451-95: Standard specification for acrylic bone cement. American Society for Testing and Materials, Conshohocken, Pennsylvania.

Annual Book of ASTM Standards. 1997. F561-97: Practice for retrieval and analysis of implanted medical devices, and associated tissues. American Society for Testing and Materials, Conshohocken, Pennsylvania.

Annual Book of ASTM Standards. 1993. F763-87: Standard practice for short-term screening of implant materials. American Society for Testing and Materials, Conshohocken, Pennsylvania.

Autian, J. and J. E. Hamner III. 1972. A toxicity profile for calcium aluminate. Journal of Dental Research, 51: 3: 880.

Bagpai, P. K., D. Wyatt, and G. Graves. 1977. Effect of calcium aluminate ceramics on the pH of distilled water, phosphate saline and human plasma. IRCS Medical Science: Biomedical technology; Connective Tissue, Skin and Bone; Surgery and Transplantation: 5.

Banks, W. J. 1986. Applied Veterinary Histology. 2nd ed. Williams and Wilkens, Baltimore, Maryland.

Barb, W., J. B. Park, G. Kenner, and A. von Recum. 1982. Intramedullary fixation of artificial hip joints with bone cement-precoated implants. I. Interfacial strengths. Journal of Biomedical Materials Research, 16: 447-458.

Baron, R., 1999. Anatomy and ultrastructure of bone. Pages 3-10 **in** M. J. Favus, ed. Primer on the Metabolic Bone Diseases and Disorders of Mineral Metabolism. Lippencott Williams & Wilkins, Philadelphia, Pennsylvania.

Berzins, A. and D. R. Sumner. 2000. Implant pushout and pullout test. Pages 463-467 **in** Y. H. An and R. A. Draughn, ed. Mechanical Testing of Bone and the Bone-Implant Interface. CRC Press, Boca Raton, Florida.

Beaumont, P. and B. Plumpton. 1977. The strength of acrylic bone cements and acrylic cement-stainless steel interfaces. Journal of Materials Science, 12: 1853-1856.

Bhaskar, S. N., J. M. Brady, L. Getter, M. F. Grower, and T. Driskell. 1971. Biodegradable ceramic implants in bone. Journal of Oral Surgery, 32:335-346.

Black, J. 1999. Biological Performance of Materials – Fundamentals of Biocompatibility. Marcel Dekker, Inc., New York, New York.

Bonucci, E. 2000. Basic composition and structure of bone. Pages 3-22 **in** Y. H. An and R. A. Draughn, ed. Mechanical Testing of Bone and the Bone-Implant Interface. CRC Press, Boca Raton, Florida.

Canale, S. T. 1998. Campbell's Operative Orthopaedics. Mosby, St. Louis, MO. Page 308.

Caputo, A., 1999. Healing of bone and connective tissues. Pages 201-216 **in** F. Bronner and R. V. Worrell, ed. Orthopaedics – Principles of Basic and Clinical Science. CRC Press, Boca Raton, Florida.

Capmas, A., D. Sorrentino, and D. Dadmidot. 1990. Effect of temperature on setting times of calcium aluminate cements. Pages 65-81 **in** R. J. Mangabhai, ed. Calcium Aluminate Cements. E. & F. N. Spon, Cambridge, Great Britain.

Carvalho, B., G. Graves, and P. K. Bajpai. 1975. Calcium and inorganic phosphate contents of implanted resorbable porous calcium aluminate ceramics. IRCS Medical Science: Biomedical technology; Connective Tissue, Skin and Bone; Surgery and Transplantation, 3: 185.

Cini, L., A. Pizzoferrato, C. Trentani, S. Sandrolini, and M. Paltrinieri. 1975. Thermodifferential analysis of ceramic implants. Journal of Biomedical Materials Research, Vol. 9: 441-451.

Charnley, J. 1972. Acrylic Cement in Orthopedic Surgery. Churchill Livingstone, London.

Crammond, N. J. 1990. Long-term performance of HAC concrete in sulphate bearing environments. Pages 208-227 **in** R. J. Mangabhai, ed. Calcium Aluminate Cements. E. & F. N. Spon, Cambridge, Great Britain.

Currell, B. R., R. Grzeskowlak, H. G. Midgley, and J. R. Parsonage. 1987. The acceleration and retardation of set high alumina cement by additives. Cement and Concrete Research, 17: 420-432.

Cussino, L. and A. Negro. 1980. Hydration of aluminous cement in the presence of silicic and calcareous aggregate. 7th Inter. Congr. Chem. Cem. Vol. 3: 62-67.

Dai, K., Y. Liu, J. Park, C. Clark, K. Nishiyama, and Z. Zheng. 1991. Bone-particle-impregnated bone cement: An *in vivo* weight-bearing study. Journal of Biomedical Materials Research, 25: 141-156.

Darr, G. M., and U. Ludwig. 1974. The incorporation of chloride in calcium aluminate hydrates. Ind. Chim. Belg., 39: 687-692.

Davies, J. P. and W. H. Harris, 1994. Tensile bonding strength of the cement prosthesis interface. Orthopedics, 17: 171-173.

Dhert, W. J., C. C. Verheyen, and L. H. Braak. 1992. A finite element analysis of the pushout test: influence of test conditions. Journal of Biomedical Materials Research, 26, 119.

Dhert, W. J. and J. A. Jansen. 2000. The validity of a single pushout test. Pages 477-488 **in** Y. H. An and R. A. Draughn, ed. Mechanical Testing of Bone and the Bone-Implant Interface. CRC Press, Boca Raton, Florida.

Donath, L. 1990. Reactions of tissue to calcium phosphate ceramics, in Heimke, G. Ed. Osseo-Integrated Implants, Vol. 1. CRC Press, Boca Raton, Florida.

Driessens, F. C., J. A. Planell, and F. J. Gil. 1995. Calcium phosphate bone cements. Pages 171-190 **in** D. Wise, D. Trantolo, D. Altobelli, M. Yaszemski, J. Gresser, and E. Schwartz, ed. Encyclopedic Handbook of Biomaterials and Bioengineering, Part B: Vol. 1. Marcel Dekker, Inc., New York, New York.

Elliott, J. C. 1994. Structure and Chemistry of the Apatites and Other Calcium Orthophosphates. Elsevier Science B. V., Amsterdam, Netherlands.

Ganong, W. F., 1995. Review of Medical Physiology, 17th Edition. Appleton & Lange, Norwalk, Connecticut.

George, C. M. 1990. Manufacture and performance of aluminous cement: a new perspective. Pages 181-207 **in** R. J. Mangabhai, ed. Calcium Aluminate Cements. E. & F. N. Spon, Cambridge, Great Britain.

Gitzen, W. H., L. D., Hart, and G. MacZura. 1957. Properties of some calcium aluminate cement compositions. Journal of the American Ceramic Society, 40 (5): 158-167.

Glenkinsop, J. C. 1963. Magazine of Concrete Research, 15:33-38.

Gruber, H. and A. Stasky. 1999. Histological study in orthopaedic animal research. Pages 115-138 **in** Y. H. An and R. J. Friedman, ed. Animal Models in Orthopaedic Research. CRC Press, Boca Raton, Florida.

Haas, S., G. Brauer, and G. Dickson. 1975. Characterization of polymethyl-methacrylate bone cement. Journal of Bone and Joint Surgery, 57A: 380-391.

Hannawayya, F. 1990. Inorganic admixture inhibits corrosion of steel embedded in mortar. Proceedings of the International Conference of Cement Microscopy, 12: 411-426.

Hench, L. 1996. Ceramics, glasses, and glass-ceramics. Pages 73-84 in B. Ratner, A. Hoffman, F. Schoen and J. Lemons, eds. Biomaterials Science-An Introduction to Materials in Medicine, Academic Press, San Diego, California.

Hentrich, R. L., G. A. Graves, H. G. Stein, and P. K. Bajpai. 1971. An evaluation of inert and resorbable ceramics for future clinical orthopedic applications. Journal of Biomedical Materials Research, 5: 25.

Hulbert, S. F., J. J. Klawitter, S. J. Morrison, and R. G. Topazian. 1981. Materials for direct skeletal attachment. Pages 371-456 in D. N. Ghista, ed. Biomechanics of Medical Devices. Marcel Dekker, Inc., New York, New York.

Hulbert, S. F., F. A. Young, R. S. Matthews, J. J. Klawitter, C. D. Talbert, and F. H. Stelling. 1970. Potential of ceramic materials as permanently implantable skeletal prostheses. Journal of Biomedical Materials Research, 4: 443-456.

Jarcho, M. 1981. Calcium phosphate ceramics as hard tissue prosthetics. Clinical Orthopaedics & Related Research, 157: 259-278.

Jee, W., 1999. Structure and function of bone tissue. Pages 3-27 **in** F. Bronner and R. V. Worrell, ed. Orthopaedics – Principles of Basic and Clinical Science. CRC Press, Boca Raton, Florida.

Kaneps, A. J., S. M. Stover, and N. E. Lane. 1994. Changes in canine cortical and cancellous bone mechanical properties following immobilization and remobilization with exercise. Bone, 15: 557.

Katsumura, T., T. Koshino, and T. Saito. 1998. Viscous property and osteogenesis induction of hydroxyapatite thermal decomposition product mixed with gelatin implanted into rabbit femurs. Biomaterials, 19: 1839-1844.

Kindt-Larsen, T., D. Smith, and J. Jensen. 1995. Innovations in acrylic bone cement and application equipment. Journal of Applied Biomaterials, 6: 75-83.

Kosmac, T., G. Lahajnar, and A. Sepe. 1993. Proton NMR relaxation study of calcium aluminate hydration reactions. Cement and Concrete Research 23: 1-6.

Kühn, K. D. 2000. Bone Cements. Springer-Verlag, New York, New York. p: 27-28.

Kurdowski, W., L. Taczuk, and B. Tybalska. 1990. Behaviour of high alumina cement in chloride solutions. Pages 222-229 **in** R. J. Mangabhai, ed. Calcium Aluminate Cements. E. & F. N. Spon, Cambridge, Great Britain.

Kuzel , H. J. 1968. X-ray investigations of some complex calcium aluminate hydrates and related compounds. Proc. 5th Int. Symp. on the Chem. of Cement, Tokyo, Supplementary paper II-19: 92-97.

Lea, F. M. 1971. The Chemistry of Cement and Concrete, 3rd edition. Chemical Publishing Co., Inc., New York, New York

Lian, J. B., G. Stein, E. Canalis, P. Robey, and A. Boskey. 1999. Bone formation: osteoblast lineage cells, growth factors, matrix proteins, and the mineralization process. Pages 14-29 **in** M. J. Favus, ed. Primer on the Metabolic Bone Diseases and Disorders of Mineral Metabolism. Lippencott Williams & Wilkins, Philadelphia, Pennsylvania.

Macdonald., W., M. Phil, E. Swarts, and R. Beaver. 1993. Penetration and shear strength of cement-bone interfaces in vivo. Clinical Orthopedics and Related Research, 286: 283-288.

Majumdar, A. J., B. Singh, and R. N. Edmonds. 1990. Hydration of mixture of 'Ciment Fondu' aluminous cement and granulated blast furnace slag. Cement and Concrete Research, 20: 179-183.

Marks, S. C. Jr. and D. Hermey. 1996. The structure and development of bone. **in** Bilezikian, J.P., L. G. Raisz, and G. A. Rodan, ed. Principles of Bone Physiology, Vol. 1. Academic Press, San Diego, California.

Marks, S. C. Jr. and Popoff, 1996. **in** Bilezikian, J.P., L. G. Raisz, and G. A. Rodan, ed. Principles of Bone Physiology, Vol. 1. Academic Press, San Diego, California.

Martini, F. H. 1995. Fundamentals of Anatomy and Physiology, 3rd edition. Prentice-Hall, Inc., Englewood Cliffs, New Jersey.

Matsuda, Y., K. Ido, T. Nakamura, H. Fujita, T. Yamamuro, M. Oka, and T. Shibuya. 1997. Prosthetic replacement of the hip in dogs using bioactive bone cement. Clinical Orthopaedics and Related Research, 336: 263-277.

McKoy, B. E., Y. H. An and R. J. Friedman. 2000. Factors affecting the strength of the bone-implant interface. Pages 439-462 **in** Y. H. An and R. A. Draughn, ed. Mechanical Testing of Bone and the Bone-Implant Interface. CRC Press, Boca Raton, Florida.

Mejdoubi, E., J. Lacout, P. Michaud, and F. Rodriguez. 1994. An hydraulic cement for biological uses. Pages 209-214 **in** Hydroxyapatite and Related Materials. CRC Press, Boca Raton, Florida.

Mendoza, J. L., A. Freese, and R. E. Moore. 1989. Behavior of calcium aluminate compositions. Ceramic Transactions, 4: 294-311.

Midgley, H.G. 1990. High alumina cement in construction – a future based on experience. Pages 1-14 **in** R. J. Mangabhai, ed. Calcium Aluminate Cements. E. & F. N. Spon, Cambridge, Great Britain.

Mirtichi, A. A., J. Lemaitre, and E., Munting. 1990. Calcium phosphate cements: study of the ß-tricalcium phosphate-dicalcium phosphate-calcite cements. Biomaterials, 11: 83-88.

Müller, R. T. and N. Schürmann. 1999. Shear strength of the cement metal interface – an experimental study. Arch. Orthop. Trauma Surgery, 119: 133-138.

Mundy, G., 1999. Bone Remodeling. Pages 30-38 **in** M. J. Favus, ed. Primer on the Metabolic Bone Diseases and Disorders of Mineral Metabolism. Lippencott Williams & Wilkins, Philadelphia, Pennsylvania.

Nade, S., L. Armstrong, E. McCartney, and B. Bagaley. 1983. Osteogenesis after bone and bone marrow transplantation. Clinical Orthopaedics and Related Research, 181:255-263.

Nilforoushan, M. R., and J. H. Sharp. 1995. The effect of additions of alkaline-earth metal chlorides on the setting behavior of a refractory calcium aluminate cement. Cement and Concrete Research, 25: 1523-1534.

Nurse, R., J. Welch, and A. Majumdar. 1965. Transactions of the British Ceramic Society, 64: 9: 416.

National Center for Health Statistics. 1998. Ambulatory and inpatient procedures in the United States, 1996. Vital and Health Statistics: Series 13, No. 139: 28.

Park, J. B. and R. S. Lakes. 1992. Biomaterials – An Introduction, 2nd edition. Plenum Press, New York, New York.

Parker, M. and P. Bourcelly. 1960. Journal of Chemical Physics, 63: 257.

Parker, T. W. 1952. The constitution of aluminous cement. Proc. Third Int. Symp. Chemistry of Cement, Cement and Concrete Association, London, 5: 485-529.

Planell, J.A., M. M. Vila, F. J. Gil, and F. C. M. Driessens. 1995. Acrylic bone cements. Pages 879-922 **in** D. Wise, D. Trantolo, D. Altobelli, M. Yaszemski, J. Gresser, and E. Schwartz, ed.

Encyclopedic Handbook of Biomaterials and Bioengineering, Part B, Vol. 2. Marcel Dekker, Inc., New York, New York.

Poellmann, H. 1986. Solid solution series of complex calcium aluminate hydrates containing Cl^-, OH^-, and CO_3^{2-}. Proc. 8th Int. Symp. on the Chem. of Cement. Rio de Janeiro, Supplementary Paper, Vol. III: 300-306.

Poellmann, H., and H. J. Kuzel. 1988. Synthesis and polymorphic transformations of solid solutions in the system $3CaO{\cdot}Al_2O_3{\cdot}CaCl_2{\cdot}nH_2O$-$3CaO.Al_2O_3.Ca(OH)_2.nH_2O$-$H_2O$. Neues Jahrb. Mineral., 5: 193-202.

Powder Diffraction File [Computer file], 1999. JCPDS-International Centre for Diffraction Data., Newton Square, PA.

Puzas, J. E. and G. D. Lewis. 1999. Biology of osteoclasts and osteoblasts. Pages 45-58 in F. Bronner and R. V. Worrell, ed. Orthopaedics – Principles of Basic and Clinical Science. CRC Press, Boca Raton, Florida.

Ratner, B., A. Hoffman, F. Schoen and J. Lemons. 1996. Biomaterials Science – An Introduction of Materials in Medicine. Academic Press, San Diego, California.

Recker, R. 1983. Bone Histomorphometry: Techniques and Interpretation. CRC Press, Boca Raton, Florida.

Reilly, D. T., A. H. Burstein, and V. H. Frankel. 1974. The elastic modulus for bone. Journal of Biomechanics, 6: 31.

Rivero, D. P. S. K. Skipor, M. Singh, R. Urban, and J. Galante. 1987. Effect of disodium etidronate (EHDP) on bone ingrowth in a porous material. Clinical Orthopaedics and Related Research, 215: 279-286.

Rixom, M. R. and N. P. Mailvaganam. 1986. Chemical Admixtures for Concrete, 2nd Edition. E & F. Spon. London, New York.

Roberts, W., P. Turley, N. Brezniak, and P. Fielder. 1987. Bone physiology and metabolism. CDA Journal. October edition.

Robson, T. D. 1967. High Alumina Cements and Concretes. John Wiley & Sons, Inc. New York, New York.

Roemhildt, M. L. 1998, Calcium phosphate compatible bone cements, Master's Thesis, Iowa State University, Ames, Iowa.

Rosen, C. and D. Kiel. 1999. The aging skeleton. Pages 57-62 in M. J. Favus, ed. Primer on the Metabolic Bone Diseases and Disorders of Mineral Metabolism. Lippencott Williams & Wilkins, Philadelphia, Pennsylvania.

Sersale, R. 1957. Ricer Scienti. 27: 777. as referenced in Lea's Chemistry of Cement and Concrete research, 205.

Stone, J., J. Rand, E. Chiu, J. Grabowski, and K. An. 1996. Cement viscosity affects the bone-cement interface in total hip arthroplasty. Journal of Orthopaedic Research, 14: 834-837.

Tanner, E., 1998. Biomaterials for orthopaedic applications. Pages 263-276 in S. Hughes and I. D. McCarthy, eds. Sciences Basic to Orthopaedics. W. B. Saunders Company Ltd., London.

Taylor, H. F. W. 1997. Cement Chemistry, 2nd edition. Thomas Telford, New York, New York.

Traetteberg, A. and P. E. Grattan-Bellew. 1975. Hydration of $3CaO{\cdot}Al_2O_3$ and $3\ CaO{\cdot}Al_2O_3$ + gypsum with and without $CaCl_2$. Journal of the American Ceramic Society, 58. No 5-6: 221-227.

Welch, J. and W. Gut. 1961. High temperature studies of the system calcium oxide-phosphorous pentoxide. Journal of Chem. Society, 4442-4444.

Williams, D. F., 1999. The Williams Dictionary of Biomaterials. Liverpool University Press, Liverpool.

Wolff, 1892 **in** Park, J. B. and R. S. Lakes. 1992. Biomaterials – An Introduction, 2nd edition. Plenum Press, New York, New York.

Zioupos, P., C. Smith, and Y. An. 2000. Factors affecting mechanical properties of bone. Pages 65-85 **in** Y. H. An and R. A. Draughn, ed. Mechanical Testing of Bone and the Bone-Implant Interface. CRC Press, Boca Raton, Florida.

Yamamoto, H., S. Niwa, M. Hori, T. Hattori, K. Sawai, S. Aoki, M. Hiano, and H. Takeuchi. 1998. Mechanical strength of calcium phosphate cement *in vivo* and *in vitro*. Biomaterials, 19: 1587-1591.

Young, J. F., 1970. Effect of organic compounds on the interconversions of calcium aluminate hydrates: hydrates of tricalcium aluminate. Journal of the American Ceramic Society, 53: 2: 65-69.

ACKNOWLEDGEMENTS

My deepest thanks to my advisor, Dr. Thomas McGee, for his enthusiastic support and encouragement throughout my graduate studies. My sincere appreciation to committee members, Dr. David Cann, Dr. Mary Helen Greer, Dr. Dennis Johnson, Dr. Surya Mallapragada, and Dr. Stanley Wagner for their advice, expertise in respective areas, and willingness to serve on my committee. Special gratitude goes to Dr. Wagner for performing surgeries for cement implantation and follow-up care and to Dr. Yosiya Niyo for providing histological evaluation.

Thanks to T. Walker, M. Bohan, J. Riney, G. Nugent, J. Evangelau, M. Hintz, K. MacAlvany, A. Crabtree, R. Neuendorf, and E. Camponesci for assistance with assorted portions of this project. Appreciation is given of J. Hildebreth for providing veterinary assistance and to the Chemistry Machine Shop for their adeptness in machining testing fixtures.

Acknowledgement of the following ISU researchers and facilities for providing technical assistance and use of equipment:

- Tracey Pepper at the Bessey Microscopy Center - Digital light micrographs,
- Margie Carter at the Image Analysis Facility – Fluorescence microscopy photographs and image analysis,
- Warren Straszheim and Scott Schlorholz at the Materials Analysis and Research Laboratory – Scanning electron microscopy and X-ray diffraction,
- Dr. Joe Gray at the Center for Non-destructive Evaluation – Microradiographs,
- Veterinary Clinical Sciences – Fluoroscope,
- Laboratory Animal Resources – Care of experimental animals,
- Microbiology Cell Facility – Fluorescence microscopy.

Finally, deepest appreciation to friends and family who too have experienced the journey of my graduate program and encouraged me along the way, especially mom, dad, Bill, Cheryl, Tim, Judy, Todd, Kim, Amy, Kevin, Cindy and Steve. Thank you!

APPENDIX A: X-RAY DIFFRACTION OF OC-CEMENT
(Scans performed from 10-70 degrees at 1.00 deg/min)

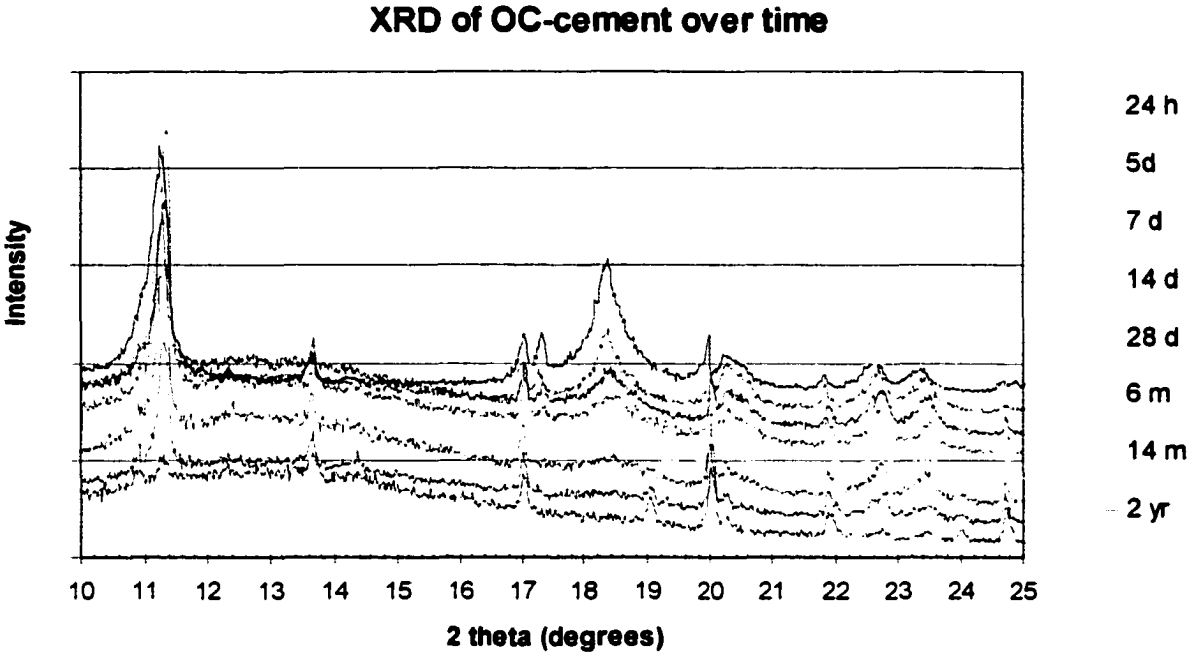

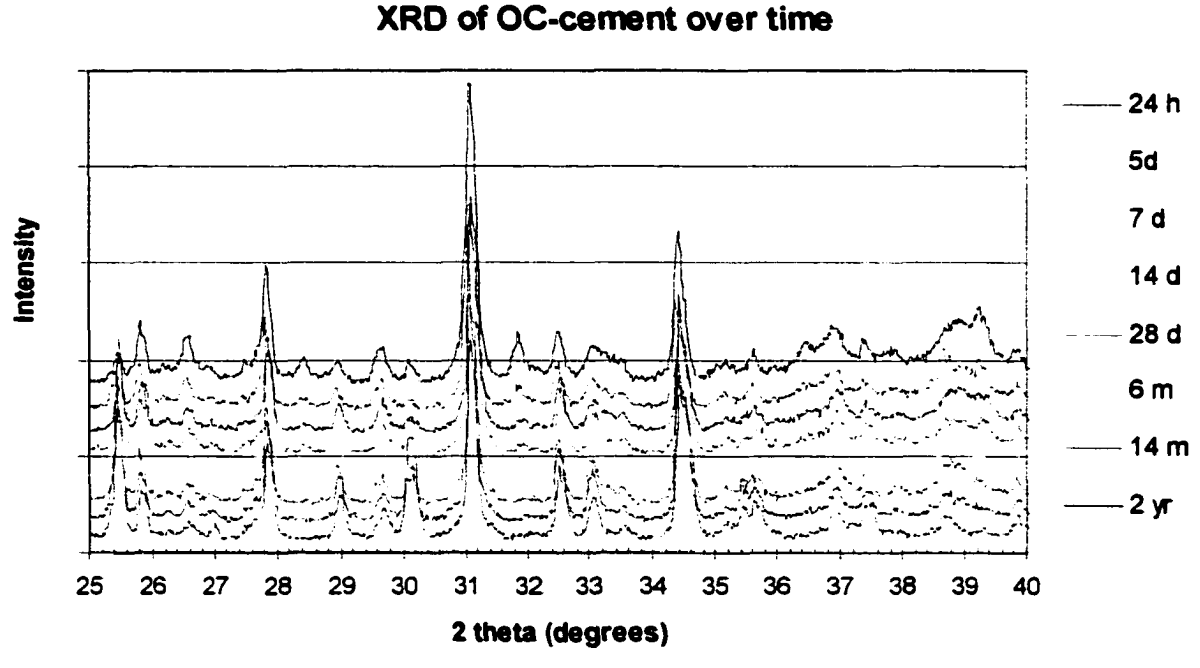

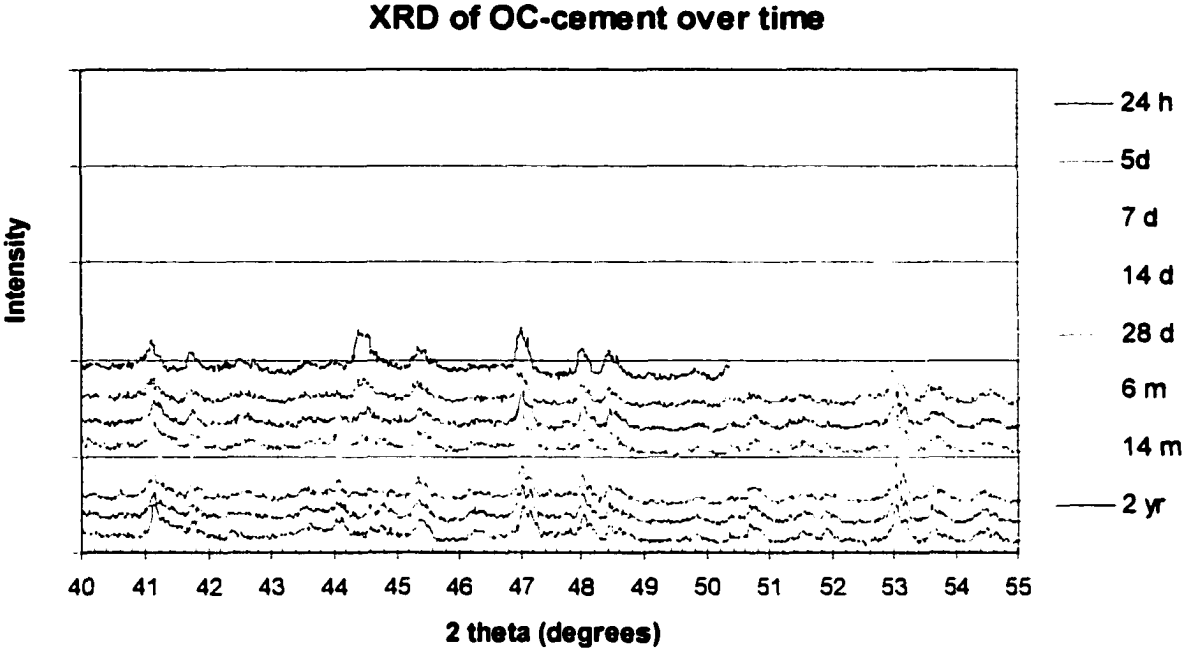
XRD of OC-cement over time
Intensity
24 h
5d
7 d
14 d
28 d
6 m
14 m
2 yr
40 41 42 43 44 45 46 47 48 49 50 51 52 53 54 55
2 theta (degrees)

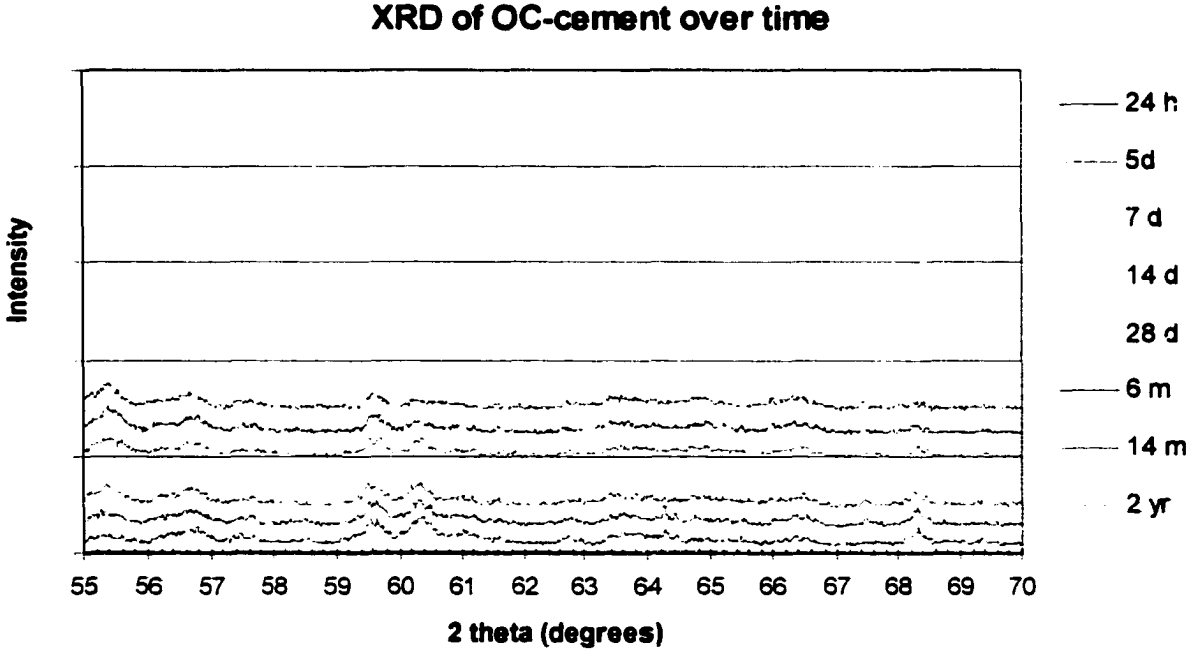
XRD of OC-cement over time
Intensity
24 h
5d
7 d
14 d
28 d
6 m
14 m
2 yr
55 56 57 58 59 60 61 62 63 64 65 66 67 68 69 70
2 theta (degrees)

Analysis of XRD of OC-cement over time

Compound	*Characteristic peaks*	*1 day*	*5 days*	*7 days*	*14 days*	*28 days*	*6 mos*	*14 mos*	*2 yrs*
CA	19.00, 30.10, 30.21	+	⇓	⇓	⇔	⇔	⇓	-	-
CA_2	20.01, (25.54, 34.45)	+	⇔	⇔	⇔	⇔	⇓	⇓	⇔
CAH_{10}	12.47, 21.17, 25.17	-	-	-	-	-	-	-	-
C_2AH_8	16.42, 24.76	+	+	⇓	⇔	⇓	⇓	*⇓	-*
C_3AH_6	17.28, 39.26, 44.43	-	-	-	-	-*	-	-	-
β-TCP	27.8, 31.05, 34.36,	+	⇔	⇔	⇔	⇔	⇔	⇔	⇔
$CACl_mH_n$	11.2-11.6, 22.5-22.8, (31.0-31.2)	-	⇑	⇑	⇔	⇑	⇔	⇑	⇑
AH_3	18.3-18.5	-	-	⇑	⇔	⇑	⇔	⇑	⇑
$CaCl_2 2H_20$	31.63	-	-	-	-	-	-	-	-
$CaCl_2 6H_20$	41.86	-	-	-	-	-	-	-	-

+ peak is present, - absence of the peak, * possibility of small peak
⇑ increase since previous time period, ⇓ decrease since previous time period, ⇔ no significant change
The location of the three principle peaks is given. Numbers in brackets indicate peaks that overlap with others.

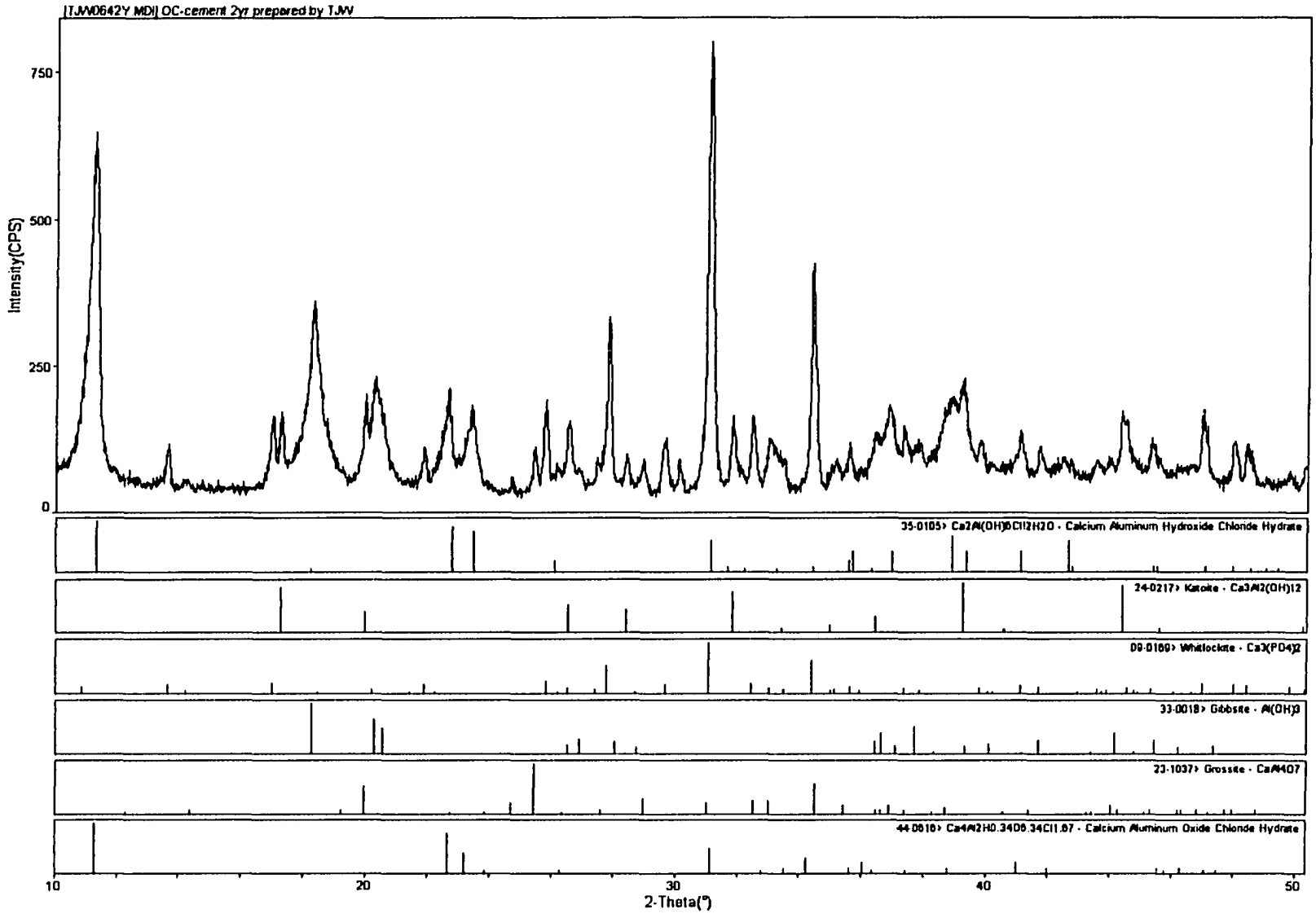
[TJW0642Y.MDI] OC-cement 2yr prepared by TJW
Intensity(CPS)
750
500
250
0
35-0105> Ca2Al(OH)6Cl.2H2O - Calcium Aluminum Hydroxide Chloride Hydrate
24-0217> Katoite - Ca3Al2(OH)12
09-0169> Whitlockite - Ca3(PO4)2
33-0018> Gibbsite - Al(OH)3
23-1037> Grossite - CaAl4O7
44-0816> Ca4Al2H0.34O6.34Cl1.67 - Calcium Aluminum Oxide Chloride Hydrate
10
20
30
40
50
2-Theta(°)

APPENDIX B: GRAPHS OF PULL-OUT DATA

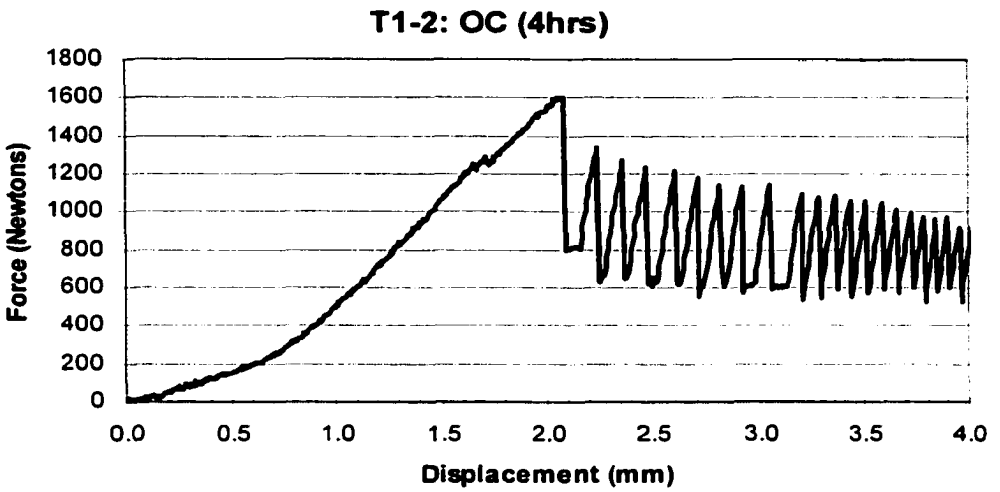

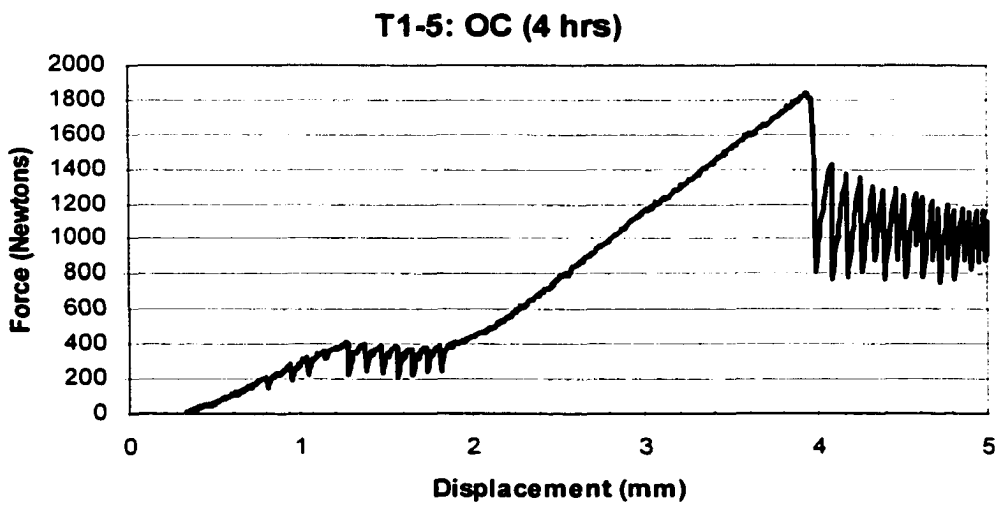

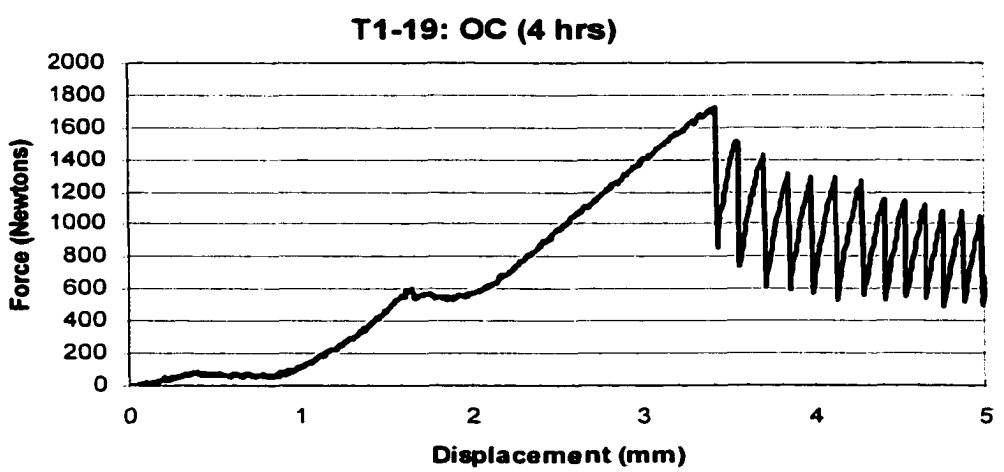

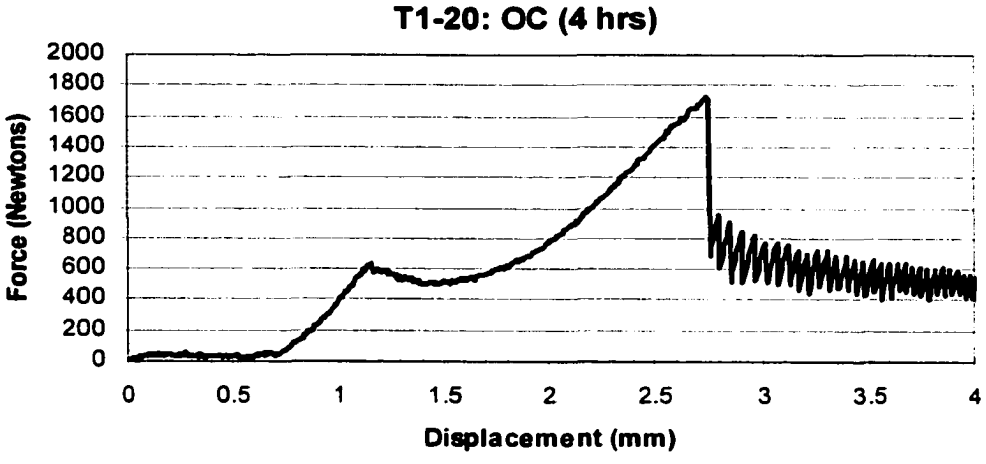
T1-20: OC (4 hrs)
Force (Newtons)
2000
1800
1600
1400
1200
1000
800
600
400
200
0
0
0.5
1
1.5
2
2.5
3
3.5
4
Displacement (mm)

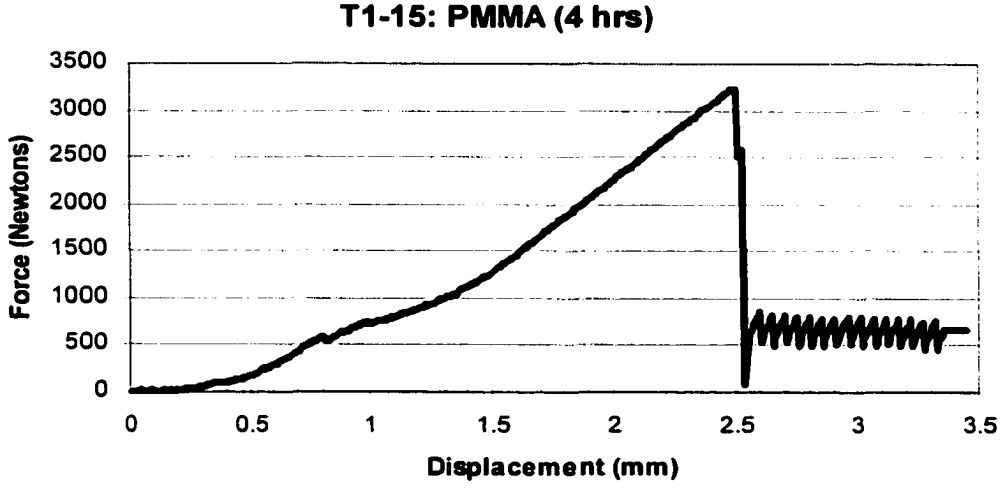
T1-15: PMMA (4 hrs)
Force (Newtons)
3500
3000
2500
2000
1500
1000
500
0
0
0.5
1
1.5
2
2.5
3
3.5
Displacement (mm)

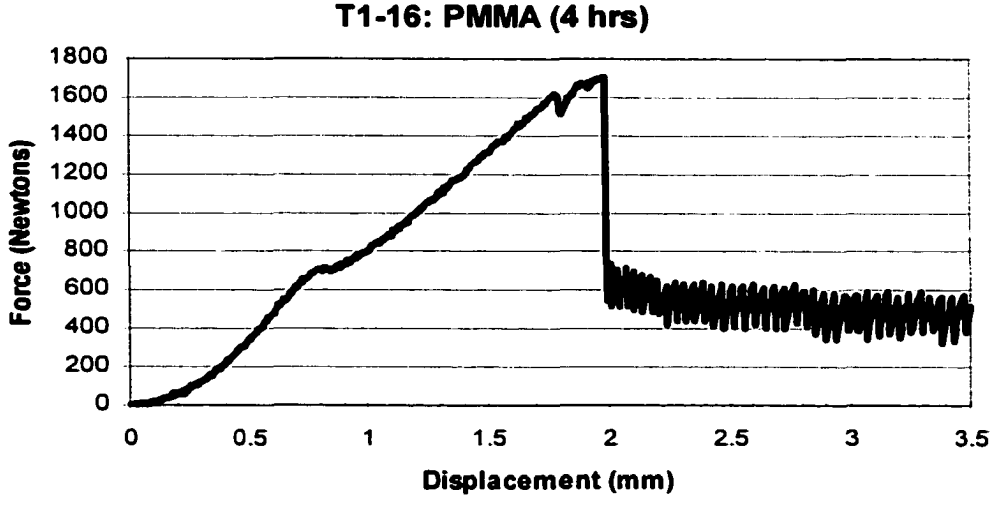
T1-16: PMMA (4 hrs)
Force (Newtons)
1800
1600
1400
1200
1000
800
600
400
200
0
0
0.5
1
1.5
2
2.5
3
3.5
Displacement (mm)

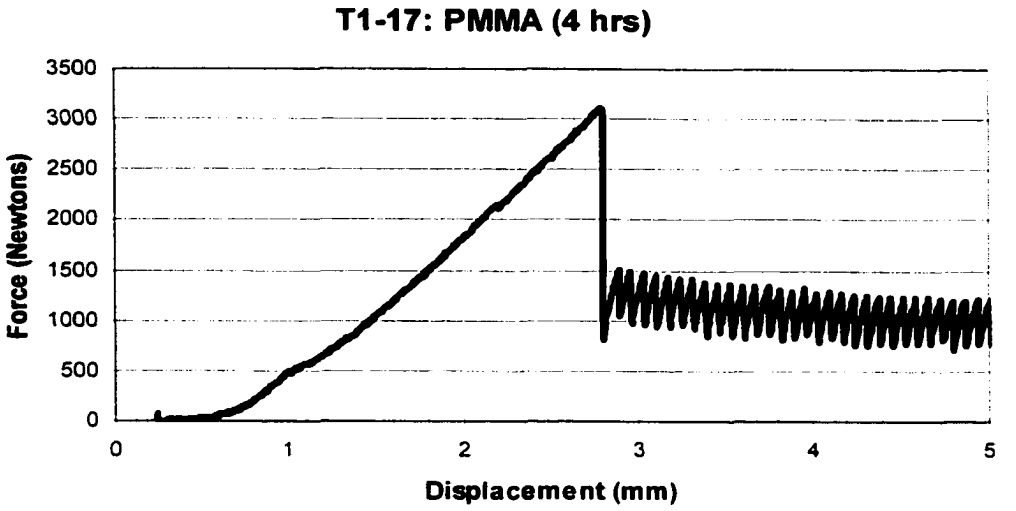
T1-17: PMMA (4 hrs)
Force (Newtons)
3500
3000
2500
2000
1500
1000
500
0
0
1
2
3
4
5
Displacement (mm)

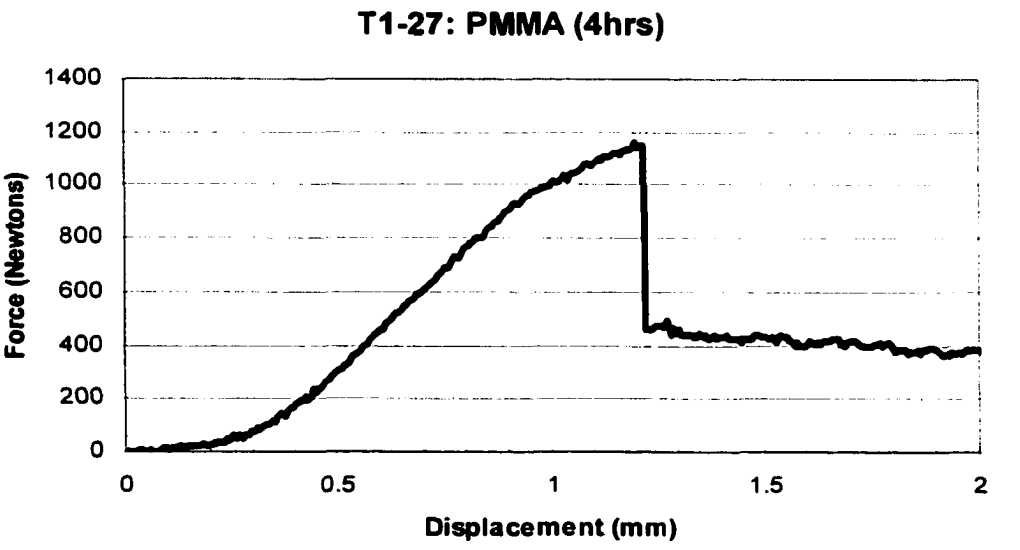
T1-27: PMMA (4hrs)
Force (Newtons)
1400
1200
1000
800
600
400
200
0
0
0.5
1
1.5
2
Displacement (mm)

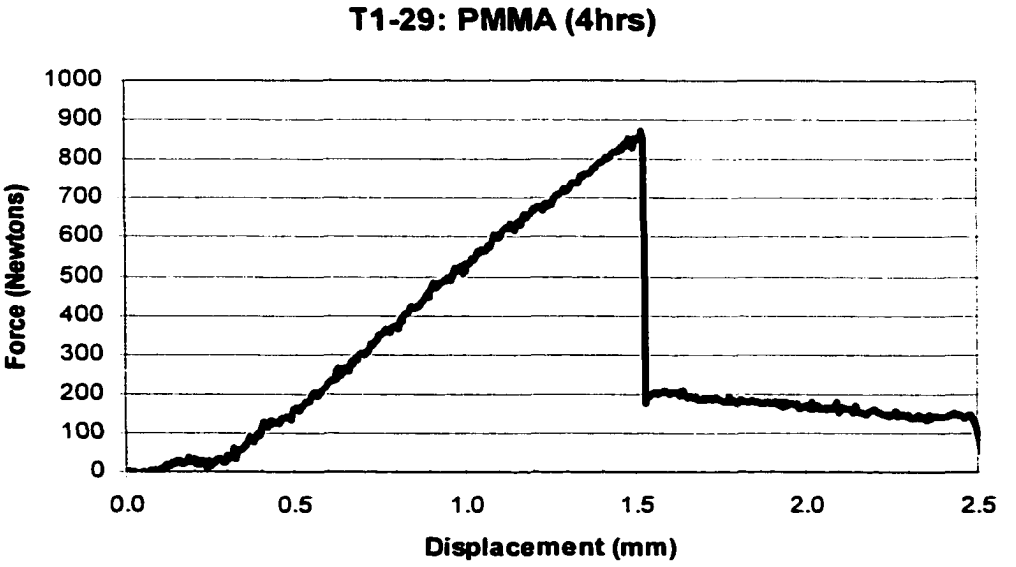
T1-29: PMMA (4hrs)
Force (Newtons)
1000
900
800
700
600
500
400
300
200
100
0
0.0
0.5
1.0
1.5
2.0
2.5
Displacement (mm)

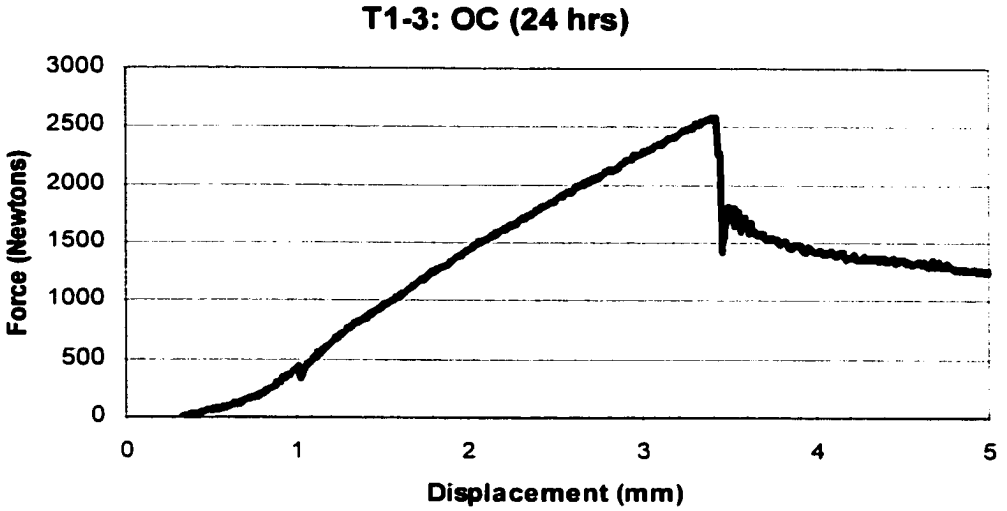
T1-3: OC (24 hrs)
Force (Newtons)
3000
2500
2000
1500
1000
500
0
0
1
2
3
4
5
Displacement (mm)

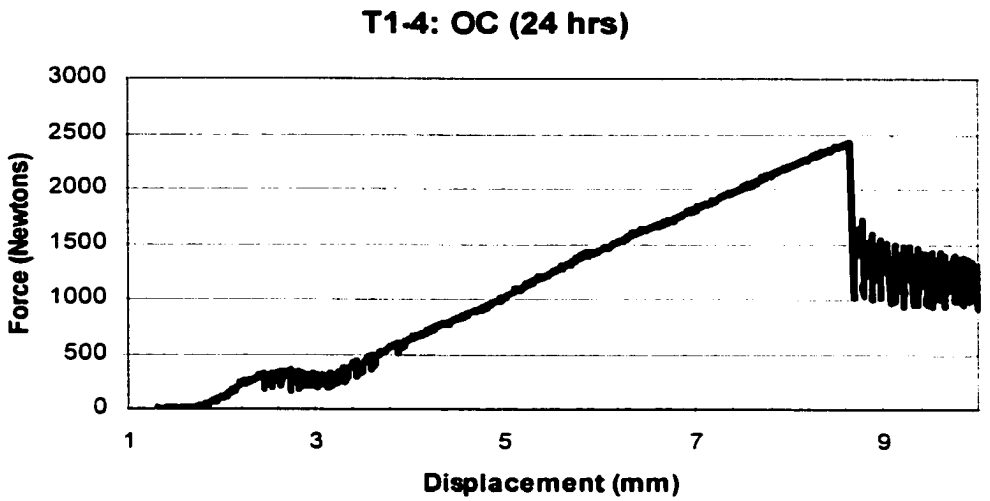
T1-4: OC (24 hrs)
Force (Newtons)
3000
2500
2000
1500
1000
500
0
1
3
5
7
9
Displacement (mm)

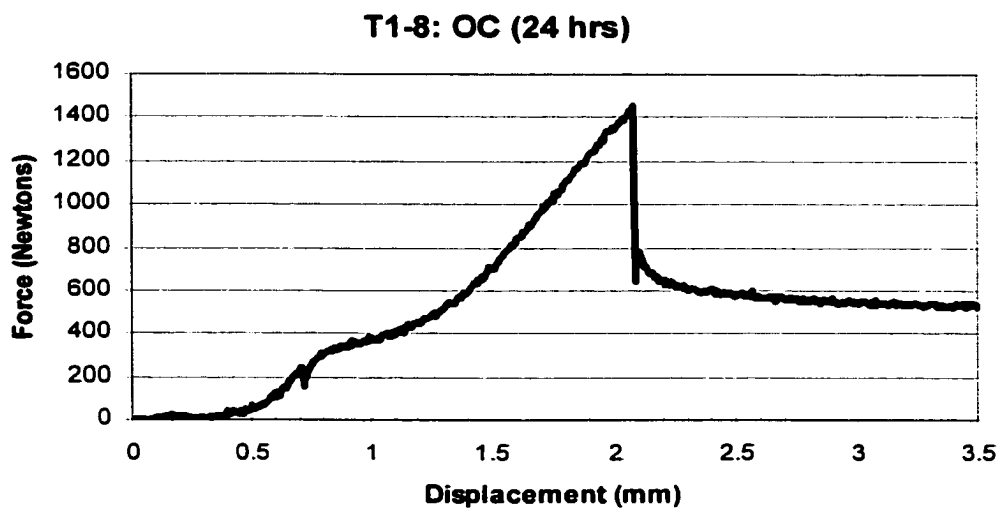
T1-8: OC (24 hrs)
Force (Newtons)
1600
1400
1200
1000
800
600
400
200
0
0
0.5
1
1.5
2
2.5
3
3.5
Displacement (mm)

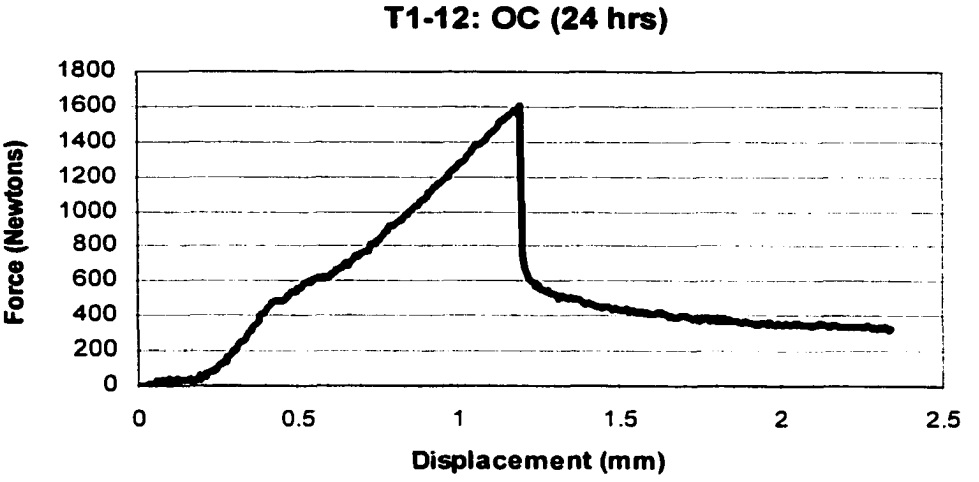
T1-12: OC (24 hrs)
Force (Newtons)
1800
1600
1400
1200
1000
800
600
400
200
0
0
0.5
1
1.5
2
2.5
Displacement (mm)

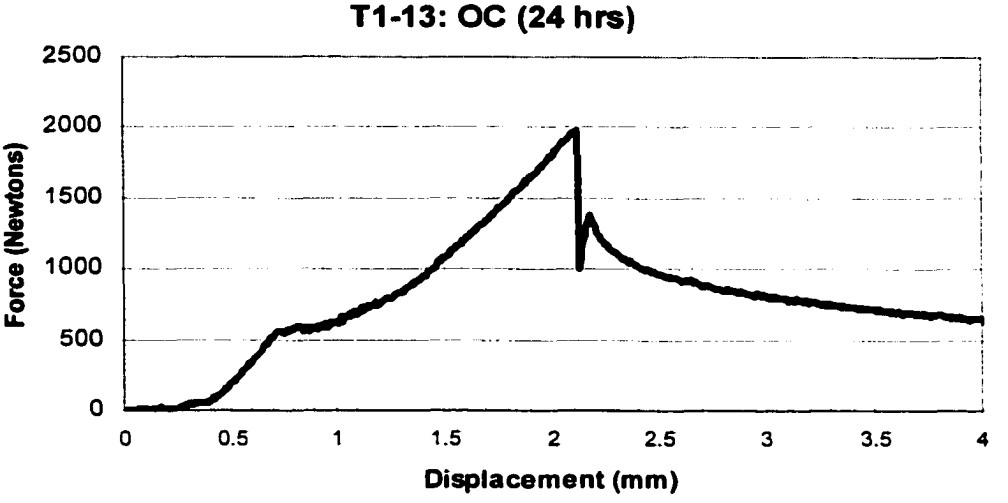
T1-13: OC (24 hrs)
Force (Newtons)
2500
2000
1500
1000
500
0
0
0.5
1
1.5
2
2.5
3
3.5
4
Displacement (mm)

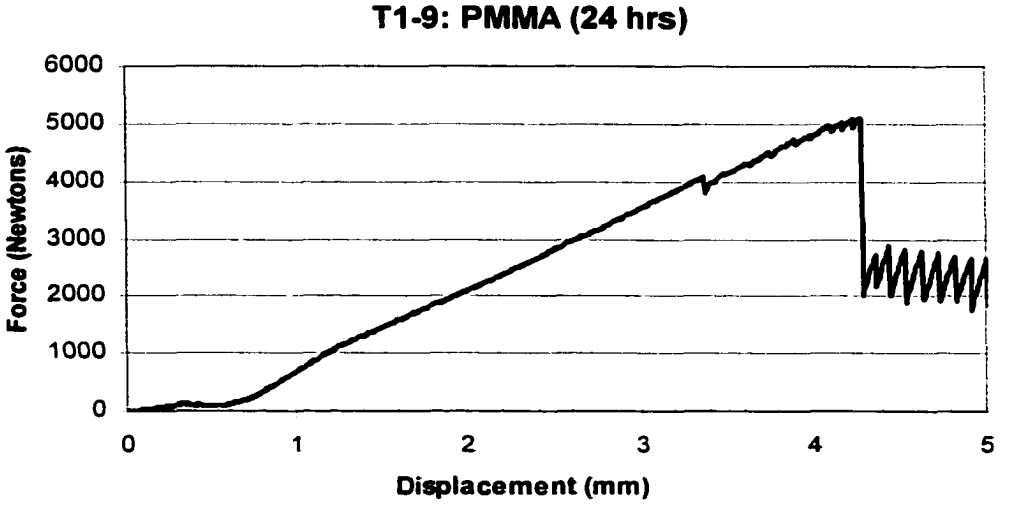
T1-9: PMMA (24 hrs)
Force (Newtons)
6000
5000
4000
3000
2000
1000
0
0
1
2
3
4
5
Displacement (mm)

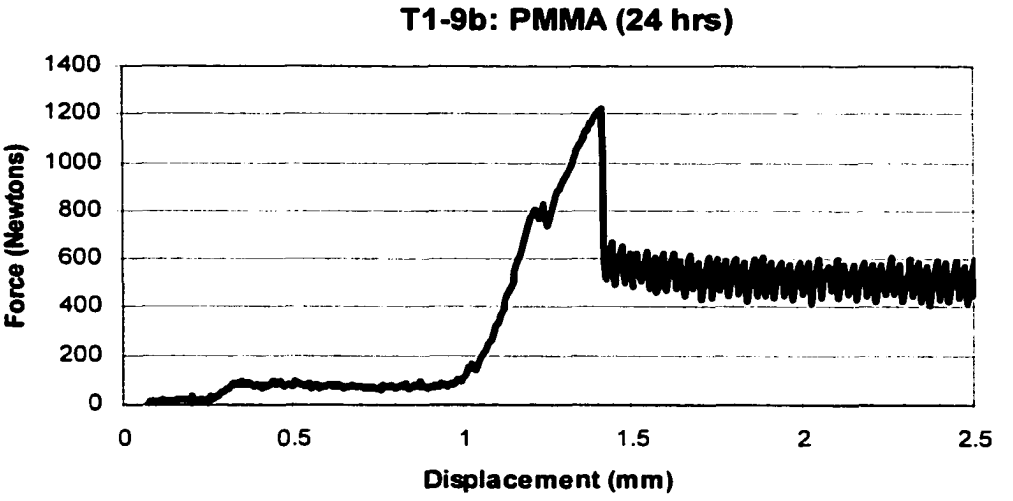
T1-9b: PMMA (24 hrs)
Force (Newtons)
1400
1200
1000
800
600
400
200
0
0
0.5
1
1.5
2
2.5
Displacement (mm)

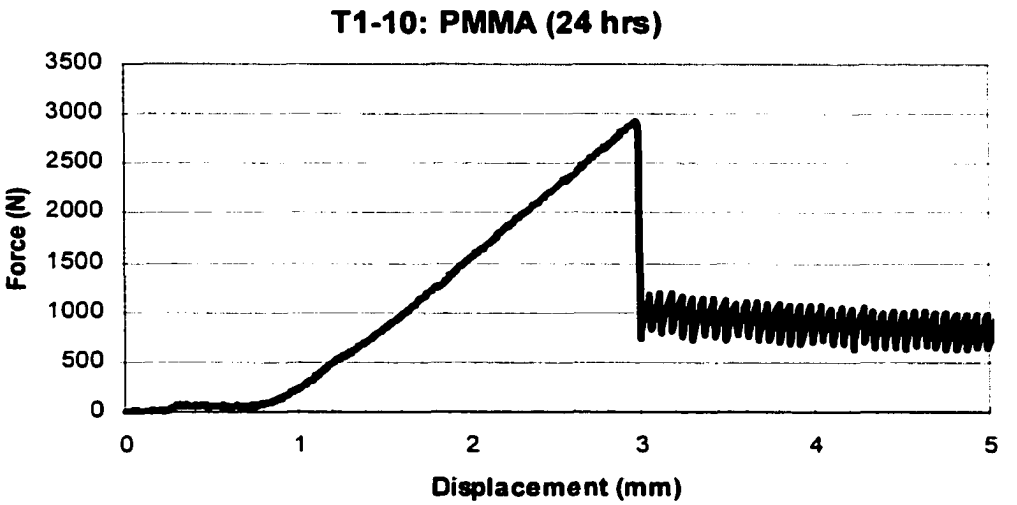
T1-10: PMMA (24 hrs)
Force (N)
3500
3000
2500
2000
1500
1000
500
0
0
1
2
3
4
5
Displacement (mm)

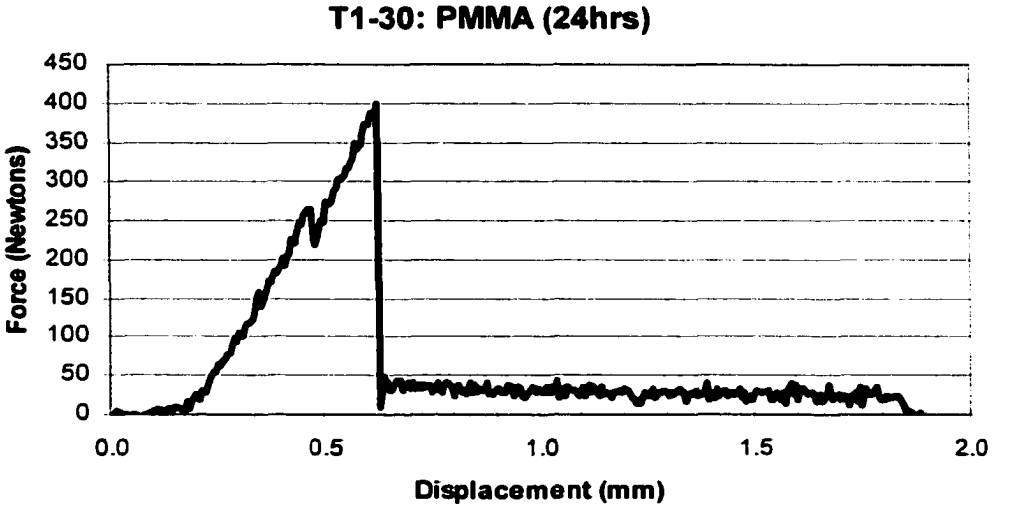
T1-30: PMMA (24hrs)
Force (Newtons)
450
400
350
300
250
200
150
100
50
0
0.0
0.5
1.0
1.5
2.0
Displacement (mm)

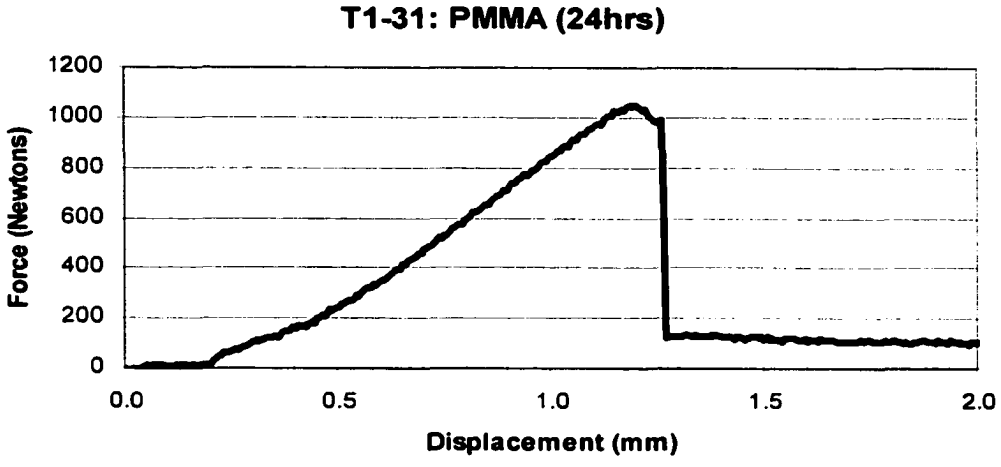
T1-31: PMMA (24hrs)
Force (Newtons)
1200
1000
800
600
400
200
0
0.0
0.5
1.0
1.5
2.0
Displacement (mm)

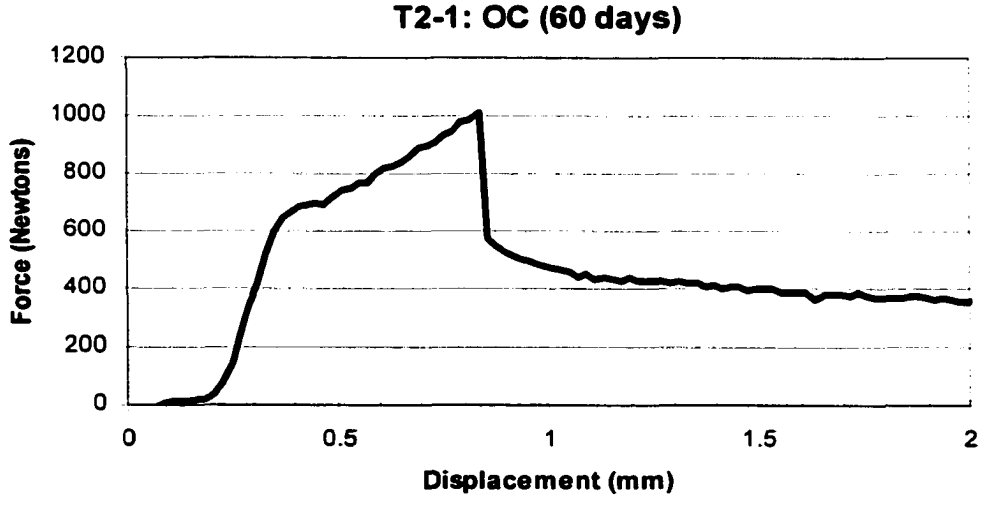
T2-1: OC (60 days)
Force (Newtons)
1200
1000
800
600
400
200
0
0
0.5
1
1.5
2
Displacement (mm)

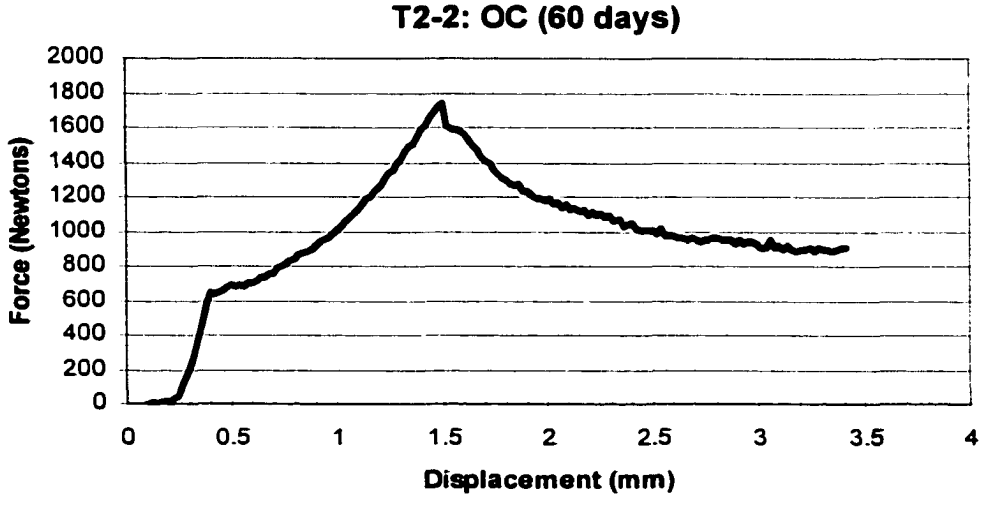
T2-2: OC (60 days)
Force (Newtons)
2000
1800
1600
1400
1200
1000
800
600
400
200
0
0
0.5
1
1.5
2
2.5
3
3.5
4
Displacement (mm)

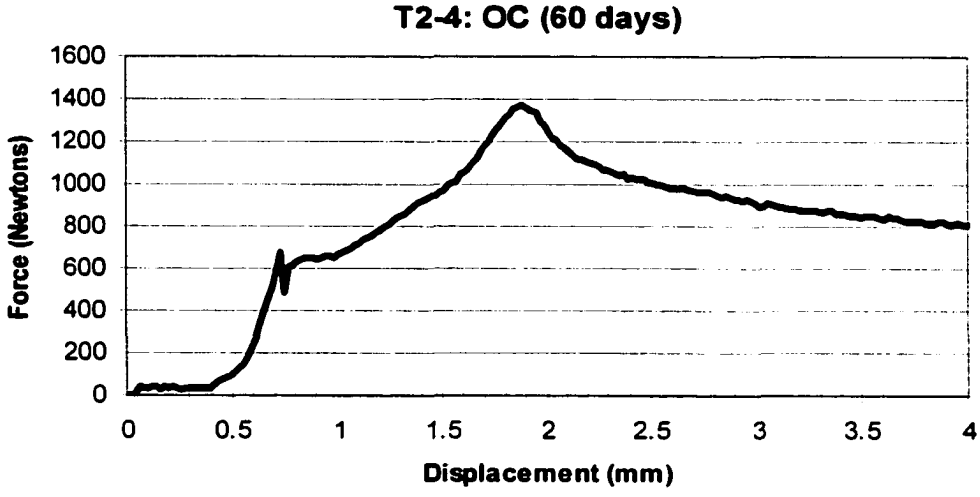
T2-4: OC (60 days)
Force (Newtons)
1600
1400
1200
1000
800
600
400
200
0
0
0.5
1
1.5
2
2.5
3
3.5
4
Displacement (mm)

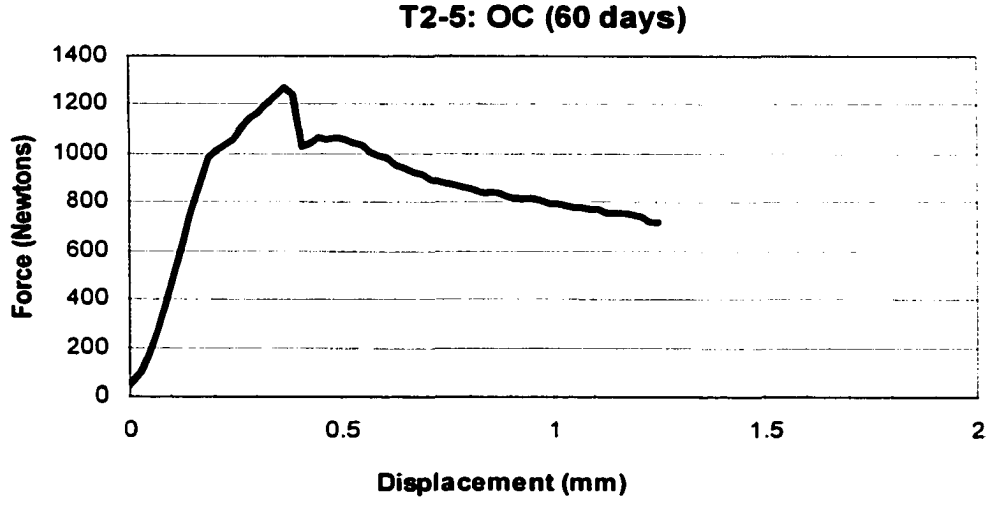
T2-5: OC (60 days)
Force (Newtons)
1400
1200
1000
800
600
400
200
0
0
0.5
1
1.5
2
Displacement (mm)

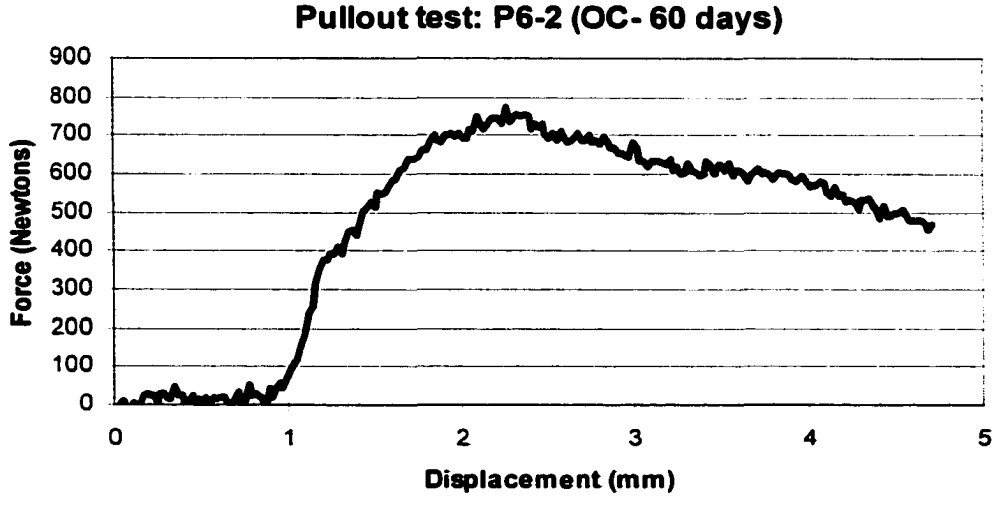
Pullout test: P6-2 (OC- 60 days)
Force (Newtons)
900
800
700
600
500
400
300
200
100
0
0
1
2
3
4
5
Displacement (mm)

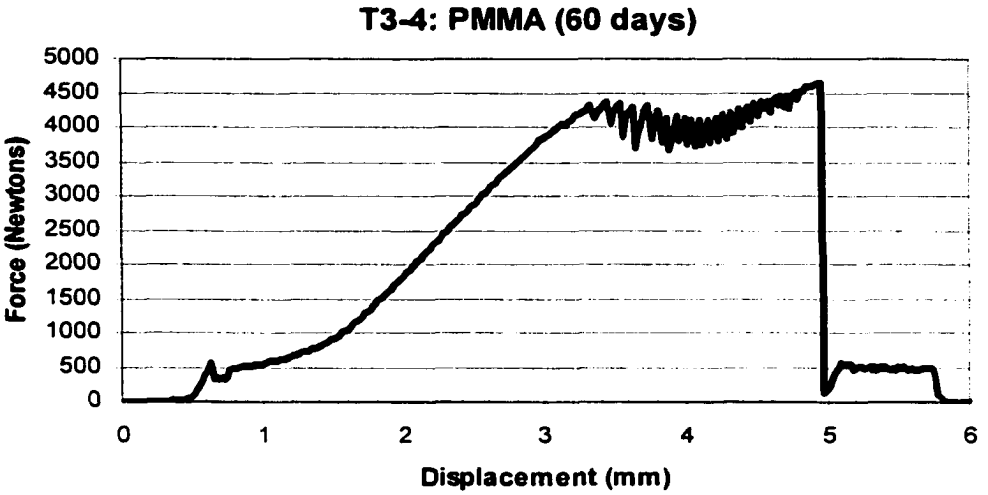
T3-4: PMMA (60 days)
Force (Newtons)
5000
4500
4000
3500
3000
2500
2000
1500
1000
500
0
0
1
2
3
4
5
6
Displacement (mm)

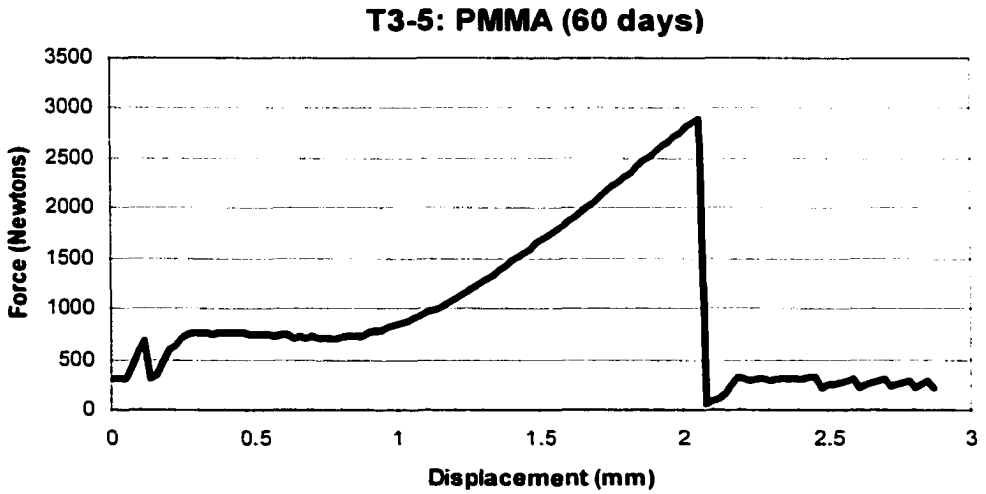
T3-5: PMMA (60 days)
Force (Newtons)
3500
3000
2500
2000
1500
1000
500
0
0
0.5
1
1.5
2
2.5
3
Displacement (mm)

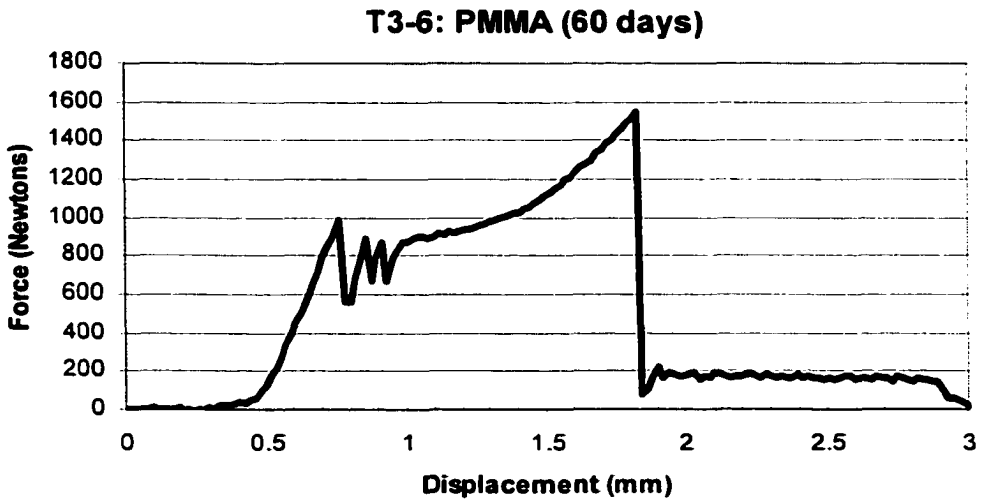
T3-6: PMMA (60 days)
Force (Newtons)
1800
1600
1400
1200
1000
800
600
400
200
0
0
0.5
1
1.5
2
2.5
3
Displacement (mm)

APPENDIX C. SURGICAL NOTES, RECOVERY OBSERVATIONS, RETRIEVAL NOTES AND RADIOGRAPH SUMMARY.

This appendix contains tables compiling observations regarding the surgical procedure, animal observations prior to euthanasia, observations made during the recovery of the femurs that had been implanted with cement, and comments regarding radiographs collected immediately following retrieval of the femur. The second table included compiles results from routine blood tests on select dogs from 4 to 16 days after cement implantation.

Summary of implantation notes, animal observations, retrieval notes, and post retrieval radiographs

ID	Type	Implantation Notes	Observations	Retrieval Notes	Post retrieval Radiograph
6629	PMMA 2 wks	Ok	Incision is healing. Dog using leg fine.	No abnormal tissue surrounding cement. Good fill.	Not available
6668	PMMA 2 wks	Ok	Incision is healing. Dog is walking and running on leg fine.	No abnormal tissue surrounding cement. Good fill	Not available
6672	PMMA 2 wks	Hole made in the diaphysis. Large amount of PMMA placed outside femur, but most was removed. Small amount of cement remained.	Incision is healing. Dog is using leg normally.	Some PMMA on the outside of femur. Scar tissue present at femur head. Narrow plug of cement implanted. Spongy bone not completely removed.	Not available
6596	PMMA 6 wks	IM nail pushed through femur. Large amount of PMMA outside femur.	Incision is healed. Dog is "walking" on leg, but not bending knee. Cannot balance on surgical leg. Suspect nerve damage.	Surrounding tissue looks ok. Synovial fluid in joint ok. Mass of cement present outside femur. Top part of femur has roughened texture on the outside.	Femur was poorly filled. Large amount of cement was placed outside the femur in two separate masses. Cortical bone was slightly thickened in some areas.
6649	PMMA 6 wks	Ok	Incision was healed. Dog was using leg normally.	No noticeable abnormalities.	Femur was fully filled. Some porosity apparent in the cement. Trabecular bone around the head of the femur filled with cement. Exterior surface of the cortical bone appears irregular in some areas in upper portion of the bone. Good contact between cement and bone in upper half of the femur.

ID	Type	Implantation Notes	Observations	Retrieval Notes	Post retrieval Radiograph
6657	PMMA 6 wks	Ok. A little cement placed outside the femur.	Incision was healed. Dog was very active and walking and running normal.	Some PMMA was outside bone (~2ml) that was surrounded by a large amount of scar tissue.	Femur was fully filled. Some porosity was observed in the cement. Trabecular bone was completely filled with cement. There was a very thin space between cement and bone in the middle of the of the femur shaft. Some regions of increased cortical bone thickness.
6587	PMMA 12 wks	Smooth procedure, one hole made in the diaphysis. Some cement placed outside femur.	Incision healed and using leg normally. Femur had fractured 35 days after surgery. Apart from 3-5 days after fracture, dog was active and using leg normally.	Diaphysis of femur appeared enlarged, with large amount of tissue adhering to the bone.	$^2/_3$ filled. Large mass of cement outside bone. Fracture of diaphysis and cement below the exterior cement mass. Cement broke at 45 degrees. Bone broke at 45 degrees and splintered. Massive callus formation.
6615	PMMA 12 wks	Smooth procedure, good filling of the canal.	Incision healed. Dog was using leg normally.	Normal, no noticeable abnormalities.	Fully filled. Some porosity within the PMMA cement. Trabecular bone filled with cement. Very thin space between cement and bone in some areas. Cortical bone is a little thickened in some areas.
6640	PMMA 12 wks	Hole through diaphysis. Large amount of PMMA initially placed outside femur. Most of this was removed, but a small piece remained.	Incision healed. Using leg ok. Slight favoring of non-surgical leg.	Knee only able to bend ½ way. Top portion of the femur appeared enlarged and was surrounded by scar tissue. Some PMMA outside femur.	Approximately ½ filled. Cortical bone appears thin or missing from ½ cm section of femur. Other view shows callus formation adjacent to this section.

ID	Type	Implantation Notes	Observations	Retrieval Notes	Post retrieval Radiograph
6669	OC 2 wks	Some cement placed outside femur near greater trochanter. Cement didn't flow well, pushed in with tube & packed.	Incision healed. Dog using leg normally.	Some necrosis of muscle tissue around head of femur. Some cement outside of femur. Bone marrow was darkened around the implant.	1/3 filled. Cement in intramedullary canal is fragmented. Upper plug is intact. Cement is not in direct contact with bone in the diaphysis region.
6673	OC 2 wks	Approach through greater trochanter. Minimal amount on soft tissue. Same solution as 6656.	Incision healing. Using leg normally.	No obvious adverse tissue reaction. Scar tissue not evident. Small ring of darkened blood around cement at most locations.	Fully filled. Cement is intact, mostly in close contact with the bone. Thin space between bone and cement in some places.
6740	OC 2 wks	Smaller than expected bones. 2 vials of cement inserted with 6mm funnel. No complications.	Incision healing. Using leg normally.	Normal post surgical granulation tissue. Some scar tissue closer to the greater trochanter.	½ filled. Cement of the lower ½ of the cement plug had fragmented. Direct contact with bone in some locations.
6746	OC 2 wks	2 vials of cement inserted with smaller than ¼" tube.	Incision began to drain slightly at 2 wks. Dog using leg normally.	Some cement was outside femur, perhaps some fibrous tissue forming.	2/3 filled. Middle portion has imprint from post in center of the cement plug. A small amount of cement was placed outside the greater trochanter. Relatively good contact.
6569	OC 6 wks	Tried to vibrate cement in place. Significant amount of cement on soft tissue.	Incision site drained periodically. At times of drainage, decreased use of leg.	Some scar tissue around the top of the femur.	¼ filled. Anterior ¾ of the intramedullary canal has increased radioopacity. Thickening of cortical bone thickness evident at mid-length of the diaphysis.

ID	Type	Implantation Notes	Observations	Retrieval Notes	Post retrieval Radiograph
6656	OC 6 wks	Approach through the greater trochanter. Used anhydrous $CaCl_2$. Mixed cement a bit more fluid. Some cement on soft tissue, tried to rinse off with Ringer's solution.	Incision healed. Dog using leg normally.	Ok. No abnormalities noticed.	½ to $^2/_3$ filled. Top portion had close contact with bone. Lower ½ of the cement was fragmented.
6698	OC 6 wks	Drilled hole through bone, some cement outside. Three plugs of cement inserted.	Incision healed. Dog using leg fine. Swinging leg out a bit.	Appears that insertion hole went through diaphysis of femur and a considerable amount of cement was placed outside adjacent to the diaphysis. Some scar tissue formed around this.	½ to $^1/_3$ filled. Inner segment not fully filled. Good cement contact with bone in regions. Cement in the middle section of the femur was somewhat fragmented.
6652	OC 12 wks	Cement inserted with plug method. Minimal amount on soft tissue.	Incision healed. Dog using leg normally.	Cement outside femur diaphysis. No noticeable adverse response. Some fibrous tissue growth around top of femur.	$^1/_3$ filled, but radiograph showed that insertion hole went through the femur and half of the cement was actually placed outside the bone.
6661	OC 6 wks	Same approach and solution as 6656. Minimal amount on soft tissue.	Incision healed. Dog using leg normally.	OK. Small amount of cement outside.	Fully filled. Cement was in close contact with bone. One area of space between cement plugs.

ID	Type	Implantation Notes	Observations	Retrieval Notes	Post retrieval Radiograph
6662	OC 12 wks	Hole drilled through femur. Partial fill, some cement on soft tissue.	Incision initially healed, but small abscess at surgical site occurred later. A little weak in the surgical leg.	Some cement outside bone. Gelatinous material consisting of fascia and cement mass outside of femur.	¼ filled. Initially inserted small plug of cement. Some cement was located on the outside.
6663	OC 12 wks	Good fill, minimal amount on soft tissue. 2½ vials inserted.	Incision healed. Dog using leg normally.	Ok. Fibrous tissue on top portion of femur (around top of cement plug)	Fully filled with cement. Mostly close contact between cement and bone.
6681	OC 12 wks	Plugs from 3 vials inserted. Small amount on soft tissue.	Incision healed. Using leg normally.	Ok. Very small amount of cement on muscle tissue.	Femur ½ filled. Middle portion of the cement was fragmented.

Table of results from routine blood tests

I.D. #	Type	Time	*WBC*	*RBC*	*HGB*	*HCT*	*MCV*	*MCH*	*MCHC*	*PLT*	*Neuts*	*AB band*	*Lymph*	*Monos*	*Eos*	*Basos*	*RDW*	*MPV*
6587	PMMA	15	11.90	8.06	17.8	51.1	63.4	22.1	34.9	683	6.66	0.0000	3.21	0.95	1.07	0.0	15.3	---
6596	PMMA	16	8.87	6.28	15.5	43.6	69.4	24.7	35.5	479	6.74	0.0887	0.98	0.98	0.09	0.0	14.4	---
6615	PMMA	15	11.50	6.96	16.1	46.3	66.5	23.1	34.8	469	7.13	0.1150	3.11	0.69	0.46	0.0	15.2	7.2
6672	PMMA	12	13.70	5.34	13.3	37.2	69.6	25.0	35.9	620	8.77	0.1370	3.01	1.37	0.41	0.0	14.7	9.23
6640	PMMA	14	5.35	7.11	16.5	47.8	67.1	23.1	34.5	319	3.10	0.0535	1.55	0.27	0.37	0.0	15.2	8.32
6649	PMMA	15	14.40	7.63	17.6	50.7	66.4	23.1	34.7	448	10.37	0.0000	2.30	1.44	0.29	0.0	15.0	8.48
6657	PMMA	15	13.50	7.41	17.1	49.8	67.2	23.1	34.4	363	10.80	0.2700	1.76	0.54	0.14	0.0	16.2	---
6652	OC	8	12.90	6.04	13.6	40.0	66.3	22.5	34.0	366	6.71	0.0000	4.52	1.16	0.52	0.0	14.3	---
6656	OC	8	14.40	5.89	14.2	40.3	68.4	24.0	35.1	413	10.80	0.0000	2.30	0.86	0.43	0.0	14.0	10.6
6661	OC	8	9.70	8.71	19.4	56.7	65.0	22.3	34.2	342	7.57	0.0000	1.26	0.68	0.19	0.0	14.7	9.98
6662	OC	5	9.80	7.01	16.5	47.3	67.5	23.5	34.8	350	7.45	0.0000	1.47	0.78	0.10	0.0	13.9	9.64
6663	OC	4	9.66	6.12	13.8	39.9	65.2	22.6	34.7	403	6.18	0.0966	1.93	0.68	0.77	0.0	14.9	8.23
6673	OC	9	18.20	7.77	18.1	51.7	66.5	23.3	35.0	223	13.83	0.1820	1.82	2.00	0.36	0.0	14.9	---
6681	OC	8	12.20	7.26	16.8	48.4	66.7	23.2	34.8	321	6.47	0.0000	4.27	0.73	0.73	0.0	16.1	---
6698	OC	8	15.00	7.52	17.4	49.8	66.3	23.1	34.8	461	7.05	0.0000	4.50	3.00	0.45	0.0	14.8	12.7
Normal (L)			6.00	5.50	12	37.0	60.0	19.5	32.0	200	3.00	0.0000	1.00	0.15	0.10	0.0	13.6	6.3
Range (H)			17.00	10.00	18	55.0	77.0		36.0	500	11.40	0.3000	4.80	1.35	0.75	0.1	16.8	11

Type = Cement type
Time = Number of days following implantation surgery until blood sample was collected
WBC = White blood cells ($10^{\wedge 3}/\mu l$)
RBC = Red blood cells ($10^{\wedge 3}/\mu l$)
HGB = Hemoglobin (gr/dl)
HCT = Hemocrit (%)
MCV = Mean cellular volume (fl)
MCH = Mean corpuscular hemoglobin (pg)
MCHC = Mean corpuscular hemoglobin concentration (gr/dl)
PLT = Automated platelets ($10^{\wedge 3}/\mu l$)
Neut = Neutrophils ($10^{\wedge 3}/\mu l$)
AB band = Absolute bands ($10^{\wedge 3}/\mu l$)
Lymph = Lymphocytes ($10^{\wedge 3}/\mu l$)
Monos = Monocytes ($10^{\wedge 3}/\mu l$)
Eos = Eosinophils ($10^{\wedge 3}/\mu l$)
Basos = Basophils ($10^{\wedge 3}/\mu l$)
RDW = Red cell distribution width(%)
MPV = Mean platelet volume (fl)

APPENDIX D: INTRAOPERATIVE FLUOROSCOPY IMAGES

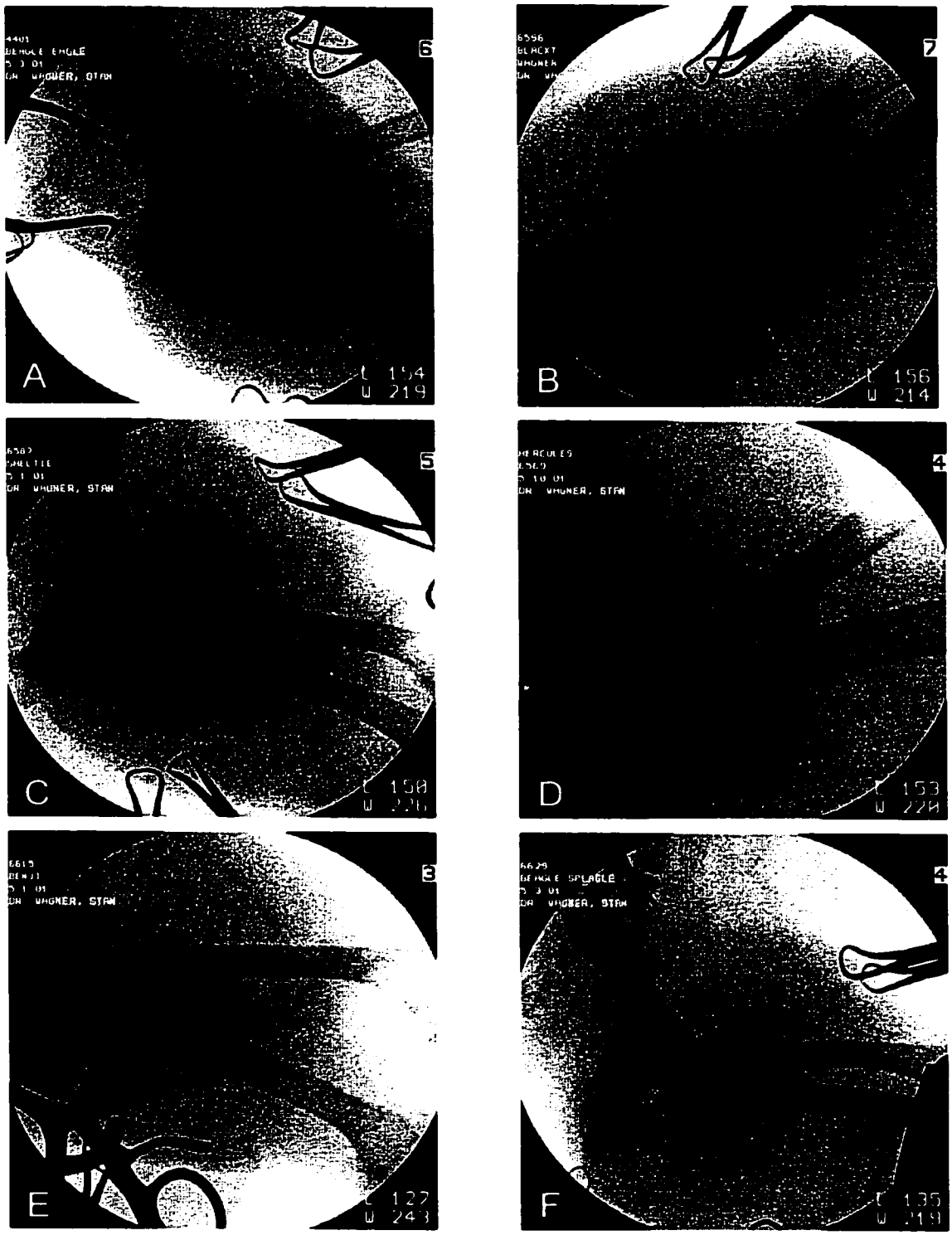

Intraoperative Fluoroscope images: A) 6640 B) 6596 C) 6587 D) 6569 E) 6615 F) 6629

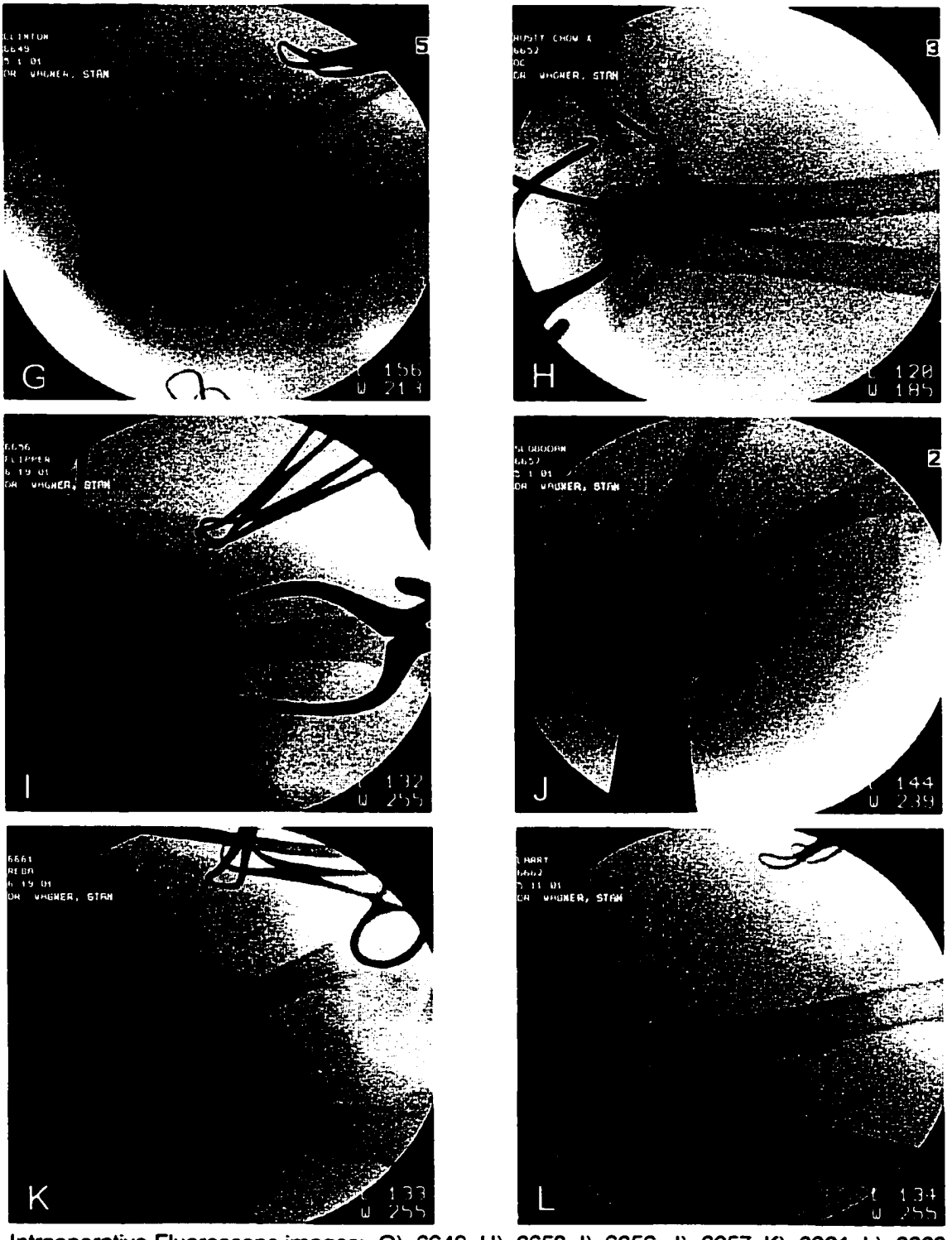

Intraoperative Fluoroscope images: G) 6649 H) 6652 I) 6656 J) 6657 K) 6661 L) 6662

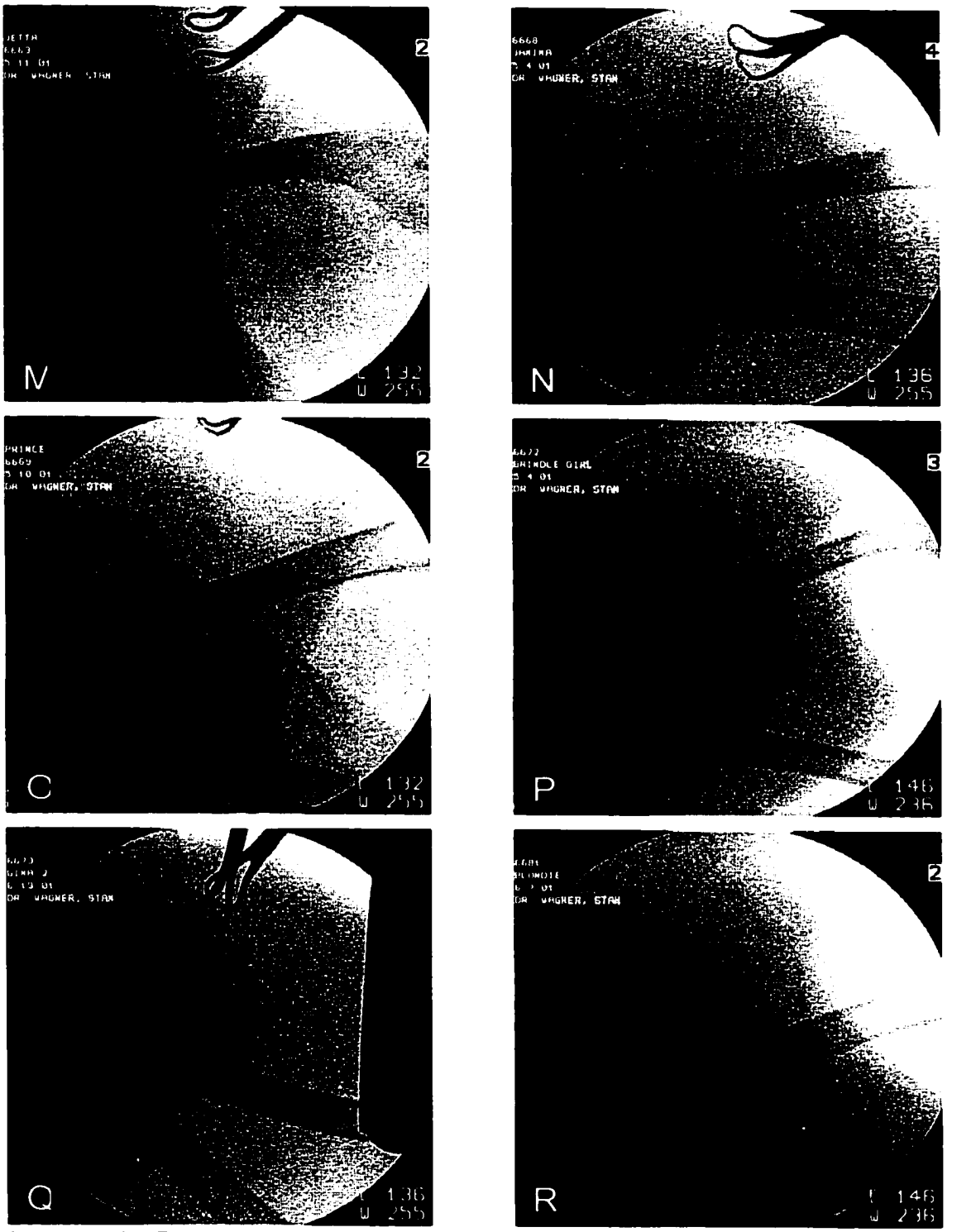

Intraoperative Fluoroscope images: M) 6663 N) 6668 O) 6669 P) 6672 Q) 6673 R) 6681

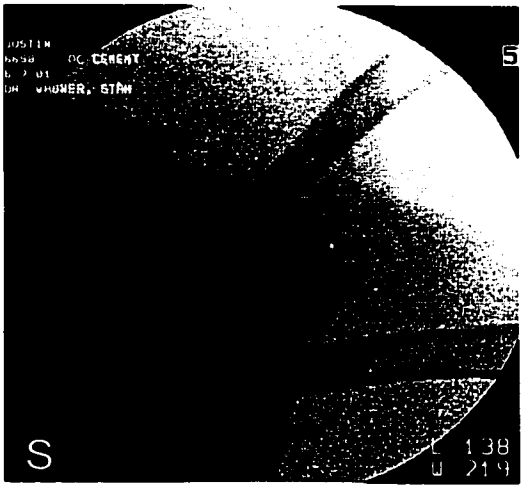

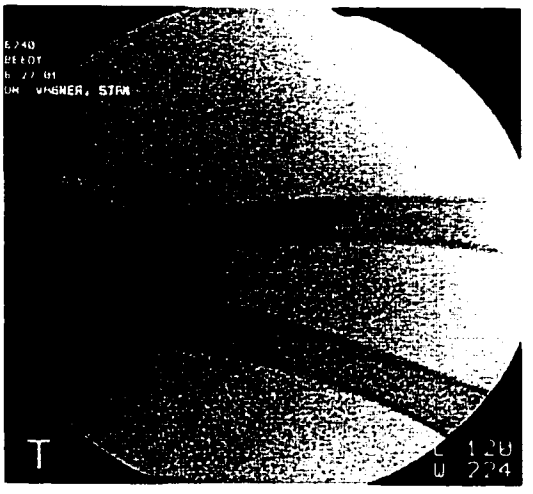

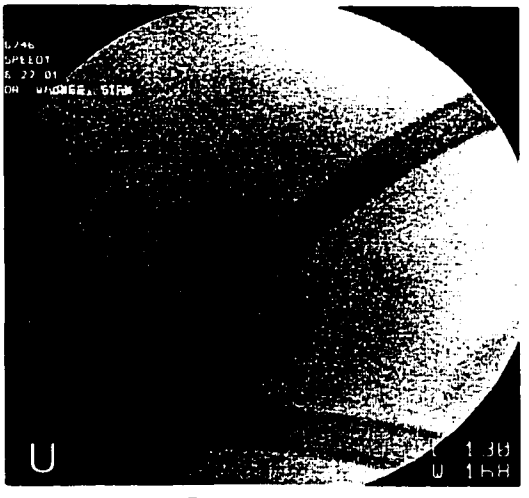

Intraoperative Fluoroscope images: S) 6698 T) 6740 U) 6746

APPENDIX E: MACRORADIOGRAPHS

Radiographs #6596: PMMA 6 wks A) Cranial-caudal B) Medial-lateral

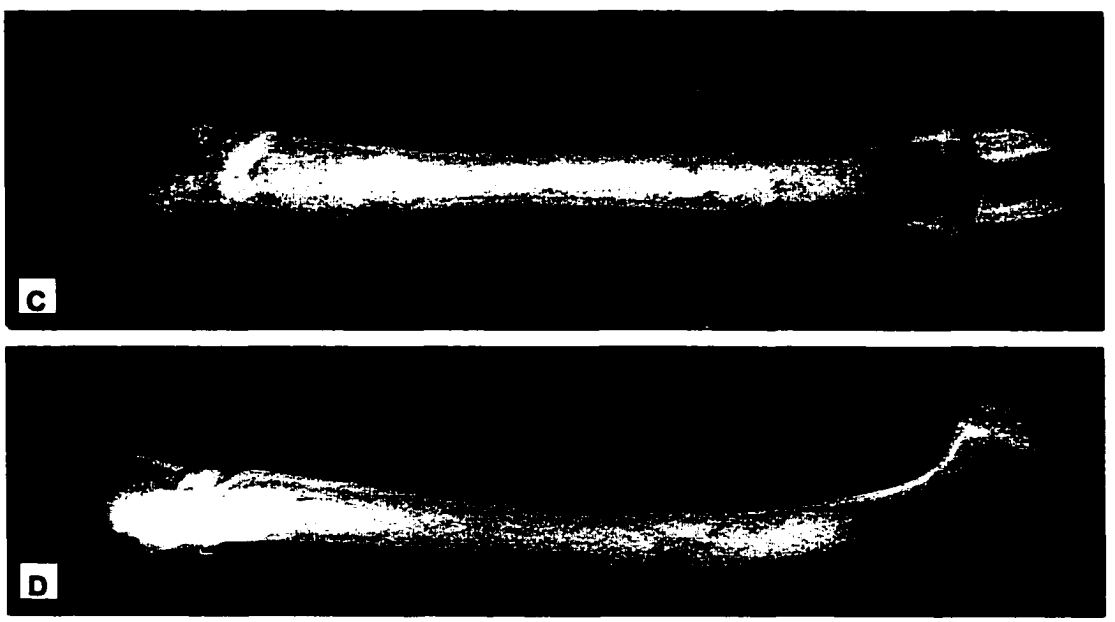

Radiographs #6649: PMMA 6 wks C) Cranial-caudal D) Medial-lateral

Radiographs #6657: OC 2 wks A) Cranial-caudal B) Medial-lateral

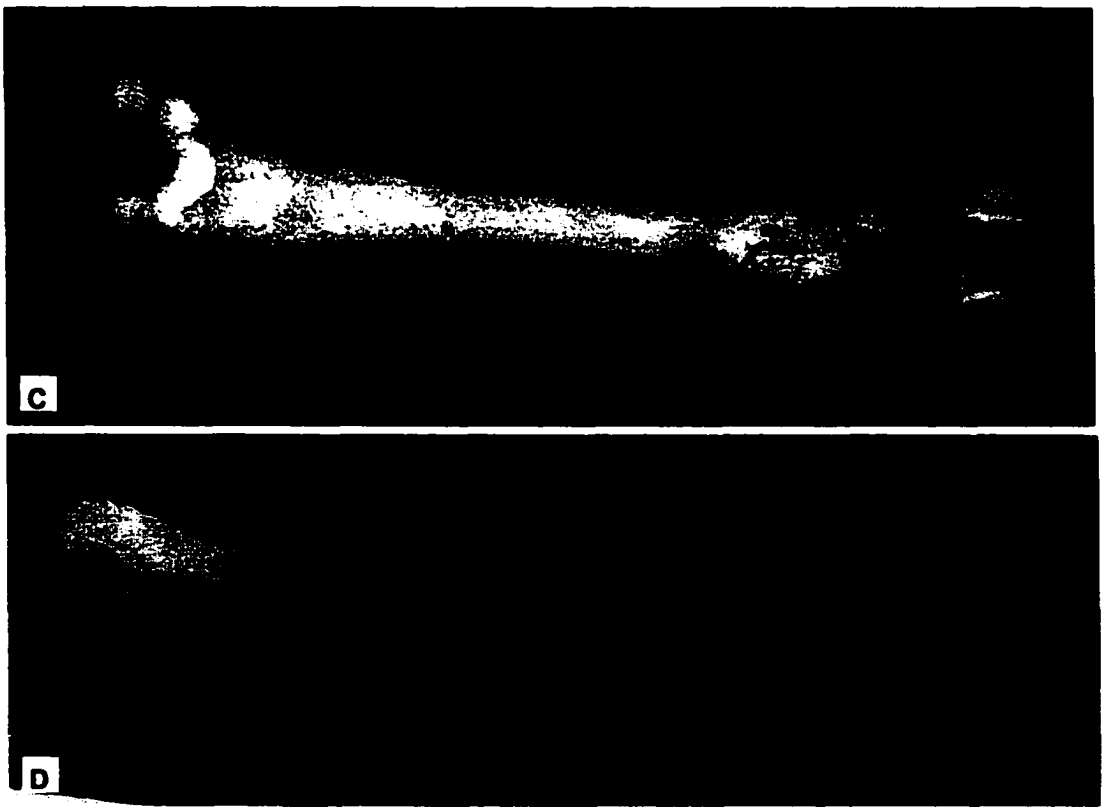

Radiographs #6615: PMMA 12 wks C) Cranial-caudal D) Medial-lateral

Radiographs #6587: PMMA 12 wks A) Cranial-caudal B) Medial-lateral

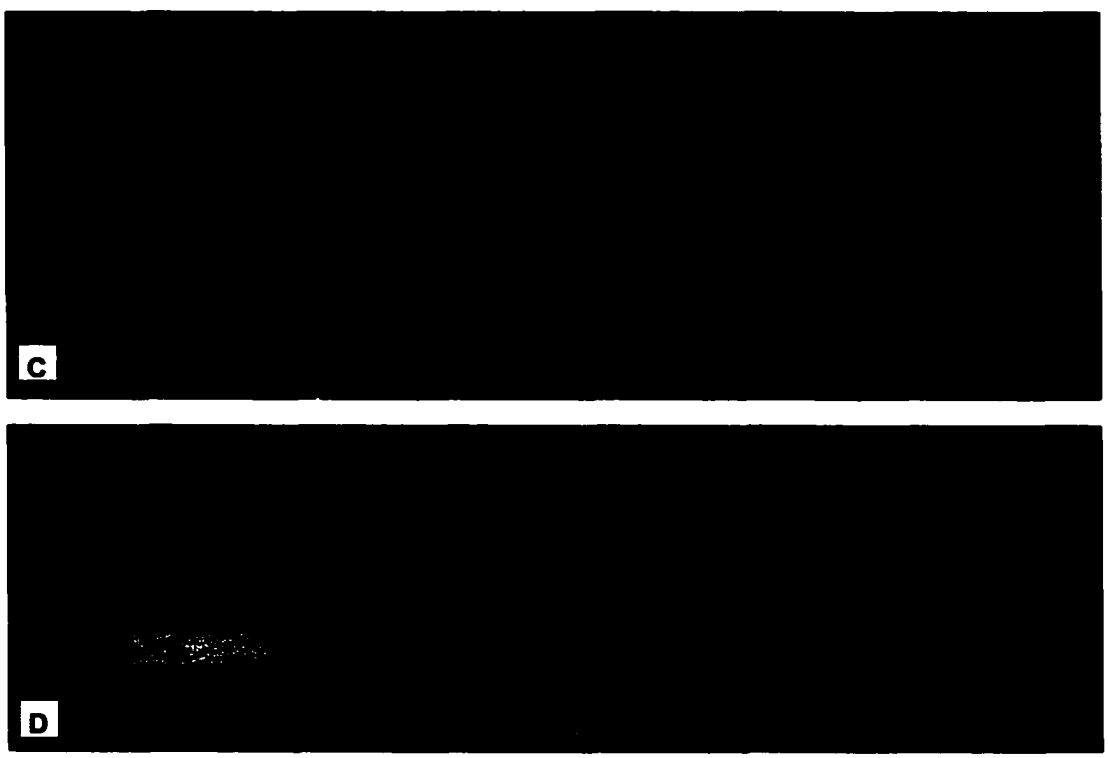

Radiographs #6640: PMMA 12 wks C) Cranial-caudal D) Medial-lateral

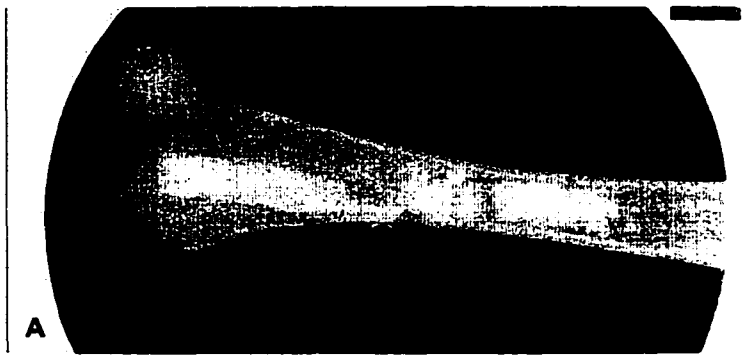

Fluoroscope image #6669: OC 2 wks A) Cranial-caudal

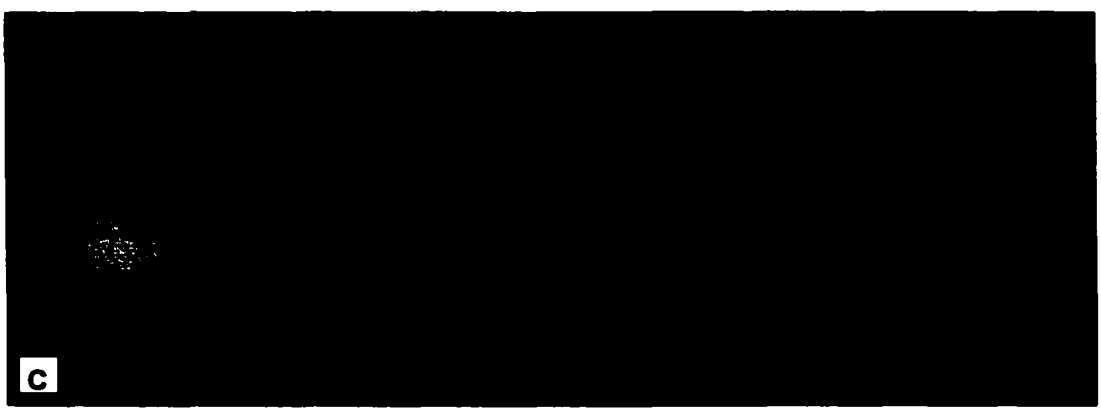

Radiographs #6673 (left femur): OC 2 wks B) Cranial-caudal C) Medial-lateral

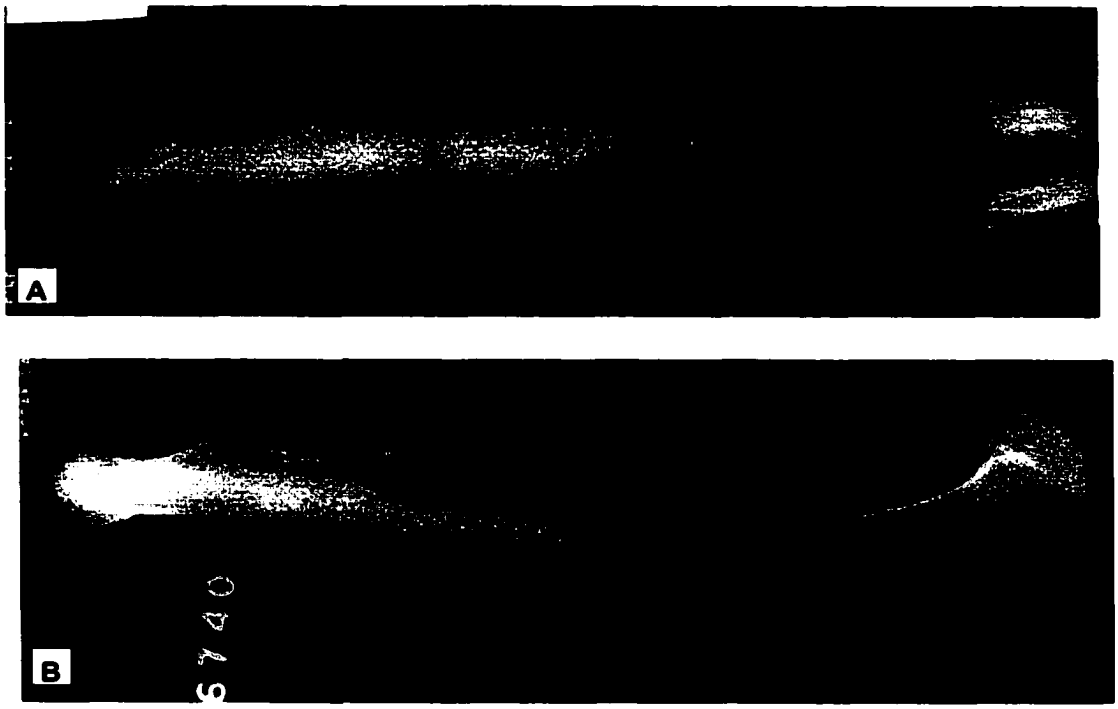

Radiographs #6740: OC 2 wks A) Cranial-caudal B) Medial-lateral

Radiographs #6746: OC 2 wks C) Cranial-caudal D) Medial-lateral

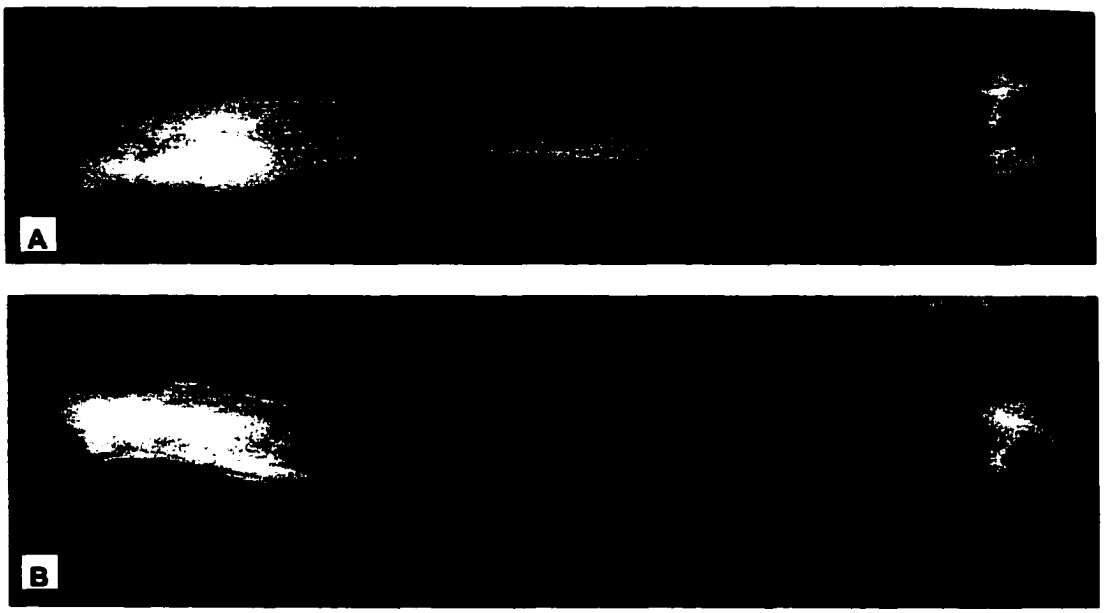

Radiographs #6569: OC 6 wks A) Cranial-caudal B) Medial-lateral

Radiographs #6656: OC 6 wks C) Cranial-caudal D) Medial-lateral

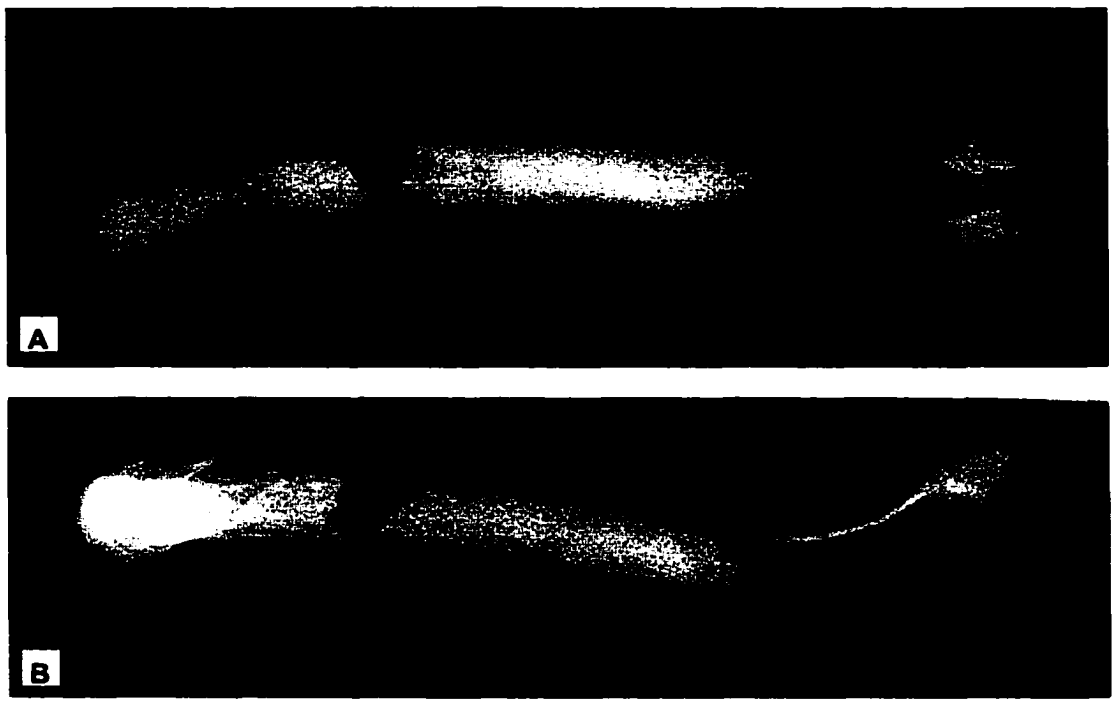

Radiographs #6661: OC 6 wks A) Cranial-caudal B) Medial-lateral

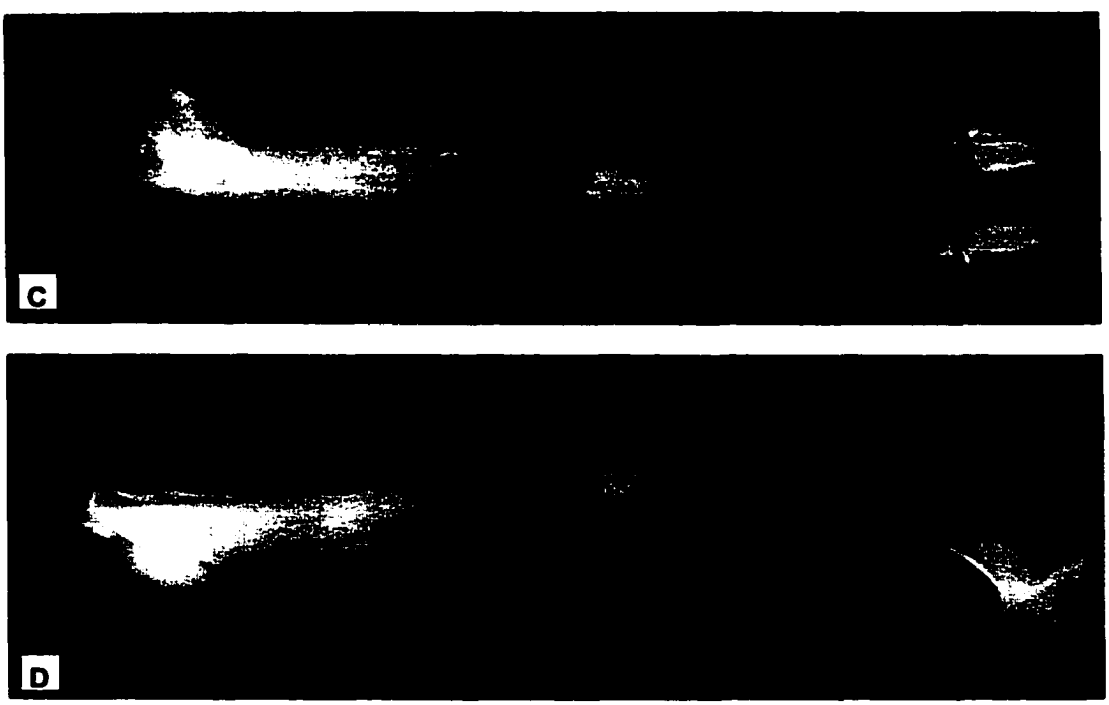

Radiographs #6698: OC 6 wks C) Cranial-caudal D) Medial-lateral

Radiographs #6652: OC 12 wks A) Cranial-caudal B) Medial-lateral

Radiographs #6662: OC 12 wks C) Cranial-caudal D) Medial-lateral

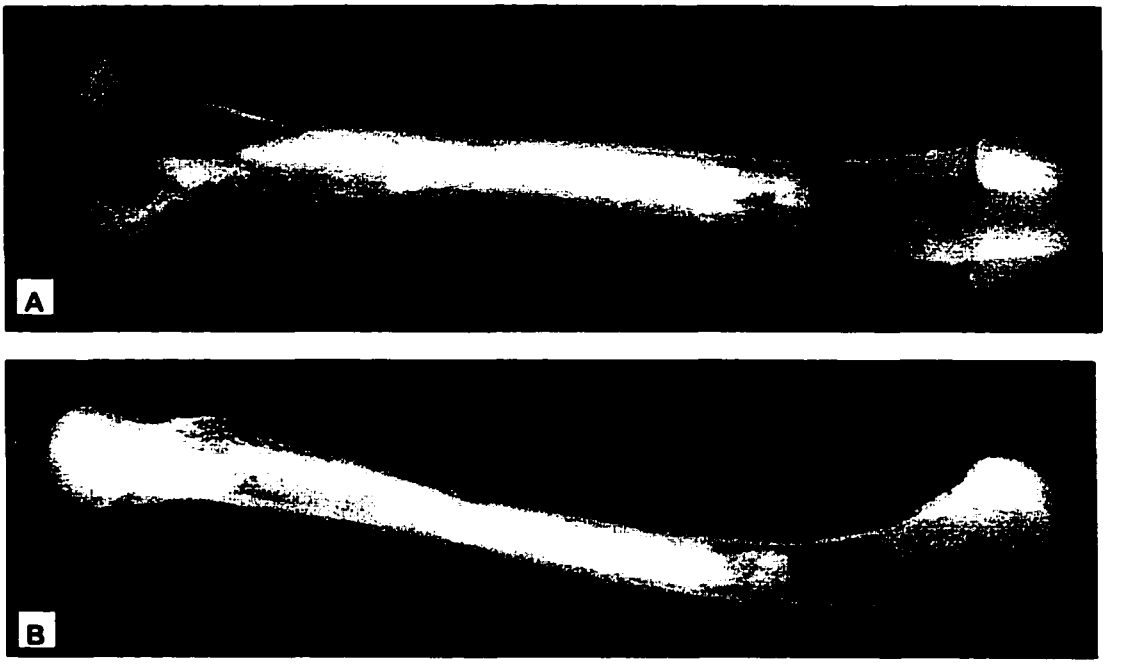

Radiographs #6663: OC 12 wks A) Cranial-caudal B) Medial-lateral

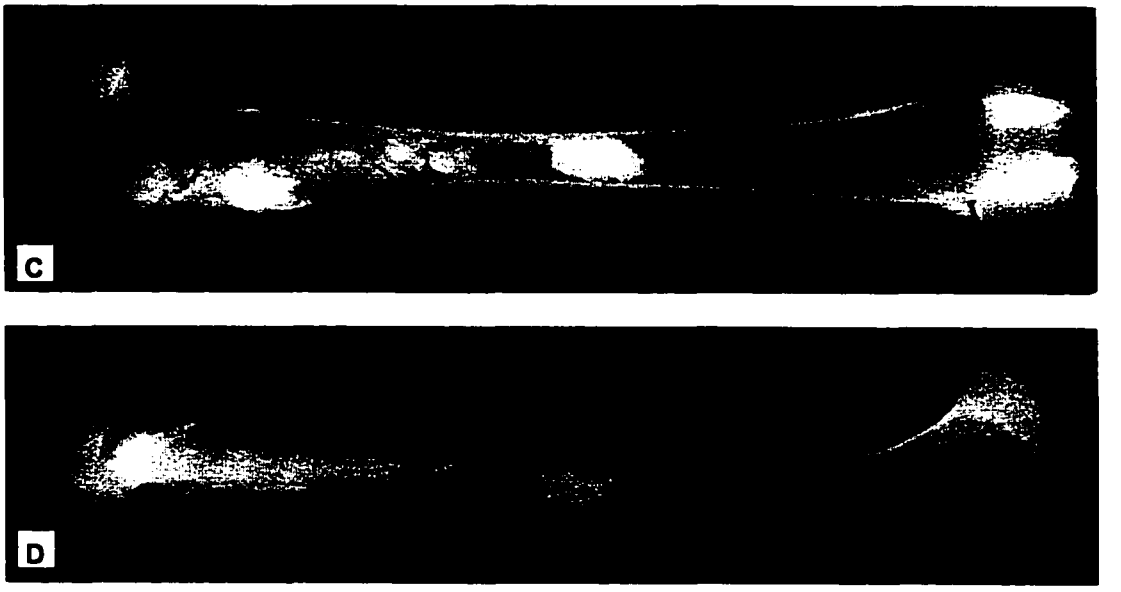

Radiographs #6681: OC 12 wks C) Cranial-caudal D) Medial-lateral

APPENDIX F: MICRORADIOGRAPHY- SUMMARY AND MICRORADIOGRAPHS

Summary of microradiograph analysis (Animal number – section number)

Specimen I.D.	*Grouping*	*Microradiograph observations*
6629-4b	PMMA 2 wks	Cancellous bone. Some penetration of cement into cancellous cells. Close contact between cement and bone. Very little periosteal bone growth.
6629-6c	PMMA 2 wks	Cortical bone. Incomplete fill of medullary cavity in this section. Thin gap between cement and bone. Significant periosteal bone growth.
6668-6b1/6b2	PMMA 2 wks	Cancellous bone. Penetration of cement into cancellous cells. Gap between cement and bone. Periosteal bone growth in some areas.
6672-5c	PMMA 2 wks	Cortical bone. Incomplete filling of medullary cavity in this section. Very little periosteal bone growth. Medullary canal contains some spongy bone surrounding the cement plug.
6657-4b	PMMA 6 wks	Cancellous bone. Penetration of cement deep into cancellous cells. Small gap between bone and cement in most areas. Significant amount of periosteal bone growth.
6657-5a	PMMA 6 wks	Cancellous bone. Penetration of cement deep into cancellous cells. Significant gap between bone and cement in most areas and much periosteal bone growth.
6657-6a	PMMA 6 wks	Cortical bone. Gap between bone and cement. Significant periosteal bone growth.
6596-3b	PMMA 6 wks	Cancellous bone. Cement penetration into cancellous cells. Shows good contact between bone and cement in most areas. Woven bone formation in upper right hand corner filling in hole in bone from surgery.
6596-4c	PMMA 6 wks	Cortical bone. Incomplete fill of medullary canal in this section. Very thin gap between bone and cement. Significant periosteal bone growth.
6649-4a	PMMA 6 wks	Cancellous bone. Cement penetrated deeply into most of the cancellous cells. Active periosteal bone growth. Very small gap between bone and cement.
6649-5b	PMMA 6 wks	Cortical bone. Small gap between bone and cement. Less periosteal bone growth.

Specimen I.D.	*Grouping*	*Microradiograph observations*
6587-4c	PMMA 12 wks	Cancellous bone. Some PMMA infiltration into adjacent cancellous cells. Some PMMA placed outside bone. Thinning of periosteal bone on remote side.
6587-5b	PMMA 12 wks	Cancellous bone. Some PMMA infiltration into adjacent cancellous cells. Large amount of PMMA placed outside bone. Some bone growth and callus formation.
6587-7b	PMMA 12 wks	Cortical bone. Fracture of diaphysis and cement. Ring of periosteal bone surrounding original cortical bone growth that is surrounded by massive callus formation. Gap between cement and bone.
6615-4	PMMA 12 wks	Cancellous bone. Cancellous cells completely filled with cement. Gap between bone and cement.
6615-5nc	PMMA 12 wks	Cortical bone. Close contact between cement and bone in $^{2}/_{3}$ of circumference. Significant periosteal bone growth ring that has been highly mineralized.
6640-4b	PMMA 12 wks	Cancellous bone. Little penetration into surrounding cancellous cells. Continuous gap between cement and surrounding bone. Intense densification of trabeculae on the right side and lower left corner.
6640-5b	PMMA 12 wks	Cortical bone. ¼ to $^{1}/_{3}$ the circumference of the cortical wall is missing. Massive periosteal bone growth and callous formation around $^{2}/_{3}$ to ¾ of the implant.
6669-3b	OC 2 wks	Cancellous bone. Cement and blood mixture in direct contact with bone. Some periosteal bone growth.
6669-5b	OC 2 wks	Cortical bone. Cement and bone mixture in contact with bone. Little periosteal bone growth.
6673-1b	OC 2 wks	Cancellous bone. Trabeculae surrounding implanted cement were damaged in surgical procedure. Little penetration of cement into cancellous cells. Some woven bone formation in some of the surrounding cancellous cells and a little periosteal bone growth.
6673-2b/2c	OC 2 wks	Cortical bone. Direct contact between cement and bone. Very little periosteal bone growth.
6740-4a	OC 2 wks	Cancellous bone. Little penetration of the cement into cancellous cells. Cement is in contact with bone. A few cancellous cells appear slightly more radio-opaque. Little or no periosteal bone growth.
6740-5b	OC 2 wks	Cortical bone. Cement is in direct contact with bone. Little periosteal bone growth.

Specimen I.D.	*Grouping*	*Microradiograph observations*
6746-4a	OC 2 wks	Cancellous bone. Cement partly placed outside of the bone. Some cancellous cells appear slightly more radio-opaque.
6746-5b	OC 2 wks	Cortical bone. Cement not penetrated into cancellous cells. Direct contact between bone and cement. Very little periosteal bone growth. Hole in the center of cement was inadvertently created at the time of implantation.
6569-4a/10e	OC 2 wks	Cancellous bone. Direct contact between bone and cement. Some infiltration of soft tissue or cement particles into cancellous cells.
6569-5d/6e	OC 2 wks	Cortical bone. No implant in these sections. Medullary canal shows infiltration of mineralized tissue that was not present on the initial post surgical fluoroscope image. Some periosteal bone growth.
6656-5a	OC 2 wks	Cancellous bone. Direct contact between bone and cement. Very little infiltration of cement into cancellous cells. No periosteal bone growth.
6656-6b	OC 2 wks	Cortical bone. Direct contact between bone and cement. Little periosteal bone growth.
6661-4c	OC 2 wks	Cancellous bone. Direct bone-cement contact. Some filling of cancellous cells with cement particles.
6661-4d	OC 2 wks	Cancellous bone. Direct contact between bone and cement. Little to no filling of cancellous cells. Growth of trabecular bone surrounding implanted cement.
6661-5c	OC 2 wks	Cortical bone. Direct bone-cement contact. Some periosteal bone growth on upper edge of the bone.
6698-5a/4b	OC 2 wks	Cancellous bone. Cement is in direct contact with bone. Little or no infiltration of the cement into cancellous cells. Growth of trabecular bone surrounding implant.
6698-3b	OC 2 wks	Cortical bone. Incomplete fill of medullary canal. Cement plug in medullary canal with spongy bone surrounding cement.
6652-4b	OC 2 wks	Cancellous bone. Cement placed outside of bone. Woven bone filling in surgical defect that was created on the top edge.
6662-4c	OC 2 wks	Cancellous bone. Surgical defect was not completely filled with cement. Some direct bone-cement contact. A lot of periosteal bone growth in the lower left corner.
6662-7b	OC 2 wks	Cancellous bone. Direct contact between bone and cement.

Specimen I.D.	*Grouping*	*Microradiograph observations*
6662-5a	OC 2 wks	Cortical bone. Small cement plug in oversized defect. Spongy bone surrounding defect. New bone growth surrounds defect. Cement is not in direct contact with new bone growth.
6663-4a	OC 2 wks	Cancellous bone. No penetration of cement into cancellous cells. Cement plug placed in circular defect with some direct bone contact. Trabecular bone around the defect area has become denser.
6663-5a	OC 2 wks	Cortical bone. Direct contact between cement and bone. Some periosteal bone growth.
6681-4b	OC 2 wks	Cancellous bone. Cement is in contact with bone. A small amount of cement in cancellous cells immediately adjacent to the implant.
6681-6b	OC 2 wks	Cortical bone. Cement plug is surrounded by marrow or blood in most places. Very small area of direct cement bone contact. Little periosteal bone growth evident.

MICROCRADIOGRAPHS OF BONE-CEMENT SECTIONS

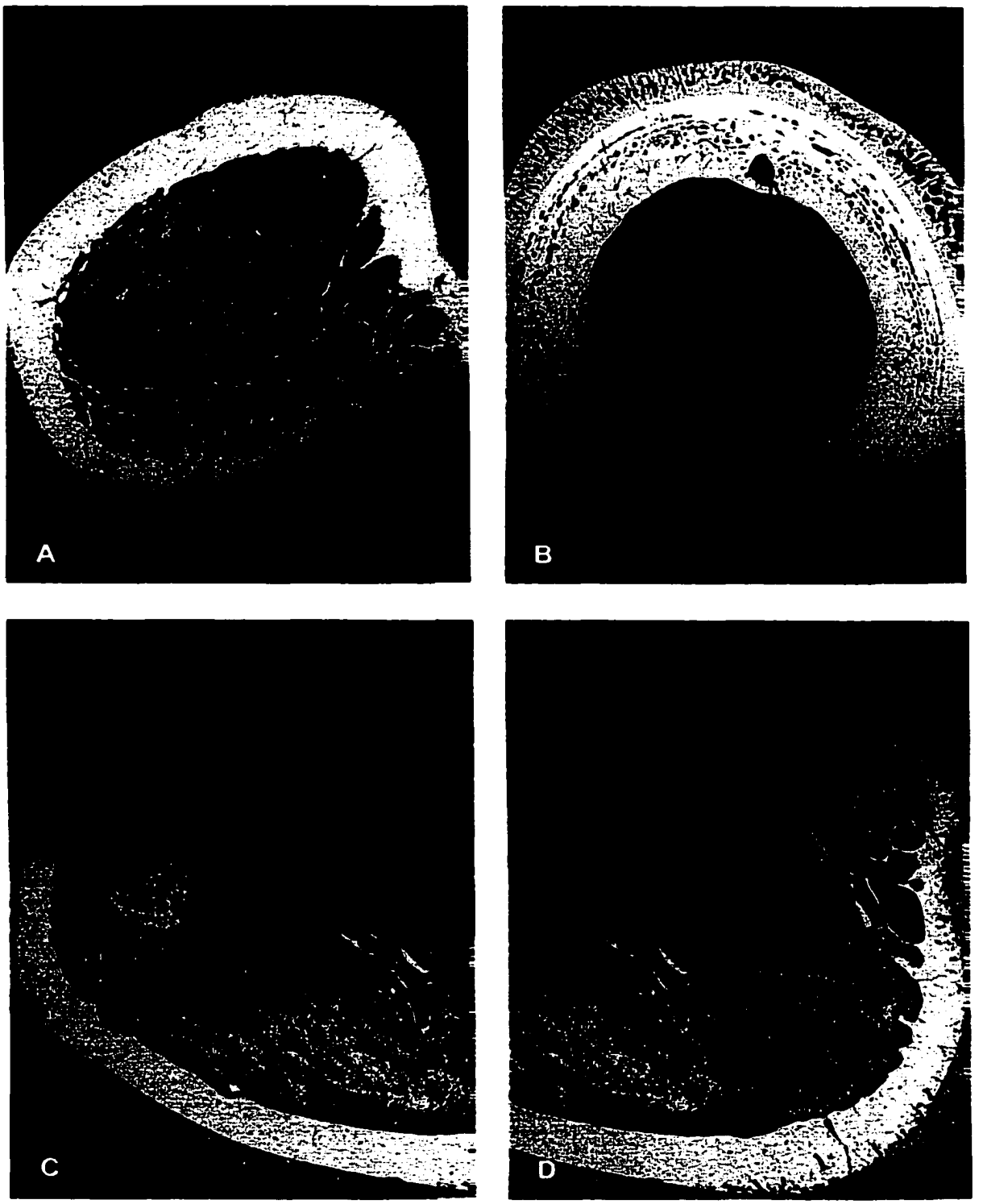

PMMA 2 wk: A) 6629-4b B) 6629-6c C) 6668-6b1 D) 6668-6b2

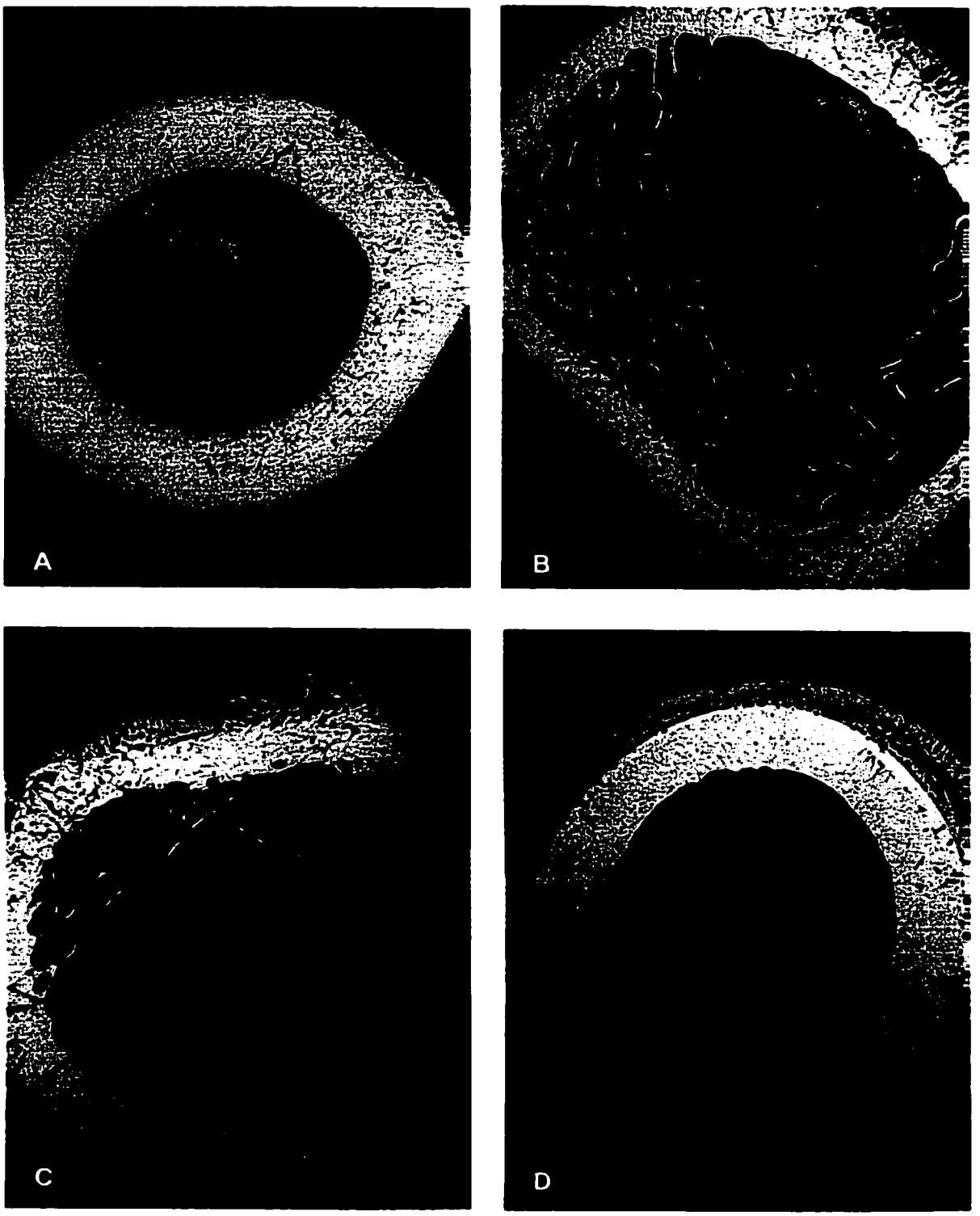

PMMA 2 wk: A) 6672-5c, 6 wks: B) 6657-4b C) 6657-5a D) 6657-6a

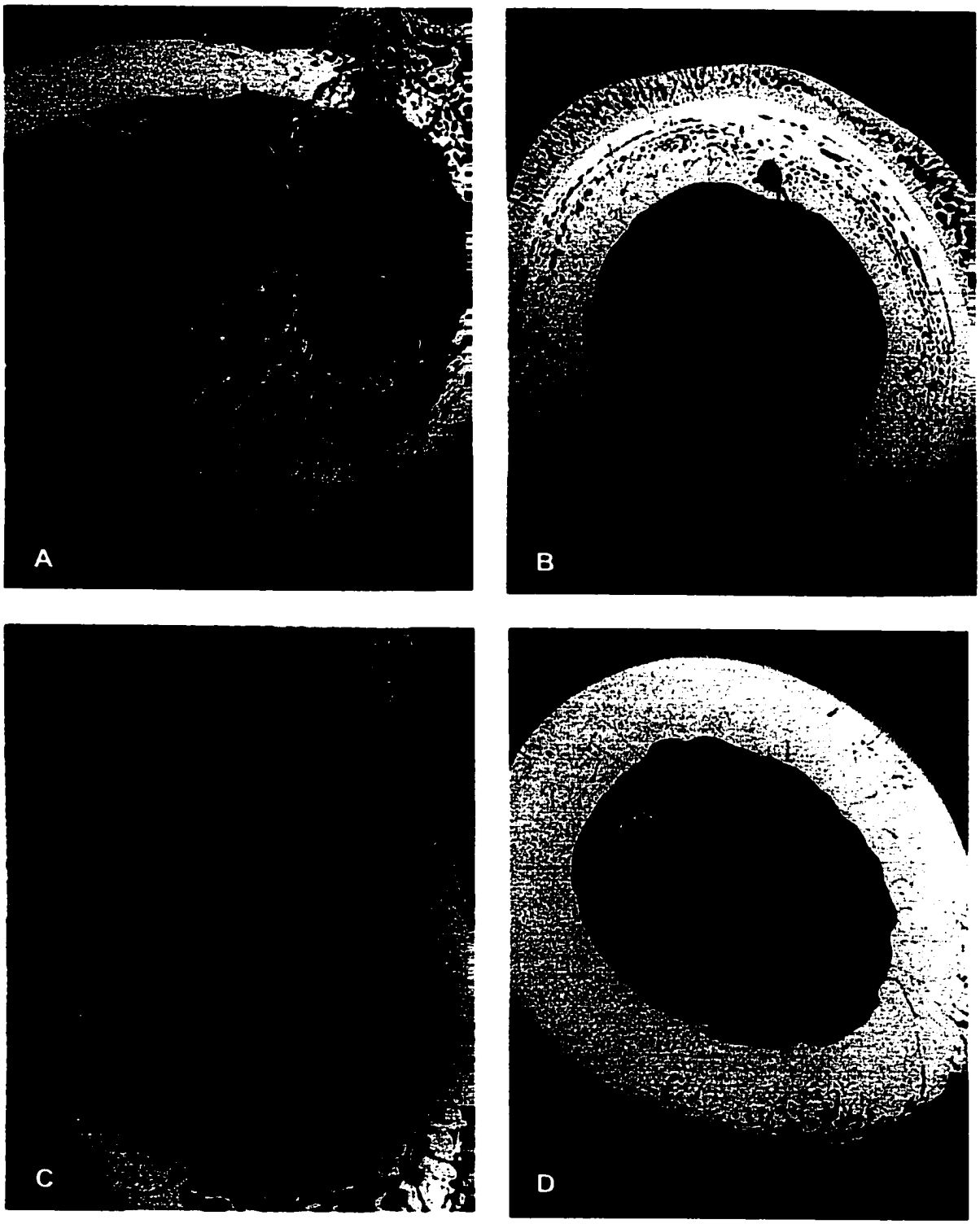

PMMA 6 wk: A) 6596-3b B) 6596-4c C) 6649-4a D) 6649-5b

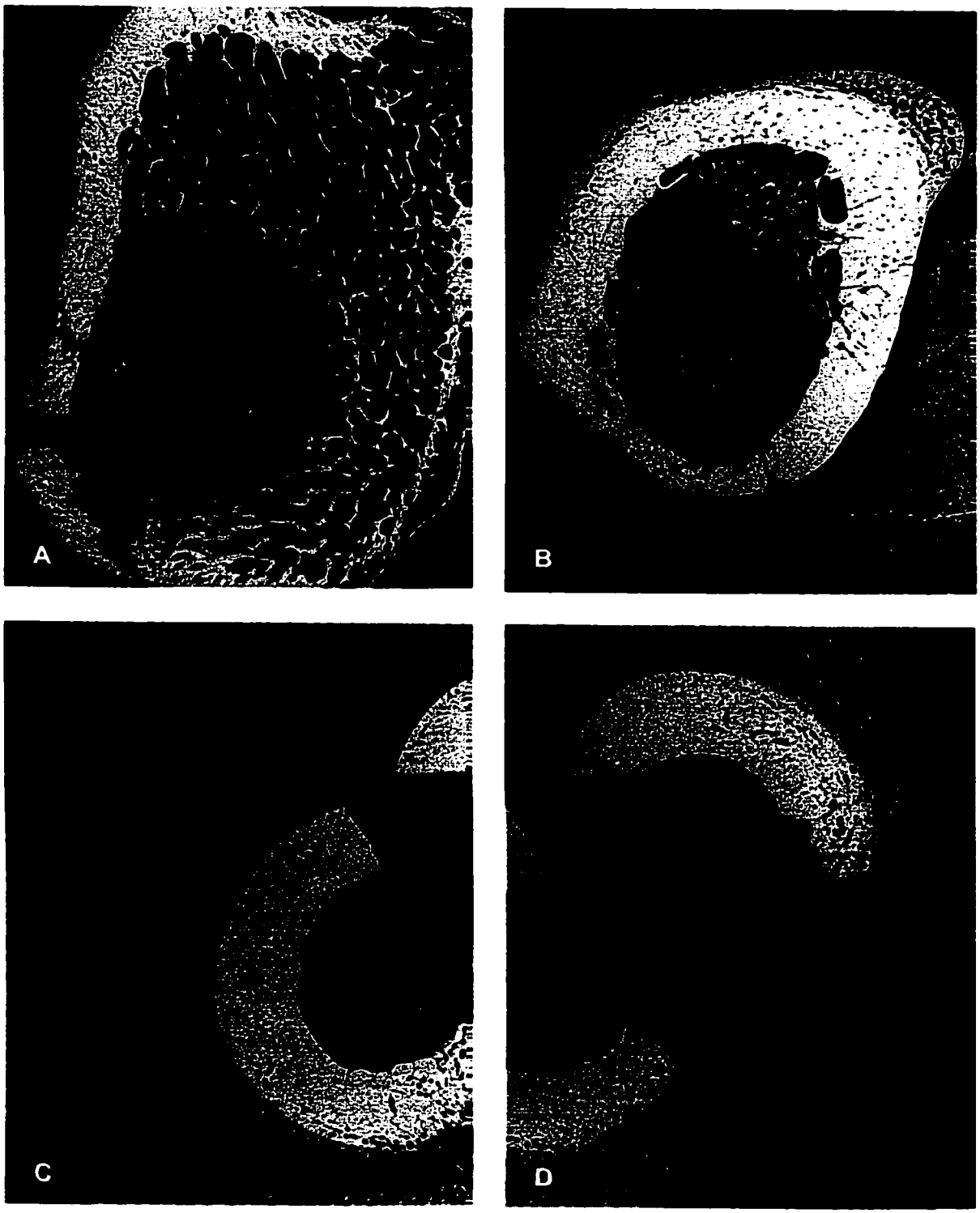

PMMA 12 wk: A) 6587-4c B) 6587-5b C) 6587-7b1 D) 6587-7b2

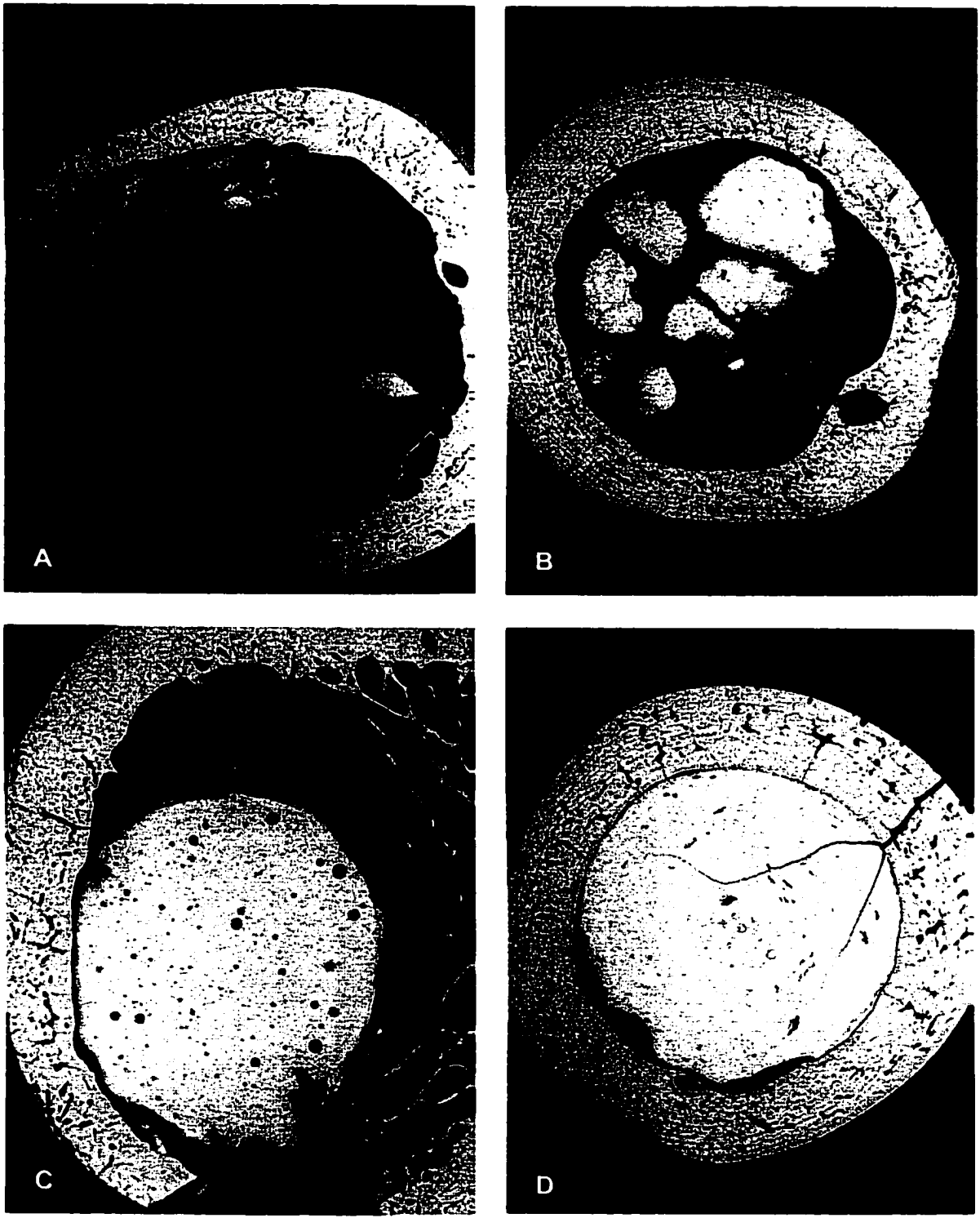

OC-cement 2 wk: A) 6669-3b B) 6669-5b C) 6673-1b D) 6673-2b

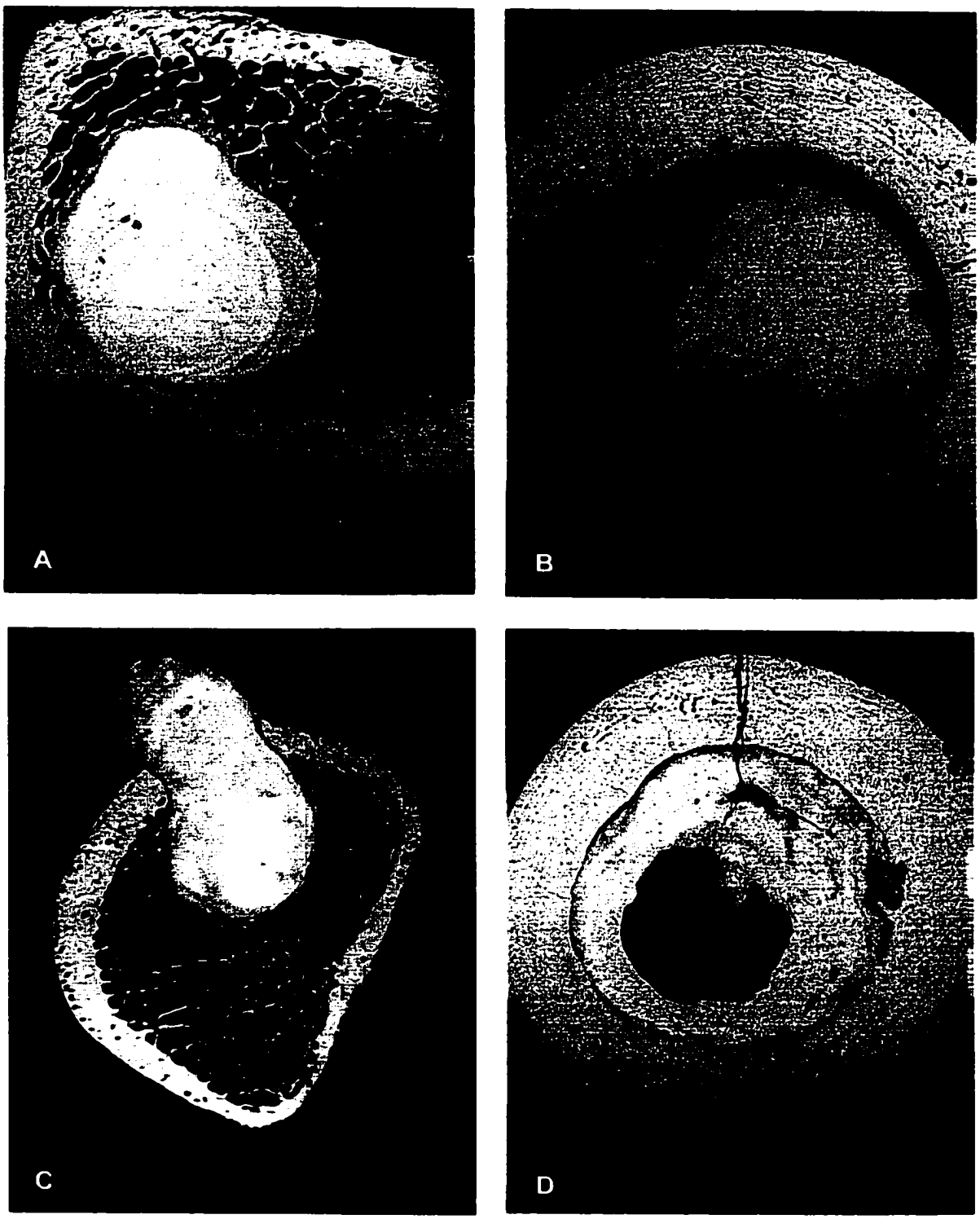

OC-cement 2 wk: A) 6740-4a B) 6740-5b C) 6746-4a D) 6746-5b

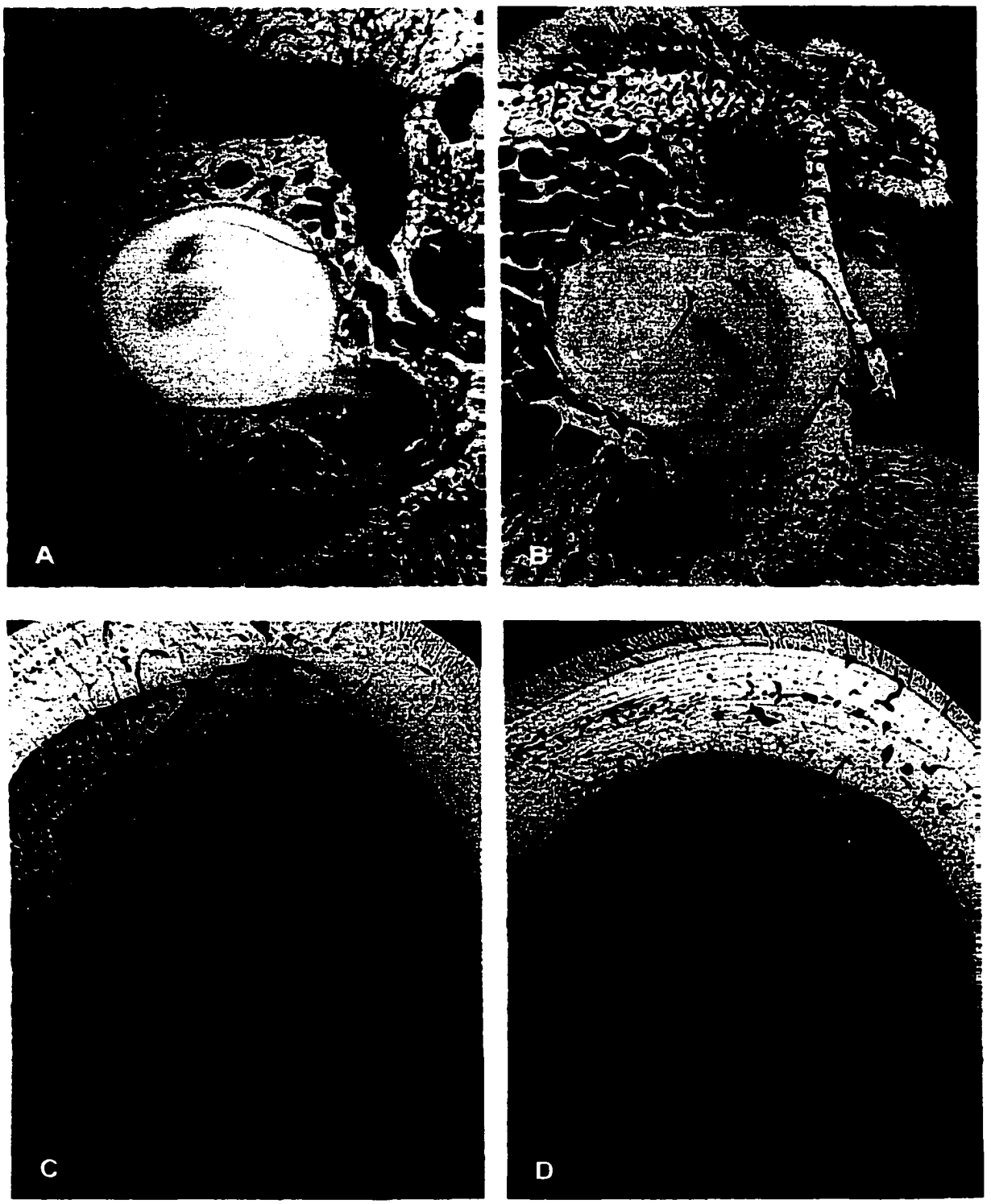

OC-cement 6 wk: A) 6569-10e B) 6569-4a C) 6569-5d D) 6569-6e

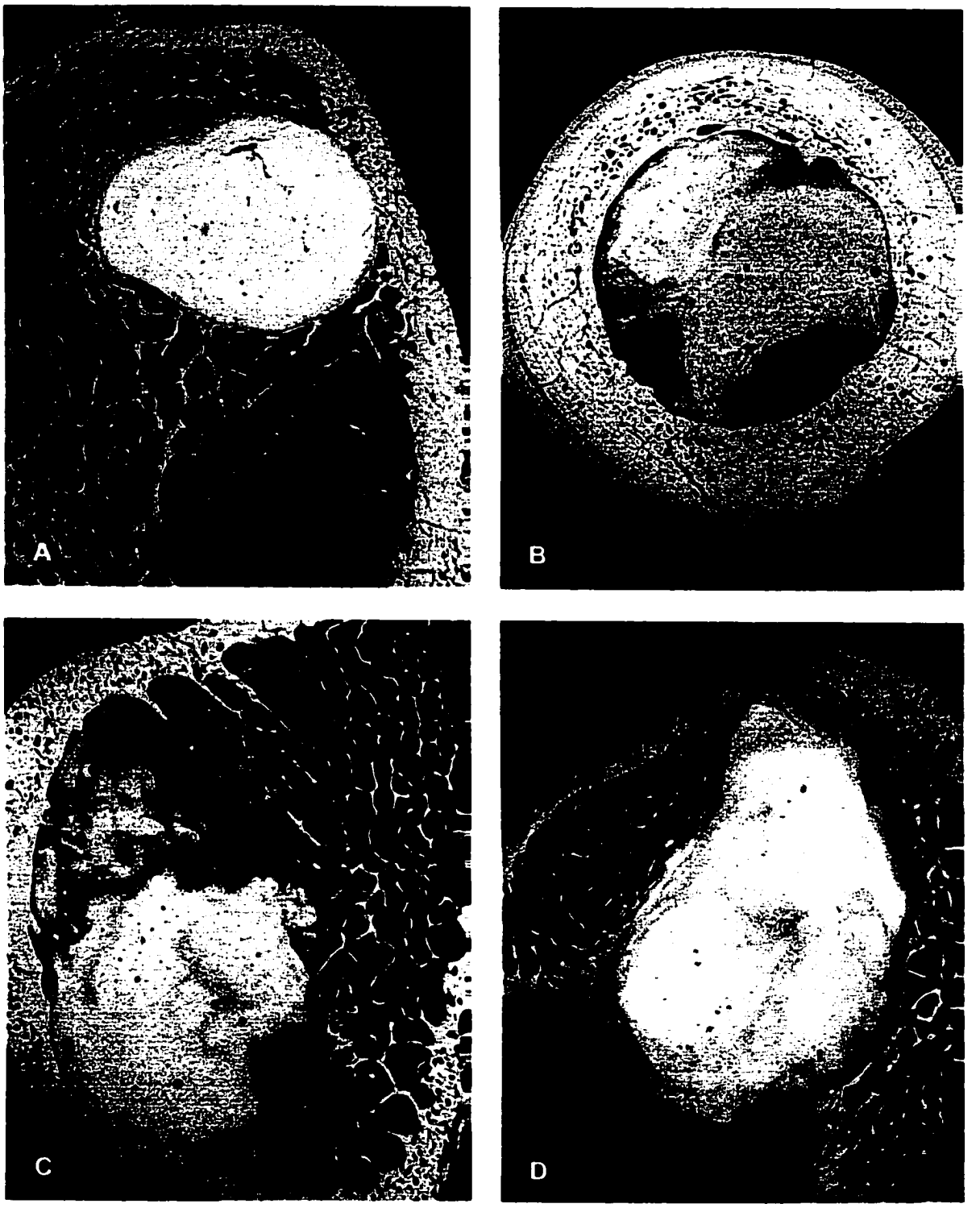

OC-cement 6 wk: A) 6656-5a B) 6656-6b C) 6661-4c D) 6661-4d

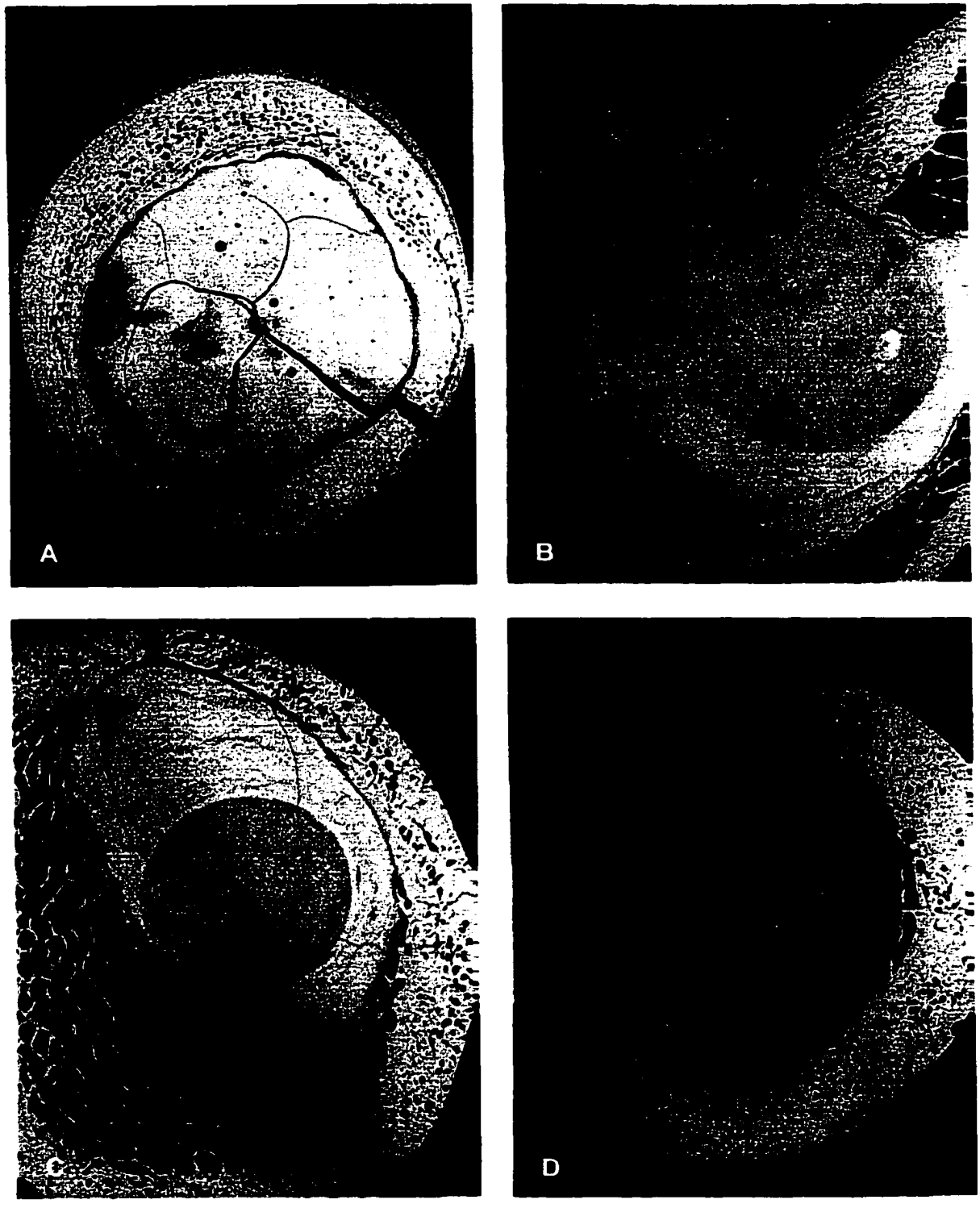

OC-cement 6 wk: A) 6661-5c B) 6698-5a C) 6698-4b D) 6698-3b

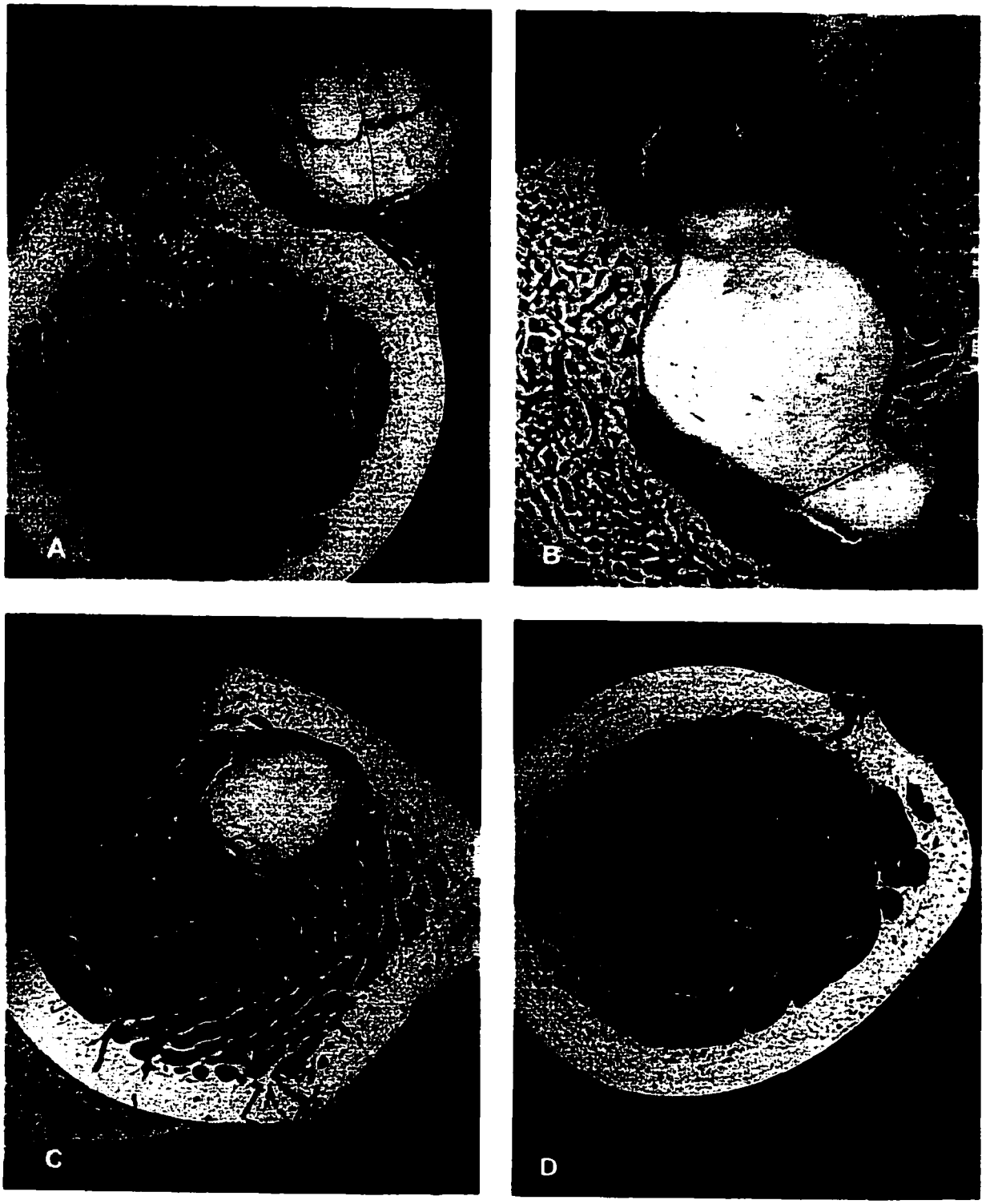

OC-cement 12 wk: A) 6652-4b B) 6662-7b C) 6662-4c D) 6662-5a

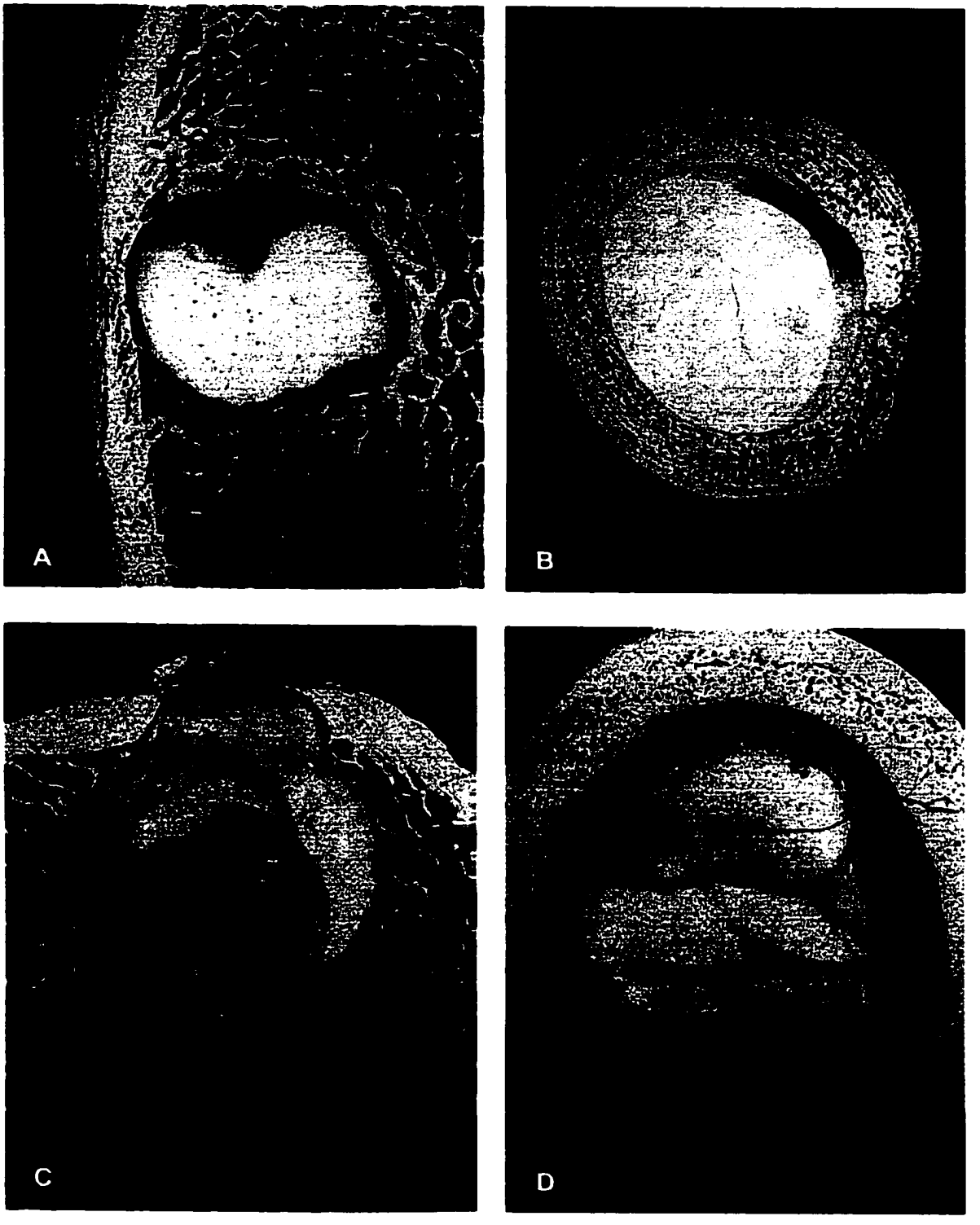

OC-cement 12 wk: A) 6663-4a B) 6663-5a C) 6681-4b D) 6681-6b

APPENDIX G: FLUORESCENCE MICROSCOPY NOTES

Slide I.D	*Grouping*	*Observations*
6569-4a	OC 6 wks	Massive periosteal bone growth. Mineralization present throughout bone. Mixture of blood and cement present between cement and growing bone.
6569-5a,b/ 6c,d,e	OC 6 wks	Thick periosteal bone formation. Some mineralization present throughout cortical bone. Thin hairline of growth observed around the lumen with spongy bone growing into intramedullary canal.
6569-10b	OC 6 wks	Massive periosteal bone growth. Growth and mineralization throughout bone. Bone directly adjacent to cement was not as active as other areas throughout the bone. Bone growth was observed along areas where a mixture of cellular and cement debris was present.
6656-5a	OC 6 wks	Thin band of growth around the periosteum. Growth in trabecular bone observed. Little growth observed at the cement-bone interface, but appeared consistent with the amount of growth in the surrounding bone.
6656-6b	OC 6 wks	Thin band of growth around the periosteum. Mineralization and remodeling was prevalent throughout the cortical bone. Typical amount of growth and thin areas of direct bone growth surrounding areas of cellular and cement debris. Very few areas of bone growth adjacent to cement.
6661-4c	OC 6 wks	Growth at the periosteum and mineralization throughout the cancellous bone. Direct contact between bone growth and cement in some trabeculae. Generally, a band of practically no growth was observed between cement and surrounding bone.
6661-5c/4d	OC 6 wks	Very thin band of periosteal bone growth around half of the bone. Prevalent mineralization and remodeling throughout cortical bone, but very little growth in bone directly adjacent to the cement. Very, thin line of growth along lumen in one, small area.
6698-3b	OC 6 wks	Fluorescence appeared faded on this slide. Very, thin band of growth around approximately 10% of periosteum. Mineralization and remodeling was observed throughout cortical bone. Mostly soft tissue surrounding cement; no direct contact between cement and bone was observed.
6698-4a/4b	OC 6 wks	Fluorescence appeared faded on this slide. Growth was observed around the periosteum. Mineralization of cancellous bone was observed throughout the specimen. Typical growth was observed up to and adjacent to cement.
6698-5a/5b	OC 6 wks	Very, thin line of growth around periosteum. Mineralization and remodeling was observed throughout cortical and cancellous bone. Little growth was found directly along implant, although occasionally observed in cancellous bone areas.

Slide I.D	*Grouping*	*Observations*
6698-6e	OC 6 wks	Cement was implanted into soft tissue. No bone growth observed.
6596-3b	PMMA 6 wks	Band of periosteal bone growth of irregular thickness observed. Mineralization adjacent to cement in trabecular bone was observed. Growth at lumen was generally separated from cement by soft tissue.
6596-4c	PMMA 6 wks	Complete, thick band of growth around periosteal bone. Typically, no growth closer to the cement. Some growth of spongy bone adjacent to the cement in the marrow cavity.
6649-4b	PMMA 6 wks	Irregular, thick band of growth found around periosteum. Mineralization was observed throughout cancellous bone. Some growth was noted adjacent to cement in areas where cement infiltrated cancellous cells.
6649-5b	PMMA 6 wks	Irregular, thin band of growth around periosteum. Very, little mineralization and remodeling were observed throughout cortical bone. A couple very, thin lines of growth in bone surrounding the lumen was observed, possibly a very, small amount of direct contact.
6657-4b	PMMA 6 wks	Large amount PMMA infiltrated into cancellous cells. Irregular, thin band of growth was found around the periosteum. Large amount of mineralization was observed in outer trabecular bone. Trabecular bone closer to cement showed less activity, but was sometimes in direct contact with cement. Mineralization was observed at bone-cement interface, but was typically separated by soft tissue.
6657-6a	PMMA 6 wks	Complete band of growth of medium thickness was observed around periosteum. Little mineralization or remodeling was found throughout the cortical bone. Very, thin line of growth found in approximately 10% of bone around lumen.
6652-4b/5c	OC 12 wks	A portion of the implant was placed outside of the bone. No bone growth was observed between cement and soft tissue. Where the cement was placed in the bone, a layer of cellular and cement debris was present between bone and implant. Bone mineralization was observed along debris-bone interface throughout the specimen. Rings of growth were present along the periosteum. Prevalent mineralization and remodeling was observed throughout cortical bone. Very, thin line of growth was present along the marrow cavity (not in direct contact with cement).
6662-4c	OC 12 wks	Implant was placed in bone, but not in direct contact with bone. Cement was surrounded by layer of cellular and cement debris. Growth was observed along the periosteum and mineralization was present throughout the cancellous bone. Soft tissue was observed between the cement and bone; no bone growth was found in direct contact with cement.

Slide I.D	*Grouping*	*Observations*
6662-5a/7a	OC 12 wks	Very, little growth was observed at the periosteum. Some mineralization was present throughout the cortical bone and up to the soft tissue interface between the cement and bone. In a small area, there was direct bone-cement contact, a little bone with consistent amount of growth was in contact with cement.
6663-4a/4c	OC 12 wks	Thin ring of new bone was observed around periosteum. Growth throughout cancellous bone. Very little bone growth in direct contact with cement. Area of cement and cellular debris surrounded the implant; this layer was typically surrounded by soft tissue.
6663-5a	OC 12 wks	Bone growth around periosteum was observed. Mineralization and remodeling observed throughout cortical bone. No mineralization was observed in ring of bone directly adjacent to the cement.
6681-4b	OC 12 wks	Little growth was observed around the periosteum. Small locations of mineralization were found adjacent to the cement, but not as much activity as in the surrounding cancellous bone.
6681-5b/6b	OC 12 wks	Very, thin, incomplete band of growth was observed at peiosteum. Mineralization and remodeling was present throughout cortical bone. Very, thin line of growth was present at bone interface with soft tissue (along approximately 10% of the diameter).
6681-7c	OC 12 wks	Entire slide had very little fluorescence. Very, little growth of periosteal bone was observed. Some remodeling and mineralization was present throughout cortical bone. No mineralization was present around the lumen.
6587-4c	PMMA 12 wks	Thin, irregular growth of periosteal bone was observed. Mineralization was found in cancellous bone. Soft tissue separated cement and bone. Approximately 50% of the trabecular bone in contact with the soft tissue showed mineralization.
6587-5b,d	PMMA 12 wks	Some periosteal bone formation was observed, followed by massive callus formation. Little mineralization and remodeling were observed throughout the original bone. Very thin line of mineralization was found around 20% of the lumen.
6615-4b	PMMA 12 wks	Thin, irregular band of growth was observed at the periosteum. Mineralization and remodeling were present throughout cancellous bone. A very, thin line of mineralization surrounded approximately 90% of the lumen, but the bone and cement were separated by soft tissue.
6615-5nc	PMMA 12 wks	Band of bone growth of medium thickness was present around periosteum. Mineralization and remodeling was observed throughout cortical bone. Two very, thin lines of mineralization were present around approximately 80% of the lumen. Cement was separated from the surrounding bone by soft tissue.

Slide I.D	*Grouping*	*Observations*
6640-4b	PMMA 12 wks	Thin, irregular band of growth was observed along the periosteum. Prevalent mineralization was observed throughout cancellous and cortical bone and around the lumen. Typically, there was soft tissue between the cement and bone growth, however, some areas in the cancellous bone appeared to have direct contact between growth and cement.
6640-5b/6b	PMMA 12 wks	Cortical bone was missing from approximately $^{1}/_{4}$ of the bone's diameter and was filled-in with soft tissue. Massive bone growth was observed around periosteum of the original bone. Growth and mineralization was prevalent throughout the cortical bone and around the lumen. Soft tissue generally separated the bone and cement. Direct contact between cement and growth of spongy bone in a few, isolated areas.

APPENDIX H: PUSH-OUT TEST DATA

Charts showing individual data points for push-out tests are compiled for OC-cement and PMMA in addition to charts presenting the average push-out strength that was determined from each animal.

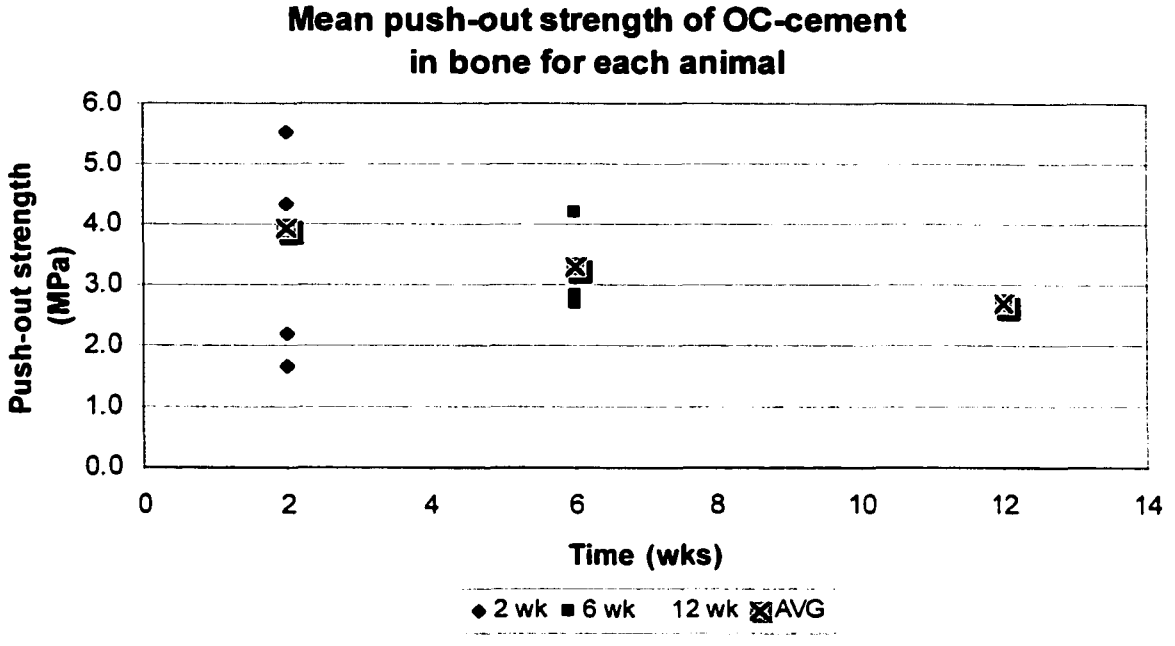
Mean push-out strength of OC-cement in bone for each animal
Push-out strength (MPa)
6.0
5.0
4.0
3.0
2.0
1.0
0.0
0
2
4
6
8
10
12
14
Time (wks)
2 wk
6 wk
12 wk
AVG

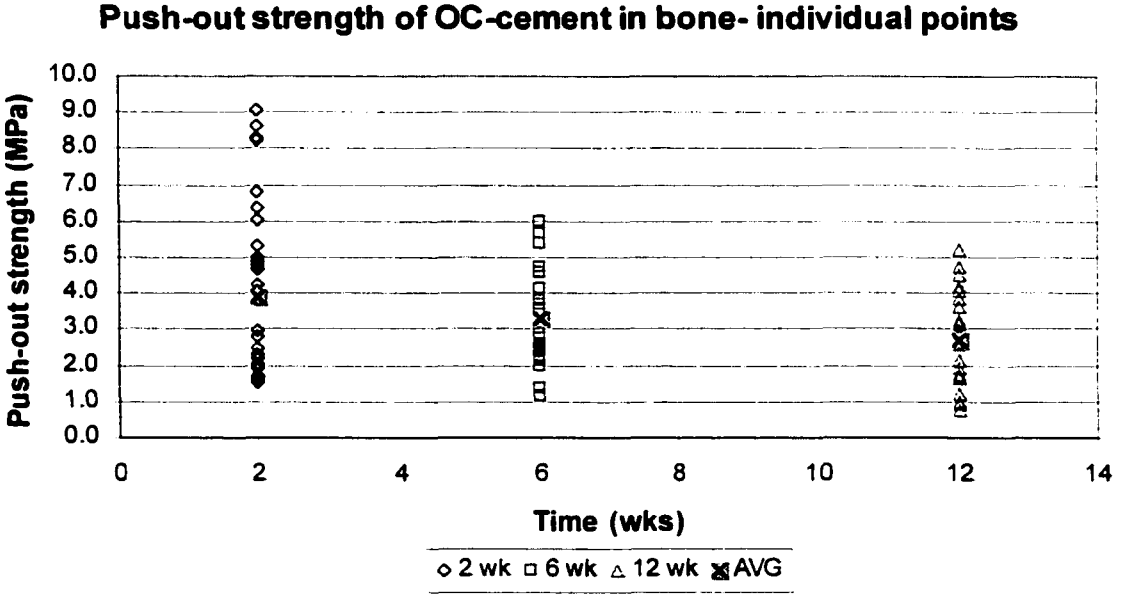
Push-out strength of OC-cement in bone- individual points
Push-out strength (MPa)
10.0
9.0
8.0
7.0
6.0
5.0
4.0
3.0
2.0
1.0
0.0
0
2
4
6
8
10
12
14
Time (wks)
2 wk
6 wk
12 wk
AVG

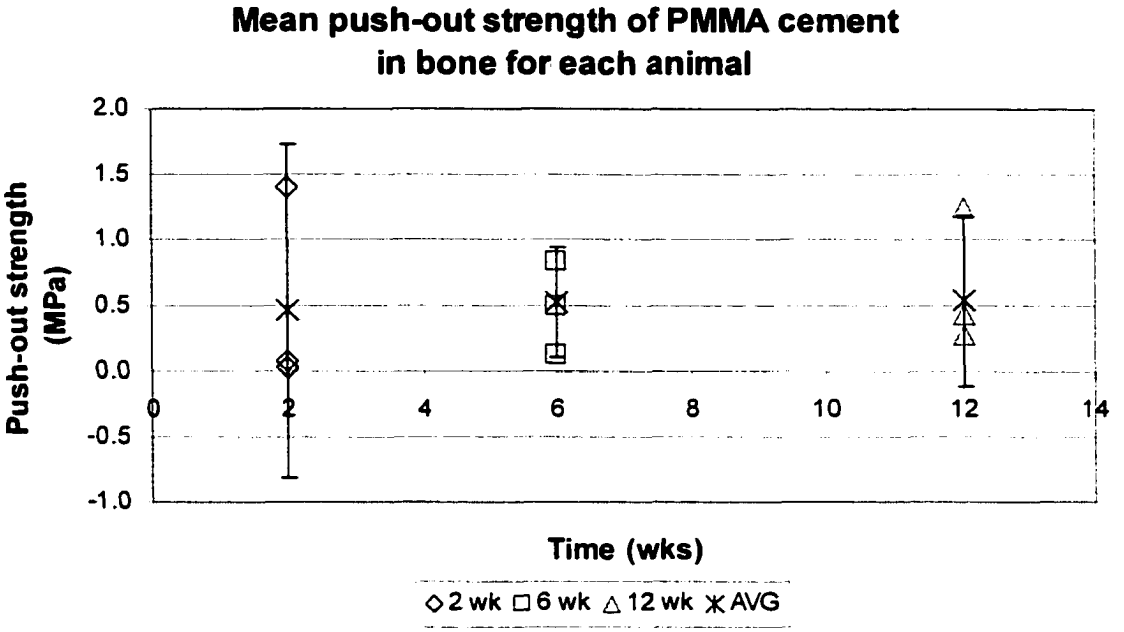
Mean push-out strength of PMMA cement in bone for each animal
Push-out strength (MPa)
2.0
1.5
1.0
0.5
0.0
-0.5
-1.0
0
2
4
6
8
10
12
14
Time (wks)
◇2 wk □6 wk △12 wk ✳AVG

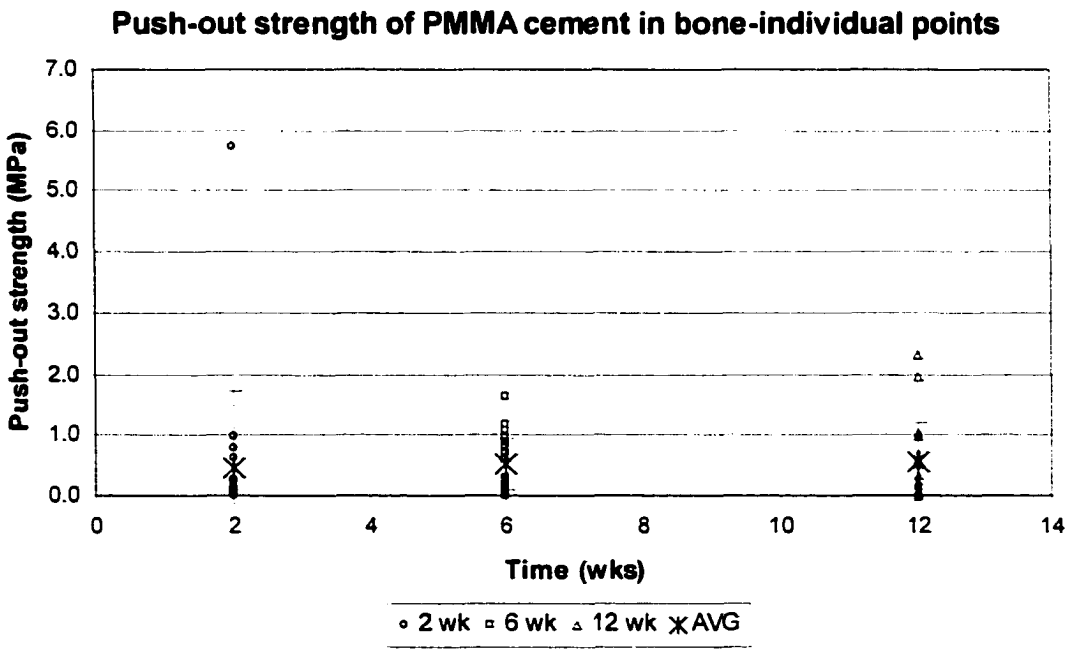
Push-out strength of PMMA cement in bone-individual points
Push-out strength (MPa)
7.0
6.0
5.0
4.0
3.0
2.0
1.0
0.0
0
2
4
6
8
10
12
14
Time (wks)
◦ 2 wk ▫ 6 wk △ 12 wk ✳AVG